Hydroxyproline O- Arabinosylation in Pollen Fertility

by

Steven Beuder

A dissertation submitted in partial fulfillment
of the requirements for the degree of
Doctor of Philosophy
(Molecular, Cellular, and Developmental Biology)
in The University of Michigan
2021

Doctoral Committee:

Professor Steve Clark, Chair
Associate Professor Scott Barolo
Assistant Professor Cora MacAlister
Professor Erik Nielsen

Steven Beuder

sbeuder@umich.edu

ORCID iD: 0000-0001-6735-2631

Dedication

To my dogs, who have no idea why I abandoned them. To my family, for supporting me through everything. And to my friends Andrew and Brittany- I miss you both.

Acknowledgements

Thank you to everyone who supported and challenged me while I was here, and of course, to those who helped me get to graduate school in the first place. While this experience was lonely at times, my growth and development did not occur in a vacuum.

Table of Contents

List of Tables

.

List of Figures

Appendix Figures:

Abstract

Sexual reproduction in flowering plants relies on the successful delivery and fusion of the male and female gametes. Ovules contain the female gametes and are located in the ovaries, which are embedded in the female reproductive tissue- collectively referred to as the pistil. The male gametes are transported through a specialized cell called the pollen tube, which must penetrate and traverse through the transmitting tract, which can be dense with carbohydrates secreted from the surrounding cells, or open- depending on the species. Therefore, successful fertilization relies on the pollen tube's ability to grow, successfully navigate to the ovules, and burst to release the sperm cells once inside the ovule. While these physiological events are well-understood, the molecular mechanisms underlying key processes are still unclear.

Sperm delivery relies on the pollen tube's ability to maintain the structural integrity of its cell wall throughout the growth process; it must be rigid enough to penetrate the female tissue and prevent premature rupture, but also extensible at the tip to allow for elongation. This is regulated by a multitude of factors that control the structural integrity of the cell wall, which include the synthesis and trafficking of cell wall materials, secretion, and the proper assembly, organization, and modification of these materials once they are deposited into the extracellular space. Many factors have been identified, but many key players and their roles have yet to be discovered.

This dissertation describes how we identified new factors that regulate pollen tube growth by influencing the structural and mechanical properties of the cell wall, by using a combination of genetic, molecular, and bioinformatic approaches. We characterized the cell wall structural defects caused by loss of protein *O*-arabinosylation in *Arabidopsis* pollen tubes which primarily included loss of cell polarity, increased bursting frequency, and decreased elongation rates which, in combination, caused poor fertility. We examined the pollen tube cell wall structure and discovered that loss of protein *O*-arabinosylation was associated with changes in the composition of the cell wall and the organization of its components which have important roles in regulating the mechanical properties of the cell wall. Through a forward genetics screen, we identified mutations in key secretory genes- including members of the exocyst complex- that suppressed the effects caused by loss of protein *O*-arabinosylation and improved pollen tube growth and fertility, and we interrogated the link between the secretory pathway and cell wall structure. We also identified a mutation in a gene involved in phosphoinositide (PI) signaling, which appears to be suppressing the effects caused by loss of *O*-arabinosylation through another pathway. By characterizing the effects of this suppressor mutation and learning more about the gene involved, we have identified another novel factor that regulates tip growth and cell wall structure in *Arabidopsis* pollen tubes. Our findings described herein demonstrate how we have contributed to the overall knowledge of the plant development and reproduction field by addressing how protein *O*-arabinosylation, secretion, and PI signaling pathways combine to influence the structural and mechanical properties of the cell wall.

Chapter 1 - Literature Review

Introduction of pollen tubes as a model to study cell wall structure and secretion

The plant cell wall is a complex extracellular matrix composed of multiple carbohydrate networks including cellulose, hemicellulose, callose and pectins, as well as proteins such as cell wall-remodeling enzymes and glycoproteins. The cell wall is essential for the proper development and growth of both the sporophytic/vegetative and gametophytic/reproductive phases of the plant life cycle by performing key functions such as providing structural support, mediating cell to cell communication, and serving as a defensive barrier against biotic and abiotic stresses, among others. During cell growth, the wall must be rigid enough to maintain structural integrity and prevent rupture, but capable of re-organization to allow for expansion. This is mediated through changes in wall structure which promote or inhibit expansion, but **how does the structure of the cell wall contribute to its mechanical properties?**

Pollen tube (PT) growth occurs through a tip-growth mechanism, which is a highly-polarized form of cell growth that also occurs in root hairs, fungal hyphae, and neuronal axons (Campàs & Mahadevan, 2009). After landing on the stigma, a pollen grain will germinate to form a tube, which elongates and delivers the sperm cells to the ovules located in the ovaries, which are embedded in the pistil. PTs must grow with enough force to penetrate the transmitting tract of the pistil, navigate into an ovule (mediated by guidance cues secreted by the female tissue) and rupture in a timely manner to release the sperm nuclei (Higashiyama & Takeuchi, 2015). Proper PT tip growth is mediated by maintaining two spatially-distinct regions of cell wall with different mechanical properties: (i) an extensible tip that allows for expansion while preventing premature rupture, and (ii) rigid subapical walls (known as the shank), which are fortified with callose and pectic crosslinking to withstand internal turgor pressure and direct it towards the tip to drive expansion (Chebli et al., 2012) (Figure 1A). The cell wall is continually expanded

throughout growth, and therefore relies on the proper synthesis and rapid secretion of cell wall materials; however, trafficking and exocytosis must be carefully balanced with endocytosis to prevent over-accumulation of materials and thickening of the tip cell wall, which inhibits growth (Ischebeck et al., 2008). PTs are an excellent system to study cell growth because expansion is occurring at a confined apical region with unique cell wall properties relative to its subapical, non-growing regions. Also, in multicellular tissues, the walls of individual cells form a shared continuous layer, and changes in individual cell morphology affect neighboring cells through this attachment (Daher & Braybrook, 2015). Because there are no neighboring cells, single- celled PTs are a convenient model to study cell growth *in vitro*.

Studying the cell wall poses unique challenges, which are largely due to its dense, acidic environment and interconnectedness of different polymers, networks, fibrils, etc. While PTs offer the convenience of a single cell, their cell wall contains low amounts of cellulose and high amounts callose, making them different than other tissues. Therefore, studying PTs allows us to identify new factors that regulate cell wall structure and growth, which may not have roles in vegetative tissues. This chapter will review what is known about how cell wall materials are structurally organized and secreted to regulate PT tip growth, and will focus on several main areas: (1) the extensin proteins and the enzymes that modify them, and how extensin structure and function regulates cell wall properties; (2) pectins, which interact with extensins and have major roles in regulating cell wall structure and mechanics through crosslinking activity; (3) how the exocyst complex regulates polarized secretion and cell growth; and (4), how phosphoinositide signaling at the plasma membrane regulates exocyst-mediated secretion and polarized growth.

1.1 Extensins

1.1.1 Overview

Although they are only a minor portion of the cell wall by weight, cell wall-associated glycoproteins- and the enzymes that modify them- are essential for the many growth and developmental processes in plants. The hydroxyproline (Hyp)-rich

glycoproteins (HRGPs) are a large family of cell-wall associated proteins in plants and they are classified into three main subfamilies: (i) extensins (EXT) and extensin-like proteins, (ii) arabinogalactan proteins (AGPs), and (iii) proline-rich glycoproteins (PRPs) (reviewed recently in (Petersen et al., 2021). However, the delineations between subfamilies are not always clear due to the existence of HRGP hybrid and chimera proteins, which may include multiple HRGP domains of different types, or HRGP domains fused with non-HRGP domains which have their own function/activity (Borassi et al., 2016). The HRGPs undergo varying degrees of posttranslational glycosylation; AGPs are highly glycosylated, the classical extensins are typically moderately glycosylated, and PRP glycosylation is usually the least extensive (Showalter et al., 2010).

Early studies showed that expression of extensins and other HRGPs is upregulated during development and in response to conditions including wounding, fungal and viral infection, and abiotic stresses (e.g. heat shock, water stress, and drought). Extensin expression was mainly associated with phloem and cambium tissues, although the means of detecting expression were limited by some of the techniques used (including tissue print protein and mRNA blots), and their insolubilization in the cell wall created difficulty for protein detection (Showalter, 1993). Insolubilization in the cell wall is mediated by multiple types of crosslinking reactions (discussed later) and is an important aspect of extensin structural function in the cell wall. Extensin increases the cell wall's resistance to enzymatic digestion, osmotic lysis (Lamport & Lamport, 1966), and pathogen infection (Esquerré-Tugayé et al., 1979; Hammerschmidt et al., 1984), and inhibited cell elongation in pea epicotyl and root sections (Cleland & Karlsnes, 1967; Sadava & Chrispeels, 1973; Vaughan & Cusens, 1973), suggesting that the primary function of extensins is strengthening the cell wall. **But how do extensins regulate the structural and mechanical properties of the cell wall, and what is the significance of glycosylation in this process?** This section will focus on literature that addresses how extensin protein structure and function are important in plant processes- with an emphasis on tip growth.

1.1.2 Extensin structure and crosslinking in the cell wall

The structures of “classical” extensins are highly periodic and amphiphilic with key features including an N-term signal peptide followed by repetitive amino acid sequences, including Ser$(Pro)_{3-5}$ motifs which alternate with lysine- and tyrosine (Y) -containing motifs (Y/VY) (and occasionally His-) (Figure 1B) (Showalter et al., 2010). The high level of proline promotes formation of a polyproline II helical structure, and early structural studies showed that extensin monomers extracted from carrot appear as elongated rods when imaged with electron microscopy. De-glycosylation of extensins using hydrogen fluoride eliminated the appearance of these elongated structures, suggesting that glycosylation is important to maintain extensins in an extended rod-like conformation. Extensins from carrot were observed to undergo Tyr-Tyr crosslinking intra-molecularly (forming isodityrosine- Idt) and inter-molecularly to form short oligomers (Stafstrom & Staehelin, 1986a).

This was corroborated in a more recent study, which showed *Arabidopsis* EXT3 molecules undergo crosslinking *in vitro*. Purified AtEXT3 monomers that were incubated with extensin peroxidase polymerized through covalent linkages between individual tyrosine residues and/or Idt motifs. Intermolecular crosslinking occurring through the formation of trimeric (pulcherosine) and di-Idt (four crosslinked tyrosines) linkages, which resulted if the monomers were aligned in parallel (or head-to-head) or staggered, respectively (Cannon et al., 2008). In the same study, a separate approach was used to examine EXT3 crosslinking, where EXT3 monomers in solution were transferred to a graphite surface (without extensin peroxidase) and visualized using atomic force microscopy (AFM). All EXT3 monomers adopted rod-like conformations and polymerized to form dendritic networks through end-on and lateral branching. Interestingly, a synthetic analog composed of repetitive extensin motfis $(SOOOOSOSOOOOYYYK)_{20}$ did not assemble to form dendritic networks, indicating importance of the YVY motif to form pulcherosine in EXT3 network assembly (Cannon et al., 2008).

Extensin crosslinking also influences the cell wall through interactions with pectin. Pectins are a family of secreted carbohydrates that have diverse structures and are described in more detail in section 1.2. However, a key component is homogalacturonic (HG) acid and is found in polygalacturonan chains which can be modified to expose free, negatively- charged carboxyl groups; calcium bridges between carboxyl groups of

neighboring HG chains form crosslinks which increases cell wall rigidity (Carpita & Gibeaut, 1993; MacDougall et al., 1996). Extensins are carry an overall net positive charge due to the abundance of lysine, and extensins extracted from tomato were shown to be ionically bound to negatively- charged pectic carboxyl groups (Smith et al., 1984). Carrot extensin was also shown to interact ionically with homogalacturonan (MacDougall et al., 2001). A synergistic effect was observed between extensin crosslinking and pectin crosslinking, suggesting that extensin oligomers can promote pectin crosslinking through ionic interactions (i.e. extensin pectate) (MacDougall et al., 2001). Furthermore, cotton extensin forms covalent interactions with another pectic component called rhamnogalacturonan-1 (Qi Xiaoyang et al., 1995). Therefore, it is hypothesized that extensin networks function as scaffolds to template the assembly of pectins (and possibly other cell wall materials) secreted in the cell wall through direct interactions (Cannon et al., 2008) (Figure 1D).

1.1.3 Functional studies of EXT and EXT-like mutants

The EXT protein family consists of the classical EXTs and EXT-like proteins including the leucine-rich repeat extensins (LRXs), formins (or formin homology- FHs), and the proline-rich extensin-like receptor kinases (PERKs) [reviewed in (Borassi et al., 2016)]. A few of these members have described functions in regulating cell wall structure and growth, which will be reviewed in this section starting with the classical EXTs.

A mutation in *Arabidopsis* causing defects in root, shoot, and hypocotyl development and seedling germination defects called *rsh* was mapped to a gene encoding an extensin. *RSH* was found to be an essential gene, as *rsh/rsh* homozygous knock out mutant seedlings do not live past ~3 weeks even under the most pampered conditions. Embryonic development was disrupted in *rsh* mutants; ~25% of *rsh* embryos showed mispositioning of the cell plate as early as the first zygotic division, leading to abnormal cell shapes. In *rsh* plants that survived to the seedling stage, cell shape was abnormal throughout the layers of the root. RSH-GFP localized to the cell wall of embryonic and root cells and was also observed at the edges of the cell plate and corresponding junction position in the mother cell wall. This study suggested that RSH

plays an important role regulating cytokinesis to influence cell shape (Hall & Cannon, 2002). A follow-up study identified *RSH* as *EXT3.* The cytokinesis defects were examined more closely and revealed the presence of wall stubs, hanging walls (the one side of the cell plate connected to the mother cell wall), and floating walls (no cell plate connections) in sections of 3-day-old roots, which further supports the role of EXT3 as a contributor of wall formation during cytokinesis (Cannon et al., 2008).

In *Arabidopsis,* loss of EXT18 caused defects in both vegetative and reproductive organs. Abnormal vegetative phenotypes in *ext18* plants included delayed seedling germination frequency, fewer and smaller leaves, shorter primary roots, and more lateral roots, which indicated that EXT18 has an important role in the development in a broad range of tissue types. *ext18* also caused a pollen- specific transmission defect. This was consistent with the observed expression pattern of the *EXT18p:GUS* reporter, which showed activity in the anthers and pollen (and vegetative tissues) but not the female reproductive organs. Compared to WT, *ext18* PTs germinated at a lower frequency and burst at a higher frequency *in vitro*; additionally, about half the *ext18* was dead when dissected from anthers, indicating that pollen development was also compromised, in addition to PT germination and growth. DAPI staining of *ext18* pollen grains showed that meiosis was occurring correctly. Therefore, it was concluded that EXT18 functions to maintain the structural integrity of the cell wall in developing pollen and the PT to promote proper cell growth and plant fertility- in addition to its role in vegetative tissues (Choudhary et al., 2015).

The leucine-rich repeat extensins (LRXs) are a subclass of the extensin family named for their chimeric structure which includes an N-terminal leucine-rich repeat (LRR) domain and a C-terminal EXT domain. The LRR domain is associated with the plasma membrane and may be involved in cell signaling by interacting with other proteins or molecules*,* while the EXT domain functions to anchor the protein in the cell wall (Fabrice et al., 2018). LRXs are also involved in tip growth of root hairs and PTs. In *Arabidopsis lrx1* mutants*,* root hairs are short and swollen with occasional branching and bursting (Baumberger et al., 2001). These defects were exacerbated in *lrx1/2* double homozygous mutants, whose root hairs were mostly either burst or very short, suggesting that. *lrx1/2* cell walls showed abnormal architecture with irregular changes in thickness, suggesting

that LRX1 and LRX2 have partially- overlapping functions in regulating maintain structural integrity to promote proper root hair tip growth (Baumberger et al., 2001). LRXs 8-11 function redundantly to promote PT germination and elongation, and higher-order mutants shown altered cell wall composition, including abnormalities in pectic, xyloglucan, callose, and glycoprotein (AGPs and EXTs) accumulation and patterning (Fabrice et al., 2018; Sede et al., 2018). These LRXs have also been shown to bind Rapid Alkalinization Factor (RALF) 4, which along with RALK19, controls cell wall composition to promote proper PT growth primarily through regulating cell wall integrity and decreasing bursting frequency (Mecchia et al., 2017).

A subset of formins (class I) contain extracellular EXT-like domain that contains Ser(Pro)$_{3-5}$ motifs, a transmembrane domain, and an intracellular formin domain which nucleates actin filament polymerization (Ingouff et al., 2005). Similar to LRXs, the extracellular EXT-like domain functions to anchor formins in the cell wall and immobilize them in the plasma membrane (Martinière et al., 2011). Formins promote actin polymerization by nucleating actin (Cheung et al., 2010) and increasing filament elongation rate (Lan et al., 2018), and formins are required for proper tip growth of both PTs (FH1 and FH3) and root hairs (FH1 and FH8) in *Arabidopsis* [reviewed in (Borassi et al., 2016)]. FH5 was also shown to be important for PT growth as well, and loss of FH3 and/or FH5 decreases overall actin filamentation levels and organization in the PT, which is associated with decreased vesicular transport in *fh3/fh5* mutants (Lan et al., 2018). Furthermore, while the EXT-like domain functions to anchor the FHs, as well as the LRXs, **it has not yet been shown if proline hydroxylation and/or subsequent *O*-glycosylation occurs on these proteins, and whether this is an important factor in cell wall anchoring.**

The proline-rich extesin-like receptor kinases (PERKs) also contain an extracellular domain with Ser(Pro)$_{3-5}$ motifs, in addition to a transmembrane helix and intracellular receptor-like kinase domain (Nakhamchik et al., 2004). There are 15 PERKs in *Arabidopsis* and microarray analysis shows that root and pollen are two tissue types with the highest PERK expression, and PERK8 and 13 are specifically expressed in root hairs while PERK6, 7, 11, and 12 are expressed specifically in pollen. Less is known about the function of the PERK family members, but several PERKs are important for cell

growth in roots and root hairs in *Arabidopsis* [reviewed in (Borassi et al., 2016)]. Importantly, the role of the PERK kinase domain is unknown because their endogenous ligands have not been identified.

1.1.4 Functional studies of O-arabinosyltransferase mutants

Prolines in Ser$(Pro)_{3-5}$ motifs are hydroxylated by proline 4-hydroxylases (P4Hs) to form hydroxyproline (Hyp), which is a substrate for additional modifications (described below) (Tiainen et al., 2005). In *Arabidopsis,* PRH4, 5, and 13 are required for normal root hair growth, as these single knockout *p4h* mutants had decreased root hair lengths; similar results were also observed using pharmacological P4H inhibition and RNA-interference knockdown lines for these genes (Velasquez et al., 2011). Hyp content was decreased in each mutant as well. *ext6, 7, 10, 11* and *12* knockout lines also showed a similar root hair growth defect, indicating that these specific extensins, and *O*-glycosylation in general, are essential for normal root hair growth. The P4Hs localized to the ER and golgi stacks, indicating that proline hydroxylation (and subsequent *O*-glycosylation) occurs during the secretory pathway (Velasquez et al., 2015).

Extensins undergo *O*-arabinosylation at Hyp residues harbored within Ser$(Hyp)_{3-5}$ motifs. Hyp-Ara can then further modified to form chains with up to 5 arabinoses (Akiyama et al. 2014). The first arabinose is added to Hyp through a β-1,4 linkage by a family of enzymes named Hyp *O*-arabinosyltransferases (HPATs) (Ogawa-Ohnishi et al., 2013); the Reduced Residual Arabinose (RRA) enzyme family extends Hyp-Ara to Hyp-Ara_2 through a β-1,2 linkage (Egelund et al., 2007; Velasquez et al., 2011); Hyp-Ara_2 is extended to Hyp-Ara_3 through a β-1,2 linkage by the Xylo-EndoGlucanase 113 (XEG113) enzyme family (Gille et al., 2009); and Hyp-Ara_3 is extended to Hyp-Ara_4 through a β-1,2 linkage by the Extensin Arabinose Deficient (ExAD) family, which were the most recently identified (Møller et al., 2017) (Figure 1C). Sometimes a fifth arabinose is added through a α-1,3 linkage, but the enzyme(s) responsible for adding this have not been identified.

Three HPATs were identified in *Arabidopsis* (HPAT1, 2, and 3). Each gene was broadly expressed across multiple tissue types, and HPAT1-GFP co-localized with the *cis*-golgi marker mRFP-SYP31. *hpat* single and double mutants showed decreased Hyp-

Ara of EXT3 and an increase in free Hyp residues. *hpat* single mutants showed no abnormal phenotype, but *hpat1 hpat2* (*hpat1/2)* double mutants had vegetative phenotypes including elongated hypocotyls with thinner cortical cell walls, suggesting that HPATs 1 and 2 function redundantly during plant growth. Average PT lengths from *HPAT1 +/- HPAT3 +/-* double heterozygotes were shorter than *HPAT1/3* WT, suggesting that in addition to vegetative development, HPAT-mediated Hyp *O*-arabinosylation of extensins is also important for reproductive growth (Ogawa-Ohnishi et al., 2013). This was confirmed, as further examination identified a strong, pollen-specific transmission defect of the *hpat1/3* double mutant due to poor PT elongation, with no defects observed in *hpat1/3* pollen grain development or viability (MacAlister et al., 2016).

Hyp *O*-arabinosylaton is not only important for PT tip growth. In the moss *Physcomitrella patens*, protonemal filaments growth through a tip-growth mechanism similar to PTs and root hairs. Interestingly, *hpata* single and *hpata/b* double mutants had increased protonemal tip growth, which is an opposite effect than observed in *Arabidopsis hpat1/3* PTs (MacAlister et al., 2016). One possible explanation is that moss protonema is that moss lack the classical extensins (but possess LRXs), and because the machinery involved in HPAT-mediated cell growth has evolved since mosses and angiosperms diverged, so have the mechanisms of tip growth. In *Arabidopsis,* each of the *rra1, rra2, rra3* and *xeg113* knockout mutants had shorter root hairs (Velasquez et al., 2011). *xeg113* mutants also had elongated hypotcotyls, similar to what was reported for the *hpat1/2* mutant (Gille et al., 2009; Ogawa-Ohnishi et al., 2013). *exad* knockout lines also had shorter root hairs (Møller et al., 2017).

It is worth noting that Hyp *O*-arabinosylation has another role in regulating cell differentiation in the shoot apical meristem. In tomato, loss of one HPAT caused a mutant phenotype with a fascinated inflorescence (*fin*) that produced a higher number of floral organs per meristem which resulted in larger fruits (Xu et al., 2015). The CLAVATA signaling pathway controls meristem size (Clark et al., 1995), and CLV/CLE peptides are normally Hyp *O*-arabinosylated (Schoof et al., 2000; Shinohara & Matsubayashi, 2013). A CLV peptide in *Arabidopsis* called CLE2 was under Hyp *O*-arabinsoylated specifically in the *hpat3* knockout mutant, showing that this modification was HPAT-dependent (Ogawa-Ohnishi et al., 2013). Interestingly, none of the *hpat* mutants, including the

hpat1/2/3 triple homozygous mutant, had a fascinated inflorescence (MacAlister et al., 2016). It is suggested that the HPATs are the only enzymes with Hyp *O*-arabinosylation activity, but it cannot be completely ruled out that other enzymes may be modifying CLE2, CLV3, or other CLV peptides. Another possible explanation for lack of inflorescence fasciation in *Arabidopsis is* that Hyp-Ara is not required for CLV peptide-mediated activation of CLV1 (MacAlister et al., 2016). No PT or phenotypes were reported for *fin,* but there are multiple FINS in tomato which may have specialized roles in tip-growing cells.

1.1.5 Functional model of how EXTs influence cell wall structural properties

Taken together, these findings indicate that extensins and undergo proline hydroxylation and subsequent Hyp *O*-arabinosylation at Ser$(Pro)_{3-5}$ motifs during their transport through the ER and golgi by a cascade of enzymes localized in these organelles, prior to secretion into the cell wall. Hyp *O*-arabinosylation appears to be important for extensin crosslinking, and extensins associate ionically with pectins, which also have a major role in cell wall structural and mechanical properties. Extensins seem to strengthen the cell wall through crosslinking to form EXT-EXT networks, which also affects pectic crosslinking in many tissues. Therefore, crosslinked EXT networks are thought to function as a scaffold to template the proper assembly and organization of secreted pectins. Extensin glycosylation is particularly important for tip-growing cells including PTs and root hairs. Loss of glycosylation reportedly increased anisotropic cell growth in hypocotyls by decreasing cell wall thickness (Ogawa-Ohnishi et al., 2013), but no other abnormal vegetative phenotypes were observed for *hpat1/3* mutants (MacAlister et al., 2016). Therefore, extensin glycosylation is largely expendable for most cell types, except PTs and root hairs, which indicates that tip growth is uniquely sensitive to extensin glycosylation. The role of extensin glycosylation (and the enzymes involved) in tip growth is likely to maintain the specialized cell wall structure to promote proper growth, **but how this occurs is still not entirely clear.**

1.2 Pectins

1.2.1 Overview

Pectins make up about 35% of the primary cell wall in dicots and are highly structurally diverse (Fry, 1988). Pectic backbones and side chains are composed of multiple polymers including homogalacturonan (HG), rhamnogalacturonan I (RG-I), rhamnogalacturonan II (RG-II), xylogalacturonan, and apiogalacturonan (Mohnen, 2008; Wolf et al., 2009). While the exact cell wall composition varies between species and tissue types, HG is the most abundant, constituting ~65% of pectin polymers (Mohnen, 2008). HG is primarily composed of *alpha*-1,4-linked-d-galacturonic acid (GalA) and is synthesized in the Golgi by a family of enzymes known as HG galacturonasyl-transferases (GAUTs) (Ridley et al., 2001; Sterling et al., 2001, 2006). Most GalA (~80%) residues in HG become highly methylesterified (me-HGs) by enzymes in the Golgi called and are secreted into the apoplast in this form (Krupková et al., 2007; Mohnen, 2008; Mouille et al., 2007; O'Neill et al., 1990). The degree of methylesterification (DM) of HG is an important factor in many plant processes including the development of vegetative tissues, reproduction, and interactions with the environment [as reviewed in (Levesque-Tremblay et al., 2015). In addition to methylation, HGs can also be O-acetylated, although how HG acetylation influences cell wall mechanical properties is not as well-understood as DM (de Souza et al., 2014). Additionally, boron-mediated crosslinking of RG-II molecules has been shown to be important for development of reproductive and vegetative tissues (Chormova et al., 2014; Iwai et al., 2002, 2006; O'Neill et al., 2004).

1.2.2 HG DM is regulated by PMEs and PMEIs

After secretion into the cell wall, HG DM is selectively modified by pectin methylesterases (PMEs). PMEs catalyze the de-methylesterification of me-HGs to form dme-HG, exposing negatively- charged carboxyl groups. Neighboring dme-HG molecules crosslink with each other via calcium bridges (referred to as the "egg-box" model) which promotes gelation and increases the overall rigidity of the cell wall (Figure 1E) (Bosch et

al., 2005; Braccini & Pérez, 2001; Catoire et al., 1998; Grant et al., 1973; Limberg et al., 2000; Wormit & Usadel, 2018).

PMEs have been found in many plants, bacteria, fungi and some animals (Kent et al., 2016). PMEs and PME inhibitors (PMEIs) are large gene families; for example, there are 66 PME genes in *Arabidopsis* and 76 genes encoding PMEIs in the *Arabidopsis* genome (Hocq et al., 2017; S. Wang et al., 2019). The presence of these large gene families suggest (i) there is a high likelihood of functional redundancy among co-expressed paralogs, (ii) that PMEs may have differences in pectic substrate preference and/or optimal conditions for enzyme activity such as apoplastic pH, and (iii) that PMEIs have differences in PME substrate preference and/or optimal conditions of binding/activity.

Plant PMEs are classified based on the presence or absence of up to 1-3 N-terminal “PRO” regions. The sequences of PRO regions contain similarities to sequences of PME inhibitor (PMEI) domains and are often referred to as such (Camardella et al., 2000; Jolie et al., 2010; Markovič & Janeček, 2004). Confusingly, PMEs that do not contain PRO regions are known as group 1/type II, and PMEs that do contain PRO regions are known as group 2/type I (Camardella et al., 2000; Micheli, 2001; Pelloux et al., 2007; Tian et al., 2006). Phylogenetic analyses showed that the PRO region is not present on PMEs of bacteria, fungi or *Physchomitrella patens*, although PRO-containing group 1/type II PMEs are abundant in higher plants including *Arabidopsis* and rice*,* suggesting that the PRO domain-containing group 2 PMEs evolved after the divergence of mosses and vascular plants (Lang et al., 2005; Markovič & Janeček, 2004; Pelloux et al., 2007)*.*

However, PMEs extracted from the cell wall did not contain PRO regions (Bordenave & Goldberg, 1993; Sénéchal et al., 2014). This early observation led to numerous hypotheses about the functional role of the PRO region, including that PRO regions may inhibit the activity of their respective, covalently- attached PMEs prior to secretion, or that they regulate the trafficking and/or folding of the mature protein (Micheli, 2001; Shinde et al., 1995). Indeed, PRO regions have important roles in PME trafficking. Deletion of the PRO region of NtPPME1-GFP (or deletion the PME region itself) inhibited transport from the Golgi to secretory vesicles, thereby preventing secretion of the protein

into the cell wall (Bosch et al., 2005). Additionally, in *Arabidopsis*, the N-terminal PRO region was shown to mediate retention of unprocessed PME proteins in the Golgi, and cleavage of the PRO regions was required for trafficking and secretion into the cell wall (Wolf et al., 2009). Therefore, PRO regions provide cells with a mechanism to post-translationally regulate PME activity in the cell wall by controlling the trafficking and secretion of PMEs.

The first PMEI protein was identified in kiwi, and PMEI genes are present in *Physcomitrella patens,* suggesting that they evolved along with the presence of pectins in cell walls; however, the origin of PMEs is still up for debate (Balestrieri et al., 1990; M. Wang et al., 2013). Despite sequence similarities, PMEIs regulate PME activity through different mechanisms than described above for the PRO regions. Analysis of the crystallized kiwi PME-PMEI complex indicated that PME inhibition occurs through direct binding at a 1:1 stoichiometric ratio which hides the PME catalytic site (Ciardiello et al., 2008; Di Matteo et al., 2005). This was corroborated in another study through *in silico* modeling and biochemical experimentation, which showed AtPMEI17 inhibits AtPME3 activity optimally in a 1:1 complex, and that PME-PMEI complex formation is pH-dependent (Sénéchal et al., 2015). Furthermore, in *Arabidopsis,* both PMEI9 and PMEI4 could inhibit recombinant PME3, but did so with different pH dependencies. PMEI9 was found to have a higher affinity (lower K_D) for PME3 than PMEI4 (Hocq et al., 2017), suggesting that PMEIs also have preferred PME binding partners.

1.2.3 Functional studies of PMEs in PTs

There is functional information available for many plant PMEs, including some that are specifically expressed in pollen. One of the first PMEs characterized in plants is VANGUARD1 (VGD1), which is a PME that is expressed specifically in *Arabidopsis* pollen (Jiang et al., 2005). *vgd1* knockout mutant PTs germinated at a normal frequency but elongated poorly *in vitro* and *in vivo. In vitro,* 93.8% of germinated *vgd1* PTs burst compared to 3.7% for WT over the same time period, indicating that *vgd1* PTs were structurally unstable. *In vivo, vgd1* PTs were not defective in ovular targeting/guidance, and *vgd1* PTs were able to fertilize the ovules they reached in the pistil. However, when

VGD1/vgd1 plants were outcrossed as males, there was a strong transmission defect observed for *vgd1* pollen compared to wild type. PME activity from *vgd1* pollen grain extracts was significantly decreased compared to wild type (Jiang et al., 2005). VGD1 was later designated as PME5.

In *Arabidopsis*, PPME1 is another PME with pollen- specific expression, and is also an important regulator of PT tip growth. *ppme1* knockout mutant pollen grains had a comparable level of decreased PME activity, and pollen grains looked phenotypically normal; however, *ppme1* PTs had several defects observed during *in vitro* growth including decreased growth rate (which resulted in shorter lengths), bulged tips and branching (defined as the appearance of a secondary tube forming from the primary tube). However, there was no observed transmission defect for *ppme1* PTs, indicating that the overall function of *ppme1* PTs was not compromised *in vivo* (Tian et al., 2006). Although the phenotypes caused by *ppme1* contrast significantly to *vgd1,* both studies are consistent with a role of PMEs in promoting proper PT growth through regulating the structural integrity of the PT cell wall.

PME48 is another *Arabidopsis* PME that is specifically expressed in pollen. *pme48* knockdown mutants had PT growth including increased bursting and branching rates, as well as increased width and growth rates and decreased germination frequency (Leroux et al., 2015). Immunolabeling showed that highly methylesterified HG epitopes (which are bound and the LM20 antibody) were present along the subapical regions of the PT, which is different than the tip-only pattern observed in WT. Biochemical analyses showed decreased PME activity in *pme48* pollen grains, and Fourier transform- infrared spectroscopy estimated that HG DM was higher in *pme48* pollen grains compared to wild type, which is consistent with the PT LM20 immunolabeling. *pme48* PT germination and growth defects were partially rescued when grown with higher levels of calcium in the growth media, which mediates crosslinking between demethylesterified HGs (Leroux et al., 2015).The findings from this study suggest that PME48-mediated HG demethyesterification and subsequent pectic crosslinking via calcium bridges formation- which increases cell wall rigidity- is required for normal PT tip growth.

Lily and tobacco PTs grown *in vitro* and treated with exogenous PME showed decreased germination frequencies and growth rates in a dose-dependent manner. Closer examination of PME-treated PTs showed thickening of the apical cell wall and loss of the tip-focused cytoplasmic calcium gradient. Tobacco (*Nicotiana tabacum*- Nt) PTs transiently transformed with the PME domain of a native pollen-expressed PME, NtPPME1, decreased PT growth and increased JIM5 labeling (an antibody that binds dm-HGs) throughout the PT cell wall (including the tip where it is usually absent), and decreased JIM7 labeling (an antibody that binds me-HGs) (Bosch et al., 2005). Interestingly, knock down of NtPPME1 also decreased PT growth, indicating that PT growth is sensitive to changes in PME activity levels in either direction (Bosch & Hepler, 2006).

1.2.4 PME inhibition and PT growth

In maize, PMEI1 is strongly expressed in anthers, and PMEI1-GFP localizes to the PT tip, which maintains extensibility by preventing me-HG conversion to dme-HG and subsequent crosslinking. *In vitro* grown PTs treated with exogenous PMEI1 showed increased bursting frequency in a dose-dependent manner, and bursting was localized to the subapical region and specifically did not occur at the tip (Woriedh et al., 2013). This suggests that PME inhibition by PMEI1 in maize PTs disrupts the cell wall structural integrity at the shank where HG DM is typically low, based on immunolabeling experiments mentioned above (Leroux et al., 2015). Furthermore, this is consistent with findings in the above section that suggest that PME activity rigidifies the subapical cell wall to promote proper growth.

AtPMEI1 and AtPMEI2 were shown to bind and inhibit AtPME1. Transient expression of AtPME1 decreased tobacco PT growth, while transient expression of AtPMEI2 had the opposite effect and increased PT growth. Transient expression of PME1-YFP showed signal along the cell wall in both the apical tip and subapical shank regions, while PMEI2-YFP showed a tip-only signal pattern, consistent with (Woriedh et al., 2013). Further examination showed that AtPMEI2-YFP, but not AtPME1-YFP, is internalized through endocytosis. This finding suggests that while PMEs and PMEIs may

be secreted normally at the tip, endocytosis of PMEIs along the subapical walls increases PME activity at these regions, which decreases HG DM and promotes crosslinking; HG DM is maintained at a high level at the tip, promoting extensibility (Röckel et al., 2008).

In a more recent study, rice PTs were grown *in vitro* and treated with commercial PME or a PME-inhibiting catechin extract called Polyphenon 60. Both treatments decreased PT germination frequency and growth, and increased bursting frequency. In PTs just beginning to germinate, PME treatment caused increased signal accumulation from LM19 (an antibody that binds HG with low levels of methylesterification) immunolabeling, with no observed effect on LM20 staining intensity or pattern; conversely, LM20 staining was increased in response to Polyphenol 60 treatment, which did not change LM19 staining- as expected. However, in longer PTs, PME-treatment caused an increase in LM19 staining throughout the tip and the shank, as well as LM20 staining at the tip. Polyphenol 60 caused similar effects as PME treatment, and also increased LM20 signal throughout the shank (which was expected) (Kim et al., 2020). These findings indicated that PME and Polyphenol 60 treatment disrupted PT growth by affecting the deposition and/or the modification of pectins in the cell wall, and the fact that each treatment caused similar effects on both PT growth and pectin immunolabeling highlight the importance of a carefully balance of PME activity for tip growing cells.

1.3 The exocyst complex

1.3.1 Overview of exocyst-mediated secretion

In eukaryotic cells, the transfer of cargos between different organelles occurs through vesicular trafficking, in which materials are transported in lipid compartments (vesicles), which pinch or bud-off from a membranous structure (donor compartment) and are transported to another structure (acceptor compartment). After arriving at their destination, vesicles must successfully tether to and fuse with the target membrane in order to expel their cargo. The secretory pathway describes the trafficking of cargo to the plasma membrane for external release, and this is how many plant cell wall components- including pectins and glycoproteins- are transported to the cell wall. Exocytosis is the final

step in the secretory pathway in which vesicles tether to and fuse with the plasma membrane. Tethering of Golgi- and endosome-derived vesicles to the plasma membrane is mediated by the exocyst complex, which is a multisubunit tethering complex (MTC) found in all eukaryotes and is composed of eight highly-conserved proteins SEC3, 5, 6, 8, 10, 15, Exo70, and Exo84. Seven other MTCs exist and facilitate vesicular tethering between different donor and acceptor compartments for both the secretory pathway (i.e. ER to Golgi or vice-versa) and vacuolar protein sorting pathway. MTC-mediated tethering acts upstream of SNARE-mediated vesicular fusion (Cai et al., 2007). Partial crystal structures have been solved for some of the exocyst components from different species, including Exo70 from yeast and mouse, yeast Sec3, Exo84 and Sec6, and Sec15 from *Drosophila* (Baek et al., 2010; Dong et al., 2005; Hamburger et al., 2006; Moore et al., 2008; Sivaram et al., 2006; Wu et al., 2005). While their primary structures are not very similar, the individual exocyst subunits are all largely alpha-helical, with helices packed in bundles interspersed by loops (He & Guo, 2009).

Most of the exoyst subunits were first identified through a yeast genetic screen as temperature-sensitive secretion (*sec*) mutants that failed to secrete enzymes, leading to internal protein accumulation in structures including vesicles, golgi and ER (Novick et al., 1980); Exo70 and Exo84 were later identified in separate studies (Kee et al., 1997; TerBush & Novick, 1995). In budding yeast, a small region of the parent cell undergoes polarized growth to form a bud, which eventually grows into a new cell. Sec8 was one of the first exocyst subunits examined, and it was observed to localize to small bud tips, where exocytosis (and cell growth) is occurring at high rate relative to other regions of the cell (TerBush & Novick, 1995). Bipolar budding patterns were disrupted in diploid *sec3, sec4,* and *sec9* single homozygous mutant yeast cells, which exhibited new bud initiation at random regions (Finger & Novick, 1997). Sec3-GFP localized to sites of polarized secretion *in vivo* after latrunculin treatment, as well as in *sec* mutant backgrounds in which ER- golgi transport was disrupted, indicating that Sec3 localization is independent of actin and a functional secretory pathway (Finger et al., 1998). These findings demonstrated that the exocyst complex localizes to areas of polarized secretion in yeast to regulate cell growth.

1.3.2 Sec3 and Exo70 promote polarized localization of the exocyst complex through interactions with proteins and phospholipids.

The polarized localization of Sec3 is mediated by a direct interaction via its N-terminus with Rho1, which is a GTPase binding protein in the Rho family that localizes to regions of active growth (Yamochi et al., 1994). However, polarized localization of Sec3 (and Exo70) was decreased but not abolished in *rho1* mutants. Also, loss of the N-terminus ($Sec3^{deltaN}$) results in mis-localization of much of the $Sec3^{deltaN}$-GFP signal, but some polarized signal was still observed, suggesting Sec3 can also be trafficked in a Rho1-independent manner. Cells expressing only $Sec3^{deltaN}$ were viable and exhibited normal secretion, growth, and polarized localization of Exo70 and Sec5, indicating that Sec3/Rho1 interaction is not entirely required for exocyst assembly and function (Guo et al., 2001). An additional important factor for polarized localization of the yeast exocyst is Ccd42, which is another GTPase binding protein in the Rho family involved in regulating cell polarization and membrane trafficking to control cellular growth. Cdc42 co-localizes with Sec3-GFP at sites of new bud formation, and *in vitro* binding assays showed that Cdc42 competes with Rho1 for binding (X. Zhang et al., 2001). Analysis of crystal structures shows that the N-terminus of yeast Sec3 folds into a pleckstrin-homology (PH) domain, which is known to bind phophoinositides including phophsotidylinositol 4,5 bisphosphate [PI(4,5)P2] (Baek et al., 2010; Lemmon, 2008).

To learn more about how the exocyst assembles at target sites, fluorescence recovery after photobleaching (FRAP) was performed to measure the kinetics of individual exocyst subunits fused to GFP. The mobility of Sec3-GFP and a fraction of Exo70-GFP were insensitive to Latrunculin treatment and displayed different recovery kinetics than the other subunits. Also, electron microscopy showed that every exocyst subunit except Sec3 associated were with secretory vesicles. This suggests that every exocyst subunit except Sec3 and a portion of Exo70 are transported via the secretory pathway to sites of polarized secretion, marked by Sec3 and Exo70, to assemble the full complex (Boyd et al., 2004). Therefore, it was hypothesized that Sec3 and Exo70 have an important role in recruiting the exocyst to the plasma membrane.

Additional studies showed that polarized localization of Sec3^{deltaN}-GFP was disrupted after Latrunculin treatment, while full-length Sec3-GFP still showed signal at the buds consistent with findings from (Finger et al., 1998). FRAP experiments showed that Sec3-GFP signal was able to recover after photobleaching in the presence of Latrunculin, while the Sec3^{deltaN}-GFP signal was unable to recover (X. Zhang et al., 2008). In the same study, Sec3 was shown to preferentially bind PI(4,5)P2 and phosphatidyl serine (PS) *in vitro* via a cluster of basic residues at positions 134-137 in the N-terminus, which is adjacent to the amino acids at positions 140-155 that important for binding Cdc42. In the presence of latrunculin B, polarized localization of Sec3 was disrupted when key residues in either N-terminal binding region were mutated, and this localization was abolished when both mutations were present. This data suggests that both interactions synergistically promote targeting to the bud tip in an actin-independent manner. Disrupting either of these interactions in the *exo70* background lead to synthetic lethality. Taken together, this data indicates that the polarized localization of Sec3, which is mediated by N-terminal binding with PI(4,5)P2 and Cdc42, is important for its cellular function. Furthermore, the localization of exocyst subunits was depolarized in *sec3 exo70* double mutants, and invertase secretion was significantly knocked down in these cells which also appeared larger and rounder (X. Zhang et al., 2008), which is consistent with Exo70 and Sec3 having important, specialized roles in promoting polarized secretion and growth.

In *Arabidopsis,* GFP-SEC3a displayed dynamic and polarized localization within the PT tip region. An enrichment of polarized signal near and at the tip apex was present during active PT growth, and appeared to localize in anticipation of growth trajectory. GFP-SEC8 appeared to mimic the localization of GFP-SEC3a. GFP-SEC3a also co-localized with the plasma membrane region directly underneath the region of the cell wall where newly- secreted pectins (labeled by propidium iodide) were deposited in growing PTs, sugging that the exocyst complex mediates pectin secretion (and possibly for other cell wall materials). The N-terminal PH domain was required for plasma membrane localization of AtSEC3a in tobacco PTs, and the YFP-SEC3a$^{N\text{-}term}$ fusion protein co-localized with the PI(4,5)P2 marker RFP-PH^{PLCd1}, suggesting that SEC3a localization at plasma membrane is mediated by an interaction between its N-terminal PH domain and

PI(4,5)P2. However, loss of the PH domain does not affect GFP-SEC3a^{deltaN} localization in *Arabidopsis* PTs, indicating that direct binding to PI(4,5)P2 is not required for SEC3a localization to the plasma membrane (Bloch et al., 2016).

The positively charged C-terminus of Exo70 binds PI(4,5)P2s *in vitro* and the plasma membrane *in vivo* (He et al., 2007). Molecular dynamics (MD) simulations showed that initial contact between the plasma membrane and yeast Exo70p occurs via a cluster of basic amino acids clustered near the C-terminus including K601, R604, and K605- which were previously shown to be important for binding PI(4,5)P2s (He et al., 2007)- and then further stabilized by PI(4,5)P2-interacting residues K168, K212, K228, and K489. MD simulations also showed that the interaction between Exo70p and the plasma membrane was PI(4,5)P2-dependent, and Exo70p binding to the plasma membrane resulted in increased PI(4,5)P2 clustering in the lipid bilayer. These residues and the overall membrane-interacting surface were highly conserved across the 150 eukaryotic Exo70s analyzed in this study (Pleskot et al., 2015), suggesting that PI(4,5)P2 binding is an important function of Exo70.

Knockdown of the yeast PI(4,5)P2-synthesizing enzyme Mss4 (a PI4P 5-kinase) abolished the normal pattern of polarized localization to the bud tip for Exo70 and other exocyst subunits, and Exo70 and other exocyst subunits -which are normally associated with the plasma membrane- were almost entirely absent from membrane fractions extracted from *mss4* cells. Normal association of exocyst subunits with the bud tip plasma membrane observed in the *sec3^{deltaN}* was absent in the *sec3^{deltaN} exo70* double mutants, which also had defects in secretion and loss of cell polarity. Exo70 is also known to bind Rho3, which is another Rho GTPase implicated in polarized exocytosis, but specifically disrupting this interaction did not cause an abnormal phenotype in the wild type nor *sec3^{deltaN}* backgrounds (He et al., 2007). Taken together, this data suggests that in addition to Sec3, the C-terminus of Exo70 has an important role in targeting the exocyst complex to the plasma membrane by binding PI(4,5)P2s to promote polarized exocytosis (Figure 1F).

1.3.3 Functional studies of exocyst components and PT growth

In *Arabidopsis, sec8* knockout mutant PTs fails to germinate *in vivo,* despite pollen grains appearing normal during gametogenesis and responding to signals to germinate. Other partially- functioning *sec8* mutant alleles showed decreased pollen transmission and PT growth (Cole et al., 2005). Loss of EXO70A1 caused multiple developmental defects including shorter hypocotyls and smaller floral organs, primarily through a defect in cell division leading to lower cell numbers, and reduced root hair tip growth (Synek et al., 2006). Decreased hypocotyl elongation was exacerbated in *exo70a1* plants when combined with partially- functioning *sec8* alleles or a *sec5a* null mutant allele- none of which caused vegetative defects on their own. Loss of function mutations in *SEC6*, and *SEC15A* significantly decreased transmission through the pollen but not the female. Pollen carrying *sec5a* or *sec5b* mutant alleles transmitted normally, but double mutant *sec5a sec5b* (*sec5a/*b) did not transmit at all through the male, indicating that SEC5A and SEC5B function redundantly to promote pollen fertility (Hála et al., 2008). The s*ec5a/b, sec6,* and *sec15a* mutations each caused a decrease in PT germination frequency and increased frequency of PTs with an abnormal appearance that were shorter, thicker, with irregularly shaped. EXO70A1 and SEC6 co-localized with SEC8 at the tips of growing PTs, which is consistent with the expected localization of the exocyst complex. Pair-wise interactions were tested using yeast two-hybrid and provide a helpful basis to begin dissecting the important protein-protein interactions required for plant exocyst complex assembly (Hála et al., 2008). Furthermore, loss of *SEC3a* (one of two SEC3 paralogs in *Arabidopsis*) specifically decreased pollen transmission similar to *sec5*, *6*, *8*, and *15a*, and *sec3a* PT germination and growth were severely compromised *in vitro* and *in vivo* (Bloch et al., 2016).

There are 23 EXO70 genes in *Arabidopsis*, in contrast to the other exocyst subunits which have 1-3 members for each gene family. They are differentially expressed throughout various tissue types and often overlap each other, but none are constitutively expressed (S. Li et al., 2010). In addition to EXO70A1 (mentioned above), other EXO70s have been reported to be important for regulating polarized secretion and growth including a subset of EXO70 isoforms which are expressed in pollen (S. Li et al., 2010; Synek et al., 2017). Loss of EXO70C2 caused a significant pollen-specific transmission defect which was exacerbated when EXO70C1 was also knocked out, suggesting that

these two isoforms function redundantly in pollen (Synek et al., 2017). PT germination was not decreased, but *exo70c2* PTs grew shorter than wild type and had abnormal morphologies caused by increased branching and sharp bending. Increased growth rates (prior to bursting), increased bursting rates, and higher amounts of accumulated cytoplasmic pectin suggested that defective growth in *exo70c2* PTs is due to compromised secretion of materials to and structural integrity of the cell wall. However, EXO70C2-GFP localized to the cytoplasm and not at the apical plasma membrane like GFP-SEC8 or SEC10-GFP, suggesting that although EXO70C2 has an important role, it may not be the canonical EXO70 isoform functioning in Arabidopsis PTs (Synek et al., 2017). Further studies indicate that this role likely belong to EXO70A2. PT germination is drastically decreased in *exo70A2* loss of function mutants, and PT growth is decreased. CRISPR-generated *exo70a2* knockdown lines produced PTs that were wider than WT, while *exo70a2-3* knockout mutant PTs appeared morphologically normal (Beuder et al., 2020; Marković et al., 2020). In both studies, EXO70A2 fluorescent fusion reporters localized to the apical plasma membrane of the PTs. Taken together, these studies indicate that EXO70A2 is likely the canonical EXO70 isoform in *Arabidopsis* pollen, and other EXO70s (C2 and C1) play important but different roles- given the differences in mutant phenotypes. How the roles of different EXO70 isoforms are distinguished remains an important question moving forward.

1.4 Phosphoinositide/ Phospholipase C signaling

1.4.1 Overview of plant PLCs.

Phospholipase Cs are enzymes that catalyze phospholipid hydrolysis to generate secondary messenger molecules, and are divided into two main categories based on their preferred substrates: phosphatidylinositol (PI)- specific phospholipase Cs (PLCs), and non-specific PLCs (NPCs). This chapter will focus on the PI- specific PLCs as they pertain to plants.

PI- specific PLCs (henceforth referred to as PLCs) are found in eukaryotes and prokaryotes (Pokotylo et al., 2014). Much of what we know about PLC activity comes from

studies in animal systems, where PLC preferentially binds and cleaves PI(4,5)P2 in a calcium-dependent manner to generate inositol 1,4,5 triphosphate (IP3) and diacylglycerol (DAG)- each of which have regulatory roles in many cellular processes. IP3 is freed from the plasma membrane and can bind receptors at the endoplasmic reticulum (ER) causing a release of ER-stored calcium and increase in cytoplasmic calcium concentration, which is an input to many different regulatory pathways. DAG remains localized to the plasma membrane, but can activate protein kinase Cs, which phosphorylate downstream effectors to regulate many cellular processes [reviewed recently in (Bill & Vines, 2020)].

Eukaryotic PLCs are classified into six subfamilies based on their structures: β, γ, δ, ε, η, and ζ (ref). Plant PLCs are of the ζ type, which resemble mammalian PLC δ isoforms without the pleckstring homology (PH) domain. Plant PLC/ζ structures include a variable EF hand domain at the N-terminus, followed by more conserved X and Y catalytic domains and a C-terminal C2 lipid binding domain (Teun Munnik & Testerink, 2009). The EF hand and C2 domains have several regions which bind calcium, which is required for both lipid binding and PLC activity (Otterhag et al., 2001; Rebecchi & Pentyala, 2000).

1.4.2 PLCs regulate stress response in Arabidopsis

Functional studies of plant PLCs have identified roles of these enzymes for an array of processes including stress response, development and growth. In *Arabidopsis, plc2* knockout mutants showed decreased seedling shoot and root growth under normal conditions, and were more sensitive to ER stress (Kanehara et al., 2015). Another *plc2* null allele caused infertility male and female gametophytic developmental defects, and these phenotypes were associated with increased auxin accumulation in the anthers and ovules during male and female gametogenesis (L. Li et al., 2015). A third study showed that *PLC2* is required for embryo development, as well as male and female gametophytic development (Di Fino et al., 2017). In light of reports by Li et al., (2015) and DiFino et al., (2017), it is interesting that Kanehara et al., (2015) were somehow able to obtain homozygous *plc2* knockout mutants with ease.

plc3 knockdown mutants showed decreased primary root elongation, lateral root number and density, as well as delayed seed germination rates. Loss of *PLC3* also decreased sensitivity to abscisic acid (ABA), which inhibited seed germination and increased stomatal closure significantly more in WT versus *plc3. PLC3*-overexpressing plants exhibited increased drought tolerance and stomatal closure under normal conditions, as well as in response to ABA treatment (Q. Zhang et al., 2018).

Decreased seedling growth in a common effect of salt stress (NaCl and $NaNO_3$), but this response was diminished in *plc4* knockout lines. *PLC4* overexpression caused hypersensitivity to salt stress, but this was rescued in lines overexpressing $PLC4^{MUT}$ isoforms which had reduced PI(4,5)P2- hydrolyzing activity *in vitro*. Furthermore, increased cytoplasmic calcium levels caused by salt stress were enhanced in *PLC4*-overexpressing lines, and calcium chelation by EGTA treatment partially rescued the hypersensitive/growth response of *PLC4*-overexpressing seedlings. Taken together, this data suggests that PLC4 activity regulates seedling response to salt stress by controlling cytoplasmic calcium levels (Xia et al., 2017).

Loss of *PLC5* decreased primary root length, lateral root number and density, while *PLC5* overexpression decreased root hair length and improved drought tolerance through increased stomatal closure, similar to *PLC3* overexpression (Q. Zhang et al., 2018). Loss of *PLC7* did not affect root growth, but *plc5/7* double homozygous mutant plants had altered leaf architecture, as well as an apparent defect in cellulose-ray formation in the seed mucilage. *PLC7* overexpression also increased drought tolerance similar to *PLC3*- and *5*-overexpression, but stomatal closure with and without ABA treatment in *PLC7*-overexpressing plants resembled WT (van Wijk et al., 2018). Loss of *PLC9* decreased thermotolerance in comparison to WT, while *PLC9* overexpression improved it (Zheng et al., 2012). In summary, multiple members of the PLC gene family in *Arabidopsis* are involved in stress response, cell growth and development.

1.4.3 PLCs regulate PT growth

In Petunia, PLC1 was found to be an important regulator of PT tip growth (Dowd et al., 2006). GFP:Pet-PLC1 localized to the apical cytoplasm and plasma membrane of

the PT. Its plasma membrane localization was dynamic, with signal was focused at the tip during periods of growth arrest, while the signal localized along the apical lateral walls and was absent from the tip during active elongation (likely mediated by endocytosis). PLC1 showed calcium-dependent PI(4,5)P2 hydrolyzing activity *in vitro*, which was abolished in the PLC1^{H126A} mutant. Expression of the inactive H126A mutant isoform in PTs disrupted tip growth and caused PT swelling, which was also associated with disruptions in the cytoplasmic calcium gradient, actin organization and golgi dynamics. These results were phenocopied when just the C2 domain was expressed. GFP-PLC1's plasma membrane localization was disrupted by the presence of either the H126A or C2-only mutants, but was rescued by increasing the amount of GFP-PLC1, suggesting that the H126A and C2-only mutants were competitively inhibiting binding at the PM, and that PLC activity is required for PT tip growth. This was corroborated in a report that showed increased PI(4,5)P2 accumulation at subapical plasma membrane [using a GFP-Pleckstring Homology (PH) fusion reporter] when the H126A or C2-only mutants were expressed (Helling et al., 2006). Furthermore, because normal GFP-PH signal was only present at the tip during the growing phase of WT PTs, the increased subapical accumulation of PI(4,5)P2 may be driving secretion at these other regions, leading to tip bulging in the H126A and C2-only mutants

While overexpression of GFP:Pet-PLC1 did not noticeably disrupt PT growth, tobacco PTs overexpressing NtPLC3 were shorter than WT, but PTs transformed with the inactive mutant NtPLC3$^{H124A, D156R}$ did not exhibit decreased growth (Helling et al., 2006). NtPLC3-YFP localized to the apical lateral plasma membrane but was excluded from the tip, and this pattern was consistent with both N- and C-terminal fusion proteins. However, expression of the N-terminal version showed fainter plasma-membrane accumulation, and PTs expressing the N-terminal fusion were shorter than PTs expressing the C-terminal version. Taken together, this data suggests that while the localization pattern of PLC3-YFP in tobacco PTs is not activity-dependent, the presence of YFP at the N-terminus partially disrupts intracellular targeting. Similar to Petunia PTs, the fluorescent PI(4,5)P2 reporter YFP-PH localized to the extreme tip in tobacco- an inverse pattern to PLC3-YFP. Combined with the observed PI(4,5)P2-hydrolyzing activity *in vitro*, it was proposed that PLC3 limits membrane PI(4,5)P2 availability, and

its localization is confined to the PT tip region. Co-expression of the Petunia C2 domain made PLC-GFP mis-localize, suggesting the C2 domain competes for binding at the same region, and therefore the C2 domain is sufficient for plasma membrane targeting (Dowd et al., 2006). This data differs from reports in tobacco PTs, where it was shown that YFP fused to either the C2, EF, or XY domains alone did not result in signal accumulation at the plasma membrane, but EF-YFP-C2 did, indicating both of these domains were required for PLC3 association with the plasma membrane in tobacco PTs (Helling et al., 2006). For the rice PLC (AK064924), the C2 domain alone was sufficient to bind lipids in a calcium-dependent manner (Rupwate & Rajasekharan, 2012). Furthermore, the N-terminus/EF domain alone of *Arabidopsis* PLC2 (residues 1-100, or "N-term") was unable to bind lipid vesicles despite being enzymatically active (Otterhag et al., 2001), providing more evidence that the C2 domain is indeed an important region of PLC structure for lipid membrane binding. However, it is possible that the overall 3D structure may be an important factor in mediating C2-lipid binding.

1.4.4 Regulation of PI(4,5)P2 levels controls PT growth

PI4P is phosphorylated at the hydroxyl group of the fifth-position carbon of the inositol head group by PI4P 5-kinases to form PI(4,5)P2. Plant PI45P 5-kinases are classified by their protein structure into either Type A (which resemble human PI4P 5-kinases) or Type B. The *Arabidopsis* genome encodes for 11 PI4P 5-kinase isoforms- 1-9 are Type B, and 10 and 11 are Type A. Several of these genes and their gene products have been studied and characterized, including PIP5K4 and PIP5K5, which have been shown to play important roles in PT germination and growth, pectin secretion, and membrane trafficking (Ischebeck et al., 2008). Single *pip5k4* and *pip5k5* knockout mutants were phenotypically normal, but *pip5k4 pip5k5* PTs had decreased growth and germination frequencies, but were morphologically similar to WT. However, overexpression of either PIP5K4 or PIP5K5 resulted in a wavy growth pattern and increased branching in *Arabidopsis* PTs. Fluorescent proteins fused to either AtPIP5K4 and AtPIP5K5 localized to the cytosol and apical plasma membrane in both Arabidopsis and tobacco PTs, and the membrane signal was localized to the lateral walls near the tip

during growth but expanded to cover the tip after growth stopped. These patterns largely overlapped with the PI(4,5)P2 reporter RedStar-PLCd1-PH, suggesting that PI(4,5)P2 production was likely an important part of how PIP5K4 and 5 influence PT growth. Intermediate overexpression of PIP5K4 or 5 caused increased branching in tobacco PTs, and this was not observed when an inactive version of PIP5K5 was expressed. High levels of overexpressed PIP5K5 was associated with higher accumulation of PI(4,5)P2 reporter signal at the apical plasma membrane, and strong overexpression of either enzyme resulted in growth inhibition, plasma membrane invaginations and an apparent thickening of the cell wall at the tip. Additionally, increased accumulation of ruthenium red signal (which stains pectins) was also observed near the tip (Ischebeck et al., 2008). Taken together, this data suggests that PI4P 5-kinase regulates PI(4,5)P2 levels in the apical plasma membrane of PTs to promote pectin secretion. Loss of PI4P 5-kinase-mediated PI(4,5)P2 production decreases PT growth, and increased enzyme activity leads to overaccumulation of PI(4,5)P2 at the tip, increased secretion of pectins and possibly other cell wall materials, which inhibits normal tip growth.

Similarly, overexpression of AtPIP5K6 in tobacco PTs caused invaginations of the plasma membrane at the tip and decreased PT elongation, as well as increased PT widths. Additionally, PIP5K6-overexpressing PTs showed increased PI(4,5)P2-reporter signal and decreased PIP4 signal near the PT tip. These abnormalities were not present in PTs overexpressing an inactive PIP5K6 mutant (Zhao et al., 2010). PIP5K6 overexpression-induced plasma membrane invaginations were shown to likely be caused by an over-initiation of clathrin- dependent endocytosis that was aborted before the endocytotic vesicles could bud off from the plasma membrane. PIP5K6 overexpression phenotypes were strongly but not completely suppressed by overexpression of AtPLC2, which in combination with other experimental data, is consistent with an overaccumulation of PI(4,5)P2 at the tip causing plasma membrane invaginations and poor growth.

1.4.5 PLC-mediated PI signaling is not restricted to PI(4,5)P2 in plants

Despite the evidence that PLC-PI(4,5)P2 signaling is important in plants, there are multiple key differences in the signaling machinery between animals and plants, which,

in combination with experimental evidence, challenges the canonical model of PI/PLC signaling. For example, plants do not appear to contain genes encoding for IP3 receptors, except for the green algae *Chlamydomonas* (Nagata et al., 2004; Wheeler & Brownlee, 2008), nor homologs for animal protein kinase Cs (PKCs) (Teun Munnik & Testerink, 2009). IP6 was shown to be responsible for internal calcium release in guard cells, which is quickly converted from IP3 (Lemtiri-Chlieh et al., 2003), suggesting that IP3 is not the main secondary messenger in plants. PI(4,5)P2 is also found at very low levels in plants, but PI4,P levels resemble animals' and is hydrolyzed as well as PI(4,5)P2 *in vitro,* suggesting that PI4,P is just as likely to be the canonical substrate for plant PLCs as PI(4,5)P2 (T. Munnik et al., 1998; Van Leeuwen et al., 2007; Vermeer et al., 2006, 2009). Furthermore, DAG phosphorylation to form phosphatidic acid (PA) occurs in response to some abiotic and biotic stresses [reviewed in (Teun Munnik, 2014)], suggesting that PA, not DAG, is an important secondary messenger of PI/PLC signaling. In summary, it appears unlikely that PLCs function in plant PI signaling is strictly confined to hydrolyzing PI(4,5)P2, and downstream effects of PI signaling may be elicited through IP6 and PA rather than IP3 and DAG.

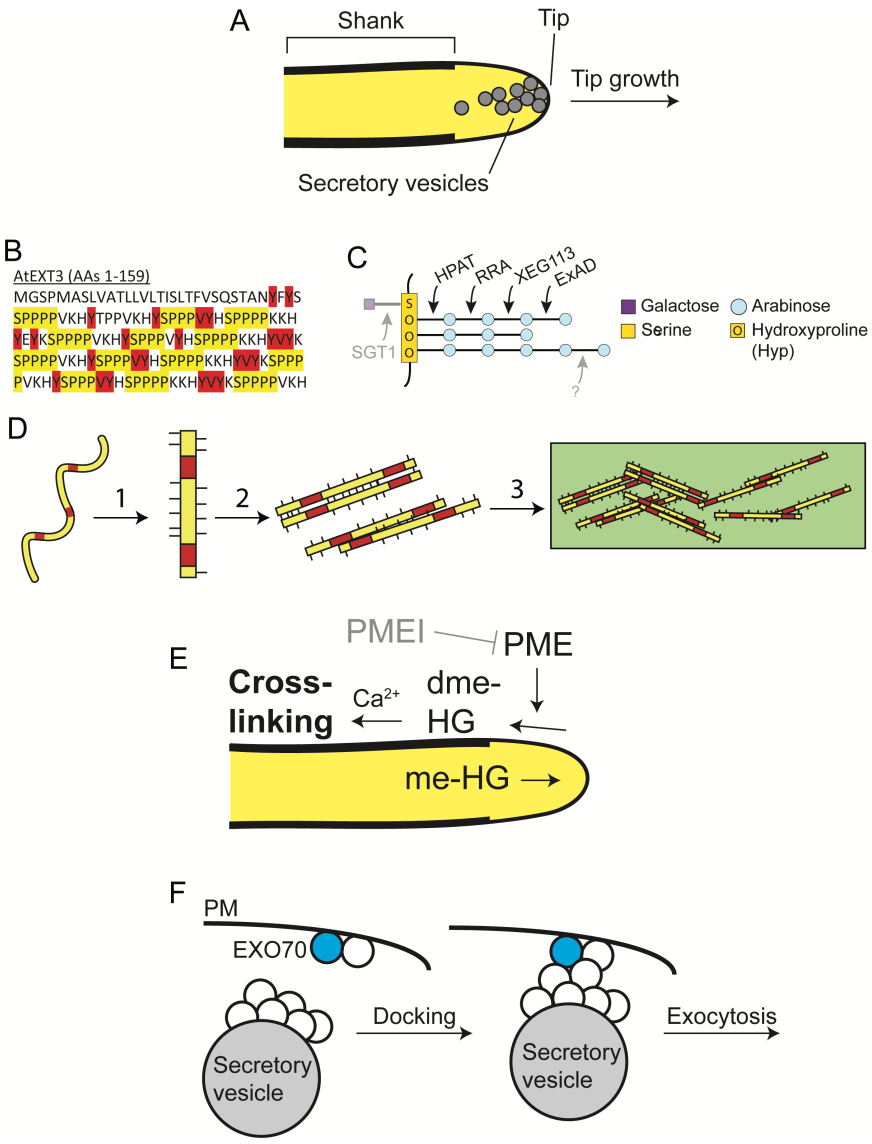

Figure 1-1. Overview of cellular processes. A) Overview of PT growth. B) Partial EXT3 sequence. C) O-arabinosylation cascade of Ser(Hyp)$_{3-5}$ motifs. D) Model of EXT crosslinking pathway. E) Schematic of HG DM regulation in PTs. F) Overview of exocyst/EXO70-mediated secretion

Chapter 2 - Isolation and Cloning of Suppressor Mutants with Improved Pollen Fertility

Authors: Steven Beuder and Cora A. MacAlister

2.1 Abstract

Mutant screens remain among the most powerful unbiased methods for identifying key genes in a pathway or process of interest. However, mutants impacting pollen function pose special challenges due to their genetic behavior. Here we describe an approach for isolating pollen mutants based on screening for suppressors of a low pollen fertility starting genotype. By identifying suppressor mutants with improved pollen fertility, we are able to identify new genes which are functionally relevant to pathway(s) causing low seed set in the original background. With this method, the low fertility of the genetic background may be due to one or more mutations or transgenes disrupting any aspect of pollen development or function. Furthermore, screening for improved pollen fertility biases toward recovery of the desired mutants due to their enhanced male transmission. The causative mutation is cloned using next-generation sequencing. The procedure uses both genetic and bioinformatics approaches to ultimately yield a very small list of candidate causative mutations speeding the transition from mutant phenotype to underlying gene.

2.2 Key Words

mutagenesis, suppressor screen, high-throughput sequencing, cloning, fertility, pollen, seed set

2.3 Introduction

Mutagenesis screens have proven to be a highly powerful method for identifying genes involved in a phenotype or biological process of interest. However, most approaches for isolating and cloning plant mutants focus on those affecting the diploid sporophyte generation. Mutants affecting the haploid gametophytes (the pollen and embryo sac) do not have the same genetic behavior as sporophytic mutants, complicating their initial isolation and cloning. Pollen mutants are especially problematic. The female gametophytes occupy fixed positions within an ovary and there is a direct correlation between the number of viable female gametophytes and ultimate seed yield. A plant that is heterozygous for a female gametophytic lethal mutant will produce seed only from the 50% of ovules containing the wild type allele. This strong reduction in seed set leads to an easily detected fertility phenotype. Pollen however, is produced in significant excess relative to the number of available ovules, leading to competition between pollen grains. Plants that are heterozygous for a pollen lethal mutation generally maintain high seed set since the 50% wild type pollen they produce is sufficient to fertilize all ovules. Though a homozygous pollen-defective mutant would have reduced seed set, such homozygotes are unlikely to appear in segregating populations due to strong bias against male transmission of the mutant allele. Therefore, a mutagenesis screen for reduced seed set is unlikely to recover pollen defective mutants. However, gametophytic mutants have been successfully identified based on screening for distorted transmission ratios. In such screens, the primary screening criteria is generally deviation from the expected Mendelian inheritance pattern of a mutagenic reporter construct (e.g. T-DNA or transposon insertion; (Christensen et al., 1998; Johnson et al., 2004; Lalanne et al., 2004; Pagnussat et al., 2005). Such screens identify mutants which are defective in male and/or female transmission and at any stage of gametophyte development or function. If a particular stage of development or molecular pathway is of interest, secondary screening criteria are required to identify appropriate mutants following the initial screen.

Here we describe a strategy for isolating novel Arabidopsis pollen mutants by screening for increased seed set in a low-fertility genetic background. If a reduced pollen fertility mutant in a pathway of interest has already been identified, for example

through reverse genetics, this low fertility background serves as a convenient starting point for a suppressor screen. Screening for suppressors with improved fertility has several advantages. Firstly, the low fertility starting genotype serves as a sensitized background allowing identification of suppressors of the original phenotype. The genetic interaction between the suppressors and the background genotype allows the direct identification of genes acting in the pathway(s) causing the low starting seed set. Secondly, both heterozygous and homozygous suppressor mutants will likely display increased seed set since increasing fertility of just half of the pollen will still allow more ovules to be fertilized. Thirdly, suppressed pollen will have a transmission advantage over non-suppressed pollen biasing toward recovery of suppressors in a segregating population (see **Note 1**).

The choice of starting genetic background is crucial for the success of a suppressor screen. The starting background must be sufficiently fertile to reliably propagate; but to efficiently screen for increased fertility, it must also have low enough seed set that an increase will be apparent. Here, we use mature silique length as the primary screening criteria since it correlates well with seed number and is an easy and rapid screening method, requiring no sample preparation and minimal handling (**fig. 1**). Unlike traditional map-based cloning, the cloning strategy described here does not require any outcrossing from the initial genetic background. Therefore, the starting phenotype can be due to a single mutation, or a more complex genotype including multiple mutations and/or transgenes regardless of their genomic locations. But, no matter how complex the background, it should be fully homozygous and phenotypically stable (i.e. the phenotype is consistent between individuals and from one generation to the next). The background mutation(s) causing low fertility also require a reliable genotyping assay. Any wild type contamination either from cross pollination or from stray seeds will behave like a strong suppressor and must be excluded based on genotype.

Once suppressor mutants are identified, our strategy for cloning the causative mutation relies on a combination of genetic and bioinformatics approaches to reduce the number of candidate suppressor mutations identified. First, the suppressor is backcrossed to the un-mutagenized parental strain to reduce the number of unlinked

induced mutations present. Second, we sequence DNA from pools of confirmed homozygous suppressors plants (*sup/sup* genotypes), non-suppressed siblings from the same family (+/+ genotypes) and the original low-fertility background. Data from the *sup/sup* sample will contain only the suppressing allele while the +/+ and background data will carry only the wild type allele for the gene causing suppression. By identifying sequence variants that are unique to the *sup/sup* sample and filtering with additional criteria, we produce a very short list of candidate sequence variants to quickly and easily confirm the causative mutation.

2.4 Materials

2.4.1 Plant Material and Growth Supplies

1. ~2,000 EMS-treated seeds of the low-fertility Arabidopsis genotype for which suppressors are sought (see **Note 2**)
2. Flats
3. Potting mix suitable for Arabidopsis
4. 32 cell flat inserts
5. 96 cell flat inserts
6. Stakes and twist ties
7. Coin envelopes for seed storage
8. Growth chamber or room suitable for Arabidopsis (see **Note 3**)
9. Fine forceps (e.g. Dumont #5)

2.4.2 Sequencing DNA Preparation

1. DNeasy Plant Mini Kit (Qiagen) and required reagents
2. 3M sodium acetate, pH5.2
3. 100% Ethanol
4. TE buffer (10mM Tris pH 8.0, 1mM EDTA)

2.4.3 Bioinformatics Resources

1. Access to a computer server or cluster capable of handling the significant volumes of data generated by Illumina sequencing.

2. Reference Genome: The *Arabidopsis thaliana* top level genome sequence can be downloaded from: ftp://ftp.ensemblgenomes.org/pub/plants/release-41/fasta/arabidopsis_thaliana/dna/

3. Software: In addition to Microsoft Excel, the steps in this protocol are performed using the open-source tools listed in Table 1.

2.5 Methods

2.5.1 Screening for Suppressors

1. Sow the mutagenized seeds on soil, distributing them evenly across nine flats containing 32-cell inserts for an average density of approximately seven seeds per cell.

2. As the plants begin to bolt, stake all plants growing in one cell together, securing them with a twist tie to limit pollen transfer between adjacent cells. Allow the M1 plants to self-fertilize and collect all seeds from one cell into a single seed envelope forming an M2 pool (see **Note 4**).

3. Sow seed from each pool into a 96-cell flat with about two seeds per cell. Following germination, thin and transplant seedlings as required so that each cell contains one plant. It is generally most convenient to sow M2 pools for screening over multiple rounds as space and manpower allow.

4. As the M2 plants begin setting seed, screen each individual for increased silique length and seed set compared to the background strain (see **Note 5**). Screening will likely require multiple rounds as the flowering time will vary. Discard non-suppressed plants. Stake each individual candidate suppressor. When dry, collect seed from all candidate suppressors individually, noting the source pool for each.

5. Sow ~50 seeds from each candidate suppressor (now the M3 generation) into 24 cells of a 96-cell flat. When flowering, phenotype for suppression as above and genotype suppressors for the background mutation(s) causing low fertility to confirm that they are not wild type contaminants. For the suppressors that prove phenotypically stable and genetically clean, chose one individual per original pool to progress further (see **Note 6**).

2.5.2 Generating the Sequencing Samples

1. Backcross the suppressor to the starting genetic background (**fig. 2**). Using the suppressor as the male parent will increase cross seed yield and favor transmission of the *sup* allele (see **Note 7**).

- Remove open flowers, small buds and the inflorescence meristem from an inflorescence of the background genotype, leaving two to four of the most mature buds.
- Using fine forceps, emasculate each bud, taking care not to damage the pistil.
- Pollinate the stigma of each emasculated bud with pollen from a young, open flower of the suppressor, applying as much pollen as the stigma will accept.
- Label the crossed inflorescence with the parent plant information and allow the seeds to mature over the next few weeks.
- When the crossed siliques are nearly ripe, collect them and allow the seeds to finish drying on the bench.

2. Sow the backcross F1 seed. When the F1s are flowering, screen for suppression and backcross as above using a suppressed F1 as the male parent. Repeat the backcross step as many times as desired (see **Note 8**).

3. When the desired number of backcrosses have been carried out, allow the F1s to self-fertilize forming the F2 generation.

4. Sow the F2 seeds to produce a minimum of 32 F2 plants (see **Note 9**).

5. When flowering, identify suppressed F2s. The suppressed plants will be a mixture of s*up/sup* and *sup/*+ genotypes.

6. Cross each suppressed F2 individual as a female to the background genotype (see **Note 10**). When ready, collect both the cross seeds and self-fertilized seeds from each F2 parent, carefully tracking the parent individual.

7. Sow the test cross seeds. When the plants are setting seed, score each individual for suppression. Categorize the parent F2 as either *sup/sup* (if all test cross plants are suppressed) or *sup/*+ (1:1 suppressed to non-suppressed test cross plants, **fig. 3**). For statistical confidence, we require a minimum of seven scored test cross progeny for a given F2 parent (see **Note 11**).

8. The test cross progeny from *sup/*+ parents will include non-suppressed (+/+) sibling plants. Collect a total of 100 mg of young leaf tissue from these non-suppressed plants to serve as the non-suppressed sibling (+/+) DNA sample. Preventing suppressor contamination in this pool is critical, so avoid collecting tissue from any questionable individuals.

9. For each confirmed *sup/sup* F2 parent, sow self-fertilized seed (now the F3 generation). Following germination, genotype each F3 population using the background mutation genotyping assay and discard any F3 populations showing wild type contamination.

10. Collect a total of 100 mg of pooled tissue from the confirmed *sup/sup* seedlings, using roughly equally amounts of tissue for each individual F3 population.

11. Sow seeds of the low fertility genetic background and collect 100 mg of seedling tissue for the background DNA sample.

12. Extract DNA from the pooled +/+ tissue, the pooled *sup/sup* tissue and the background genotype tissue using the Qiagen DNeasy Plant Mini Kit following the manufacturer's instructions.

13. To concentrate the purified DNA, add 20 µl of 3M sodium acetate, pH 5.2 and 600 µl of Ethanol to the 200 µl of eluted DNA. Mix by inversion and freeze at -20°C overnight.

14. Spin DNA samples at 4°C for 30 minutes at maximum speed in a standard microcentrifuge.

15. Gently decant the supernatant and allow the tube to dry. Resuspend the DNA pellets in 30 µl of TE.

16. Submit the purified DNA samples for whole-genome library preparation and sequencing (see **Note 12**).

2.5.3 SNP-Mapping Pipeline

The programs used in this pipeline are open-source and can be downloaded from the sources listed in table 1. Alternatively, if you have access to a server and computer cluster with the software installed, then no downloads and installations are necessary, other than loading programs when needed. The command scripts are designed to be typed into a command-line interpreter program- otherwise known as a shell (e.g. "Terminal" for Mac and Linux, or a Unix shell emulator, like Cygwyn, for Windows).

The SNP-mapping pipeline described here consists of several main steps: (1) mapping sequence reads to a reference genome, (2) calling and filtering variants to identify suppressor-specific mutations, and (3) filtering variants based on additional criteria including variant type, sequencing depth, and variant frequency. It is important to note that most steps generate output files which will be used in subsequent steps. Prepare a

work space by creating an empty folder that will serve as the working directory in which multiple subdirectories will be created to store files.

1. Create a new subdirectory called “tair10ref” to store the fasta file of the reference genome sequence. Download the most recent Arabidopsis genome assembly, “Arabidopsis_thaliana.TAIR10.dna.toplevel.fa.gz” and transfer it to the “tair10ref” folder.

2. Create a subdirectory named “raw_reads”, download the raw sequencing reads, and store them in this folder. As an example, here are two “mates” of raw reads from the same sample/pool of DNA; “R1” and “R2” in the file name denotes each mate for a single sample. The “.gz” indicates that the file was compressed.

112369_ATCACG_S1_L004_R1_001.fastq.gz
112369_ATCACG_S1_L004_R2_001.fastq.gz

3. The first action to perform on sequence read files is a quality check using FastQC. Run the following command to perform quality analysis on your raw reads.

```
fastqc Raw_reads/112369_ATCACG_S1_L004_R1_001.fastq.gz
```

This will generate an output filed named “112369_ATCACG_S1_L004_R1_001_fastqc.zip”. Download and open this file to unpack it and open the .html file. This will bring up the FastQC report page. Analyze each section listed in the summary (see **Note 13**).

4. Indices for the reference genome must be generated before performing alignment. To do this, load Bowtie2 (Langmead et al. 2012) and run the following command from your working directory.

```
bowtie2-build tair10ref/Arabidopsis_thaliana.TAIR10.dna.toplevel.fa.gz
```

tair10ref/TAIR10

This will generate multiple files with “.bt2” extensions. This command specifies that all the .bt2 files will have the base name “TAIR10”, and they will be directed to the “tair10ref” folder. The reference genome and the .bt2 index files must be present in the same subdirectory to perform alignment.

5. Create a new subdirectory called “aligned”. Run the following command to align the sequence reads to the reference genome. This will create an output file named “11269.sam”, which will be directed to the “aligned” folder. Be sure to include “-1” or “-2” before each file name to denote that these files contain paired-read mates, otherwise the reads will be aligned without taking pairing into account.

bowtie2 -x tair10ref/TAIR10 -1

Raw_reads/112369_ATCACG_S1_L004_R1_001.fastq.gz, -2

Raw_reads/112369_ATCACG_S1_L004_R2_001.fastq.gz -S aligned/11269.sam

6. Convert SAM files to BAM files. SAM and BAM files contain the same information, but SAM files are a human-readable text format and BAM files are a machine-readable binary version. The BAM format is used for downstream analysis. Create a subdirectory called “bams”. Run the following command to convert the SAM file to a BAM file named “11269.bam” and direct the output file to the “bams” folder.

samtools view aligned/112369.sam > bams/112369.bam

7. Create a subdirectory named “sorted_bams”. Run the following command to sort a BAM file and create an output file named “112369sorted.bam” directed to the “sorted_bams” folder.

samtools sort bams/112369.bam -o sorted_bams/112369sorted.bam

8. Create a new subdirectory named “bams_rmdup” Run the following command to remove PCR duplicates from a sorted .bam file. This command generates an output file named “112369rmdup.bam”, which will be directed to the “bams_rmdup” folder.

samtools rmdup sorted_bams/112369sorted.bam bams_rmdup/112369rmdup.bam

9. Variant-calling tools (including Freebayes) require an index for a .bam file. Run the following command to create an index for a .bam file. Although it is not written in the command, the output file will be directed to the subdirectory containing the .bam file to be indexed, and the output file will have the same name plus “.bai” at the end (e.g. the above command will generate a new file called 112369rmdup.bam.bai that will appear in the “bams_rmdup” folder). Leave the files together in the same subdirectory.

samtools index bams_rmdup/112369rmdup.bam

2.5.4 Identify Sequence Variants and Filter for Candidate Causative Mutations

1. Create a new subdirectory called “VCFs” to store output files. To call variants using Freebayes, run the following command.

freebayes -f tair10ref/Arabidopsis_thaliana.TAIR10.dna.toplevel.fa

bams_rmdup/112369rmdup.bam > VCFs/112369.vcf

The .vcf files can be opened with Microsoft Excel and will contain a large header at the top with the variants listed below. Details of the variants are specified in different columns, of which, the following are the most important (see **Note 14**):

- the chromosome that a variant was found in is listed in the “CHR” column
- the position of the variant on the chromosome are listed in the “POS” column
- the nucleotide(s) present in the reference genome in the “REF” column
- the variant listed in the “ALT” column
- other information, including the number of times the reference and variant sequences were counted in the sample, read coverage, and sequencing quality is listed in the “INFO” column. The header contains key information to interpret data listed in the INFO column.

2. Annotate the suppressor variants (see **Note 15**). Knowing the possible consequences for a given variant on gene function will be useful data for later analysis. Here we use SnpEff to predict the effect of the sequence variants (Cingolani et al. 2012) Though several filtering steps remain, it is convenient to annotate the variant effect now, since SnpEff takes a .vcf file as input and the file format will be altered in later steps. This step is only required for the *sup/sup* data can be skipped for the +/+ and background data. Using the below command, SnpEff will automatically install the required Arabidopsis genome database, annotate the .vcf file with a new data column and save the results as a new file “112368ann”.

java –Xmx4g –jar snpEff.jar Arabidopsis_thaliana 112369.vcf >112369ann.vcf

3. For downstream analysis the information in the INFO column must be split into individual columns. Open the annotated .vcf file in Microsoft Excel and preform the following steps:

- Delete the header
- Highlight the INFO column
- In the “Data” tab, click “Text to Columns”

- Select “Delimited” and set delimiters as “Semicolon”
- Save as a .csv file.

4. Remove common variants. When all files have been processed, there will be two pairs of .csv files for each sequenced suppressor (the *sup/sup* and the +/+ pools) along with the .csv file for the genetic background. The causative mutation will be present in the *sup/sup* sample but absent from the background and the +/+ samples. In this step, we remove variants from the *sup/sup* sample that also occur in the +/+ sample and/or the background sample (see **Note 16**). The following steps are performed with R Studio.

- Move the .csv files to the working directory.
- Install the “DBI” and “dplyr” packages if not already installed.
- Import the .csv files for comparison using the “Import Dataset” function with the “no header” option selected.

The following commands takes the annotated suppressor variant list (data frame ‘112369ann’) and removes any lines which share the same chromosome number (column V1), position (column V2) and alternate sequence (column V5) as any variant in the +/+ pool (data frame ‘112370’). We further subtract the non-mutagenized background variants (‘112371’) from the intermediate result (‘112369ns’) to produce the final list of unique *sup/sup* variants (‘u112369’). The resulting list is saved as a new .csv file. The variant number is typically reduced by ~40% following this step.

```
library(dplyr)

112369ns <- anti_join(`112369ann`,`112370`, by= c("V1", "V2", "V5"))

u112369 <- anti_join(`112369ns`,`112371`, by= c("V1", "V2", "V5"))

write.csv(u112369, file = "u112369.csv")
```

5. Determine variant frequency in the unique variant list:

- Open the unique *sup/sup* variant .csv file in Excel

- Find and highlight the column with information that says “RO=n”, where n is the number of times a read included the reference nucleotide and use the find and replace tool to delete the “RO=” from each cell.
- Repeat these steps for the alternate nucleotide observation column with the “AO=n” information to remove the “AO=”.
- Insert a new column and label it “AO freq”. Divide the values in the “AO” column by the sum of the values in the “RO” and “AO” column for each row. These values are the frequencies with which a variant was found in that sample.

6. Using the Filter tool, you can now filter the file to show only the variants meeting the filtering criteria:

- To filter by allele frequency, highlight the “AO freq” column, select Filter, and filter for values greater than or equal to your cutoff value. We generally use 0.8.
- To filter by sequencing depth, filter the “AO” column. We generally require a minimum of five reads.
- There is also a column containing the type of change, “type=n”, where n refers to a type of variant, such as a single nucleotide polymorphism (SNP), insertion, etc. Since EMS typically induces transition mutations, filter for “type=SNP”.

Following these filtering steps, the total number of candidate variants will be significantly reduced, generally to <2% of the starting unique variant number. Most of these variants will occur in one chromosomal region which includes the causal mutation and those linked to it. The remaining few dozen candidates can be further filtered based on their annotated effect. Missense or non-sense mutations occurring in pollen-expressed genes near the center of the cluster are the most likely causative mutations.

2.6 Notes

1. We do not screen for enhancers (mutants with reduced pollen fitness and lower seed set) since they would be under a strong male-transmission disadvantage, making their recovery difficult. Though sterile mutants are a frequently recovered class in any mutagenesis screen, such sterility is likely caused by an unrelated sporophytic mutation.

2. The induction of Arabidopsis mutants by seed treatment with Ethyl methanesulfonate (EMS) has been described several times previously (Dinh et al., 2014; Qu & Qin, 2014; Weigel & Glazebrook, 2006). We generally treat seeds of the starting genotype with 0.2% EMS for 16 hours. It is advisable to check for segregation of albino seedlings in the M1 generation as an indicator of mutagenesis success.

3. Fertility is influenced by many factors, both genetic and environmental. Therefore, growth conditions should be as consistent and as favorable as possible. We have found that high air movement is a major contributing factor to contamination by wild-type pollen. Pollen contamination can be limited by using lower airflow growth areas or by excluding flowering wild type plants from the growth area.

4. The M1 plants may be screened directly for increased seed set. However, the M1s will be chimeras with sectors carrying different mutations so only some of their siliques may be carrying the suppressive mutation, which can complicate screening. If the M1s are screened, it is still advisable to screen the M2s of any pools that did not produce any suppressor candidates.

5. Older plants are generally easier to screen since they will have more siliques available for comparison. The choice of which siliques to consider is also important. The first few flowers produced by a plant should be avoided for phenotyping purposes as these often have low fertility, even in wild type plants. We also avoid scoring siliques produced late in life or from tertiary branches as these often have low fertility.

6. Multiple unique suppressor mutations may exist in a single M2 pool. Unfortunately, due to the haploid nature of gametophytic mutants, complementation tests are not possible and allelic mutants can only be recognized after their cloning. Therefore, we progress a single candidate suppressor per pool as a reasonable compromise between total number of suppressors isolated and the highest likelihood of recovering independent mutations, and therefore novel alleles and genes.

7. We assume here that suppression is due to an improvement in pollen fertility. This has always been the case in our experience, but it is possible that female suppression pathways may exist. To determine whether suppression is due to improved fertility of the pollen itself or through compensation by the female tissue, perform reciprocal test crosses with the suppressor plants and the background genotype. If the suppressor acts by improving pollen fertility, the crossed siliques will have high seed set when the suppressor is used as the male parent (similar to the suppressor self-fertilized siliques), but low seed set when it is used as the female parent (similar to the self-fertilized background genotype).

8. We generally backcross for four generations, but this number may be reduced (or increased) as desired. If time is a constraint, reducing the number of backcrosses is preferable to eliminating the test cross step. Much of the power to filter candidate mutations comes from filtering based on the allelic frequency in the *sup/sup* data. If the suppressors sequenced were not confirmed homozygotes, the stringency of this filtering must be significantly reduced to account for heterozygous suppressors.

9. A *sup/sup* F2 plant is homozygous for the causative mutation, but may be homozygous for unrelated mutations as well. By pooling F2 individuals we reduce the allele frequency of non-causative mutations. We expect about half of the suppressed individuals used for test crosses will prove homozygous. We target a minimum of ten homozygous F2s to include in the sequencing DNA pool, but have used as few as five with good success. We start with an F2 population of 32 plants, allowing for some non-suppressed F2s, some test crosses which fail to produce enough progeny to screen and other potential problems.

10. Due to the male transmission advantage expected for a suppressor, the test crosses *must* be done using the suppressors as the female parent. However, the low male fertility of the background genotype will reduce the total seed yield from crosses when it

is used as the male parent. Therefore, more flowers may need to be pollinated than is typical to ensure sufficient cross seed yield.

11. From a *sup/+* female parent, each individual test cross progeny has a 50% chance of inheriting the non-suppressive (+) allele and appearing non-suppressed. The probability of all progeny of sample size N inheriting the + allele by chance is calculated as 0.5^N. For seven individuals, the overall likelihood is 0.5^7=0.0078 or 0.78%. In practice, we sow all cross seed and discard any crosses for which fewer than seven individuals can be scored. We also generally discard test crosses if the segregation ratio is not clearly one of the expected classes (100% suppressed or 50% suppressed).

12. We have used both in-house DNA sequencing core facilities and commercial sequencing operations to both prepare the libraries and carryout the sequencing with good success. We typically sequence the libraries as paired-end 150 bp reads using an Illumina HiSeq 4000 sequencer, pooling 16 libraries per lane with a target sequencing depth of 20-30 fold per sample (James et al., 2013). The specific type of sequencing run is not critical and single-end sequencing and/or different read lengths can be used with only minor adjustments to data analysis. If a different read type, length or sequencer will be used, Illumina offers an online sequence coverage calculator to determine how many libraries may be pooled per lane (https://support.illumina.com/downloads/sequencing_coverage_calculator.html).

13. A tutorial to guide beginners through interpreting FastQC reports is available at the FastQC link in Table 1.

14. The total list of sequence variants will be long (in our experience ~40,000 per sequenced line) and include many classes of variants (e.g. induced mutations, sequencing errors, polymorphisms between the sequenced line vs. the genome release, etc.). Therefore, the variant number should not be taken as an indication of mutation rate.

15. The read mapping and variant calling steps are computationally too intensive for a standard personal computer and will require use of a server or cluster. However, all of the remaining steps after variant calling can be done on a standard laptop or desktop computer.

16. In this step, any variant that is found in the non-suppressed sibling (+/+) sample or the background genotype sample will be removed from the suppressor variant list. Even a small amount of suppressor contamination in these samples will eliminate the causative mutation since no account is made for the frequency or the quality of the variant. If the analysis does not yield promising candidate mutations, this is the most likely point of failure. For a less stringent approach this step can be skipped leaving a longer list of candidate variants.

Table 2-1: Tools for data analysis

Tool	**URL**
Bowtie2 ***(5)***	http://bowtie-bio.sourceforge.net/bowtie2/index.shtml
FastQC	http://www.bioinformatics.babraham.ac.uk/projects/fastqc/
Freebayes	https://sourceforge.net/projects/acoros/files/acoros/stable/pool/main/f/freebayes/
R Studio	https://www.rstudio.com/products/rstudio/download/
Samtools	http://www.htslib.org/
SnpEff ***(6)***	http://snpeff.sourceforge.net/index.html

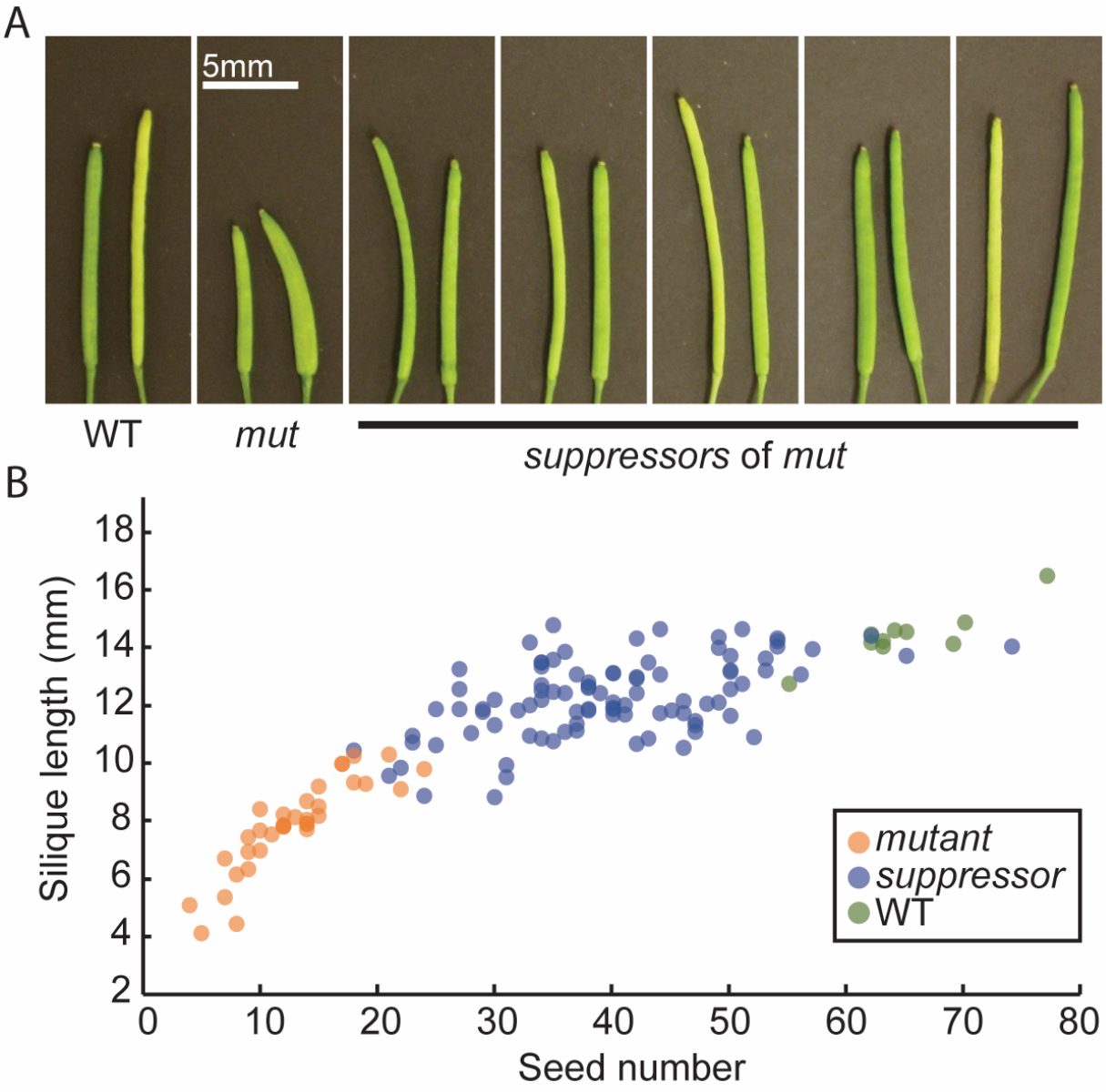

Figure 2-1. Silique length approximates seed set. A) Two representative nearly mature siliques from wild type (WT), the low- fertility starting background mutant (mut) and five different suppressors of mut. Note that the mutant background siliques are shorter

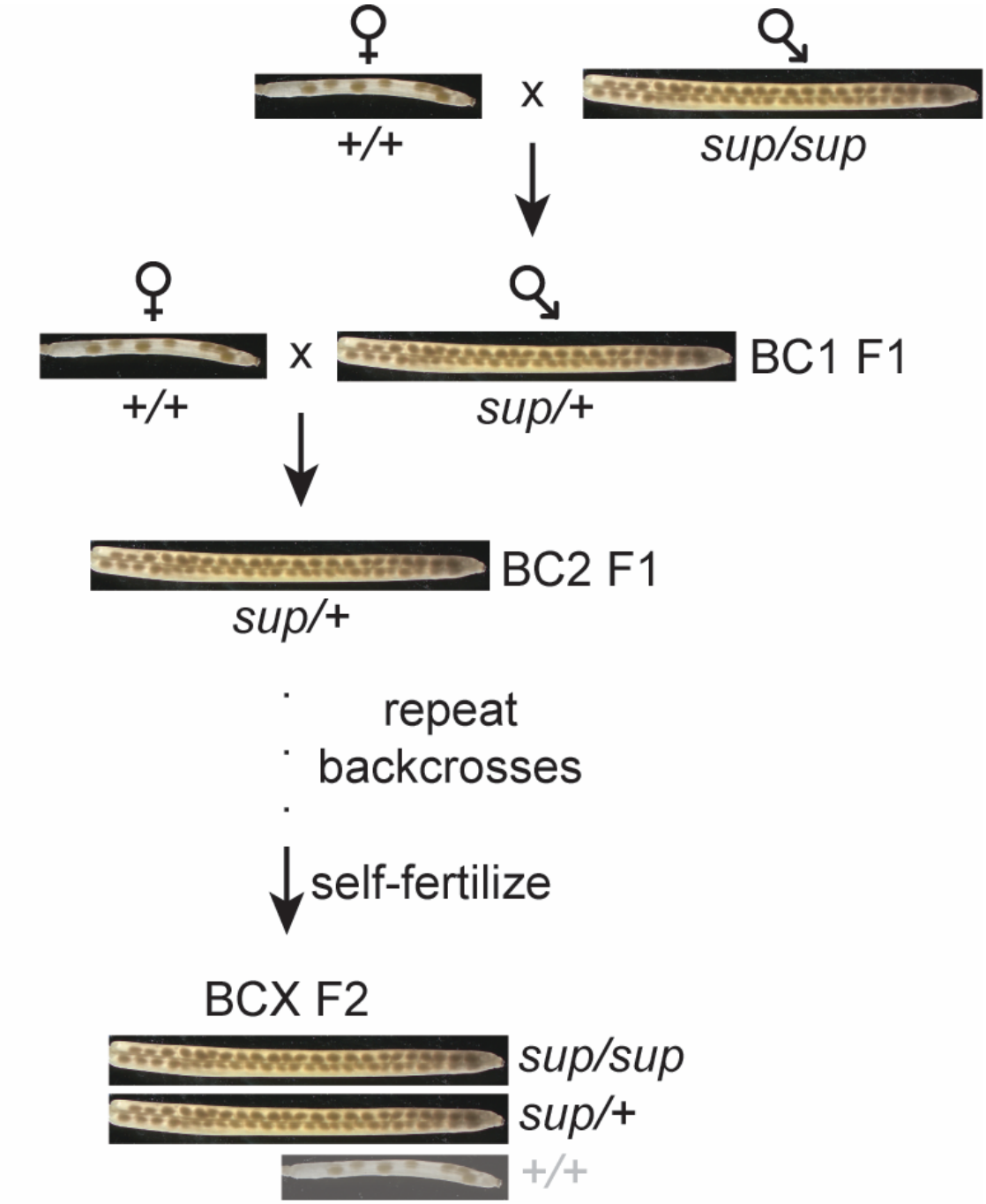

Figure 2-2. Backcrossing the suppressor reduces the number of superfluous mutations. Mutagen treatment will produce not only the desired sup mutation, but other random mutations as well. Backcrossing the suppressor to the parental background will dilute these.

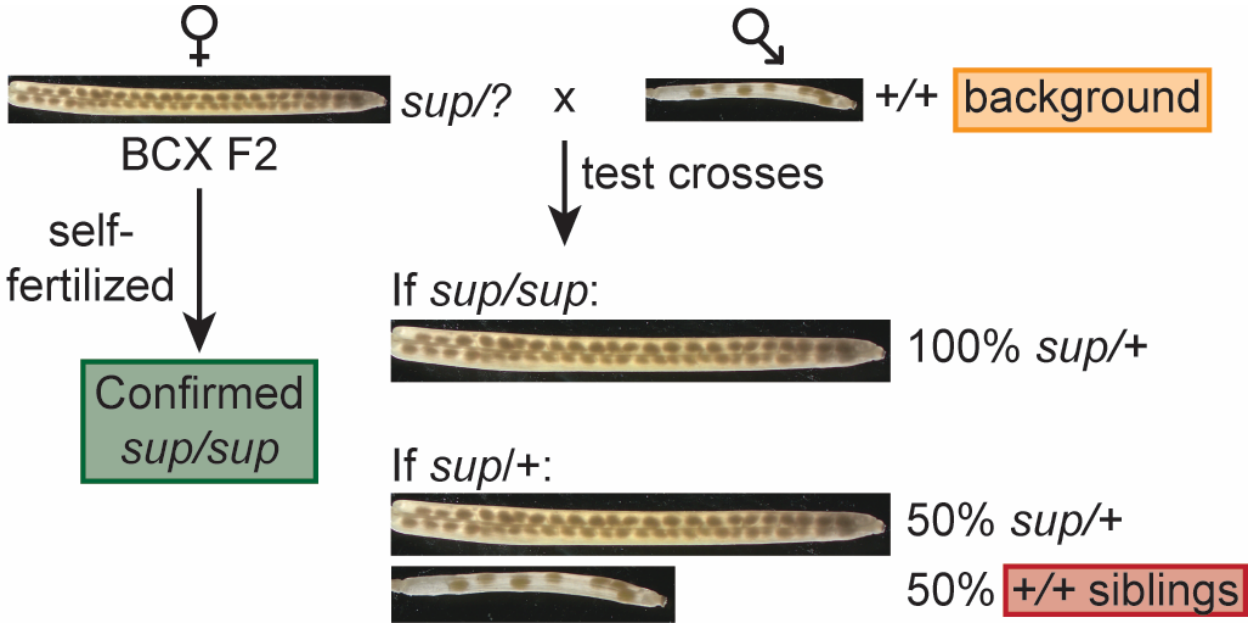

Figure 2-3. Source of tissue samples for DNA sequencing.The backcross F2 generation will be composed primarily of suppressed individuals which are either sup/sup or sup/+ genotypes. Determining the genotype of a given plant requires a test cross with the background.

Chapter 3 - Exocyst Mutants Suppress Pollen Tube Growth and Cell Wall Structural Defects of *Hydroxyproline O-arabinosyltransferase* Mutants

Steven Beuder[1], Alexandria Dorchak[1], Ashwini Bhide[1], Svenning Rune Moeller[2], Bent L. Petersen[2] and Cora A. MacAlister[1,*]

1. University of Michigan, Department of Molecular, Cellular and Developmental Biology
2. University of Copenhagen, Faculty of Science, Department of Plant and Environmental Sciences
* corresponding author, macalist@umich.edu

3.1 Summary

HYDROXYPROLINE O-ARABINOSYLTRANSFERASEs (HPATs) initiate a post-translational protein modification (Hyp-Ara) found abundantly on cell wall structural proteins. In *Arabidopsis thaliana HPAT1* and *HPAT3* are redundantly required for full pollen fertility. In addition to the lack of Hyp-Ara in *hpat1/3* pollen tubes, we also found broadly disrupted cell wall polymer distributions, particularly the conversion of the tip cell wall to a more shaft-like state. Mutant pollen tubes were slow growing and prone to rupture and morphological irregularities. In a forward mutagenesis screen for suppressors of the *hpat1/3* low seed set phenotype, we identified a missense mutation in *exo70a2*, a predicted member of the vesicle-tethering exocyst complex. Suppressed pollen had increased fertility, fewer morphological defects and partially rescued cell wall organization. A transcriptional null allele of *exo70a2* also suppressed the *hpat1/3* fertility phenotype as did mutants of core exocyst complex member *sec15a*, indicating that reduced exocyst function bypassed the PT requirement for Hyp-Ara. In a wild-type background, *exo70a2* reduced male transmission efficiency, lowered pollen germination

frequency and slowed pollen tube elongation. EXO70A2 also localized to the PT tip plasma membrane, consistent with a role in exocyst-mediated secretion. To monitor trafficking of Hyp-Ara modified proteins, we generated an HPAT-targeted fluorescent secretion reporter. Reporter secretion was partially dependent on *EXO70A2* and was significantly increased in *hpat1/3* PTs compared to wild type, but reduced in the suppressed *exo70a2 hpat1/3* tubes.

3.2 Introduction

For plant cells to grow, the cell wall must be sufficiently extensible to accommodate cell expansion while maintaining enough strength to prevent cell rupture from the high turgor pressure of the cytoplasm. This balance is especially critical to tip growing cell types, like pollen tubes (PTs) and root hairs, where expansion happens at a single growing point. Due to their inherent growth polarity, tip-growing cells may be divided into two general cell wall domains, an extensible tip and a rigid shaft. Cell wall properties depend on its polymer composition and the tip and shaft region differ in functionally significant ways (Bosch & Hepler, 2005; Chebli et al., 2012; Dardelle et al., 2010; Rounds et al., 2011). PTs are generally rich in pectic polysaccharides which are initially secreted in a methyl-esterified form. The methyl-esterified pectins are de-esterified in the wall by pectin methylesterases (PMEs), after which they are able to form a gel through divalent ion cross linking, contributing to cell wall rigidity (Bosch & Hepler, 2005; Wolf et al., 2009). In PTs, the shaft is further reinforced by the deposition of callose (1,3-β-D-glucan) (Schlupmann et al., 1994; VanDerWoude et al., 1971). In contrast to other plant cell types, PTs contain relatively little cellulose (1,4-β-D-glucan). While cellulose and callose are synthesized at the plasma membrane, other wall polymers are synthesized by ER and Golgi-resident enzymes and must be delivered, along with other secretory cargos, by secretory vesicles, though much is unknown about the process (Cosgrove, 2005; Sinclair et al., 2018).

To support the rapid growth of PTs, secretion must also be very rapid in these cells (Campanoni & Blatt, 2007). Cell expansion and cell wall accumulation are temporally related with secretion leading to thickening of the wall followed by an

increase in growth rate during oscillatory PT growth (McKenna et al., 2009). The vesicle dynamics at the tip of the PT are complex and include a mix of exocytic vesicle movement, plasma membrane fusion and endocytic recycling of excess membrane (Bove et al., 2008). Multiple components of the PT secretory pathway have been described including several members of the vesicle tethering exocyst protein complex. The exocyst is an octomeric complex composed of one of each of its subunits (SEC3, SEC5 SEC6, SEC8, SEC10, SEC15, EXO70 and EXO84). The exocyst is well conserved across Eukaryota (Mei & Guo, 2018) and in plants, exocyst complex members have been implicated in several important biological processes including casparian strip formation (Kalmbach et al., 2017), compatible pollen reception by the stigma (Safavian et al., 2015; Samuel et al., 2009), tracheary element development (S. Li et al., 2013), polar organ growth, root hair elongation (Synek et al., 2006), root growth (Cole et al., 2014) and pollen germination and tube elongation (Bloch et al., 2016; Cole et al., 2005; Hála et al., 2008; Y. Li et al., 2017). However, the rules by which various secretory cargo are packaged and trafficked and how these cargoes become incorporated into a functional wall upon secretion remains poorly understood. The PT is an excellent system for studying these processes given its rapid growth, heavy dependence on secretion and the importance of maintaining proper cell wall organization in these cells.

We have previously shown that successful PT elongation and fertilization requires protein glycosylation, specifically of the hydroxyproline *O*-arabinosylation (Hyp-Ara) type (MacAlister et al., 2016). O-linked protein glycosylation, like Hyp-Ara, begins in the endoplasmic reticulum with the conversion of peptidyl proline to Hyp by prolyl-4 hydroxylases (Adams & Frank, 1980). In plants, Hyp can be modified by O-linked glycosylation in the form of Hyp-Ara or Hyp O-(arabino)galactosylation (Showalter & Basu, 2016; Tan et al., 2010). Which type of modification a given Hyp receives depends on the protein context; contiguous and non-contiguous Hyps are arabinosylated while clustered but discontinuous Hyp, like those occurring in the arabinogalactan proteins are galactosylated (Kieliszewski & Shpak, 2001; Ohyama et al., 2009). For Hyp-Ara, arabinose sugars are sequentially added until a linear chain of up to 4-5 sugars is formed (Lamport & Miller, 1971). The first, (β1,4-linked) arabinofuranose is added by the

Golgi-localized HYDROXYPROLINE O-ARABINOSYLTRANSFERASE 1-3 (HPAT1-3) enzymes which are classified as glycosyltransferase family GT95 members (Ogawa-Ohnishi et al., 2013). The single arabinose (Hyp-Ara_1) may then be extended by the GT77 family members REDUCED RESIDUAL ARABINOSE 1-3 (RRA1-3) and XYLOGLUCANASE113 (XEG113) which add a second (β-1,2-linked) and a third (β-1,2-linked) arabinofuranose, respectively (Egelund et al., 2007; Gille et al., 2009; Velasquez et al., 2011). The fourth (α-1,3-linked) arabinofuranose is added by the GT47-classified EXTENSIN ARABINOSE DEFICIENT TRANSFERASE (ExAD) (Møller et al., 2017). An enzyme activity for addition of the rare fifth arabinose has not been assigned. In the absence of HPAT activity Hyp-oligoarabinosides are not produced (MacAlister et al., 2016). In Arabidopsis, mutants of the three-member *HPAT* gene family have reported pleiotropic effects including reduced hypocotyl length, reduced cell wall thickness, accelerated senescence in *hpat1 hpat2* double mutants, and disrupted root hair elongation (Ogawa-Ohnishi et al., 2013; Velasquez et al., 2015). *HPAT1* and *HPAT3* are redundantly required for full male fertility; *hpat1 hpat2 hpat3* triple mutants and *hpat1 hapt3* double mutants display low male fertility and PT growth defects leading to reduced male transmission and low seed set (MacAlister et al., 2016).

The largest known group of HPAT-target proteins are members of the EXTENSIN (EXT) family of repetitive cell wall structural glycoproteins (Brownleader & Dey, 1993; Lamport, 1967; Lamport & Miller, 1971; Showalter et al., 2010). Following heavy Hyp-Ara modification, EXTs are secreted into the apoplast where they assemble into an insoluble covalent network by peroxidase-mediated cross-linking of tyrosine residues (Everdeen et al., 1988; Held et al., 2004). The glycosylation of the EXTs contributes to their rod-like, extended poly-Pro-II left-handed helical conformation and increases tyrosine cross-linking *in vitro* (Chen et al., 2015; Stafstrom & Staehelin, 1986a, 1986b; van Holst & Varner, 1984). This EXT network is hypothesized to serve as scaffold for further cell wall assembly, specifically through acid-base and/or covalent interactions with pectins (Cannon et al., 2008; Qi Xiaoyang et al., 1995). Proteins with EXT-like regions fused to other domains are also predicted to carry Hyp-Ara modifications. These “EXT-chimeras” have many proposed functions, with the EXT-like region generally proposed to act in cell wall binding or sensing. EXT-chimeras include

the leucine-rich repeat extensin (LRX) proteins, the proline-rich extensin-like receptor kinase (PERK) proteins and the class I formin homology (FH) proteins (Borassi et al., 2016; Showalter et al., 2010).

With the aim of understanding the requirement for Hyp-Ara in PT growth, we carried out a genetic suppressor screen to identify additional factors in the HPAT pollen fertility pathway. Here we report the cloning and characterization of two such suppressor mutants, both of which encode members of the exocyst complex, pointing to an important link between regulation of secretion, protein glycosylation and cell wall structure in the PT.

3.3 Results:

To identify mutations suppressing the pollen fertility defect of *hpat1 hpat3* double mutants (*hpat1/3* for brevity) we mutagenized ~2,000 *hpat1/3* seeds by treatment with 0.2% ethyl methanesulfonate. Self-fertilized progeny were screened for increased silique length and seed set (see also Material and Methods section). The identified suppressor mutants, named *fertility restored in hpat1/3* (*frh*), were confirmed to be homozygous for the original *hpat1* and *hpat3* insertion mutations and to display consistently increased fertility between generations and following backcrosses with the parental strain.

3.3.1 frh1 *improves the fertility of* hpat1 hpat3 *pollen*

In contrast to the *hpat1/3* genetic background, suppressed *frh1 hpat1/3* plants showed increased silique length and higher seed set, but appeared otherwise morphologically normal (Fig. 1). To confirm that *frh1* suppression was the result of improved pollen fertility we analyzed seed set following reciprocal crosses between the suppressed line and *hpat1/3*. The *hpat1/3* fertility defect is limited to the pollen; seed set can be fully rescued by pollination with wild-type (WT) pollen (MacAlister et al., 2016). Similarly, seed set was high when *frh1 hpat1/3* was used as the pollen parent, but not when it was used as the seed parent with *hpat1/3* pollen, demonstrating that suppression in *frh1* was due to increased pollen fertility (Fig. 1B). This enhanced pollen

fertility coupled with the Arabidopsis habit of producing excess pollen relative to ovule number, impacted the genetic behavior *frh1 hpat1/3* and its pattern of inheritance. Seed set was significantly increased in both homozygous and heterozygous (i.e. backcross F1) *frh1 hpat1/3* plants (Fig. 1B). In the *frh1/+ hpat1/3*, the increased fitness of pollen carrying the *frh1* mutation also drove high *frh1* male transmission and reduced the number of non-suppressed progeny recovered. In a backcross F2 population, only 9% of plants displayed low, *hpat1/3*-like fertility, a significant deviation from the 25% expected in the absence of a transmission bias (N=123, χ^2 P-value = 1.55×10^{-5}).

Given that *frh1* improved *hpat1/3* pollen fertility *in vivo*, we next analyzed the phenotype of *frh1 hpat1/3* PTs directly. When grown on *in vitro* pollen germination media *hpat1/3* PTs displayed a number of defects including reduced PT length, the initiation of secondary tips (i.e. “branched” PTs), high frequencies of PT rupture and modestly increased PT width. We found *frh1* partially suppressed all of these defects (Fig. 1D-E and Fig. S1). Interestingly, we also found that *frh1 hpat1/3* pollen germinated at a lower frequency than either WT or *hpat1/3* pollen. The apparent reduction in germination in *hpat1*/*3* is at least partially a result of their poor PT growth. *hpat1/3* PTs often rupture and can do so before a tube becomes sufficiently apparent to consider a pollen grain germinated. However, this was not true for *frh1 hpat1/3* pollen grains which had reduced frequency of PT rupture, but further reduced germination frequency. In a comparison of sustained PT growth rates for each genotype, we found an overall reduction in *hpat1/3* PTs which was suppressed by *frh1* (Fig. S1I). Though the *frh1 hpat1/3* growth rate was even higher than the WT rate, this did not translate into an increase in the overall length of PTs after 5 hours of growth (Fig. 1D). We also noted that *hpat1/3* PTs would often arrest growth for extended periods of time before ultimately rupturing. The average duration of this pre-rupture pausing was 24.5 minutes and ranged from less than five minutes to greater than 100 minutes (N=11).

3.3.2 frh1 does not restore Hyp-Ara, but partially rescues cell wall organization

The most direct mechanism for suppressing the *hpat1/3* phenotype would be restoration of the Hyp-Ara protein modification itself. In order to assess the Hyp-Ara

status of *frh1*, we sought an antibody capable of specifically recognizing this modification. The Extensin (EXT) family of cell wall structural proteins are known to be heavily Hyp-Ara modified and several monoclonal antibodies have been previously raised against purified EXTs. We tested three of these for Hyp-Ara specificity [JIM11, JIM19 and JIM20; (M. Smallwood et al., 1994; Margaret Smallwood et al., 1995). We found JIM20 recognized protein samples from WT seedlings, but not *hpat* triple mutant seedlings, which we have previously shown to lack detectable Hyp-Ara [Fig. S2A-B;(MacAlister et al., 2016)]. Furthermore, JIM20 did not recognize protein from mutants of the arabinosyltransferases adding the second and third 1→2 linked β-Arabinofuranoses (the *rra2 rra3* double mutants and the *xeg113-3* mutant; (Egelund et al., 2007; Gille et al., 2009). JIM20 did however recognize protein from *exad1-1* plants, therefore, the fourth, 1→3 linked α–arabinofuranose added by ExAD is not required for JIM20 recognition (Møller et al., 2017).We immuno-labeled pollen grains and PTs with JIM20 to determine the localization of Hyp-Ara in these cells. We found robust staining of the WT pollen grain and tube cell wall (Fig. 2A, Fig. S2C). In *hpat1/3* pollen, we detected no JIM20 signal, as in WT secondary antibody alone controls (Fig. S2D-E). As in *hpat1/3*, no Hyp-Ara was detected in *frh1 hpat1/3* tubes (Fig. S2F). Therefore, *frh1* did not suppress the *hpat1/3* phenotype by directly restoring Hyp-Ara, but through another mechanism.

The *hpat1/3* pollen phenotypes are consistent with defective cell wall integrity. In order to gain insight in the molecular basis for these defects and *frh1*'s suppression of them, we compared the organization of key PT cell wall polymers. Given the importance of pectin for PT growth and the proposed function of EXTs in pectin organization we hypothesized that compromised EXT Hyp-Ara may alter pectin distribution in the cell wall. We used the monoclonal antibodies LM19 and LM20 (Verhertbruggen et al., 2009) to assess the distribution and abundance of demethyl-esterified homogalacturonan (dme-HG) and methyl-esterified HG (me-HG), respectively, in WT, *hpat1/3* and *frh1 hpat1/3* PTs. A key functional difference between these two forms of pectin is their ability to form calcium salt bridges. dme-HG is able to form a cross-linked structure while the methyl-ester groups present on the me-HG prevent this (Micheli, 2001). In WT PTs, the me-HG recognized by LM20 was enriched at the PT tip while the calcium

cross-linkable dme-HG recognized by LM19 was excluded from the tip and enriched in the shaft, consistent with previous reports [Fig. 2C-D; (Bosch & Hepler, 2005; Chebli et al., 2012; Dardelle et al., 2010; Rounds et al., 2011). This pattern was disrupted in *hpat1/3* PTs. The LM20 epitope (me-HG) signal enrichment at the tip region was weaker in *hpat1/3*. Moreover, the overall level of LM19 epitope (cross-linkable dme-HG) was increased in the shaft region and enriched, rather than excluded from the tip (Fig. 2C-D). However, *frh1 hpat1/3* PTs had intermediate levels of dme-HG (LM19) signal, and reduced me-HG (LM20) at the tip relative to the shaft, though the pattern was not restored to that of WT. Increased cell wall rigidity at the PT tip in *hpat1/3* due to accumulation of dme-HG in this region is consistent with the poor expansion ability of this genotype. The reduced accumulation of this polymer in *frh1* is also consistent with its improved growth and the suppressed phenotype. Interestingly, in *frh1 hpat1/3* PTs, the tip enrichment of me-HG (LM20 signal) was almost completely missing and the expression was generally flat across the length of the PT (Fig. 2C).

The PT shaft is also reinforced with callose (Schlupmann et al., 1994; VanDerWoude et al., 1971) We stained PTs with aniline blue fluorochrome (ABF) to compare callose distribution between genotypes. As expected, in WT PTs we found high levels of ABF binding along the shaft and low signal at the tip. Again, consistent with the poor expansion ability of *hpat1/3* pollen, we found high levels of ABF signal at the PT tip. This enrichment was abrogated in *frh1 hpat1/3* tubes, though not restored to WT levels, again, consistent with the improved growth of suppressed PTs (Fig. 2B).

3.3.3 frh1 suppression is caused by a mutation in exo70a2

To identify the mutation conferring increased seed set and improved PT growth in *frh1* plants, we used a high-throughput sequencing strategy (Beuder & MacAlister, 2020). *frh1* was backcrossed to the parental strain for four generations and allowed to self-fertilize forming the BC4 F2 generation. To identify homozygous *frh1* individuals for sequencing, the BC4 F2 plants were used as females in test crosses with *hpat1/3* pollen. Homozygous *frh1* plants produce only suppressed F1 progeny while heterozygous females produce a 1:1 ratio of suppressed and non-suppressed progeny.

A minimum of 11 test cross progeny per parent were scored for 25 BC4 F2 individuals. Twelve were found to be homozygous (100% suppressed progeny, N=149 total), while the remaining 13 were heterozygous (49.4% suppressed progeny, N=170 total). We extracted DNA from three groups of plants: the self-fertilized progeny of the confirmed homozygous *frh1* plants (the *frh1/frh1* pool), the non-suppressed progeny segregating from the heterozygous plant test crosses (the *FRH1/FRH1* pool) and the *hpat1/3* genetic background.

Following paired-end 150 bp DNA sequencing, quality control and read mapping, we identified sequence variants from all three DNA samples relative to the Columbia reference genome (Table S1). From the variants identified in the *frh1/frh1* data, we removed all variants shared with the background strain (*hpat1/3*) or the *FRH1/FRH1* pool, leaving 18,287 unique *frh1* variants. We filtered this set for single nucleotide polymorphisms, as expected for an EMS-induced mutation, supported by a minimum of four reads leaving 16,001 variants. After filtering for a minimum variant sequence read frequency of 80%, we were left with 48 variants, eight of which were predicted missense mutations. Thirty of these variants were clustered within a 5.7 Mbp region on chromosome 5, presumably containing the causative mutation and those linked to it (Table S2). Near the middle of this region, we identified a missense mutation converting glycine 319 to a glutamic acid in EXO70A2, a predicted subunit of the vesicle-tethering exocyst complex. The altered amino acid position (Glycine 319) is conserved in eight of the 23 Arabidopsis EXO70s including the A, E, F and G subfamilies and is directly C-terminal to a phenylalanine that is conserved in all Arabidopsis EXO70s (Fig. S3).

We tested for co-segregation between the *exo70a2*^{G319E} variant (hereafter *exo70a2-2*) and the suppressive phenotype in an *frh1* BC5 F2 population using a PCR-based genotyping assay. As expected for the causative mutation, we found a significant bias against recovery of homozygous wild-type plants and perfect concordance between *exo70a2-2* genotype and suppressive phenotype, including intermediate seed set values for heterozygous plants (Fig. S4). To confirm that the *exo70a2* mutation is the cause of the *frh1* suppression, we expressed the wild-type genomic *EXO70A2* sequence from a transgene in the *frh1 hpat1/3* background. Transgenic *frh1* “rescue” would be a return to the low fertility of the *hpat1/3* parental strain. We cloned a 3,971 bp

region of the EXO70A2 locus including the native promoter, full coding region and ~450 bp of 3' sequence and recombined this fragment into a plant expression vector containing a seed-expressed fluorescent transformation marker (Shimada et al., 2010). We compared the transgene transmission efficiency in three independent single-loci insertion hemizygous lines and found a significant and robust male-specific transmission defect for the *EXO70A2* transgene for all lines (Fig. S5). The same plasmid backbone carrying a strong pollen-specific promoter (Lat52) driving expression of the florescent protein, mNeonGreen, had no effect on male or female transmission [Fig. S5B; (Bate & Twell, 1998; Shaner et al., 2013). Furthermore, in *exo70a2-2 hpat1/3* lines homozygous for the transgene, seed set was reduced to the level of the *hpat1/3* background while non-transgenic sibling plants had *frh1*-like high seed sets (Fig. S5C). Thus confirming that the *exo70a2-2* mutation confers the increased fertility observed in *frh1 hpat1/3* plants.

3.3.4 EXO70A2 *is required for efficient pollen germination and pollen tube growth*

Given the effect of *exo70a2-2* on *hpat1/3* pollen fertility, we next determined the phenotypic consequence of this mutation in an otherwise WT background. From a Col outcross population, we isolated *exo70a2-2* homozygous mutants which were wild-type for *HPAT1* and *HPAT3*. We observed no statistically significant change in seed set between Columbia and *exo70a2-2* (Fig. 3C). However, using a more sensitive competitive fertilization assay, we found significantly reduced male transmission of the *exo70a2-2* allele vs. the WT allele (16.7% transmission efficiency, N=84; χ^2 P-value=5.89×10^{-11}). Therefore, in an otherwise WT background, *exo70a2-2* reduced pollen fitness.

Since we had observed partial rescue of cell wall organization in suppressed PTs (Fig. 2), we compared the PT cell wall organization between WT and *exo70a2-2*. We again used LM19 and LM20 to compare the distribution of dme-HG and me-HG, respectively along with ABF staining to compare callose accumulation. In all three cases, the overall pattern of signal was similar between WT and *exo70a2-2* tubes (Fig. S6). The only difference we observed was an overall reduction of signal intensity for

LM19 (dme-HG) in *exo70a2-2*, though the pattern of low signal at the tip and increasing signal in the shaft was the same for both genotypes. We next used the JIM20 antibody to compare distribution of Hyp-Ara. Similar to our observations for LM19 staining, the overall intensity of JIM20 signal was reduced in *exo70a2-2* PTs, though the pattern was generally flat across the PT length in both genotypes. Therefore, while *exo70a2-2* partially restores PT cell wall organization in the *hpat1/3* background, it did not alter cell wall polarity in the wild-type background.

Our transgenic rescue data (Fig. S5) suggests that the G319E allele is likely a loss or reduction of function allele and the only previously published allele (*exo70a2-D*) is a promoter-region insertion with increased transcript expression with no reported pollen fertility phenotypes (Synek et al., 2017). To gain further insight into the function of this gene, we identified an additional allele with an insertion in the fifth intron of *EXO70A2* among the available insertion mutant collections. Based on RT-PCR analysis of flower cDNA, we found that this insertion mutant (*exo70a2-3*) was a transcriptional null allele (Fig. 3B). Seed set was modestly reduced in homozygous *exo70a2-3* plants compared to the WT background (Fig. 3C-D) and the male transmission efficiency of *exo70a2-3* was also reduced to about half of the *exo70a2-2* value (8.3% transmission efficiency, N=130, χ^2 P-value=5.03×10^{-22}). We next tested *exo70a2-3* for suppression of the *hpat1/3* low-fertility phenotype. Self-fertilized progeny of *exo70a2-3/+ hpat1/3* plants displayed a significant bias towards inheritance of the *exo70a2-3* mutant allele, consistent with a suppressive effect conferring improved transmission of the triple mutant pollen (13% WT, 49% heterozygous, 37% homozygous mutant, N=67 total, χ^2 P-value=7.06×10^{-9}). Seed set in *hpat1/3 exo70a2-3* triple mutants was also significantly increased compared to the *hpat1/3* background, though the *exo70a2-3* allele did not increase seed set to the same degree as the *exo70a2-2* allele (Fig. 3C).

Since *exo70a2* mutants exhibit reduced male fitness in the wild-type background, we analyzed their pollen phenotypes directly. When grown *in vitro* we observed a moderate and strong reduction in pollen germination frequency for *exo70a2-2* and *exo70a2-3*, respectively (Fig. 3E-G). The non-germinated pollen grains appeared morphologically normal and all pollen appeared similarly viable based on Alexander staining [Fig. 3H-J; (Peterson et al., 2010)]. We hypothesize the observed germination

defect was due to failure to target secretory vesicles to the germination site, similar to the pollen germination defect described for other exocyst mutants including *sec3a,* sec6, *sec8, sec15a* and *sec5* (Bloch et al., 2016; Cole et al., 2005; Hála et al., 2008; Y. Li et al., 2017). We examined germination plaque formation using Ruthenium red which stains pectin accumulation (Y. Li et al., 2017). Though WT pollen accumulated pectin at the germination site as expected, most *exo70a2-3* pollen did not, consistent with the low germination frequency in this line (Fig. 3K-L). We further noted that the mutant pollen which successfully germinated produced shorter PTs than the wild type after five hours of growth (Fig. 3M), though they were otherwise morphologically normal (Fig. 3O-P). To determine if this was due to slower rates of PT growth or an indirect effect of delayed germination, we measured the sustained PT growth rate. Following successful germination, *exo70a2-3* PTs elongated at about half the rate observed in WT though the rate of *exo70a2-2* PT growth was not significantly different from that of the WT (Fig. 3N). Therefore, *exo70a2* mutants have both impaired pollen germination and tube elongation, phenotypes consistent with a secretion defect, with the *exo70a2-3* null allele being more severely impaired than the missense allele *exo70a2-2*.

3.3.5 EXO70A2 *localizes to the tip of growing pollen tubes*

Available microarray, mRNA sequencing and proteomic data indicates that *EXO70A2* is most strongly, if not exclusively expressed in pollen and PTs (Grobei et al., 2009; Hruz et al., 2008; Klepikova et al., 2016; Synek et al., 2017). To validate this expression data and determine the sub-cellular localization of EXO70A2, we generated a C-terminal mNeonGreen fusion protein including the native promoter region and full genomic sequence (EXO70A2-mNG). In stably transformed wild-type plants, we observed reporter expression in *in vitro* grown PTs, with no detectable expression in other tissues, in agreement with the reported expression data. To determine if the fusion protein was functional, we transformed homozygous *exo70a2-3* plants with this construct. In contrast to the low germination frequency of *exo70a2-3* pollen, pollen from three independent T1 plants had a significantly higher proportion of germinated pollen grains after two hours and the vast majority of T1 PTs were positive for mNeonGreen

fluorescence, demonstrating that pollen carrying the reporter construct was able to germinate and form elongating PTs while the non-transgenic mutant pollen largely failed to do so (Fig. S7). A similar experiment using the EXO70A2^{G319E} point mutant fused to mNeonGreen resulted in much weaker rescue of pollen germination frequency, suggesting that this mutant is a hypomorph with reduced activity relative to the wild-type sequence (Fig. S7B). In addition to the weaker rescue by the mutant protein, the resulting PTs had noticeably weaker fluorescence than the corresponding wild-type EXO70A2-mNG expression lines, suggesting the mutant protein may be less stable *in vivo*, potentially accounting for its lower activity.

In budding yeast, EXO70p localizes to the target membrane, along with SEC3p, through phospholipid interactions and recruits the remaining, vesicle-associated complex members to the site of tethering (He et al., 2007; Liu et al., 2007). Given the importance of proper vesicle targeting during tip growth, we examined the localization of the EXO70A2:mNG fusion protein in PTs and observed signal at the tip plasma membrane (Fig. 4). This localization pattern was similar to the immunolocalization pattern reported by Hála et al., (2008) in tobacco PTs using an antibody raised against the highly similar EXO70A1. Furthermore, a C-terminal YFP fusion to the tobacco EXO70A2 homologue (NtEXO70A2) was reported to localize to the PT tip, but only occasionally to show PM localization (Sekeres et al., 2017).

3.3.6 exo70a2 mutants reduce Hyp-Ara modified protein secretion at the pollen tube tip

EXO70A2's localization to the PT tip (Fig. 4), combined with the reduced pollen germination and slower PT growth of *exo70a2-3* mutants (Fig. 3) suggested that EXO70A2 is a positive regulator of PT tip growth and likely acting as a canonical exocyst complex member. Therefore, we hypothesized that the suppression of *hpat1/3* by *exo70a2* mutants was due to reduced rates of secretion of one or more key exocyst cargo(s). Hyp-Ara modified proteins themselves are a strong candidate for exocyst-mediated secretion. To develop a secretion reporter to allow us to follow Hyp-Ara modified proteins, we used a portion of a directly validated HPAT substrate, EXT3

(Ogawa-Ohnishi et al., 2013), specifically an arabinosylation motif (SPPPP) and adjacent sequence (KSPPPPVKHLY) inserted into an exposed loop of GFP (Fig. 5A). Insertion into the GFP sequence has been shown to stabilize glycoprotein fusions which are otherwise often subject to terminal tag cleavage and degradation (Yang et al., 2012). We used the EXT3 signal peptide sequence to drive the protein into the secretory pathway and expressed the resulting fusion, GF(EXT3)P, under the Lat52 promoter for pollen expression (Bate & Twell, 1998). We stably transformed this construct into *hpat1/3* plants. To limit potential confounding effects due to expression level variation between independent transgenic lines, we crossed a single, robustly expressing *hpat1/3* GF(EXT3)P line to Col, *exo70a2-2*, *exo70a2-3* and *hpat1/3 exo70a2-2* and isolated the desired genotypes from the resulting F2 populations. As a control, we also transformed a GFP construct with no signal peptide (Lat52::GFP) into Col.

We were able to detect GF(EXT3)P from PT protein samples with an anti-GFP polyclonal antibody at the expected molecular mass of the fusion, ~34 KDa (Fig. 5B). To determine if the fusion protein was arabinosylated, we probed with the JIM20 Hyp-Ara antibody. No native arabinosylated proteins of the GF(EXT3)P mass were observed in un-transformed Col PTs, but we detected JIM20 signal at the observed reporter mass in the GF(EXT3)P transgenic Col line (Fig. 5B). No JIM20 signal was detected from *hpat1/3* or *exo70a2-2 hpat1/3* transgenic samples, consistent with the absence of Hyp-Ara in these genotypes.

In *in vitro* grown GF(EXT3)P-expressing PTs, we observed robust intracellular fluorescence, likely due to the presence of the reporter in the secretory pathway (ER, Golgi and secretory vesicles). To determine if the protein was secreted, we plasmolyzed PTs by transfer to high sucrose media. In PTs, plasmolysis occurs preferentially at the tip region, separating the plasma membrane from the cell wall (Hill et al., 2012). We observed fluorescence signal remaining at the vacated PT tip, suggesting that the protein was secreted into the cell wall space (Fig. 5C). To quantitatively compare secretion between genotypes, we calculated a “Secretion Index” (SI) as a ratio of fluorescence intensity of the cytoplasm-free tip region to the intracellular signal after subtraction of non-tube background. The Col GF(EXT3)P SI was significantly higher

(~3-fold greater) than that of the control GFP construct, demonstrating that the GF(EXT3)P construct was actively secreted (Fig. 5D). This secretion was also partially dependent on *EXO70A2;* the SI was significantly lower in *exo70a2-3* compared to WT PTs, though it was still greater than the SI of the control (Fig. 5E). Interestingly, the SI was increased by ~40% in *hpat1/3* mutants compared to Col, suggesting more rapid secretion of HPAT-target proteins in the absence of the HPATs, despite the lower growth rate of the *hpat1/3* tubes (Fig. S1I). Finally, we found that the Secretion Index was significantly reduced in the suppressed *hpat1/3 exo70a2-2* PTs compared to *hpat1/3*, but was not significantly different from the *exo70a2-2* value. Thus, in addition to the cell wall defects of *hpat1/3* PTs noted above, increased secretion of un-modified HPAT-target proteins may be further confounding the cell wall structure of the mutant PTs.

3.3.7 sec15a mutants also suppress the hpat1/3 fertility phenotype

The above data suggests an important function for *EXO70A2* in the secretion of glycoproteins in PTs. The *exo70a2* mutant phenotypes were also consistent with the defects observed for mutants in other exocyst complex members (Bloch et al., 2016; Cole et al., 2005; Hála et al., 2008; Y. Li et al., 2017). If the underlying mechanism of *hpat1/3* suppression by *exo70a2* is a reduction of exocyst-mediated secretion, mutants in other members of the core exocyst should also suppress the *hpat1/3* fertility defects. Fortuitously, in the course of sequencing additional *frh* suppressor lines, we identified a line carrying a mutation in exocyst complex member *SEC15A,* converting serine 213 to phenylalanine (Table S3, Fig. 6A). *SEC15A* is one of two Arabidopsis *SEC15* genes and is required for male transmission, pollen germination and PT growth (Hála et al., 2008). In the BC5 F2 generation of this suppressor family, we found strong bias against recovery of plants homozygous for the wild-type *SEC15A* allele, as expected for an *hpat1/3*-suppressing mutation (Fig. 6B-C, χ^2 P-value = 1.57×10^{-5}). Following pollination of *hpat1/3* pistils by pollen from *sec15a-3/+ hpat1/3* plants, 90% of the progeny inherited the *sec15a-3* allele (61 heterozygous vs. 7 WT progeny, χ^2 P-value = 5.8×10^{-11}), confirming increased male transmission of the *sec15a*^{S213F} mutation (hereafter *sec15a-*

3) in the *hpat1/3* background. We also found perfect co-segregation between *sec15a-3* and the suppressive phenotype including intermediate seed set values for heterozygous individuals (Fig. 6D). Like *exo70a2-2*, the *sec15a-3* mutant also increased PT lengths *in vitro* in the *hpat1/3* background (Fig. 6E). After outcrossing our suppressor allele to the wild-type Columbia background to remove the *hpat1* and *hpat3* mutations, *sec15a-3* mutants did not display significantly different seed set compared to WT, similar to our observations for *exo70a2-2* (Fig. 6D and Fig. 3C). However, the transmission efficiency of the mutant allele was reduced in the WT background (TE=60.6%, N=249, χ^2 P-value = $1.1x10^{-4}$), indicating a modest fertility cost to pollen carrying the mutant allele.

Given that loss of function *exo70a2* mutants were able to suppress the *hpat1/3* phenotype, we reasoned that the suppression by *sec15a-3* was also due to a loss of function of this core exocyst complex member. Therefore, we next crossed *hpat1/3* to a previously published transcription null T-DNA insertion allele of *sec15a* (*sec15a-2*, SALK_067498; Hála et al., 2008). In plants homozygous for the *hpat1* and *hpat3* mutations, the presence of a *sec15a-2* allele increased seed set with homozygous *sec15a-2* plants being more strongly impacted (Fig. 6D), thus confirming that loss of function of *sec15a* can suppress the *hpat1/3* phenotype. The recovery of homozygous *sec15a-2* plants in the *hpat1/3* background was somewhat surprising since this allele is essential for male transmission in the WT background (Hála et al., 2008).

If *exo70a2* and *sec15a* both suppress the *hpat1/3* fertility defect through disruption of the same protein complex, plants carrying both mutations should exhibit no further suppression relative to the single suppressor mutants. We crossed the two suppressor families to establish the genetic relationship between them. In the double suppressor genotype (i.e. *hpat1/3 exo70a2-2 sec15a-3* quadruple mutants) we observed the same level of seed set as sibling *hpat1/3 exo70a2-2* plants and a minor, but statistically significant (T-test P-value 0.03) increase compared to the *hpat1/3 sec15a-3* siblings (Fig. 6G), consistent with the hypothesis that both suppress through disruption of the core exocyst complex.

3.4 Discussion

PTs grow by the targeted secretion of new cell wall material to their tip. We have previously shown that the plant-specific protein modification hydroxyproline O-arabinosylation (Hyp-Ara) is required for proper PT growth and full male fertility (MacAlister et al., 2016). Here, we report major changes in the organization of the PT cell wall in *hpat1/3* mutants, specifically a loss of PT cell wall polarity and the conversion of the normally extensible cell wall structure at the PT tip into a more shaft-like state (Fig. 2). While immunolocalization studies of cell wall epitopes must be interpreted with caution due to potential epitope masking by interaction between polymers, our results demonstrate a change in cell wall organization in the *hpat1/3* PTs. Once the tip wall is disrupted as in the *hpat1/3* tubes, one would expect cell expansion to be compromised, leading to growth arrest and/or PT rupture. The “branching” observed for *hpat1/3* PTs may be the result of growth being re-directed to a more viable sub-apical cell wall region (Fig. S1). The EXT family of cell wall structural glycoproteins are heavily Hyp-Ara modified, therefore, the most direct explanation for the disrupted cell wall organization of the *hpat1/3* PTs is that the lack of Hyp-Ara prevents proper EXT function in the cell wall, broadly disrupting cell wall organization. The un-modified EXTs may also be toxic to cell wall structure; their presence as un-arabinosylated proteins causing greater disruption to the wall than their absence would. Loss-of-function mutants of the exocyst components *exo70a2* and *sec15a* suppress the *hpat1/3* pollen fertility phenotype, suggesting that reducing the rate of secretion of one or more key exocyst cargoes allows *hpat1/3* PTs to compensate for their defects. This is apparent as a partial restoration of PT cell wall organization, particularly a reduction of the anomalous accumulation of dme-HG and callose at the PT tip (Fig. 2) and an increased PT growth rate (Fig. S1I).

To determine if HPAT-modified proteins themselves are trafficked through the exocyst, we generated a Hyp-Ara modified secreted reporter (GF(EXT3)P). The secretion index (SI) of GF(EXT3)P was significantly reduced in PTs of the null *exo70a2-3* allele compared to WT PTs (Fig. 5), indicating that reporter secretion was, at least partially, *EXO70A2* dependent. However, the *exo70a2-3* GF(EXT3)P SI was still above the SI of the GFP control. Thus, there may be exocyst-independent secretion of

GF(EXT3)P, or functional redundancy within the 23 member *EXO70* gene family. Several other *EXO70* genes are expressed in PTs and two (*EXO70C1* and *EXO70C2*) have demonstrated PT functions, though their mutant phenotypes are qualitatively distinct from those of other exocyst complex mutants, suggesting they may be regulators of exocyst function rather than canonical exocyst components (et al., 2009; Li et al., 2010; Synek et al., 2017; Hruz et al., 2008; Klepikova(Chong et al., 2010; Grobei et al., 2009; Klepikova et al., 2016; S. Li et al., 2010; Synek et al., 2017). A recent preprint characterizing a CRISPR/Cas9 induced *exo70a2* mutant allele agrees with our findings with respect to the importance of *EXO70A2* for pollen germination and pollen tube elongation, further supporting its central role in PT exocytosis (Marković et al., 2019). Furthermore, reduced secretion of Hyp-Ara modified proteins in *exo70a2* mutants would also be consistent with the reduced levels of JIM20 staining we observed in *exo70a2-2* PTs (Fig. S6). The reduced SI of the GF(EXT3)P reporter in the *exo70a2* mutant indicates that the protein is being retained cytoplasmically. This retention may be occurring in secretory vesicles, at earlier points in the secretory pathway (e.g. the Golgi apparatus), or in another compartment. Determining the site of retention will require co-localization with sub-cellular markers. We also found that *hpat1/3* PTs had the highest GF(EXT3)P SI of any genotype (Fig. 5). Enhanced secretion of a glycoprotein in the absence of the relevant glycosyltransferases has been previously noted in other systems, though the underlying mechanism is unknown. For example, in budding yeast, mutation of mannosyltransferases required for N-linked hypermannosylation of cell wall glycoproteins resulted in increased secretion of modified heterologous proteins (Tang et al., 2016). Knockdown of Golgi stacking proteins also led to reduced glycosylation and accelerated secretion (Xiang et al., 2013). The underlying cause of increased glycoprotein secretion in *hpat1/3* is unclear. Partial arabinosylation could serve as a Golgi retention signal, preventing premature target protein secretion, and since the *hpat1/3* PTs cannot initiate arabinosylation, such a retention signal would be absent. Alternatively the presence of the HPAT enzymes themselves may be required for target protein retention. The *hpat1* and *hpat3* alleles are transcriptional nulls (MacAlister et al., 2016), thus any protein/protein interactions they participate in would be disrupted in *hpat1/3* mutants. Alternatively, other compensation

pathways may be activated in the hapt1/3 tubes, leading to an indirect increase in secretion. Regardless of the cause of the elevation in *hpat1/3* PTs, the secretion index was significantly reduced in *exo70a2-2 hpat1/3* PTs.

While the GF(EXT3)P secretion reporter showed that the secretion rate was altered for a synthetic HPAT-modified protein, which native protein(s) are important for PT growth is more difficult to determine. The list of candidate proteins for HPAT-modification is long, and includes the 20 classical Arabidopsis EXTs and multiple EXT-chimera families including the LRX, PERK and class I FH proteins (Showalter et al., 2010). Several members of each of these gene families are expressed in pollen. For example, six members of the *PERK* family of 15 genes are highly or exclusively expressed in pollen samples in Arabidopsis (Borassi et al., 2016). The class I Formin Homology genes, *FH3* and *FH5*, are also expressed in pollen and known to be important regulators of PT growth through their regulation of the actin cytoskeleton (Cheung et al., 2010; Cheung & Wu, 2004; Ye et al., 2009). The *LRX* genes include four members (*LRX8-11*) which are expressed specifically in pollen and have been shown to redundantly contribute to pollen fertility. Higher order *lrx* mutants displayed reduced pollen germination, abnormal PT morphology and frequent tube (Fabrice et al., 2018; Feng et al., 2017; Sede et al., 2018). LRX proteins have also been shown to bind to the RALF4/19 peptides and participate in an autocrine signaling loop maintaining PT integrity until reaching the ovule (Mecchia et al., 2017). Furthermore, Fabrice et al. (2018) also demonstrated reduced levels of JIM20 signal in *lrx8/9* and *lrx8/9/11* mutant PTs. This could be interpreted as a direct reduction in Hyp-Ara in these mutants due to reduced LRX protein levels, though an indirect effect involving feed-back with other modified proteins can't be ruled out.

In addition to the EXTs and EXT-chimeras, a second, unrelated group of HPAT-modified proteins is currently known, the small secreted signaling peptides of the CLAVATA3/EMBRYO-SURROUNDING REGION-RELATED (CLE) family. Mutants of HPAT family members from tomato, Medicago truncatula and Lotus japonicus function in the regulation of shoot meristem size and the determination of nodule number through their effect on CLE peptide arabinosylation (Imin et al., 2018; Kassaw et al., 2017; Schnabel et al., 2011; Xu et al., 2015; Yoro et al., 2019). While the participation of

an HPAT-modified CLE peptide in PT growth is an intriguing possibility, no candidates for such a pollen-expressed CLE are forthcoming (Kanaoka & Higashiyama, 2015).

Moreover, while we demonstrated reduced secretion of a Hyp-Ara modified reporter protein in the suppressed PTs (Fig. 5D), this does not preclude the trafficking of other cargoes through the exocyst. Slowing the delivery of cell wall polysaccharides or non-arabinosylated cell wall modifying enzymes may also contribute to *hpat1/3* suppression by exocyst mutants. In the PT, pectins are initially secreted in the methyesterified form and then de-methylesterified in the wall by pectin methyl esterases (PMEs), which are in turn regulated by PME inhibitors [PMEIs; (Bosch & Hepler, 2005)]. Altering the rate of delivery of pectin, PME and/or PMEI proteins could alter the timing of de-methylesterification in the PT wall. There is evidence of exocyst involvement in pectin secretion in the specialized seed coat mucilage cells (Kulich et al., 2015). The exocyst is also involved in the secretion of cellulose synthase complexes (Zhu et al., 2018) and may be trafficking other, similar complexes in the PT, for example, callose synthases.

Evidence is mounting that secretion is likely to be more complex than a simple bulk flow of Golgi material to the plasma membrane. Data from budding yeast has shown distinct post-Golgi secretory vesicles carrying different sets of cargoes marked by the presence of Bgl2p or invertase, with mutations in *exo70* predominantly blocking secretion of Bgl2p-containing vesicles (Harsay & Bretscher, 1995; He et al., 2007). In plant cells there is also evidence of distinct trafficking pathways for reporter proteins vs. cell wall polysaccharides (Leucci et al., 2007). The trafficking landscape of PTs is likely to be complex and subject to tight regulation.

3.5 Materials and Methods

3.5.1 Plant growth conditions and materials

Arabidopsis thaliana plants of the Columbia-0 ecotype were grown under 16-hour light: 8-hour dark cycles in a temperature-controlled growth room maintained at 23˚C. Recovery of *hpat1-2* (Salk_120066) *hpat3-1* (Salk_085603) double mutants has been

previously described (MacAlister et al., 2016). *frh* mutants were induced by treatment of *hpat1/3* seeds with 0.2% EMS for 12 hours. Seeds from the mutagenized plants were collected in pools of 5-10 M1 plants and ~96 M2 individuals per pool were screened for increased silique length and higher seed content. *frh* candidates were genotyped for the *hpat1* and *hpa3* mutant alleles to confirm homozygosity and backcrossed to the *hpat1/3* background for four generations. The *exo70a2-3* [WiscDsLoxHs216_02A; (Woody et al., 2007) and *sec15a-2* (SALK_067498; Alonso et al., 2003) insertion alleles were obtained from the ABRC. Mutants were genotyped using the primers listed in Table S4. RT-PCR for *exo70a2-3* knockout validation used the *EXO70A2* primers given by Synek et al. (2017) and primers from Table S4. The *rra2* (SAIL_244_A03)*, rra3* (Gabi 223B05), *xeg113-3* (SALK_058092)*,* and *exad1-1* (SAIL_843_G12) insertion alleles were genotyped using the primers listed in Table S4. To clear siliques for seed counts, fully expanded, but unripe siliques were transferred to 70% ethanol for at least two days, after which, the ethanol was replaced with 50% glycerol for several more days.

3.5.2 Whole-genome sequencing

After four generation of backcrossing of the *frh* plants to *hpat1/3*, suppressed F2 plants were crossed as females to *hpat1/3* plants to identify homozygous and heterozygous individuals based on suppression segregation in the cross progeny. Self-fertilized seeds from confirmed homozygous BC4 F2 plants were germinated on MS media plates for DNA extraction as were seeds of the *hpat1 hpat3* background strain. Tissue for the FRH/FRH pool was collected from non-suppressed plants produced by the heterozygous test cross progeny. DNA was extracted from the tissue pools using the Qiagen Plant DNA Mini kit according to the manufacturer's instructions, followed by concentration by ethanol precipitation. Libraries were generated using Illumina TruSeq DNA kits and barcoded for multiplexing by the University of Michigan DNA Sequencing Core. Samples were sequenced on the Illumina HiSeq-4000 platform with paired-end 150 bp cycles. Sequence reads were checked for quality using FastQC then aligned to the TAIR10 genome using Bowtie2, and sequence variants were called using Freebayes. Additional analysis steps were performed with Samtools. We identified all

the mutations in each suppressor family and removed mutations that were also present in the *hpat1/3* and/or the FRH/FRH samples. We then filtered the mutations based on allelic frequency ≥ 0.8, mutation type = SNP and read number ≥ 4. We annotated the sequence variants for context and predicted effect using a custom PERL script.

3.5.3 JIM20 dot blot and western blot analysis

Total non-covalently-bound protein was extracted from Col, *hpat1/2/3*, *rra2/3*, *xeg113* and *exad* seedlings grown on MS plates using a procedure modified from Fry (1988). Tissue was ground in liquid nitrogen and resuspended in freshly prepared solution A (100ml acetic acid, 250ml 80% w/w phenol), stirred rapidly in a fume hood at 70°C for 30 minutes, and cooled prior to filtering through GF/C glass fiber paper in a 4.25cm porcelain Buchner funnel (VWR, 470153-508). The residue was rinsed twice with 5ml of solution B (35ml solution A, 5ml H_2O), then 2.5ml of 10% ammonium formate. 255ml acetone was added to the filtrate, and incubated on ice for an hour. The protein precipitate was spun in PYREX™ round-bottom glass centrifuge tubes (Fisher, 05-558-5B) for 5 minutes at 2,500 x g, the supernatant discarded, and the pellet resuspended in 10ml 10% acetone. After a second spin for 5 minutes at 2,500 x g, the protein was resuspended as much as possible in a minimal volume of H_2O (1-5ml) and its concentration determined using a BCA protein assay kit (Pierce, 23225). For dot blots, 5μg of total protein extract was spotted onto 0.2μm nitrocellulose and allowed to dry prior to immuno-processing. For western blots, 15μg of total protein extract was separated by 10% mini-PROTEAN® TGX™ (Bio-Rad, 456-1033) gel electrophoresis and transferred onto a 0.2μm PVDF membrane (Bio-Rad, 170-4156) using the Trans-Blot® Turbo™ transfer system. Dot blots and western blots were then blocked for 1 hour (5% milk, in 1x TBST), probed with 1:10 JIM20 monoclonal rat IgM primary antibody (Carbosource) in blocking buffer in a sealed polypropylene envelope overnight at 4°C, washed 3 times with 1x TBST for 10 minutes, probed with goat anti-rat IgG H+L secondary antibody (Fisher, PI31629), washed twice with 1x TBST for 10 minutes, once with 1x TBS for 10 minutes, treated with chemiluminescent substrate (Immobilon, WBKLS0500) and analyzed on CL-XPosure film (Fisher, 34090).

3.5.4 Pollen assays

All pollen germination and growth assays were carried out using *in vitro* pollen growth media (PGM) modified from (Rodriguez-Enriquez et al., 2013) composed of 10% sucrose, 0.01% boric acid, 1mM $CaCl_2$, 1mM $Ca(NO_3)_2$, 1mM KCl, 0.03% casein enzymatic hydrolysate, 0.01% myo-inositol, 0.1 mM spermidine, 10mM γ-Aminobutyric acid, 500μM methyl jasmonate, pH adjusted to 8.0 and solidified with 1% low melting temperature agarose. The agarose was dissolved by slow heating on a 100°C stir plate and the media was poured into 35 mm petri plates. When solidified, the media was covered with a piece of cellophane. To germinate and grow PTs *in vitro*, pollen from recently opened flowers was dusted directly onto the cellophane and the PGM plates were placed in a humid chamber consisting of a plastic box with damp paper towels. For PT length measurements pollen was allowed to grow for five hours before tubes were imaged with a dissecting microscope equipped with a camera. PTs were measured using ImageJ. For PT width measurements PTs were imaged on a compound microscope using a 20X objective after 3 hours of growth *in vitro*. Three measurements were made across the width of each tube ≥ 10 μm from the pollen grain and tip using ImageJ. The measurements were averaged to generate a single width measurement per tube. To determine PT rupture frequency PTs were imaged after 3 hours of growth and the number of ruptured tubes was divided by the total number of PTs analyzed.

To measure PT growth rates, pollinated PGM plates were immobilized in 100 mm x 15 mm petri dishes with double-sided tape, and pieces of damp paper towel were placed in the larger petri dish to maintain high humidity. These plates were then placed directly on the stage of a dissecting microscope (equipped with a camera) and not moved for 3 hours of imaging. To determine sustained growth rates, images of the same field of PTs were taken at 20-minute intervals. PT lengths were measured at each time point, the change in length calculated and growth rate determined by dividing the number of minutes between images. The growth rates from every interval of every PT for each genotype was averaged to generate an overall “global” growth rate value. At least 30 PTs were analyzed for each genotype. To determine the length of pre-rupture

growth stalling in *hpat1/3* PTs, the above procedure was followed with the imaging interval reduced to 5 minutes and the time of rupture noted.

Protein extraction from pollen tubes and western blot analysis

Protein extraction from PTs was performed as described in (Chang & Huang, 2017) with slight modifications. Flowers were collected in 1.5 ml microcentrifuge tubes and suspended in 1 ml agarose-free PGM. The tubes were vortexed for 1 minute and incubated at room temperature in the dark for 3-5 hours with agitation. Flower debris was removed with forceps and PTs were collected by centrifugation at 12,000 RPM for 2 minutes. The supernatant was removed and the pollen pellet tube was placed on ice. Using a polypropylene pestle, the pellet was ground for 1 minute and then incubated in K-HEPES protein extraction buffer buffer (20 mM HEPES, pH 7.0, 110 mM K-acetate, 2 mM $MgCl_2$, 0.1% Tween 20, 0.2% Triton X-100, 1 mM PMSF) for 1 hour on ice. The tubes were then centrifuged at 14,000 RPM for 20 minutes. The soluble fraction in the supernatant was removed and the insoluble fraction/pellet was resuspended 2x Laemmli sample buffer with β-mercaptoethanol, diluted 1:1 with K-HEPES buffer, and then heated to 95°C for 10 minutes. For western blots, the insoluble protein extract was separated by SDS-PAGE (15% polyacrylamide) and transferred onto a nitrocellulose membrane using the Trans-Blot® Turbo™ transfer system. Membranes were then blocked for 1.5 hours with 5% milk in 1x TBST, and probed with either 1:10 JIM20 monoclonal rat IgM primary antibody (Carbosource) or 1:1000 anti-GFP polyclonal rabbit IgG (Life Technologies) in blocking buffer in a sealed polypropylene envelope overnight at 4°C with agitation. The next day, membranes were washed 3 times with 1x TBST for 10 minutes, probed with either goat anti-rat HRP-conjugated secondary antibody (for JIM20) or anti-rabbit HRP-conjugated secondary antibody (for anti-GFP), sealed in a polypropylene envelope and incubated at room temperature for 1.5 hours with agitation. Membranes were then washed twice with 1x TBST for 10 minutes, once with 1x TBS for 10 minutes, treated with chemiluminescent substrate (SuperSignal West Femto Maximum Sensitivity Substrate) for 5 minutes and imaged with a LI-COR Odyssey Fc Dual-Mode Imaging System.

3.5.5 Cloning

For the transgenic rescue construct, the *EXO70A2* gene was amplified from Columbia-0 in a single fragment including the native promotor (376 bp), coding region and the 3' sequence up to the first predicted Polyadenylation site using the primers in Table S4 with Phusion® High-Fidelity DNA Polymerase (NEB, M0530S). For C-terminal fusion to mNeonGreen, the *EXO70A2* sequence was amplified from the promoter to the last coding codon from either Columbia-0 or the *exo70a2-2* mutant. The resulting fragments were cloned into Gateway® entry clones via BP Clonase II™ (Invitrogen, 11789-020). The transgenic rescue construct was recombined via LR Clonase II™ (Invitrogen, 11791-020) into the pFAST-G01 binary vector (Shimada et al., 2010) and the localization reporters were recombined into a modified pFAST-R07 vector in which the GFP sequence was replaced with mNeonGreen. Due to restriction site limitations, a portion of the pFAST-R07 vector was amplified, using the Phusion® High-Fidelity DNA Polymerase (NEB, M0530S) alongside the mNeonGreen fusion protein, and the two fragments joined by overlap extension PCR. The GFP sequence was removed from pFAST-R07 by NruI and MluI restriction digestion and the mNeonGreen-containing fragment inserted using T4 DNA Ligase (Promega, M1801) to make pFAST-mNG.

The GF(EXT3)P construct was generated through the following steps. *pPS48-35SPro-GF-Muc1-P-35S-term* is an intermediate vector previously assembled for embed *GFP* cloning (Yang et al., 2012) where the signal sequence (*At*SS) was derived from the N-terminal signal peptide sequence of *A. thaliana* Basic endochitinase B (Uniprot: P19171). Firstly, the *GF-Muc1* fragment was obtained by *PstI*/*BamHI* double digestion and used as template for PCR with primers FReplace and RReplace. The resulting GF-Muc1 fragment was cloned into the multiple cloning site of pPS48. The two EXT3 encoding oligos, pYi1 and pYi2 were inserted into the NcoI/BamHI site of pPS48 vector. The entire fragment CaMV35S-*At*SS-GF(EXT3)P-NosTerm was excised using *XbaI* and ligated into pGreen0179, yielding the plant expression plasmid pGreen0179-35SPro-*At*SS-GF(EXT3)P-NosTerm. The *At*SS sequence in this construct was substituted with the signal sequence of EXT3 (At1g21310) by an In-Fusion cloning (Takara #638933), using the primer sets p162 and p164 on *35SPro-At*SS-*GF(EXT3)P-NosTerm* to obtain the fragment containing the 35S promoter from pGreen and EXT3

signal peptide overlap and the primer set p163 and p165 on *35SPro-AtSS-GF(EXT3)P-NosTerm* to obtain signal peptide overlap, imbed GFP and 35S terminator. The vector fragment was obtained from V26 (pUC57, including Synthetic gene fragments and AttL sites, obtained from Genescript) digested with SpeI and XbaI for directed insertion of *35SPro-EXT3ss* and *EXT3ss-GF(EXT3)P-NosTerm* into the vector fragment using the In-Fusion Cloning kit. The LAT52 promoter for pollen expression was amplified from tomato genomic DNA using the primers in Table S4. The EXT3ssGF(Ext3)P fragment was amplified from the *EXT3ss-GF(EXT3)P-NosTerm* plasmid, incorporating attB2 and attB5 sites in the forward and reverse primers, respectively (GF(EXT3)P F and GF(EXT3)P R). The LAT52pro and EXT3ssGF(EXT3)P fragments were cloned into their respective Gateway® entry vectors via BP Clonase II™ (Invitrogen, 11789-020). The LAT52pro and EXT3ssGF(EXT3)P entry clones were combined with the pFAST-G01 vector (Shimada et al., 2010) by two-fragment recombination using LR Clonase II™ (Invitrogen, 11791-020). The control LAT52:GFP construct was generated by one-fragment LR Clonase II™ (Invitrogen, 11791-020) recombination between a LAT52pro entry vector and pFAST-G07, which contains the GFP coding sequence (Shimada et al., 2010).

3.5.6 Microscopy

For immunolocalization, PTs were fixed, imaged and analyzed as described in Chebli et al. 2012, with several modifications. PTs were grown in agarose-free PGM for at least 2 hours, then the media with PTs was transferred to a 12 x 75mm polystyrene culture test tube. PTs were collected by centrifugation at 1000 rpm for 2 minutes with low acceleration and deacceleration and the growth media was removed. For fixation, PTs were resuspended in 3.5% formaldehyde in PIPES buffer (50 mM PIPES, 1 mM EGTA, 5 mM $MgSO_4$, 0.5 mM $CaCl_2$, pH 7) and vacuum infiltrated for 20 minutes. After fixation, PTs were washed three times with PIPES buffer and then three times with PBS + 3% BSA. After the final wash, PTs were resuspended in primary antibody and incubated at 4°C overnight with gentle agitation. Primary antibodies were diluted in PBS + BSA to the following concentrations: JIM20- 1:5, LM19- 1:10, LM20- 1:5 (antibodies

obtained from PlantProbes). The next day, the tubes were spun and down and primary antibody was removed, and PTs were washed three times in PBS + BSA. Anti-rat-FITC-conjugated secondary antibody (diluted 1:100 in PBS + BSA), was added, and the tubes were incubated at room temperature in the dark for 2 hours. After incubation, PTs were washed three times with PBS followed by three washes with DI water. PTs were then resuspended in mounting media (0.1% gelatin and 10% ethanol), transferred to slides with a pipette, and slides were stored overnight in the dark at room temperature to allow PTs to settle onto the mounting media. The next day, VectaShield was added to the slides, covered with a #1.5 coverslip, sealed with nail polish, and stored at 4^{o} C.

Imaging was performed with a Leica SP5 laser-scanning confocal microscope. To image FITC signal, we used a 488 nm excitation laser, an RSP 500 dichroic beam splitter, and detectors were set to capture light with a wavelength range of 495-600 nm. For each different experiment, the imaging settings including laser intensity, gain, line averaging and frame accumulation were adjusted so that the signal from the overall brightest tube was just below saturation; all images for a single experiment were taken with identical settings. Z stacks were taken throughout the entire volume of each PT. Z slice step sizes were automatically optimized and maximum intensity projections were generated using LAS-AF software. N ≥ 30 PTs for each genotype. Images were analyzed using ImageJ. To measure fluorescence signal intensities, a line was drawn using the segmented line tool along the periphery of the PT starting from the center of the PT tip towards the pollen grain, or as far as the possible. Two measurements were performed for each PT along each periphery/side. ImageJ's "Plot profile" tool was used to measure pixel grey value along distance, with distance = 0 representing the tip apex. For a single PT, the values of each side were averaged to generate a single measurement, and the measurements of all PTs were averaged within each genotype.

For aniline blue staining, PTs were grown *in vitro* on PGM plates with cellophane for 2 hours. A drop of 0.1 mg/ml aniline blue fluorochrome (ABFC, Biosupplies Australia Pty. Ltd.) diluted 1:70 in 0.1 M KH_2PO_4, pH 10 was added to a microscope slide, and PTs were transferred to the slide by dabbing the cellophane on the ABFC solution. Nail polish was applied to the slide surrounding the PTs and a coverslip was mounted onto the nail polish. PTs were imaged with a Leica SP5 laser-scanning confocal microscope,

using a UV excitation laser with 405 nm wavelength, a Substrat dichroic beam splitter, and detectors were set to capture light with 411-502 nm wavelengths. Image acquisition and analysis was carried out as above for immunolocalization.

For imaging of EXO70A2-mNG fusions PTs were grown *in vitro* on PGM plates with cellophane for 2 hours. After growth time, the cellophane was transferred to a slide and a drop of agarose-free PGM with 4 µM FM4-64 was added on top of the cellophane and PTs. Nail polish was applied to the slide and a coverslip was added on top of the nail polish, covering the liquid media. PTs were imaged using a Leica SP5 laser-scanning confocal microscope 10 minutes after FM4-64 application. To image EXO70A2-mNG*,* we used an excitation laser with 488 nm wavelength, a RSP500 dichroic beam splitter, and detectors were set to capture light with a wavelength range of 494-575 nm. To image FM4-64, we used an excitation laser with 514 nm wavelength, a DD 458/514 dichroic beam splitter, and detectors were set to capture light with a wavelength range of 620-783 nm.

To analyze secretion of the GF(EXT3)P reporter, PTs were grown for 1-2 hours under normal *in vitro* conditions on PGM plates with a layer of cellophane. To induce plasmolysis, PTs were transferred to PGM plates containing 25% sucrose (vs. 10% for standard plates), without cellophane. Plasmolysis could be observed within a few minutes of transfer. Plasmolyzed PTs that were expressing GF(EXT3)P were imaged at 40x magnification using a Leica DM5500 compound microscope. To measure fluorescent signal intensity at the plasmolyzed cell wall region, a region of interest (ROI) was drawn in the entire plasmolyzed region using the differential interference contrast (DIC) channel, excluding the plasma membrane boundary. This ROI was then added to the fluorescent channel and mean fluorescence intensity was measured. For the cytoplasm measurements, two ROIs approximately 5 μm^2 were selected about 10-20 µm from the plasma membrane, and the mean fluorescence intensities of each cytoplasmic ROI were averaged. The average of three background measurements was subtracted from both the cell wall and cytoplasm measurements. The secretion index (SI) was calculated as the ratio of cell wall/cytoplasm signal. A minimum of 30 tubes per genotype were measured and statistical significance was determined using the Benjamini–Hochberg False Discovery Rate with FDR = 0.05.

3.6 Data Availability Statement

High-throughput sequence data is available from the NCBI Sequence Read Archive (https://www.ncbi.nlm.nih.gov/Traces/study/?) under project accession number PRJNA574113. All other material and data are available upon request from the corresponding author.

3.7 Acknowledgments

This material is based upon work supported by the National Science Foundation under Grant No. IOS-1755482. This work was also supported by the Danish Councils for Strategic and Independent Research (12-125709, 12-131859) and the Copenhagen University Excellence Program for Interdisciplinary Research (CDO2016). We wish to thank Gregg Sobocinski for microscopy assistance and advice.

3.8 Author Contributions

Cora MacAlister designed the study, conducted the *frh* mutant screen and wrote the paper. Steven Beuder carried out all immunofluorescence, microscopy, bioinformatic analysis of whole genome sequences to identify candidate suppressor mutations, functional rescue assays, and performed crosses and PT phenotyping. Bent L. Petersen and Svenning Rune Moeller generated the 35S::EXT3ssGF(EXT3)P construct and the *rra2/3* double mutant. Alexandria Dorchak carried out all other cloning and the JIM20 dot blot and western blots. Ashwini Bhide conducted genotyping and genetic co-segregation experiments. All authors edited the manuscript.

3.9 Conflicts of Interest

The authors declare no conflicts of interest.

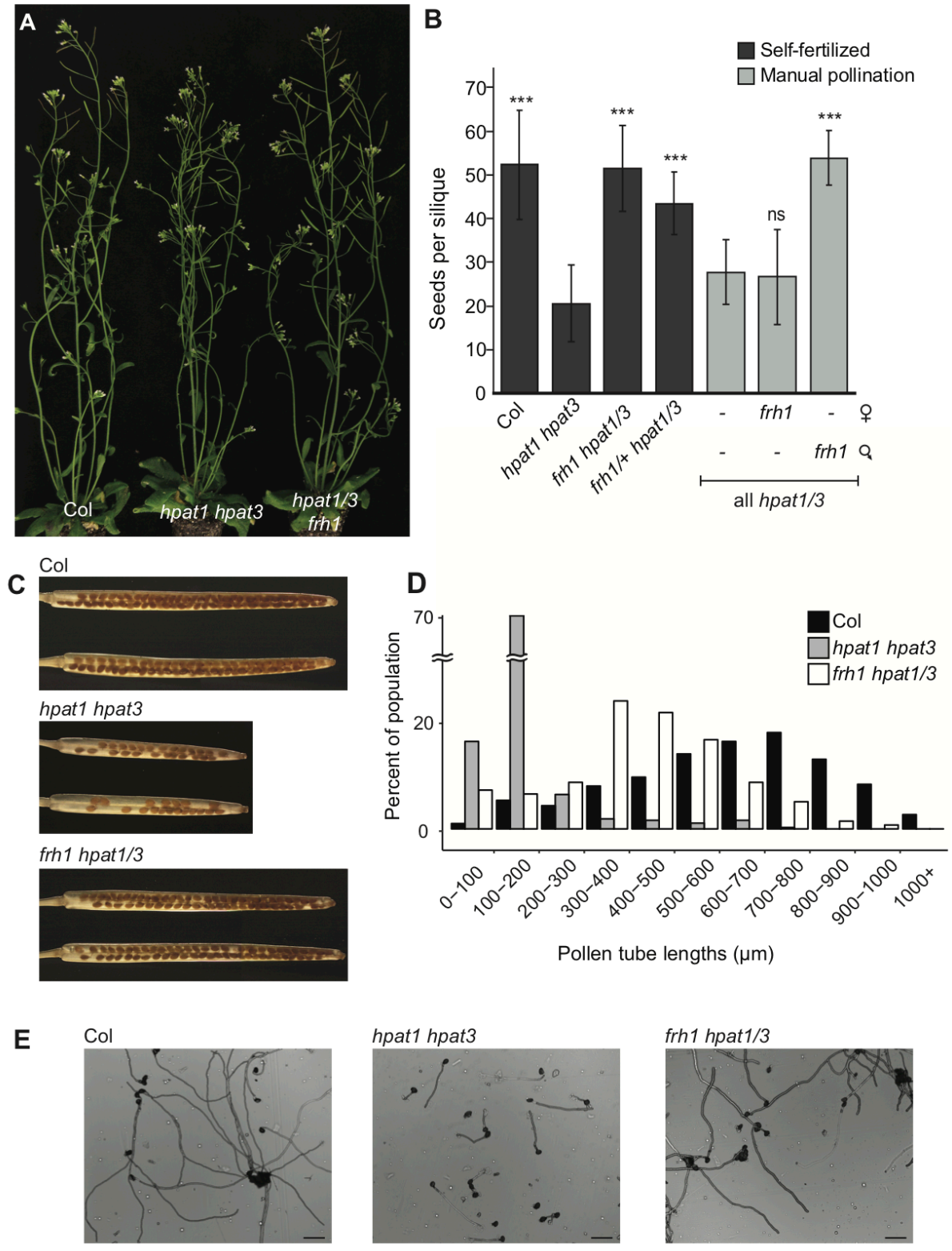

Figure 3-1. Suppressor mutant frh1 increases the pollen fertility of hpat1 hpat3 plants. A) Both double mutant hpat1/3 plants and the suppressed triple mutant frh1 hpat1/3 plants appeared morphologically

*normal aside from differences in seed set. B) Average number of seeds per silique (±SD, N≥10 per genotype) for the indicated genotypes. The low seed set phenotype of hpat1/3 double mutants is suppressed by frh1. High seed set is also observed for heterozygous frh1 plants. Reciprocal crosses between hpat1/3 and frh1 hpat1/3 plants demonstrated that frh1 suppression occurs in the pollen. '***' indicates a statistically significant difference (T-test P-value <0.0005) compared to the hpat1/3 value for either the self-fertilized siliques or manually pollinated samples. NS is not significantly different. C) cleared siliques of WT Columbia, hpat1 hpat3 and frh1 hpat1/3 plants. WT and frh1 hpat1/3 images are composite images to allow full silique imaging. D) Histogram of distribution of PT lengths after five hours of in vitro growth for the indicated genotypes. Data for all genotypes are statistically significantly different from both other genotypes (T-test P-value <0.005). E) In vitro grown PTs of the indicated genotypes. Scale bar = 100 µm.*

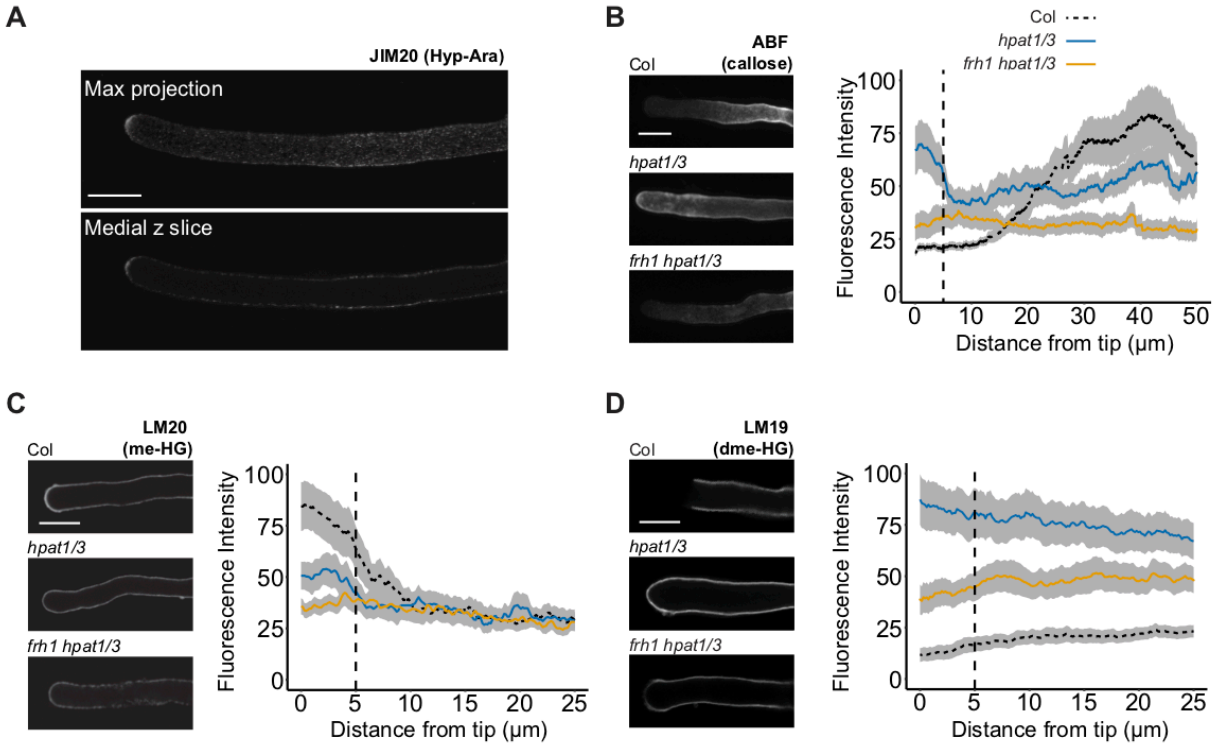

Figure 3-2. frh1 partially suppresses the disrupted polarity of cell wall polymers in hpat1/3 pollen tubes. A) Wild-type Columbia-0 PT stained with JIM20 primary antibody and anti-rat FITC-conjugated secondary antibody. B) Left: Maximum projections of PTs stained with aniline blue fluorochrome (ABF). Right: quantification of signal intensity from the tip (distance on x-axis = 0) to 50 µm down the shaft of the PT (see Materials and Methods for more details concerning image analysis). Colored lines represent the mean fluorescent intensities for each genotype, and shading represents standard error. N ≥ 30 for each genotype. Vertical dashed line represents the approximate region of the PT where the apical dome transitions to the shaft. C) Left: Medial Z-slices of PTs stained with LM20 primary antibody and anti-rat FITC-conjugated secondary antibody. Right: quantification of fluorescence intensity as in B except measurements were taken to 25 µm from the tip. D) Left: Medial Z-slice of PTs stained with LM19 primary antibody and anti-rat FITC-conjugated secondary antibody. Right: quantification of signal intensity as in C. All images were acquired by confocal microscopy at 100x magnification and all scale bars = 10 µm.

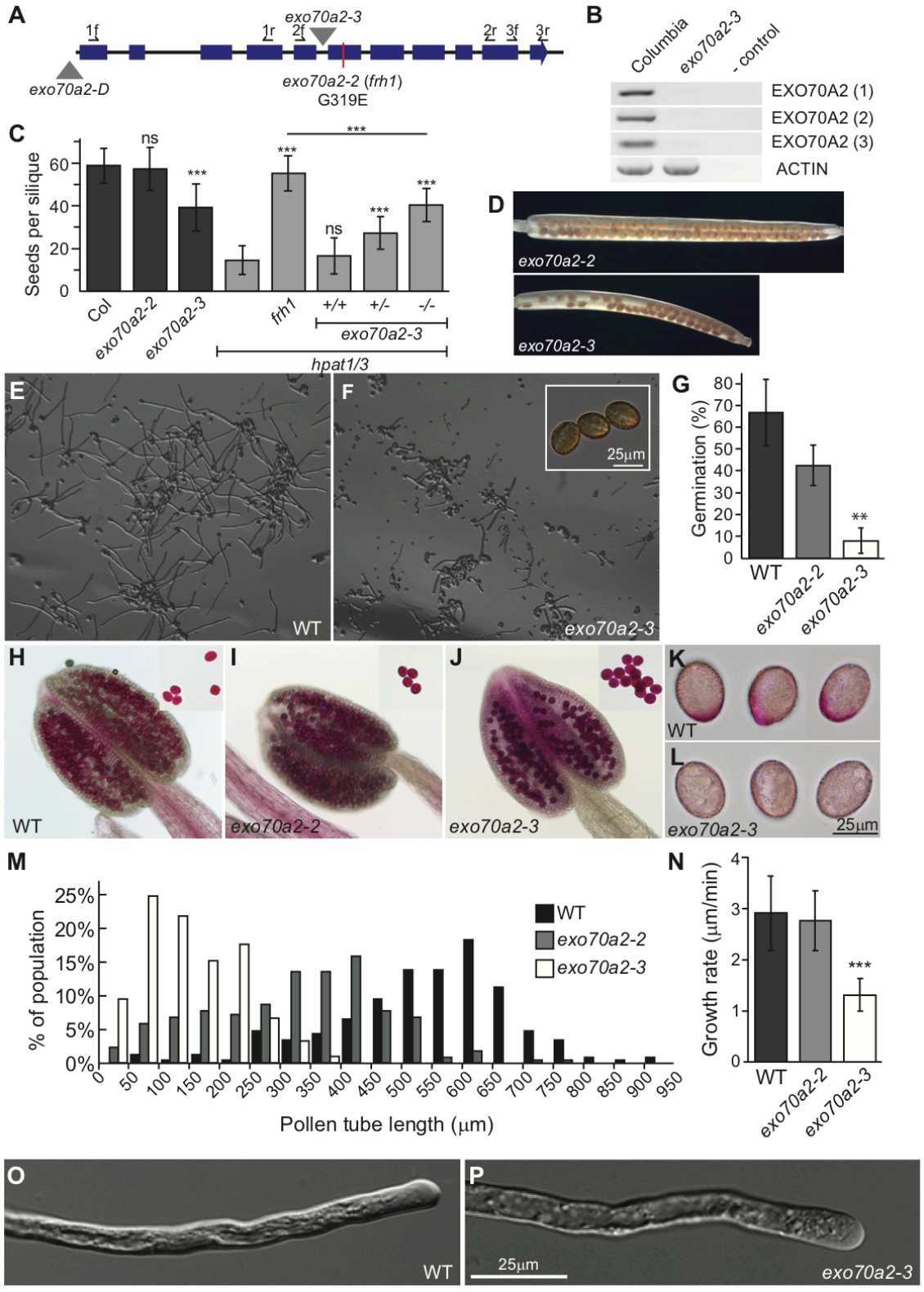

Figure 3-3. EXO70A2 is required for efficient pollen germination and pollen tube growth. A) Diagram of the EXO70A2 coding sequence with the position of the exo70a2-2 (G319E) missense mutation and insertion mutants exo70a2-D (Hála et al., 2008) and exo70a2-3 marked. B) Semi-quantitative RT-PCR of

*flower cDNA samples from the indicated genotypes showing absence of transcript in the exo70a2-3 plants using the primer pairs indicated in A. C) Average number of seeds per silique (±SD) for plants of the indicated genotype. Note the modest reduction in seed set for exo70a2-3 in the wild-type background along with partial suppression of the hpat1 hpat3 phenotype by this mutation. '***' mark statistically significant differences with the corresponding background (Columbia or hpat1 hpat3, T-test P-value <0.0005, N≥12). D) Cleared siliques of the exo70a2 mutant alleles in the Columbia background, see Fig. 1D for Col comparison image. E and F) in vitro pollen germination samples of Columbia (E) and exo70a2-3 (F) three hours after transfer to growth media. Inset in F shows non-germinated exo70a2-3 pollen grains. G) Quantification of pollen germination frequencies for WT, exo70a2-2 and exo70a2-3. Mean of three replicates of ≥740 pollen grains, +/- SD. '**' marks significant difference between WT (T-test P-value <0.005). H-J) Alexander viability staining of anthers of WT (H), exo70a2-2 (I) and exo70a2-3 (J). Insets show free pollen grains. Note no difference in viability staining between genotypes. K and L) Pollen grains stained with Ruthenium red to mark pectin accumulation at the germination plaque. M) Histogram of PT lengths after five hours of in vitro growth for the indicated genotypes. Data for all genotypes are statistically significantly different from both other genotypes (T-test P-value <0.005, N≥200 per genotype). N) sustained growth rate of PTs of the indicated genotype. Mean, N≥21 tubes, ±SD. O and P) Differential interference contrast (DIC) micrograph of PTs.*

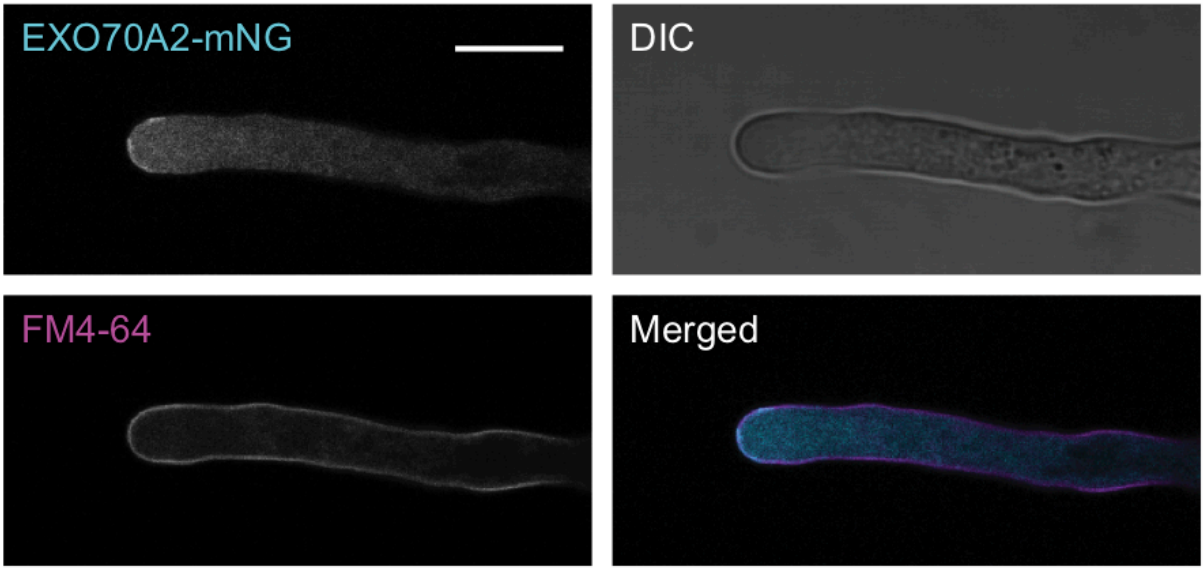

Figure 3-4. EXO70A2 localizes to the tip of growing pollen tubes.Representative PT expressing EXO70A2:mNG under its native promoter and co-stained with FM4-64 to visualize the plasma membrane. Single channels and merged image shown; overlapping signal is false-colored white. Imaged with confocal microscopy at 100x magnification. Scale bar represents 10 µm.

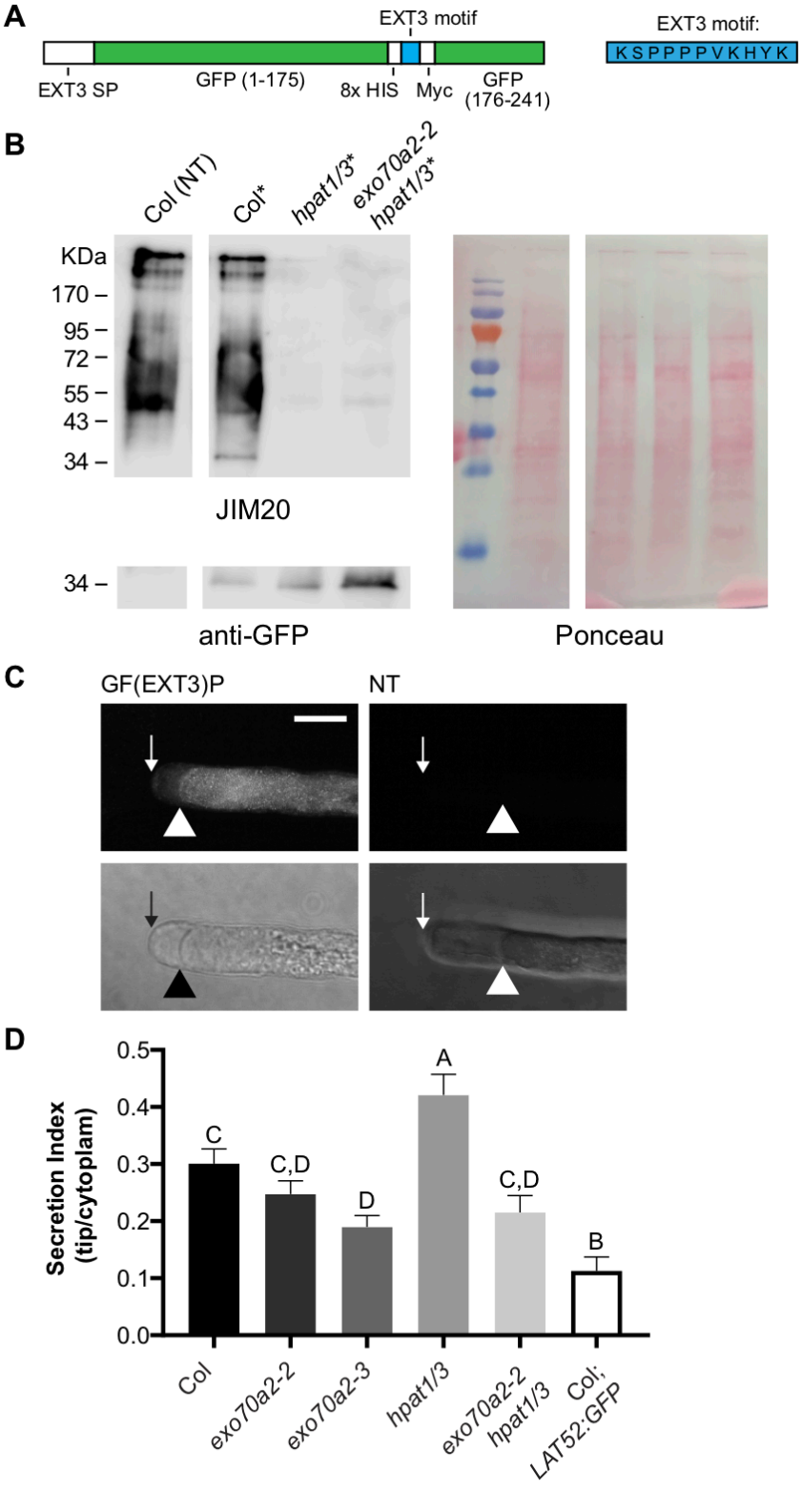

Figure 3-5. Secretion of GF(EXT3)P is decreased in hpat1/3 exo70a2-2 pollen tubes. A) Schematic of the GF(EXT3)P construct, which includes the EXT3 signal peptide (SP), amino acids 1-175 of GFP, an 8x

*HIS tag, a portion of EXT3, a Myc tag, and amino acids 176-241 of GFP. B) Western blots (left) and corresponding Ponceau-stained membrane (right) of PT protein samples. * marks samples from plants carrying the LAT52:GF(EXT3)P transgene, NT is non-transgenic. An anti-GFP polyclonal antibody detects the fusion protein in the transgenic lines at the expected mass (~34 KDa). The reporter is also detected by the Hyp-Ara monocolonal antibody JIM20 only in the transgenic Col sample. C) Images of plasmolyzed PTs expressing LAT52:GF(EXT3)P (left) and non-transgenic control (right). Scale bar represents 10 µm. Arrows indicate the location of the PT cell wall tip, and arrowheads mark the plasma membrane. D) Quantification of secreted GFP signal reported as a secretion index (SI- see Materials and Methods for details, SI mean ± SE, N ≥ 30 PTs per genotype). Samples labeled with the same letter are not significantly different (Benjamini–Hochberg FDR ≤ 0.05).*

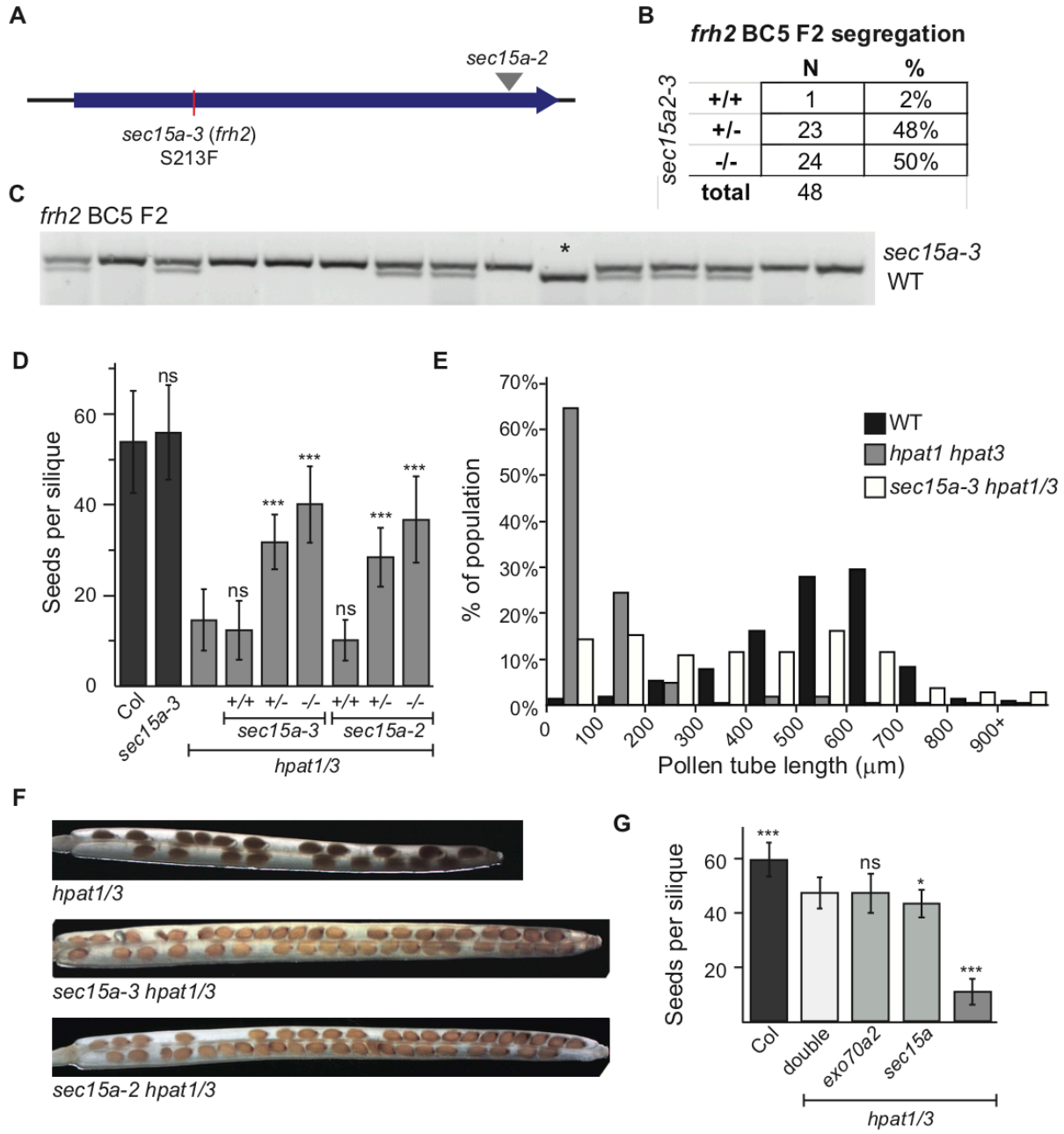

Figure 3-6. Mutations in exocyst complex member sec15a also suppress the hpat1/3 fertility phenotype. A) Gene model diagram showing the relative position of insertion in the sec15a-2 allele and the

suppressor allele identified in frh2 (sec15a-3). B) Segregation of the sec15a-3 mutation in the frh2 hpat1/3 BC5 F2 population. As expected for an hpat1 hpat3 suppressing mutation, the number of homozygous wild-type SEC15A plants identified (+/+) was significantly below the expected value based on Mendelian segregation (chi-squared p-value =1.57 x 10-5. C) Sample sec15a-3 genotyping data for 15 frh2 hpat1/3 BC5 F2 individuals visualized on an agarose gel. The wild-type allele is cleaved by digestion with MnlI. The single homozygous wild-type individual marked by '' did not have the suppressive phenotype. D) Average number of seeds per silique (±SD) for plants of the indicated genotypes. sec15a-2 is not transmitted through the male and not recoverable as a homozygous mutant (Hála et al., 2008). Both sec15a alleles suppress the hpat1/3 phenotype with homozygous mutants showing stronger suppression than heterozygotes. 'ns' marks samples which were not statistically different from their corresponding background genotype. '***' marks statistically different samples (T-test P-value <0.0005, N≥11). E) Histogram of PT lengths after five hours of in vitro growth for the indicated genotypes. Data for all genotypes are statistically significantly different from both other genotypes (T-test P-value <0.005, N≥100 per genotype). F) Cleared siliques of the indicated genotypes. G) Average number of seeds per silique (±SD) for the indicated genotypes. All hpat1/3-based genotypes were siblings segregating from the same F2 population. '***' marks statistically different samples (T-test P-value <0.0005), '*' marks statistically significant samples T-test P-value <0.05, N≥15).*

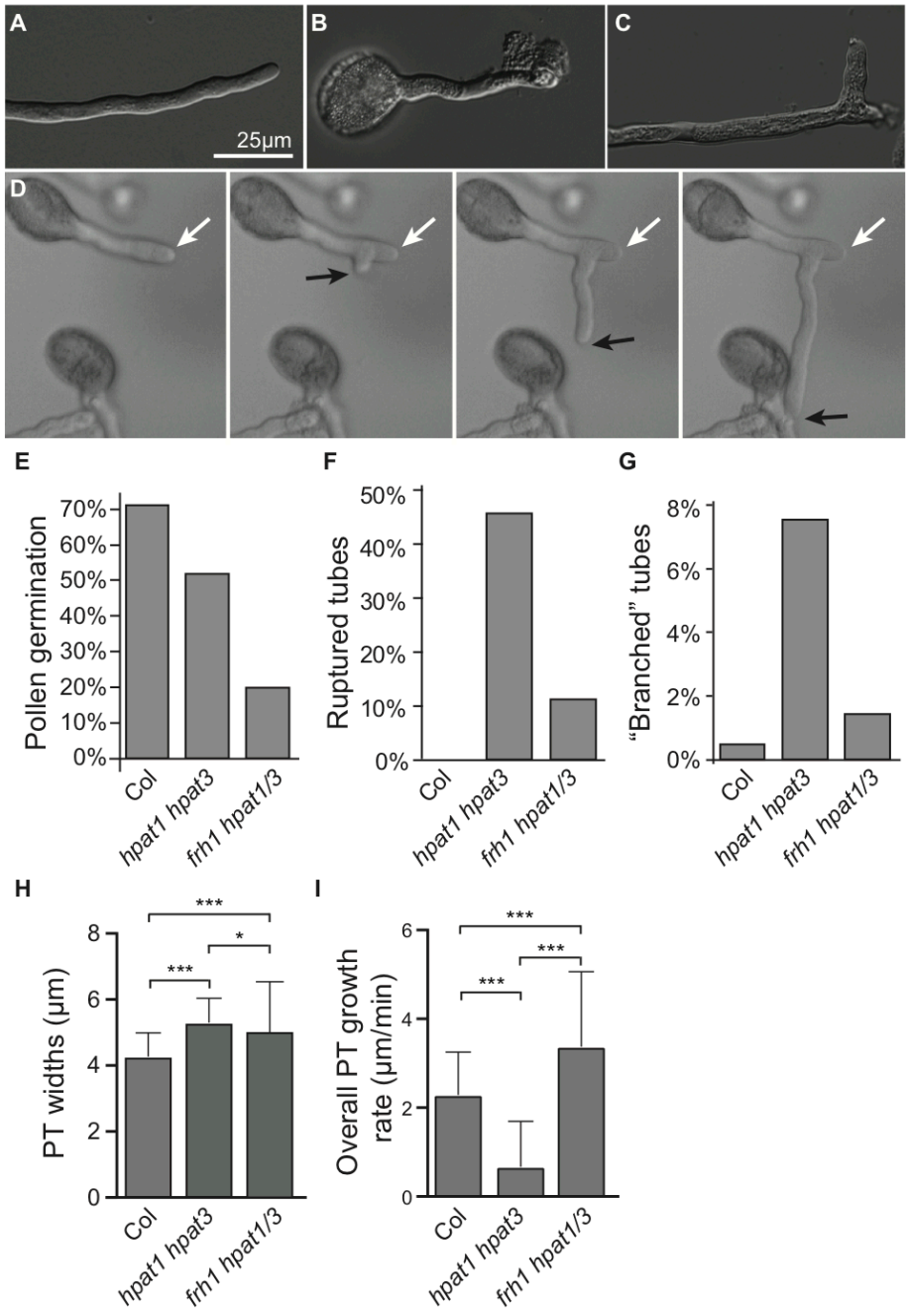

Figure 3-7 (Supplemental Figure 1) - frh1 suppresses most, but not all hpat1/3 pollen tube phenotypes. A-C) Differential interference contrast (DIC) images of PT phenotypic classes. A) a morphologically normal PT typical of the wild type, B) a ruptured PT and C) a "branched" PT typical of hpat1/3 mutants. D) Time course of an hpat1/3 branching event imaged at 5-minute intervals. White arrow marks the original tip region; black arrow marks the newly formed tip derived from a sub-apical portion of the PT. E) Frequency of in vitro pollen germination after 3 hours of growth. Pollen were considered germinated if a visible tube of at least one half the length of the pollen grain was identifiable. Note that the reduced germination in hpat1 hpat3 is in part due to their poor tube elongation. N>600 per genotype. F) Frequency of PT rupture for the indicated genotypes. No ruptured tubes were observed in WT. N>500 per genotype. G) Percentage of tubes with two morphologically distinct tip regions after 5 hours of in vitro PT growth. N>200 per genotype. H) Average PT widths (±SD, N ≥ 103 for each genotype). I) PT growth rates.

Asterisks in H and I mark statistically significant T-test p-values; '' indicates p-value ≤0.05 and '***' indicates p-value ≤0.0005.*

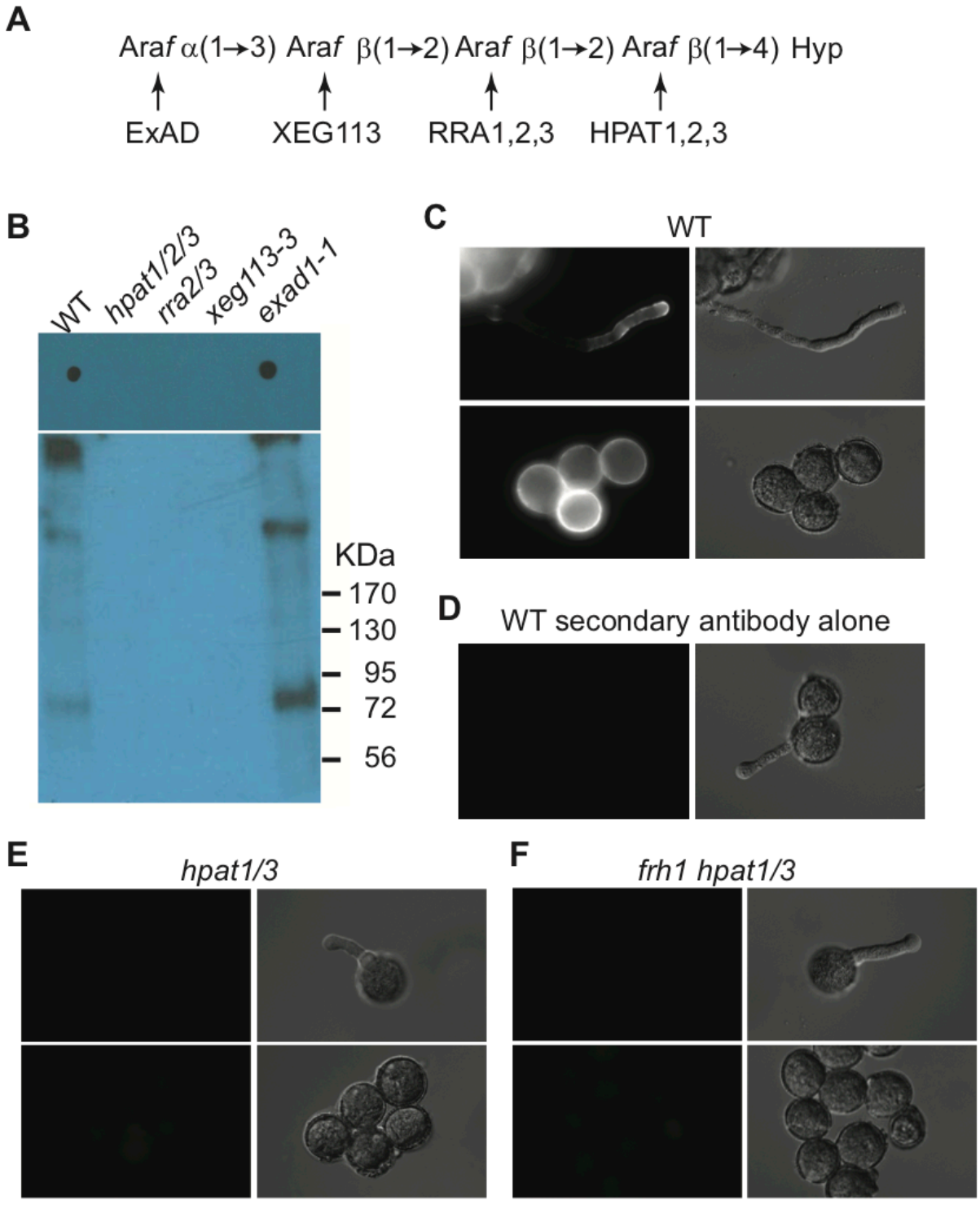

Figure 3-8 (Supplemental Figure 2). The JIM20 monoclonal antibody recognizes Hyp-Ara. A) Illustration of the Hyp-Ara modification and the enzymes responsible for the addition of each arabinose. B) The EXT antibody JIM20 requires Hyp substituted with at least three arabinoses, i.e. the presence of the HPAT, RRA and XEG113 enzymes, for recognition. Dot blot and SDS-PAGE Western blot analysis of protein isolated from seedlings (top, Dot blot) or extracted from rosette leaves (bottom, Western blot) of the indicated genotypes and probed JIM20. C-E) JIM20 immunostaining visualized with a FITC-conjugated

secondary antibody (left) of PTs (top) and pollen grains (bottom) compared to the corresponding DIC images (right). Images taken at 20x magnification. C) Wild-type Columbia-0 pollen samples produced robust JIM20 signal in both pollen grains and PTs, particularly near the PT tip. D) Secondary antibody alone control staining did not produce detectable signal. E) In hpat1/3 pollen samples no JIM20 signal was detected. F) frh1 hpat1/3 and hpat1/3 pollen displayed similar appearance with no detectable JIM20 signal. All immunolocalizations were imaged using the same light intensity and exposure settings.

```
EXO70A1   QIFRGFD--SLSDQCFAEVTVS-SVSMLLSFGDAIA----RSKRSPEKLFVLLDM  364
EXO70A2   QILDGVE--SLRDQCFGEVTVN-SVAVLLSFGEAIA----KSKRSPEKLFVLLDM  338
EXO70A3   QILDGVE--PFRDQSFAEITTI-SFGMLLSFGYAIA----ISRRSPEKVFVILDM  292
EXO70B1   RVF--FGFSSAADLSFMEVCRG-STIQLLNFADAIA----IGSRSPERLFKVLDV  335
EXO70B2   RVFSDLPVSSVTDLSFMEVCRG-TTTQLLNFADAIA----LGSRLPERLFKVVDL  319
EXO70C1   AVFPDQDHSSVRKRLFTGLVSA-VTIRFLDFSGAVV----LTKRSSEKLFKFLDM  345
EXO70C2   RIFPGDE-----GNLFCIVTHG-LAIQFLGFAEAVA----MTRRSTEKLFKILDI  390
EXO70D1   HVFESVGAVNIHEACFMETVKG-PAIQLFNFAEAIS----ISRRSPEKLFKILDL  319
EXO70D2   QIFEG----TMEETCFMEIVKT-SALQLFNFPEAIS----ISRRSPEKLFKILDL  307
EXO70D3   QLFDGI-CTAMDETCFMETVKA-SALRLFTFPEAIS----ISRRSPEKLFKILDL  313
EXO70E1   QIFGDLN--EIGLTCFVDTVKA-PMMQLLNFGEAVS----LGPRQPEKLLRILEM  336
Exo70E2   QILGDFE--SISTACFIEISKD-AILSLLNFGEAVV----LRSCKPEMLERFLSM  343
EXO70F1   EIFSSSE--SSKEVCFNETTKS-CVMQLLNFGEAVA----IGRRSSEKLFRILDM  374
EXO70G1   DVFERLG-LNVWMDCFSKIAAQAGMLAFLQFGKTVT----DSKKDPIKLLKLLDI  366
EXO70G2   DVFEDIG-EDVPLRCFGEIASNSVILQLLRFGSRIS----KCKREPPKLIKLLDC  326
EXO70H1   HVFSAS--NSTRESCFYEIANE-AATNLFKFPEFVA----KEKKSHERIFPLMDL  315
EXO70H2   HVFSAS--STIRESCFYEIVNE-AGINLFKFPELVA----EKKPSPERIFRLMDL  314
EXO70H3   EIFESS--VSLREFCFRDISKE-GALLLFGFPETITLRD-KKNPHPEKIFPLLDM  301
EXO70H4   HVFESS--DAIRESCFSDISRD-GALLLFGFPEIINTKTSKKHSPPEKVFRLLDM  307
EXO70H5   HVFSPS--VSVAESCFTEITLD-SALTLFIFPVSVA----RCKKTVEKIFLTLDI  288
EXO70H6   HIFS----SSVAESCFVDITLQ-SALNLFIFSLTVA----KSRKTAEKIFPTLDV  306
EXO70H7   HVFSSS--GLIVESSFTEITQE-GALILFTFPEYASK---IKKLTPEKMFRFLDM  299
EXO70H8   HVFSSSS-STIRESAFAEITSQ-TALALFTFPEKMA----KCRKSPEKIFLTLDV  281
           ::           *          :: *               :   :.
```

Figure 3-9 (Supplemental Figure 3). Alignment of Arabidopsis EXO70 protein sequences in the region of the exo70a2-2 G319E mutation. Clustal Omega multiple sequence alignment of the whole proteins sequences were trimmed to the region of interest. The EXO70A2 G319 position is marked with red highlight. Conserved residues are marked with "", ":" marks positions with conservation of amino acids with strongly similar properties, "." marks conservation between weakly similar amino acid properties.*

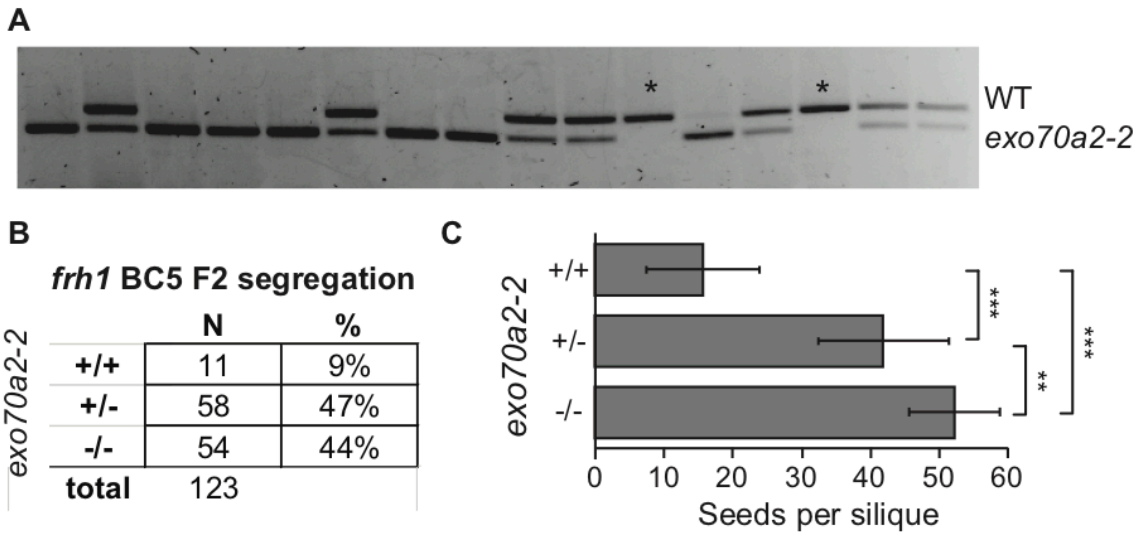

Figure 3-10 (Supplemental Figure 4). The exo70a2-2 mutations co-segregates with the frh1 suppressive phenotype. A) PCR and restriction enzyme mediated genotyping of 20 frh1 BC5 F2 individuals visualized on an agarose gel. The exo70a2-2 mutation creates a TaqαI restriction enzyme recognition site. The upper band is the un-cut wild-type product and the lower band is the cleaved exo70a2-2 product. The two individuals with a non-suppressed phenotype are marked by '' and both are homozygous WT. B) Table of the exo70a2-2 genotype distribution for 123 frh1 BC5 F2 plants. The 11 wild-type individuals (+/+) were all non-suppressed, all remaining plants (heterozygous, +/-; homozygous mutant, -/-) were phenotypically suppressed. Note also the significant distortion of genotype ratio compared to the Mendelian 25%:50%:25% ratio (chi-squared p-value = 2.42x10-7). This bias against the recovery of homozygous wild-type plants is consistent with the genetic behavior of frh1. C) Average number of seeds per silique (+/- SD, N≥16) in the BC5 F2 population grouped by exo70a2-2 genotype. Asterisks mark statistically significant T-test p-values, '**' indicates p-value ≤0.005 and '***' indicates p-value ≤0.0005.*

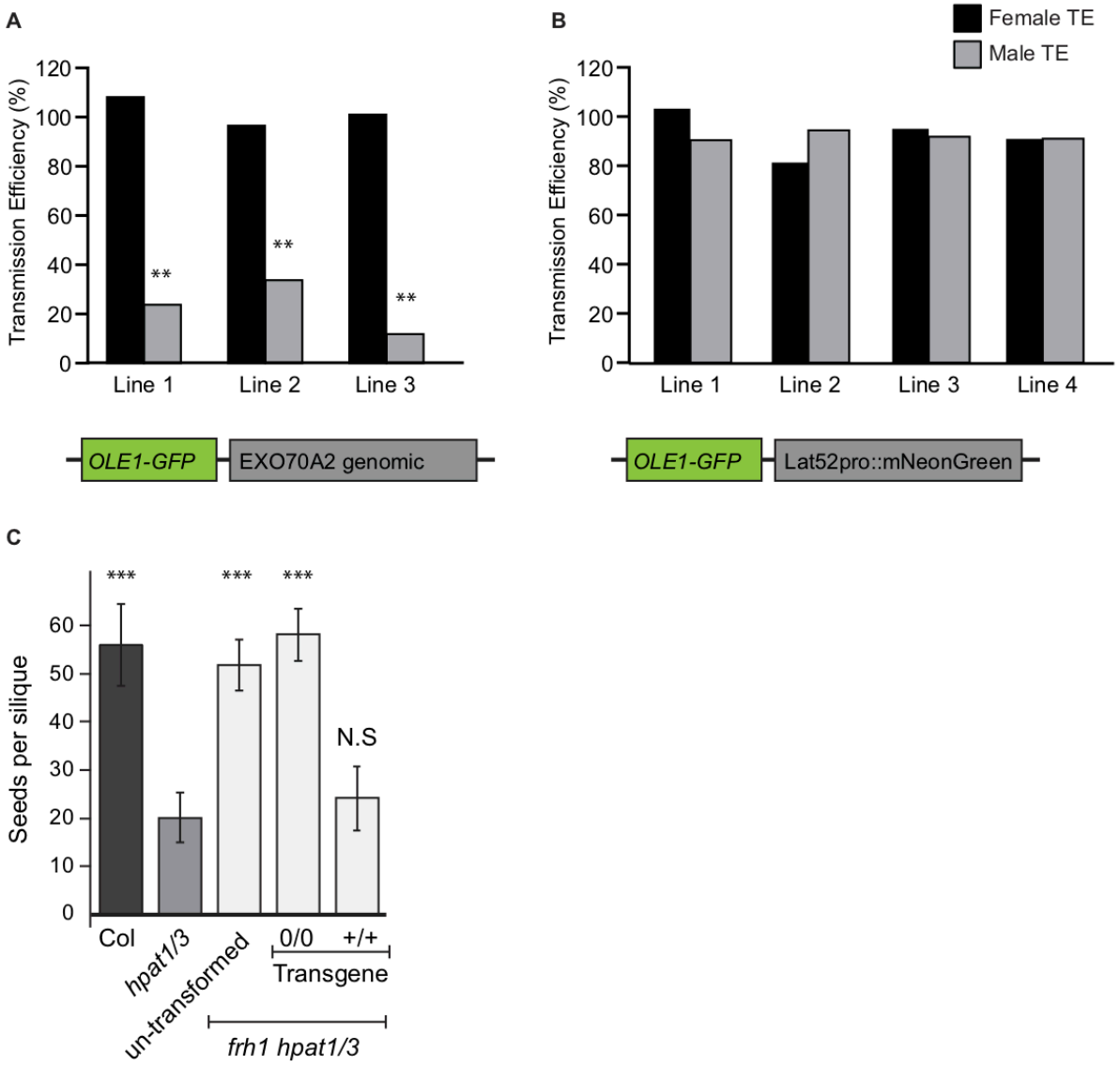

*Figure 3-11 (Supplemental Figure 5). frh1 suppression is due to a mutation in exo70a2. A) frh1 hpat1/3 plants were transformed with a rescue construct containing the wild-type genomic EXO70A2 region and seed-expressed fluorescence reporter selection cassette (OLE1-GFP; Shimada and Hara-Nishimura, 2010). Transgene transmission efficiency (TE) for three independent hemizygous single loci insertion transgenic lines. '**' marks significant difference from the expected TE for no effect of the transgene on transmission (100%, T-test P-value <0.005, N≥185). B) Transmission of a control construct containing the strong pollen promoter (Lat52) driving expression of the fluorescent protein mNeonGreen in four independent frh1 hpat1/3 lines (N≥72). C) Seed counts of T3 plants segregating for the rescue construct. Plants not carrying the rescue construct (0/0) maintained suppressor-levels of seed set. Seed set of plants homozygous for the presence of the rescue construct (+/+) was not statistically different from the hpat1/3 background ('***' indicates p-value < 0.0005; Student's T-test vs. hpat1/3; N ≥ 15 siliques).*

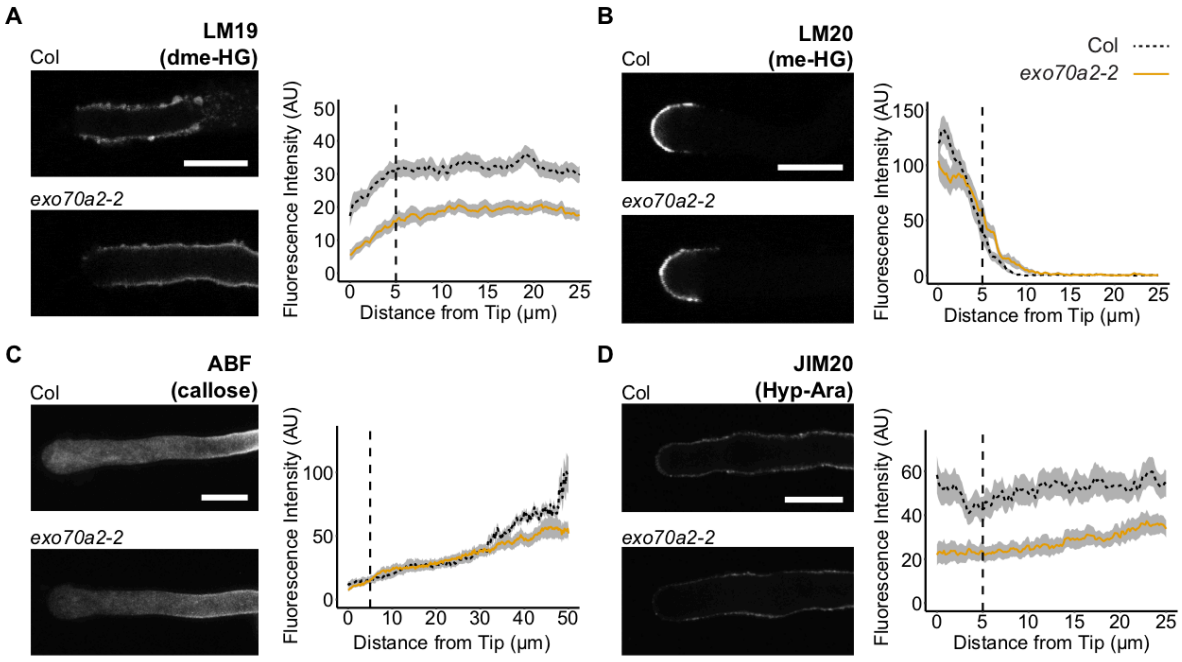

Figure 3-12 (Supplemental Figure 6). exo70a2-2 PTs maintain cell wall polymer polarity in the WT background. A) Medial Z-slices of PTs stained with LM19 primary antibody and anti-rat FITC-conjugated secondary antibody, and corresponding quantification of fluorescent signal intensity along the PT periphery, starting at the tip (distance on x-axis = 0 μm) to 25 μm down the shaft. B) Medial Z-slices of PTs stained with LM20 primary antibody and anti-rat FITC-conjugated secondary antibody, and corresponding quantification of fluorescent signal intensity as in (A). C) Maximum projections of PTs stained with aniline blue fluorochrome (ABF) and corresponding quantification of fluorescent signal intensity starting at the tip (distance on x axis= 0) to 50 μm down the shaft of the PT. D) Medial Z-slices of PTs stained with JIM20 primary antibody and anti-rat FITC-conjugated secondary antibody, and corresponding fluorescent signal quantification as in (A) and (B). Colored lines represent means and shading represents standard error. Vertical dashed line represents the approximate region of the PT where the apical dome transitions to the shaft. N ≥ 30 PTs for each genotype per experiment. All images were acquired by confocal microscopy at 100x magnification and all scale bars = 10 μm.

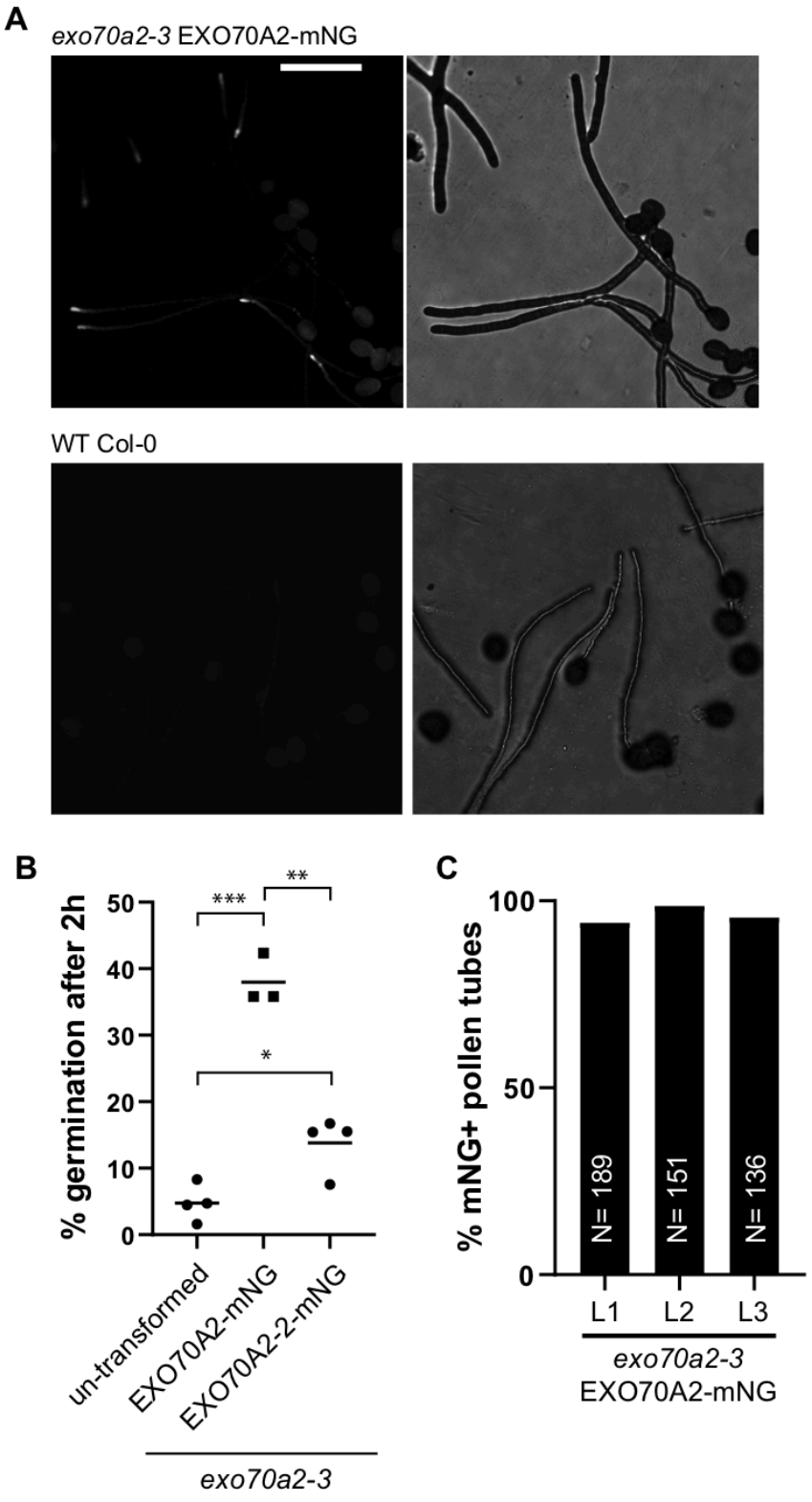

Figure 3-13 (Supplemental Figure 7). EXO70A2-mNG rescues pollen tube germination in the exo70a2-3 mutant. A) PTs were grown in vitro for 2 hours and imaged with GFP filter (left) and DIC optics (right). Wild-type un-transformed Columbia are shown as a negative control for fluorescence. B) pollen

*germination frequency in exo70a2-3. The presence of EXO70A2-mNG significantly increased pollen germination compared to the background. The point mutant allele EXO70A2-2 (G319E) also increased pollen germination to a smaller degree. Each point is data from a single independent T1 plant, N ≥ 321 pollen grains per T1. '***' indicates p-value < 0.0005, '**' indicates p-value < 0.005, '*' indicates p-values < 0.05. C) Percentage of fluorescent PTs for exo70a2-3 EXO70A2-mNG hemizygous lines.*

Table 3-1 (Supplementary Table 1). Illumina sequencing read information. DNA samples of the indicated genotype, all in the hpat1/3 background, were sequenced by paired-end Illumina sequencing. At least 97% of reads aligned to the Columbia reference genome yielding estimated genome coverage between 18 and 63 fold.

Genotype	***Total # of reads***	***Read length (bp)***	***% of reads aligned***	***Estimated average genome coverage***
frh1/frh1	16,495,587	150x2	97.93	18.64x
FRH1/FRH1	19,803,838	150x2	97.75	22.34x
frh2/frh2	55,907,035	150x2	99.15	63.96x
FRH2/FRH2	41,150,402	150x2	99.15	47.08x
hpat1 hpat3	31,918,383	150x2	97.02	35.73x

Table 3-2 (Supplementary Table 2). Full list of sequence variants passing filtering for frh1. AO- alternate observations (number of reads with the alternative nucleotide), RO- reference observations (number of reads carrying the reference nucleotide), TO- total observations (AO + RO). Allele frequency is estimated from reads as (AO/TO). Gene function, annotations for missense mutations are show in black; silent, UTR or intronic mutations are in grey. Double lines separate chromosomes. The exo70a2 mutation is in bold.

Chr	**Position**	**REF**	**ALT**	**QUAL**	**AO=**	**RO=**	**TO=**	**Allele freq**	**Location of mutation**	**Nature of change**
1	3,567,966	C	T	0.000693	4	1	5	0.80	AT1G10740	intron 1
1	5,720,122	G	T	16.1796	5	1	6	0.83	AT1G16710	intron 12

1	14,220,334	T	G	75.0463	4	0	4	1.00	Outside gene.	--
1	14,607,997	G	A	13.4014	5	0	5	1.00	Outside gene.	--
1	14,824,768	A	T	0.00556	5	1	6	0.83	Outside gene.	--
1	16,515,445	CG	T	304.618	95	13	108	0.88	Outside gene.	--
1	24,892,361	C	A	22.7986	10	1	11	0.91	AT1G66740	5' UTR
2	3,609,013	G	T	0.004568	12	3	15	0.80	Outside gene.	--
2	19,697,782	C	A	247.713	115	20	135	0.85	Outside gene.	--
3	985,535	G	T	34.8725	6	0	6	1.00	Outside gene.	--
3	13,693,041	T	C	2.7709	4	0	4	1.00	Outside gene.	--
3	13,693,069	C	A	2.37516	4	0	4	1.00	Outside gene.	--
3	13,790,444	A	G	2.59478	4	1	5	0.80	Outside gene.	--
3	13,790,522	A	G	2.83585	8	1	9	0.89	Outside gene.	--
4	3,979,241	T	C	0.017781	523	121	644	0.81	Outside gene.	--

4	4,009,421	T	G	0	658	81	739	0.89	Outside gene.	--
5	2,572,378	G	T	0.000765	4	0	4	1.00	AT5G08020	intron 2
5	11,731,813	A	C	52.3084	411	53	464	0.89	Outside gene.	--
5	18,317,951	G	A	463.66	18	4	22	0.82	AT5G45240	CDS L579L (silent)
5	18,513,821	G	A	826.928	31	4	35	0.89	AT5G45650	CDS A692V
5	19,091,266	G	A	824.113	33	7	40	0.83	AT5G47030	intron 2
5	19,128,169	G	A	592.682	22	3	25	0.88	AT5G47090	CDS K203K (silent)
5	19,717,448	G	A	370.763	25	4	29	0.86	AT5G48620	CDS D15N
5	19,743,633	G	A	434.364	18	3	21	0.86	Outside gene.	--
5	20,049,429	G	A	501.066	18	2	20	0.90	AT5G49440	CDS G171E
5	20,073,319	G	A	387.251	14	2	16	0.88	Outside gene.	--
5	20,315,382	G	A	296.135	11	1	12	0.92	Outside gene.	--

5	20,461,314	G	A	789.133	25	0	25	1.00	AT5G50280	CDS R661K
5	20,763,754	G	A	913.518	32	3	35	0.91	Outside gene.	--
5	20,789,260	G	A	724.419	24	0	24	1.00	AT5G51150	CDS G76E
5	20,841,395	G	A	871.516	29	0	29	1.00	AT5G51280	5' UTR
5	20,853,117	G	A	699.976	25	1	26	0.96	AT5G51310	CDS L239L (silent)
5	21,130,649	G	A	447.567	18	2	20	0.90	AT5G52040	intron 1
5	**21,252,591**	**G**	**A**	**768.668**	**27**	**3**	**30**	**0.90**	**AT5G52340**	**CDS G319E**
5	21,307,338	G	A	731.535	22	0	22	1.00	AT5G52510	CDS G48E
5	21,457,979	G	A	664.373	25	5	30	0.83	AT5G52910	CDS S1074F
5	21,686,079	G	A	606.121	23	5	28	0.82	AT5G53440	intron 1
5	21,751,206	G	A	612.563	22	2	24	0.92	AT5G53540	5' UTR
5	21,843,162	G	A	335.542	20	4	24	0.83	Outside gene.	--
5	22,211,139	G	A	681.526	22	2	24	0.92	AT5G54670	intron 5

5	22,459,739	G	A	949.649	30	1	31	0.97	Outside gene.	--
5	22,882,056	G	A	976.49	30	0	30	1.00	AT5G56510	CDS L112L (silent)
5	22,947,474	G	A	874.072	28	0	28	1.00	AT5G56730	intron 1
5	22,993,211	G	A	859.642	27	1	28	0.96	Outside gene.	--
5	23,146,548	G	A	839.257	27	3	30	0.90	AT5G57130	CDS E387E (silent)
5	23,185,068	T	A	312.105	12	3	15	0.80	Outside gene.	--
5	23,509,421	G	A	528.342	18	2	20	0.90	AT5G58100	intron 8
5	24,040,295	G	A	280.778	12	2	14	0.86	AT5G59662	intron 1

Table 3-3 (Supplementary Table 3). Full list of sequence variants passing filtering for frh2. AO- alternate observations (number of reads with the alternative nucleotide), RO- reference observations (number of reads carrying the reference nucleotide), TO- total observations (AO + RO). Allele frequency is estimated from reads as (AO/TO). Gene function, annotations for missense mutations are show in black; silent, UTR or intronic mutations are in grey. Double lines separate chromosomes. The sec15a mutation is in bold.

Chr	**Position**	**REF**	**ALT**	**QUAL**	**AO=**	**RO=**	**TO=**	**Allele freq**	**Gene**	**Nature of change**
1	14658163	GT	GA	38.7457	19	1	20	0.95	Outside gene.	--

1	14659168	A	G	0.168275	5	1	6	0.83	Outside gene.	--
1	14824773	A	T	2.1747	4	1	5	0.80	Outside gene.	--
1	28369259	C	A	152.176	10	0	10	1.00	Outside gene.	--
2	3618201	TTG	TTT	1534.16	3306	287	3593	0.92	AT2G08986	intron 2
2	3622048	GTCG	GTCA	258.401	1129	173	1302	0.87	AT2G08986	intron 22
3	13685761	TA	TC	9.55E-09	12	0	12	1.00	Outside gene.	--
3	13701267	T	C	20.3445	4	1	5	0.80	Outside gene.	--
3	13704892	C	A	0.0947526	8	1	9	0.89	Outside gene.	--
3	13798787	AC	AT	0.23112	19	3	22	0.86	Outside gene.	--
3	17838331	C	T	1170.32	42	4	46	0.91	Outside gene.	--
3	17925311	C	T	1895.62	73	13	86	0.85	AT3G48400	CDS P545L
3	18089552	C	T	1275.46	45	4	49	0.92	AT3G48780	intron 2
3	18190535	C	T	1145.41	44	9	53	0.83	AT3G49060	CDS A150T
3	18523069	C	T	1147.05	44	9	53	0.83	AT3G49950	CDS P167L
3	18703613	G	A	1203.6	48	9	57	0.84	AT3G50390	3' UTR

3	19091528	C	T	1441.65	53	7	60	0.88	AT3G51450	CDS D150D (silent)
3	19297541	C	T	1892.53	69	8	77	0.90	AT3G52010	CDS T359T (silent)
3	19417671	C	T	1377.8	50	5	55	0.91	AT3G52370	CDS D41D (silent)
3	19691797	C	T	1936.06	66	5	71	0.93	AT3G53120	CDS V92I
3	19739873	G	A	679.917	31	4	35	0.89	Outside gene.	--
3	20331049	C	T	1666.84	67	16	83	0.81	AT3G54870	CDS R82C
3	20935829	C	T	1742.57	61	5	66	0.92	AT3G56470	CDS Q306*
3	**20982601**	**C**	**T**	**2102.68**	**71**	**4**	**75**	**0.95**	**AT3G56640**	**CDS S213F**
3	21652112	C	T	1305.18	51	9	60	0.85	AT3G58560	intron 1
3	21746773	C	T	1849.82	60	1	61	0.98	Outside gene.	--
3	21793787	C	T	1700.27	62	5	67	0.93	Outside gene.	--
3	21823345	C	T	1137.85	38	2	40	0.95	AT3G59040	intron 1
3	21948650	C	T	2228.74	75	3	78	0.96	Outside gene.	--

3	22051051	C	T	1139.8	43	7	50	0.86	AT3G59695	intron 1
3	22070801	C	T	853.45	41	3	44	0.93	AT3G59750	CDS G312E
3	22119802	C	T	662.741	37	1	38	0.97	Outside gene.	--
3	22271130	C	T	1822.18	67	8	75	0.89	AT3G60250	CDS G188E
3	22285405	C	T	1635.22	53	0	53	1.00	AT3G60300	CDS A12V
3	22499825	C	T	1521.02	61	13	74	0.82	AT3G60900	CDS P339P (silent)
3	23184009	C	T	1330.38	52	8	60	0.87	Outside gene.	--
4	2961652	CTAG	CTAT	8.65493	4	1	5	0.80	AT4G05612	intron 11
4	3985743	TG	TC	0.619921	560	95	655	0.85	Outside gene.	--

Table 3-4 (Supplementary Table 4). Primers used in this study

Genotyping	**Name**	**Sequence 5' -> 3'**	**Notes**
hpat1	SALK_120066 LP2	GTGATTATGATATGAAGgtaagc	

	SALK_120066 RP2	aaatctagtggagaccagac	
hpat3	SALK_040668 LP2	aagatactgcagtaaggtcc	
	SALK_040668 RP2	gacaagaagggaagtaaagg	
sec15a-2	SALK_067498 LP	ACCAAGTTGGACGAGTTCATG	
	SALK_067498 RP	CTGAGCCTGTGAGCCATAAAG	
xeg113-2	SALK_058092 LP	ACACCCAAATTTTACCCAAGG	
	SALK_058092 RP	TCTACGCGACTGTGATCATTG	
	Salk LB1.3	ATTTTGCCGATTTCGGAAC	
rra3	GABI_223B05 LP	GAGGCTAAAACAAAGACTTGGG	
	GABI_223B05 RP	TCTCTGGATTGAAATTCCGTG	
	GABI LB o8409	ATATTGACCATCATACTCATTGC	
rra2	SAIL_244_A03 LP	TAAGCCAGTGTACCCTGGATG	
	SAIL_244_A03 RP	GGATCAGAGATAAAGGCAGGG	
	Sail LB1	GCCTTTTCAGAAATGGATAAATAGCCTTGCTTCC	

exo70a2-3	Wisc216_02A LP	TGGTGGAAAGACTCATGATCC	
	Wisc216_02A RP	ACCTCAGGCTGAAGCTCTCTC	
	WiscHSLB4	TGATCCATGTAGATTTCCCGGACATGAAG	
exo70a2-2 (G319E)	A2-RT-LP	AGCTGCGGTGTTGGAACAGA	mutant product is cleaved by TaqaI
	Exo70A2 CAPs RS	ACCTCAGGCTGAAGCTCTCTC	
sec15a-3 (S213F)	SEC15A-S213F f	AGGACAGTTTTACCATGCCC	Wild type product is cleaved by MnlI
	SEC15A-S213F r	AAGCGGTGAGGCCAATAGCA	
RT-PCR			
Actin control	Actin1RTf	ggcgatgaagctcaatccaaacg	

	Actin1RTr	ggtcacgaccagcaagatcaagacg	
EXO70A2 RT-PCR	A2-RT-LP	AGCTGCGGTGTTGGAACAGA	from Synek et al., 2017
	A2-RT-RP	CTCGACTGAACCGTGAGACACT	
Construct cloning		attB recombination sequences in red	
Genomic rescue construct	Exo70A2 pro B1 F	GGGGACAAGTTTGTACAAAAAAGCAGGCTactatgagaaaggggtaacg	
	Exo70A2 CDS B2 R	GGGGACCACTTTGTACAAGAAAGCTGGGTgacacaaatcatatgcgacg	
mNG reporter fusion	Exo70A2 pro B1 F	as above	
	Exo70A2 mNG B2 R	GGGGACCACTTTGTACAAGAAAGCTGGGTATCTCTTTGGCTCACTCCATG	
pFASTmNG cloning	R07 MluI F	acgcgtGGATCCGGCTTACT	
	R07 mNG R	cataccgcggGATATCACCACTTTGTACAAGAAAGCTG	

	mNG R07 F	tggtgatatcCCGCGGTATGGTGAGCAAG	
	mNG NruI R	tcgcgaTTACTTGTACAGCTCGTCCATGC	
generation of EXT3ssGF(EXT3)P	FReplace	CTGCAGATGGGTAAGACTAATCTTTTTCTCT	
	Rreplace	GGATCCATGGGATCCCGG	
	pYi1	CATGGCAAGTCCCCTCCACCACCGGTTAAGCATTACAAGG	
	pYi2	GATCCCTTGTAATGCTTAACCGGTGGTGGAGGGGACTTGC	
	p162	AAAGCAGGCTACTAGGATCCGTCAACATGGTGGAG	
	p164	AGATTGTTAAGACAAGCAAAGTTGCCACTAAAGAGGCCATTGG AGACCCCATCTGCAGGTCGTCCTCTCCA	
	p163	GAAAGCTGGGTCTAGAGATCGTACCCCTGGATTTTGG	
	p165	TTGTCTTAACAATCTCTCTCACCTTTGTATCTCAATCAACCGCTA ACTATTTCGAGCAAGTGAGCAAGGGC	
	GF(EXT3)P B2 F	ggggacaactttgtatacaaaagttgATGGGGTCTCCAATGGCCTC	
	GF(EXT3)P B5 R	ggggaccactttgtacaagaaagctgggtCGTACCCCTGGATTTTGGTT	
Lat52 promoter cloning	LAT52 B1 F	ggggacaagtttgtacaaaaaagcaggctCGACATACTCGACTCAGAAGGT	
	LAT52 B5r R	ggggacaactttgtatacaaagttgTTTTAAATTGGAATTTTTTTTTTTGG	

	LAT52 B2 R	ggggaccactttgtacaagaaagctgggtaTTTTAAATTGGAATTTTTTTTTTT GG	

Chapter 4 - PLC6 Regulates HPAT- Mediated Pollen Tube Growth in *Arabidopsis*

Steven Beuder[1], Xuesi Hua[1], Alexandria Dorchak[1], and Cora A. MacAlister[1]*

1. University of Michigan, Department of Molecular, Cellular and Developmental Biology
* Corresponding author, macalist@umich.edu

4.1 Introduction

Pollen tubes (PTs) elongate through a highly polarized growth mechanism called tip growth, which relies on the careful regulation of structural and mechanical properties of the cell wall. For proper tip growth, PTs must maintain an extensible apical tip to allow for expansion, and rigid subapical walls to prevent multidirectional expansion (leading to PT branching) and premature bursting. In order to maintain two spatially- distinct regions of the cell wall with different mechanical properties, PTs differentially regulate the structures of these two wall regions. The plant cell wall is a complex extracellular matrix composed of multiple carbohydrate networks including cellulose, hemicellulose, callose and pectins, as well as proteins such as cell wall-remodeling enzymes and glycoproteins. Pectins have a major influence on the mechanical properties of the cell wall, and mutations in genes that control pectic structure severely impair tip growth and pollen fertility, leading to decreased seed production and fitness (Jiang et al., 2005; Leroux et al., 2015; Röckel et al., 2008).

Pectins are a family of structurally diverse) carbohydrates, with homogalacturonan (HG) being the most abundant polymer type (Mohnen, 2008). HG is composed of *alpha*-1,4-linked-d-galacturonic acid (GalA) and is highly methylesterified (me-HGs) by enzymes in the Golgi prior to secretion (Krupková et al., 2007; Mohnen, 2008; Mouille et

al., 2007; O'Neill et al., 1990; Ridley et al., 2001). After secretion into the cell wall, pectin methylesterases catalyze the de-methylesterification of me-HGs to form dme-HG, exposing negatively- charged carboxyl groups. Neighboring dme-HG molecules then undergo crosslinking interactions via calcium bridges, referred to as the "egg-box" model, which promotes gelation and increases the overall rigidity of the cell wall (Grant et al., 1973; Pelloux et al., 2007). In PTs, me-HG is localized to the cell wall and enriched at the tip, while dme-HG localizes to the subapical walls and is absent from the tip (Chebli et al., 2012).

Negatively- charged pectic groups interact ionically with extensins (Smith et al. 1984), which are a family of hydroxyproline (Hyp)- rich glycoproteins that regulate cell wall formation and structural integrity (Choudhary et al., 2015; Hall & Cannon, 2002). The structures of "classical" extensins are amphiphilic and highly repetitive, consisting primarily of alternating $Ser(Pro)_{3-5}$ motifs and Tyr/Tyr-Val motifs, and are also typically rich in Lys, giving them an overall positive charge (Showalter et al., 2010). Tyr- containing motifs facilitate intermolecular crosslinking of extensin monomers to form networks, which are thought to serve as a scaffold for pectin assembly and possibly regulate crosslinking of dme- HG (Cannon et al., 2008; MacDougall et al., 2001).

Extensins also undergo significant posttranslational modifications prior to secretion into the cell wall. Prolines found in $Ser(Pro)_{3-5}$ motifs are hydroxylated by prolyl 4-hydroxylases (P4Hs) to form Hyp (Tiainen et al., 2005), which are then *O*-arabinosylated by a cascade of Golgi-localized glycosyltransferases to form linear oligoarabinosides that are typically 3-5 residues long (Akiyama et al., 1980). The first arabinose is added by enzymes called Hyp *O*-arabinosyltrasferases (HPATs), which are encoded by a three member gene family in *Arabidopsis* (Ogawa-Ohnishi et al., 2013). Loss of HPAT1 and HPAT3 (*hpat1/3*) drastically decreases seed production due to poor growth and decreased fertility of *hpat1/3* PTs (MacAlister et al., 2016). In addition to poor elongation, *hpat1/3* PTs burst more frequently and exhibited morphological defects including increased widths branching frequency compared to WT, consistent with a loss of structural integrity. Through immunolabeling and other staining techniques, we identified and characterized multiple differences in the cell wall structure of *hpat1/3* PTs compared to wild type (WT). One notable difference was that more dme-HG signal was detected

throughout the cell wall of *hpat1/3* PTs, including at the tip where it is usually absent (Chebli et al., 2012), suggesting that overall rigidity is increased *hpat1/3* PT cell walls and tip extensibility is decreased (Beuder et al., 2020).

We performed a suppressor screen and identified secondary mutations that suppress the *hpat1/3* pollen fertility defect, which were mapped using whole-genome sequencing. We previously characterized one *hpat1/3* suppressor mutant called *fertilization restored in hpat1/3 1* (*frh1*), in which the suppression-causing mutation was identified as a G319E missense mutation in *EXO70A2* (*exo70a2-2*), which encodes an EXO70 isoform (Beuder et al., 2020). EXO70 is a member of the exoycst complex, which facilitates tethering of secretory vesicles to the plasma membrane prior to SNARE-mediated membrane fusion and exocytosis. *hpat1/3* PT growth defects were strongly rescued in the *hpat1/3; exo70a2-2/frh1* suppressor, and dme-HG immunolabeling and other structural defects were also partially suppressed. Furthermore, apical secretion of a GFP-based reporter with an extensin $Ser(Pro)_{3-5}$ motif [GF(EXT3)P] was increased in *hpat1/3* PTs. This was rescued/decreased in the *exo70a2* mutants, suggesting that extensins and extensin-like proteins are secreted by the exocyst complex. We also showed that the GF(EXT3)P reporter is Hyp *O*-arabinosylated in an HPAT-dependent manner; therefore, our data suggested that Hyp *O*-arabinosylation may regulate the rate of EXO70A2-mediated extensin secretion.

EXO70 binds PI(4,5)P2 at the plasma membrane to promote exocyst-mediated secretion (He et al., 2007; Pleskot et al., 2015). PI(4,5)P2 levels are regulated by PI-specific phospholipase Cs (PLCs) which bind and cleave PI(4,5)P2 to form the secondary messengers DAG and IP3. PI(4,5)P2 was observed to localize to the plasma membrane at the tip of tobacco PTs and PLC3 localized to the subapical walls, suggesting that PLC3-mediated PI(4,5)P2 hydrolysis at these regions confines P(4,5)P2 to the tip (Helling et al., 2006). PI(4,5)P2s are formed by the phosphorylation of PIP4 by PIP4 5-kinases. Knockdown of PI4P 5- kinase activity decreased PT growth rates and germination frequency, and PI4P 5-kinase overexpression increased pectin accumulation and thickened the cell wall of PT tips tip (Ischebeck et al., 2008). In addition to mediating secretion, PI(4,5)P2 signaling is important for other cellular processes. In plants, IP3 is quickly converted to IP6 which triggers the release of intracellular calcium stores to

increase cytoplasmic calcium concentration (Lemtiri-Chlieh et al., 2003). PTs maintain a tip-focused calcium gradient which controls growth directionality (Herbell et al., 2018; Taiz, 1984), but it is unclear if this is mediated though PLC-PI(4,5)P2 signaling.

Much of what we know about PLC-PI signaling comes from animal systems, and plants lack some of animals' signaling machinery. For example, plant PLCs lack an N-terminal pleckstrin homology (PH) domain, which directly binds PI(4,5)P2s. PI(4,5)P2 levels are also particularly low in plant cell plasma membranes, suggesting that there may be other endogenous PLC ligands *in planta*. Plant PLC structures include a variable EF hand domain at the N-terminus, followed by conserved X and Y catalytic domains and a C-terminal C2 lipid binding domain (Teun Munnik & Testerink, 2009). Calcium is required for PLC activity, and both the EF hand and C2 domains have calcium-binding regions (Otterhag et al., 2001; Rebecchi & Pentyala, 2000). For the rice PLC (AK064924), the C2 domain alone was sufficient to bind lipids in a calcium-dependent manner (Rupwate & Rajasekharan, 2012). However, PLC3 in tobacco required both the EF and C2 domains to bind the plasma membrane in tobacco PTs (Helling et al., 2006).

Here, we describe another *hpat1/3* suppressor mutation found in *PLC6*. *PLC6* (At2g40116) is one of nine PLCs (*PLC1* through *9*) encoded in the genome of *Arabidopsis thaliana,* and its function has not been characterized yet. We show that PLC6 is an important regulator of PT growth by influencing cell polarity and mediating growth response to calcium, and we interrogate the potential links between *PLC6*, *EXO70A2,* and secretion in HPAT-mediated PT growth. Furthermore, while AtPLC2 has already been implicated in male and female gametophytic development (Di Fino et al., 2017; L. Li et al., 2015), our data indicates that PLC6 is a major PLC isoform functioning in PT growth, but it is likely that other PLCs have roles in this process as well.

4.2 Results

4.2.1 frh3 suppresses hpat1/3 PT growth and fertility defects to improve seed production

WT *Arabidopsis* plants typically produce large siliques filled with seeds due to efficient self-fertilization of all or most ovules for each flower. Self-fertilized *hpat1/3* plants produce fewer seeds due to poor growth of *hpat1/3* PTs, which drastically decreases fertilization efficiency (MacAlister et al., 2016). Seed production is strongly rescued in *frh3* plants due to suppression of *hpat1/3* PT growth defects and improved fertility (Figure 1); however, the mechanism through which poor pollen fertility in *hpat1/3* was improved in *frh3* was unknown.

We reasoned that increased seed production in *frh3* plants could be caused by directly improving growth and fertility of *hpat1/3* PTs, or possibly due to improved reception of the female tissue to complement poor PT growth. To distinguish between these two modes, we performed reciprocal crosses between un-mutagenized *hpat1/3* plants and *frh3* suppressors. *frh3* pistils crossed with *hpat1/3* pollen produced few seeds, with silique sizes and seed sets resembling those of normal *hpat1/3* plants, while *hpat1/3* pistils crossed with *frh3* pollen resulted in large, full siliques (Figure 1B). Furthermore, *hpat1/3* pistils manually pollinated with excess *hpat1/3* pollen still produced low seed sets resembling self-fertilized *hpat1/3* siliques (Figure 1B), demonstrating that manual pollination alone does not improve seed yield. These results indicate that seed production in *frh3* is specifically caused by improved fertility of *hpat1/3* PTs.

To learn more about how pollen fertility is improved in *frh3*, we asked if *hpat1/3* PT growth and morphological defects were suppressed in *frh3* PTs. To address this, we performed multiple *in vitro* PT growth assays and measured the frequencies of these observed phenotypes. *frh3* PTs grown for 4 hours *in vitro* were much longer than *hpat1/3* PTs and approached near-WT lengths (Figure 1D, E). The high frequency of bursting and increased width of *hpat1/3* PTs were also significantly reduced in *frh3* (Figure S1), suggesting that improved growth and fertility of *frh3* PTs is due to suppression of cell wall defects caused by the loss of HPAT activity. *hpat1/3* PTs also germinated at a slightly lower frequency compared to WT, and this was not rescued in *frh3* PTs (Figure S1).

We wanted to measure how secretion of HPAT-modified proteins was affected in the *frh3* background. We previously cloned a GF(EXT3)P reporter, whose structure includes a single EXT3 motif loop embedded in a GFP molecule, and showed that the GF(EXT3)P reporter protein was Hyp *O*-arabinosylated in an HPAT-dependent manner

(Beuder et al., 2020). We transformed *hpat1/3* plants with this construct, crossed a strongly-expressing line into the WT Col and *frh3* backgrounds, and measured apical secretion of the GF(EXT3)P protein in the same manner as described in Beuder et al. 2020. Consistent with our previous results, *hpat1/3* plants showed higher levels of GF(EXT3)P secreted into the cell wall than Col (Figure S1). This phenotype was partially suppressed in *frh3* PTs, which showed lower levels of GF(EXT3)P secretion compared to *hpat1/3*, but still significantly higher than Col. These results suggest that *FRH3* is involved in promoting the secretion of HPAT-modified proteins in PTs.

4.2.2 frh3 mapped to a mutation in PLC6

To identify the *hpat1/3* suppression-causing mutation in *frh3*, we performed whole-genome sequencing of BC4F2-generation *frh3* suppressor plants, as well as non-suppressed siblings and *hpat1/3* plants. Sample preparation, sequencing strategy, bioinformatic analysis and other steps were performed as previously described (Beuder & MacAlister, 2020). Briefly, we first identified sequencing variants unique to *frh3,* then filtered this list of variants (Var_{frh3}) based on the following criteria: (i) mutation type= single nucleotide polymorphisms (SNPs), as EMS primarily causes G to A substitutions (Greene et al. 2003), (ii) total read coverage > 3 at each position, and (iii) alternate allele frequency > 0.7. This revealed a cluster of 41 mutations spanning 6.7 million base-pairs on chromosome 2 (Table S1). We then selected for (iv) mutations in protein-coding gene regions, (iv) missense or nonsense mutations, and (v) mutations found in genes expressed in pollen. This led to the identification of a guanine to adenine substitution at genomic position 16754174, which mapped to *AtPLC6* (At2g40116) and is predicted to cause a glutamic acid to lysine change at protein position 569 (Figure 7A, B).

To validate our sequencing results, we designed dCAPS primers to detect this candidate SNP in *frh3*. Primers were designed to create a full-length PCR product of 207 base pairs, and the forward dCAPS primer contained a mismatch that created a recognition site for the restriction enzyme Hyp188III only when the SNP was also present in the PCR product. Therefore, the WT sequence (containing guanine) would not be cut, while the mutant sequence (containing adenine) would be cut to generate two fragments

of sizes 186 bp and 21 bp, which distinguishable using gel electrophoresis with a 2-3% agarose gel. A reliable genotyping protocol was developed and enabled us to successfully identify the mutation in *frh3* suppressor plants, thereby validating our whole-genome sequencing results. The results of our genotyping scheme are shown in Figure 2A, with samples from a population segregating for the *plc6-E569K (plc6-1)* mutation.

Next, we sought to demonstrate that *plc6-1* was actually the mutation responsible for improving poor *hpat1/3* PT fertility. We hypothesized that the causal mutation should co-segregate with the suppressed phenotype as we propagate the *frh3* line. To test this, we backcrossed *frh3* plants (which were confirmed to be homozygous for *plc6-1*) with *hpat1/3* plants and allowed the F1s to self-fertilize. Out of 65 BC5F2 progeny genotyped, we identified only 2 plants that were homozygous WT for *PLC6*, indicating that there was a strong transmission bias in favor of the mutation (Figure 2B). Additionally, the suppressed phenotype perfectly co-segregated with *plc6-1* in 63 BC5F2 plants, as the two F2 *PLC6* +/+ plants recovered in this generation were phenotypically identical to normal, non-suppressed *hpat1/3* plants (Figure 2C, D). Plants that were heterozygous for *PLC6* (*hpat1/3; PLC6/plc6-1*) had significantly higher seed counts than those that were $PLC6^{WT}$ (*hpat1/3; PLC6/PLC6*), indicating that seed set is markedly improved when only half of the pollen carry the suppressive mutation; however, seed counts were highest in triple homozygous mutants (*hpat1/3; plc6-1/plc6-1*).

In order to confirm the identify of *plc6-1* as our *frh3* suppressor mutation, we tested the ability of the WT *PLC6* gene to rescue the suppressor phenotype, i.e. reverting the high-fertility phenotype of suppressed pollen to the low-fertility phenotype of *hpat1/3* pollen. We cloned the genomic sequence of the *PLC6* gene and its native promoter into the binary vector pFASTG01, which contains a convenient seed coat GFP selection marker (Figure S2 top) (Shimada et al., 2010), and transformed this into *frh3* plants. Positive transformants were crossed reciprocally with WT, and we examined the resulting ratios of GFP+:GFP- seeds to measure transmission efficiency. Because of this approach, we had to accurately determine which T1 plants had transgene insertions at a single loci, so that we could expect to observe a 1:1 ratio of GFP+:GFP- seeds if the transgene did not affect transmission (50% GFP+ seeds = 100% transmission efficiency of the inserted transgene). To do this, we first analyzed the crosses in which T1 plants

were used as females, as we did not expect this insertion to affect female transmission. 7 T1 plants were identified as having single-loci transgene insertions when crossed as females with WT pollen. The GFP+:GFP- seed ratios were then examined from crosses in which these 7 single loci-insertion T1 plants were used as males. For all 7 T1s, there was a statistically significant decrease in the number of observed GFP+ seeds compared to the expected value, indicating that the presence of the transgene specifically reduced transmission efficiency through the pollen (Figure S2, graph). Our interpretation of this data is that the presence of the *PLC6p:PLC6* transgene restored normal *PLC6* activity in *frh3* pollen, which countered the suppressive effect conferred by the *plc6-1* mutation, thereby rescuing suppression and causing reversion towards *hpat1/3*. The results indicated to us that *plc6-1* was indeed the causal mutation in the *hpat1/3* suppressor family *frh3*, and that *plc6-1* is a recessive mutation which is consistent with a loss of function allele.

4.2.3 hpat1/3; frh3/plc6-1 suppressors are not improved by the addition of the frh1/exo70a2-2

Because EXO70A2 may be binding PI(4,5)P2 , and PLC6 may be regulating PI(4,5)P2 levels at the PT plasma membrane, we wanted to interrogate the link between the *frh3/plc6-1* and *frh1/exo70a2-2* suppressor mutations. Specifically, we wanted to know if the *frh3/plc6-1* suppressor is acting through the same mechanism as *frh1/exo70a2-2*, or if there was an additive effect caused by the presence of two suppressor mutations. To address this, we crossed the *frh1* and *frh3* suppressor lines and obtained *hpat1/3; exo70a2-2; plc6-1 (+/-)* and *hpat1/3; exo70a2-2 (+/-); plc6-1* plants. We test crossed each line as a male with WT females and observed that in both cases, there was a strong transmission bias against the quadruple mutant pollen compared to the triple mutant pollen (Tables 6 and 7). Furthermore, quadruple homozygous mutant plants (“double suppressors”) had lower seed counts than triple homozygous (normal “single suppressors”) plants, and were therefore less suppressed (Figure 3).

We reasoned that if the mutations were acting through the same pathway, we would have observed a 1:1 ratio of progeny fertilized by double and single suppressor

pollen. This data suggests that the *frh1/exo70a2-2* and *frh3/plc6-1* mutants are not improving *hpat1/3* PT growth through identical mechanisms, because we would have observed a 1:1 transmission ratio of quadruple mutant pollen compared to triple mutant pollen. However, this data does not rule out the possibility that *frh3/plc6-1*-mediated suppression occurs by disrupting normal EXO70A2-mediated secretion in a similar manner as *frh1/exo70a2-2*; rather, it is possible that additive knockdown of EXO70A2-mediated secretion by *frh3/plc6-1* in the *frh1/exo70a2-2* genetic background (or vice-versa) is too strong of an effect, leading to sub-optimal *hpat1/3* suppression. This is supported by the observation that the partial knockdowns of exocyst-mediated secretion in *frh1/exo70a2-2* and *frh3/sec15a-3* improved *hpat1/3* fertility more than the stronger knockout mutations *exo70a2-3* and *sec15a-2*. Furthermore, it is possible that *PLC6* functions outside of exocyst-mediated secretion in *Arabidopsis* PTs, and the *frh3/plc6-1* suppressive mechanism may not be confined this pathway.

4.2.4 plc6-1 decreases pollen transmission in vivo and polarized growth in vitro

To learn more about *PLC6*'s role in PT growth, we wanted to examine how the *plc6-1* mutation affects pollen fertility in a WT genetic background. We crossed *frh3* suppressors with WT plants, allowed the F1s to self-fertilize, and genotyped the F2s to identify *plc6-1* plants that were homozygous WT for both *HPAT1* and *HPAT3*. To compare the transmission efficiency between mutant *plc6-1* and wildtype *PLC6* pollen, *plc6-1* heterozygotes (*HPAT1/3; PLC6/plc6*-1) were outcrossed as males with WT females. We genotyped the resulting progeny for the presence or absence of the *plc6-1* allele and discovered an approximate 2:1 ratio between *PLC6 +/+: PLC6/plc6-1* progeny, which differed significantly from a 1:1 ratio expected for normal transmission (Table 1) and indicates that *plc6-1* PTs were outcompeted by WT.

To identify the underlying causes of decreased *plc6-1* pollen transmission, we performed *in vitro* PT growth assays. Surprisingly, *plc6-1* PTs appeared drastically different compared to WT, with curvy and hooked shapes signifying erratic directional changes during growth (Figure 4A, and quantified in Figure 8C). This phenotype was also not observed in *hpat1/3; plc6-1/frh3* PTs, whose appearance strongly resembled WT

(Figure 1E), indicating that *hpat1/3* suppresses the abnormal "crooked growth" phenotype of *plc6-1* PTs. We also observed decreased length and increased width in *plc6-1* PTs, suggesting that cell polarity during tip growth is compromised (Figures 4B, D). We also observed lower germination frequencies of *plc6-1* PTs- a phenotype consistent with previously- characterized exocyst secretion mutants [Figure 4D, (Beuder et al., 2020)]. *plc6-1* self-fertilized siliques contained fewer seeds than WT (Figure 4C, 4D). Notably, positions with no seeds were typically found near the basal end of the silique, suggesting that decreased PT elongation is a primary cause of lower seed counts rather than meandering PT growth, ovular targeting, or rupture. To examine if *plc6-1* PT growth *in vivo,* we manually pollinated WT pistils with either WT or *plc6-1* pollen and collected them 24 hours after pollination. We fixed the pistils and stained them with aniline blue fluorochrome, which binds (1→3)-β-glucans enriched in PT cell walls, to visualize PTs within the pistil. Both WT and *plc6-1* PTs appeared to grow straight through the transmitting tract and reached the distal end of the pistil (Figure S3, top and bottom right); however, it is possible that fewer *plc6-1* PTs reached the distal end than WT, as we did not analyze this quantitatively. Individual PTs emerged from the transmitting tract and appeared to target ovules, and there were no erratic growth paths or other obvious abnormalities phenotypes observed in *plc6-1* PTs compared to WT (Figure S3). This could be due to the physical support provided by the pistil tissue *in vivo,* which may force PTs to grow straighter and mask the crooked growth phenotype observed *in vitro*. Also, guidance cues provided by the pistil may be reinforcing PT growth directionality, and the absence of these cues *in vitro* leads may cause frequent reorientation of PT growth. Taken together, this data suggests that *PLC6* promotes pollen fertility by helping PTs maintain cell polarity during growth *in vitro*, but this may not be essential for *in vivo* PT growth and seed production. However, the pattern of seed production (or rather, the lack thereof) indicates that *PLC6* promotes PT growth required for full fertility.

4.2.5 plc6 insertion mutants do not suppress hpat1/3 fertility defects

Because the suppressive effects of *plc6-1* were rescued by the WT *PLC6* gene, we hypothesized that *plc6-1* was a loss of function allele. Therefore, we wanted to

determine if knocking out *PLC6* expression would also suppress *hpat1/3* pollen fertility defects. We obtained three *plc6* mutant lines with TDNA insertions located in different regions of the *PLC6* gene (Figure 7A). We extracted RNA from flowers and made cDNA libraries to check for *PLC6* expression in WT and our three mutant lines. We tested for disruption of gene expression using two primer combinations spanning exons 1-4 (region 1) and exons 6-9 (region 2). In WT flower cDNA, we were able to amplify both regions from the cDNA template, indicating that the predicted transcript is produced. In both the CSHL_GT4996 (*plc6-2*) and the SALK_090508 (*plc6-3*) mutants, we were unable to robustly amplify region 1, likely caused by disruption by the presence of the TDNA insertion; however, faint bands were visible (Figure 7D). We were also able to amplify region 2 from both *plc6-3* and *plc6-2* cDNA templates, indicating that some *plc6* C-terminal mutant isoform may be still expressed in these lines. Conversely, we were able to amplify region 1 from SALK_0401365 (*plc6-4*) cDNA, but we were unable to amplify region 2, which leaves open the possibility that a truncated PLC6 mutant isoform could be produced in *plc6-4.* We decided to focus on characterizing the *plc6-2* and *plc6-3* mutants because we reasoned that they were most likely to produce non-functional protein products.

To test for *hpat1/3* suppression, we crossed the *plc6-2* and *plc6-3* TDNA lines into *hpat1/3* and obtained plants that were heterozygous for either TDNA mutation (*hpat1/3 plc6-2 +/-* and *hpat1/3 plc6-3+/-*). We test crossed *hpat1/3; plc6 +/-* plants as males with WT females with the expectation if either *plc6* TDNA allele was suppressing *hpat1/3* pollen fertility defects, then we would observe a transmission bias in favor of the mutation. Interestingly, we observed a strong bias against transmission for *plc6-2* and *plc6-3* (Tables 3 and 5), indicating that these mutations decreased *hpat1/3* pollen fertility. We obtained *hpat1/3 plc6-2* and *hpat1/3 plc6-3* triple mutant plants and performed seed counts. Compared to their *hpat1/3 PLC6*^{WT} siblings, *hpat1/3; PLC6/plc6-2* and *hpat1/3; plc6-2* triple homozygous mutants had significantly lower seed counts (Figure 5D), as did *hpat1/3; plc6-3* triple homozygous mutants (Figure 5J). Since this is the opposite of what we expected, we examined pollen phenotypes of these mutants more closely through *in vitro* PT growth assays. PT lengths were comparable between both *hpat1/3; plc6* transgene insertion triple mutants and *hpat1/3* double mutants (Figure 5A,C,G and I). PT

bursting occurred at a high frequency in *hpat1/3*, and this appeared unchanged in both triple mutants (Figure 5E and K); however, PT germination frequencies were significantly decreased in both triple mutants (Figure 5F and L). This data indicates that neither *plc6-2* nor *plc6-3* suppress *hpat1/3* pollen fertility defects; on the contrary, they acted as enhancers of the low pollen fertility phenotype, primarily through decreasing PT germination frequency. This data also suggests that the *plc6-1* allele is not acting as a full loss-of-function allele.

To further examine the role of *PLC6* in pollen fertility, we also wanted to determine if *plc6-2* and *plc6-3* mutations affected pollen transmission and growth in an otherwise WT genetic background. We performed test crosses with plants that were heterozygous for either *plc6-2* or *plc6-3* as males (*PLC6/plc6-*), and, surprisingly, we observed no transmission bias either for or against either transgene (Tables 2 and 4). We compared seed sets of *plc6-2* and *plc6-3* homozygous mutants to WT and found that the seed counts appeared similar to WT (Figure 6B, D, F and H). Furthermore, the lengths and overall appearance of *in vitro*-grown *plc6-2* and *plc6-3* PTs both strongly resembled WT (Figure 6A, C, E and G). A possible explanation for why we did not observe an abnormal PT growth phenotype in either *plc6* TDNA insertion mutants could be functional redundancy among pollen-expressed *PLCs.*

***PLC* gene expression across reproductive and vegetative tissues**

To explore the possibility that PLCs could be functioning redundantly in PTs, we wanted to compare individual *PLC* gene expression levels in pollen. We downloaded a RNA-sequencing dataset (Loraine et al., 2013) and extracted the RPKM values for each *PLC* gene in both pollen and (average) seedling and plotted these values on a $\log_{10}$ scale (Figure 7E). Every gene had detectable levels of expression in both sample types except for *PLC1,* which was not found to be expressed in pollen. Notably, *PLC6* was found to be the most highly- expressed *PLC* in pollen, with an RPKM value almost one full order of magnitude higher than the second most-highly expressed *PLC* in pollen, *PLC4*; *PLC6* also had the lowest level of expression in seedlings. In addition to *PLC4* and *6, PLC5* and *9* also had higher levels of expression in pollen than in seedlings. This data spotlights

PLC6 as potentially being the major, canonical *PLC* isoform in pollen, but does not rule out the possibility that other *PLCs* are also playing important roles.

We also wanted to examine *PLC* expression patterns across different tissue types. To do this, we used the RNA-sequencing data published on the Klepikova Atlas on TAIR (Klepikova et al., 2016) to generate expression profiles for a small range of flower and vegetative tissue types. We compared data from this category for each *PLC* gene in anthers (pollen was not available), carpel, root, and leaf samples (see Figure 7F legend for more details). In this small set of tissue types, *PLC6* expression was highly enriched in the anthers, and highest in this tissue type compared to the other PLCs. *PLC1* and *7* gene expression was higher in anthers compared to carpel, but their highest expression levels were found in vegetative tissues (Figure 7F). *PLC4* expression was highest in anthers compared to other tissue types, corroborating the previous report that *PLC4p::GUS* promoter-reporter expression was observed in mature pollen (Hunt et al., 2004).

We also generated expression profiles using microarray data (Schmid et al., 2005) for each *PLC* gene except for *PLC6*, for which data was unavailable (Figure 7G). We observed that *PLC3, 4, 5,* and *7* expression was high in mature pollen and very low in carpel; each of these were expressed in at least one vegetative tissue (root), while *PLC4* expression was highly enriched in pollen. *PLC1, 2, 8* and *9* had relatively high expression in vegetative tissues and low levels of expression in mature pollen. *PLC2* expression was also observed in the carpel (Figure 7, G), consistent with its known role in female gametogenesis (Di Fino et al., 2017). In summary, our gene-expression analyses indicate that *PLC6*'s expression profile is unique among the PLCs, with high expression levels in developing and mature pollen (and possibly anther tissue itself), suggesting that it is a major PLC isoform present in growing PTs. However, most *PLCs* are expressed at some level in anthers and pollen, so it is possible that multiple *PLCs* are functioning redundantly to promote proper PT growth in *Arabidopsis*. Among these, *PLC4*'s male-enriched expression profiles are aligned with having a specialized role in pollen.

4.2.6 plc6-1 mutation is located in the C2 domain at a calcium-coordinating motif

Because our data suggests that *plc6-1* is not a full loss of function allele, we wanted to learn more about how the *plc6-1* mutation affects PLC6 function by further examining the nature of the mutation. We aligned the primary structures of *Arabidopsis* PLCs and found that the E569 position is located in the C2 domain, and this residue was conserved in five out of nine PLC sequences (Figure 7B). We also aligned the primary structure of PLC's C2 domain to the C2 domains of three protein kinase Cs from rat and human, for which protein structures have already been determined (Corbalan-Garcia & Gómez-Fernández, 2014; Pike et al., 2007; Sutton & Sprang, 1998; Verdaguer et al., 1999). This revealed that the E569 position in PLC6 falls between key aspartic acid residues involved in calcium-coordinating, as well as other residues involved in PI interactions [Fig S4A;]. To determine the spatial positioning of this residue we used a homology modeling approach using the Phyre 2 protein fold recognition server (Kelley et al., 2015). The full-length, predicted PLC6 protein sequence was modeled against a protein fold library and the best model returned was fold library ID c1djyB, which was modeled using a crystal structure for the phosphoinositide-specific PLC C δ1 from rat complexed with inositol-2,4,5-trisphosphate (Essen et al., 1997) as a template; this model returned a with a 100% confidence score for 87% of the PLC6 sequence. The mutated residue (E569K) occurred on an external loop in the C2 domain and was in particularly close proximity to calcium-coordinating aspartic acid residues in this 3D structure. The charge inversion of the *plc6-1* allele is therefore likely to interfere with the electrostatic interactions taking place in this region.

4.2.7 plc6-1 PTs are sensitive to high calcium levels

Based on our *in silico* analysis of the *PLC6* C2 domain, the E569 residue resides within a cluster of negatively-charged aspartic residues that appear to be a crucial location for coordinating calcium ions. Therefore, we hypothesized that the *plc6-1/E569K* mutation may be inhibiting PLC6's ability to bind and coordinate calcium, which is required for C2 lipid biding and PLC activity in general (Otterhag et al., 2001; Rebecchi & Pentyala, 2000). Therefore, we wanted to examine how *plc6-1* affected the PT growth response to calcium. To do this, we performed *in vitro* growth assays to analyze both PT elongation and

curliness in response to varying calcium concentrations in the growth media. After 2.5 hours of growth on normal 2 mM calcium, *plc6-1* PTs were shorter than WT, as we had observed previously (Figure 8A, B, Figure 4B). WT PTs were largely insensitive to changes in calcium level with a statistically significant reduction in average length observed only at 8 mM calcium levels compared to 2 mM ($Length_{0.5mM}$ = 236.6967 ± 109.1968 μm, $Length_{2mM}$= 252.8587 ± 93.9361 μm; Student's t-test $p\text{-value}_{0.5\ mM\ vs\ 2\ mM}$ = 0.076671; $Length_{4mM}$ = 257.3808 ± 98.4054; Student's t-test $p\text{-value}_{2mM\ versus\ 4\ mM}$ = 0.598274; $Length_{8mM}$ = 165.0201 ± 79.9379 μm; Student's t-test $p\text{-value}_{2mM\ vs\ 8mM}$ = 2.28463E-26) . *plc6-1* PTs, however, were sensitive to changes in calcium level. *plc6-1* PT growth was optimal at 1 mM calcium, and PT lengths decreased as calcium concentrations increased ($Length_{0.5mM}$ = 162.5113 ± 62.4751 μm, $Length_{2mM}$= 136.7914 ± 51.4164 μm; Student's t-test $p\text{-value}_{0.5\ mM\ vs\ 2\ mM}$ = 6.93687E-07; $Length_{4mM}$ = 119.9213 μm ± 41.2006 μm; Student's t-test $p\text{-value}_{2mM\ versus\ 4\ mM}$ = 5.66779E-05; $Length_{8mM}$ = 70.2689 ± 31.7174 μm; Student's t-test $p\text{-value}_{2mM\ vs\ 8mM}$ = 1.6223E-51).

The PT "curly index (CI)" was determined by first measuring two values- the total PT length, and the shortest length between the pollen grain and the tip of the tube ("minimal length"). CI values are calculated by dividing the total length by the minimal length; a value of 1 means the PT was perfectly straight. At each concentration, the curly index values for *plc6-1* were lower than WT, indicating that *plc6-1* PTs were curlier than WT across all concentrations (statistical analyses described in figure legends) (Figure 8C). Furthermore, WT PT curliness was unaffected at 0.5X compared to 1X ($CI_{0.5X}$ = 0.924536 ± 0.082286, CI_{1X} = 0.897569 ± 0. 0.09692; Student's t-test p-value= 0.082793), and WT PTs actually became slightly straighter at 2X calcium levels compared to 1X (CI_{2X}= 0.977564707 ± 0.190625387; Student's t-test p-value= 0.002225355). Similarly, *plc6-1* PT curliness was not significantly affected at 0.5X calcium levels compared to 1X ($CI_{0.5X}$= 0.8318 ± 0.193786, CI_{1X}= 0.800275 ± 0.167353; Student's t-test p-value= 0.322287), but *plc6-1* PTs were significantly curlier at 2X calcium compared to 1X (CI_{2X}=0.591686 ± 0.252526; Student's t-test p-value = 1.42817E-06), which is an opposite response than observed for WT PTs. This data indicates that *plc6-1* PT growth is sensitive to higher environmental calcium levels; however, the link between *PLC6,* calcium, and PT growth is still unclear.

4.2.8 Subcellular localization of PLC6-mNG

To confirm that PLC6 is expressed in PTs, and to determine its subcellular localization, we cloned and transformed plants with a construct encoding the *PLC6* genomic sequence fused with a C-terminal mNeonGreen (mNG) under the native *PLC6* promoter (*PLC6p:PLC6-mNG*). PI(4,5)P_2 and other PLCs have been shown to localize to the apical and subapical plasma membrane in PTs, respectively, (Dowd et al., 2006; Helling et al., 2006) so we hypothesized that PLC6-mNG would localize to the subapical plasma membrane as well. Using confocal microscopy, we examined the pattern of mNG signal in PTs from three positive, independent T1 plants. We observed diffuse signal throughout the cytoplasm, with no enrichment at the plasma membrane (Figure 9). However, to our surprise, we observed enrichment of mNG signal in the shape of two connected circles far from the apical tip. Using DAPI to visualize the sperm and vegetative nuclei, we confirmed that mNG signal was enriched in the endomembrane surrounding the sperm nuclei (Figure 9). These patterns were consistent among all three T1 plants.

To determine if the PLC-mNG C-terminal fusion protein was functional, we wanted to test its ability to rescue suppression of *frh3* pollen in the same manner as described earlier (Figure S2). We transformed the construct into *frh3* suppressor plants and crossed positive T1s reciprocally with WT. We selected T1s that showed a 1:1 ratio of fluorescent seeds when crossed as females, which indicates that they were single loci-insertion transformants. Then, we analyzed the seeds produced when these plants were crossed as males. For 8 single loci-insertion T1 plants, 4 of these plants produced significantly less then 50% fluorescent seeds when used as pollinators, indicating that suppression was being rescued in *frh3* pollen carrying the construct, which suggests the PLC-mNG fusion protein is functional (Figure S5). The other 4 T1 plants produced seed sets with approximately a 1:1 ratio of fluorescent to non-fluorescent seeds, indicating no transmission bias for pollen carrying the construct. We believe this data suggests that the PLC-mNG C-terminal fusion protein is likely functional.

4.3 Discussion

Similar to our findings for the *hpat1/3* suppressor mutations *exo70a2-2/frh1, exo70a2-3, sec1a-2* and *sec1a-3/frh2* (Beuder et al., 2020)*, plc6-1/frh3* also strongly rescued poor pollen fertility of *hpat1/3* by improving PT elongation, decreasing morphological defects, and decreasing bursting frequency. Also, the elevated apical secretion of the GF(EXT3)P reporter protein in *hpat1/3* is decreased in *plc6-1/frh3* (Figure S1)*,* suggesting that *PLC6* also plays a role in promoting secretion of Hyp *O*-arabinoside-containing cargos. Because of these similar phenotypes and the known link between PLCs and EXO70s, it is possible that *PLC6* may play a role in regulating exocyst-mediated secretion. PT germination is drastically decreased in *exo70a2* and *sec15a* secretion mutants, and *plc6-2* and *plc6-3* decreased PT germination frequency in the *hpat1/3* background, consistent with *PLC6* having a role in promoting secretion in PTs.

It is interesting that *plc6-2* and *plc6-3* did not affect PTs in the WT background. One possibility is that multiple PLCs function redundantly in PTs. No individual *PLCs* are significantly up- or down-regulated in *hpat1/3* pollen grains (RNA sequencing data not shown), but this may be different in PTs and/or because of loss of *PLC6.* If *PLC* gene expression is mis-regulated in *hpat1/3* PTs, then that could explain why there are different phenotypes for *plc6-2* and *plc6-3* in WT versus *hpat1/3* genetic backgrounds. Another possibility is that PLCs are not perfectly redundant, and *hpat1/3* PTs are simply more sensitive to changes that have little or no effect on WT PTs.

There are also important differences between the *plc6-1/frh3* and exocyst mutant suppressors. *exo70a2* and *sec15a* PTs did not elongate as much as those of WT, but were phenotypically normal otherwise (Beuder et al., 2020). This contrasts to the looped and crooked appearance of *plc6-1* PTs, which suggests that *PLC6* plays a role in regulating cell polarity during tip growth. Because of these phenotypic differences between *plc6-1* and exocyst mutant PTs, *plc6-1* is not likely causing robust knockdown of global exocyst-mediated secretion to slow down growth in the same manner as *exo70a2* or *sec15a*. Rather, this suggests that *PLC6* helps maintains PT polarity during growth.

Previous research shows that $PI(4,5)P_2$ availability is a limiting factor for EXO70 binding at the plasma membrane (Pleskot et al., 2015), and $PI(4,5)P_2$ accumulation

caused by PI5P kinase overexpression resembles the *plc6-1* phenotype (Ischebeck et al., 2008; Zhao et al., 2010). Our genetic data suggests that *plc6-1* is a recessive mutation, which is consistent with *plc6-1* as a loss of function allele. Therefore, one possibility is that PLC6-1 may be defective in PI(4,5)P_2 binding and/or cleavage to form IP3 and DAG, which would expand PI(4,5)P_2 availability at sub-apical regions along the PT plasma membrane and cause dispersion of exocyst-mediated secretion and decrease cell polarity and tip growth. In this model, apical secretion of Hyp *O*-arabinoside-containing cargos in *hpat1/3* (as seen with the GF(EXT3)P reporter) is decreased at the apical tip through this dispersion mechanism caused by *plc6-1*, which decreases apical extensin accumulation and restores tip extensibility and polarized growth in *hpat1/3* PTs. In the WT background, loss of polarized exocytosis misdirects apical secretion, leading to curly growth paths and wider PTs.

However, PLC6-mNG signal not observed at the plasma membrane, but rather it was localized to the cytoplasm and was enriched in the sperm endomembrane system. While the ER is considered to be the main internal calcium store in animals (Segal et al. 2014), other organelles likely contribute to cytoplasmic calcium levels. In human sperm, the nuclear envelope and surrounding endomembrane compartments contain calcium channels, which may be involved in regulating cytoplasmic or nuclear calcium levels (Costello et al., 2009). Less is known about calcium storage in plant cells, but cyclic nucleotide-gated ion channels (CNGC) which transport calcium are localized to the nucleus (Costa et al., 2018). Glutamate receptor-like channels (GLRs) transport calcium through the plasma membrane to modulate cytoplasmic calcium concentrations and control PT growth, and *glr1* knockout mutants show defects in tip growth somewhat similar to *plc6-1* (Michard et al., 2011). Similar to PLC6-mNG, GLR3-GFP localizes to the sperm endomembrane in PTs (Wudick et al., 2018), suggesting that this organelle may have a role in storing calcium to regulate cytoplasmic or nuclear calcium concentration. Therefore, rather than regulating PI(4,5)P2 at the plasma membrane, it is probably more likely that PLC6 controls PT growth by locally regulating PI signaling at the sperm endomembrane, which may affect calcium transport.

Based on our structural analysis, it is likely that the charge inversion caused by the *plc6-1 E569K* mutation impairs calcium coordinating at this region. This is consistent with

a loss-of-function effect, and our genetic data indicates that *plc6-1* is a loss-of-function allele. Furthermore, extra calcium induced curly growth in *plc6-1* but not WT PTs. But how are these phenotypes related? What is the connection between PLC6/PLC6-1 activity, calcium-coordinating, cytoplasmic calcium levels, and PT growth? To better understand *PLC6's* role in regulating PT growth, and to further elucidate the mechanism underlying *frh3/plc6-1*-mediated suppression of *hpat1/3* PT fertility defects, we must address several key questions. (1) Is PLC6 activity is affected in *plc6-1,* and if so, then how? (2) Is PI(4,5)P2 present at the sperm endomembrane? If so, then (3) does PLC6 regulate PI(4,5)P_2 availability at the sperm endomembranes, and to what end? Lastly, (4) how are cytoplasmic calcium levels affected in *hpat1/3,* and does PLC6 regulate this as well? Answering these questions will greatly improve our understanding of PLC6's role in regulating HPAT-mediated PT growth.

4.4 Materials and Methods

4.4.1 Plant growth conditions

Columbia-0 WT *Arabidopsis* mutants were grown under 16- hour light/ 8- hour dark conditions in controlled growth room maintained at 23^{O} C.

4.4.2 Suppressor screen

Mutagenesis of *hpat1/3* seeds, suppressor phenotyping and selection, whole-genome sequencing and analysis steps were performed as previously described in (Beuder et al., 2020; Beuder & MacAlister, 2020).

4.4.3 PT assays and seed counts

All pollen germination and growth assays were carried out using *in vitro* pollen growth media (PGM) modified from (Rodriguez-Enriquez et al., 2013) consisting of 10% sucrose, 0.01% boric acid, 1mM CaCl2, 1mM Ca(NO3)2, 1mM KCl, 0.03% casein enzymatic hydrolysate, 0.01% myo-inositol, 0.1 mM spermidine, 10mM γ-Aminobutyric acid, 500μM

methyl jasmonate, pH adjusted to 8.0 and solidified with 1% low melting temperature agarose. PTs were grown on cellophane placed on top of the media and placed in a homemade humid chamber (glass box with wet paper towls) and grown in the dark. Length, width, germination, and bursting frequency assays were performed as previously described in Beuder et al., 2020).

4.4.4 Cloning

The genomic suppressor rescue construct (*PLC6p:PLC6*) was cloned by amplifying the genomic *PLC6* coding sequence and the entire upstream region before the end of the previous gene using the Phusion® High-Fidelity DNA Polymerase (NEB, M0530S) from WT Col-0 DNA extracted from leaf tissue. *PLC6:PLC-mNeonGreen* (mNG) was cloned by fist amplifying the same region, with a different reverse primer to omit the stop codon, and then amplifying the mNG sequence from plasmid DNA,. We fused mNG to the *PLC6* C-terminus using the Gateway cloning system. Constructs were cloned into the binary vector pFASTG01 (*PLC6p:PLC6*) or pFASTR01 (*PLC6p:PLC6-mNG*) (Shimada et al., 2010) and transformed into plants with Agrobacterium.

4.4.5 Microscopy

PTs were imaged for growth, bursting, germination, and morphological assays were imaged with a Leica DM5500 compound microscope with DIC optics at 10X magnification. GF(EXT3)P+ PTs were imaged using the same microscope but with the GFP filter. For imaging of PLC6-mNG fusions, PTs were grown *in vitro* on slides with rubber spacers containing PGM for 2 hours in a humid chamber in the dark. After growth time, liquid PGM with 4 µM FM4-64 was added on top of the PTs and covered with a coverslip. PTs were imaged using a Leica SP5 laser-scanning confocal microscope 10 minutes after FM4-64 application. To image PLC6-mNG, we used an excitation laser with 488 nm wavelength, a RSP500 dichroic beam splitter, and detectors were set to capture light with a wavelength range of 494-575 nm. To image FM4-64, we used an excitation laser with 514 nm wavelength, a DD 458/514 dichroic beam splitter, and detectors were set to capture light with a wavelength range of 620-783 nm. Images were overlayed with Fiji.

4.5 Acknowledgments

This material is based upon work supported by the National Science Foundation under Grant No. IOS-1755482. We wish to thank Gregg Sobocinski for microscopy assistance and advice.

4.6 Author Contributions

Cora MacAlister designed the study and conducted the *frh* mutant screen.. Steven Beuder wrote the paper and carried out microscopy, bioinformatic analysis of whole genome sequences to identify candidate suppressor mutations, functional rescue assays, and performed crosses and PT phenotyping. Bent L. Petersen and Svenning Rune Moeller generated the 35S::EXT3ssGF(EXT3)P construct. Xuesi Hua performed genotyping and PT phenotyping. Alexandria Dorchak carried the cloning.

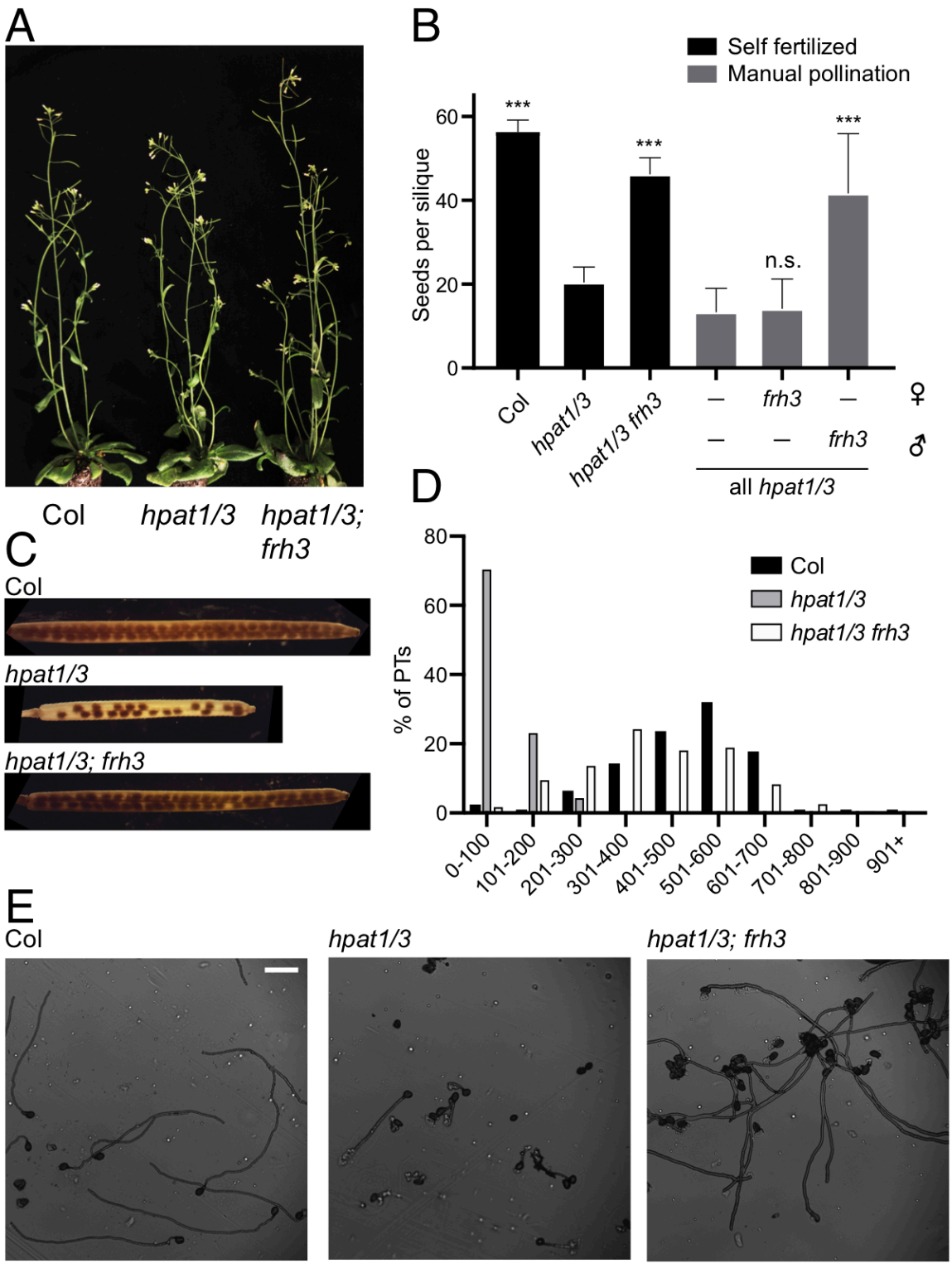

Figure 4-1. hpat1/3 pollen fertility defects and seed production are rescued in frh3. A) hpat1/3 and hpat1/3; frh3 (frh3) plants show no vegetative abnormalities. B) Seed counts (number of seeds per silique) for WT, hpat1/3 and frh3. Bars represent average seed counts and error bars represent standard

*deviation. (N ≥ 10 siliques per genotype). Statistical analysis performed using Student's t-test. *** denotes p-value ≤ 0.0005. C) Representative siliques from each genotype cleared in 70% ethanol. D) Lengths of PTs grown in vitro for 5 hours; N ≥ 203 PTs per genotype. E) Representative PTs from each genotype from (D), imaged at 10X magnification with DIC optics; scale bar represents 100 microns.*

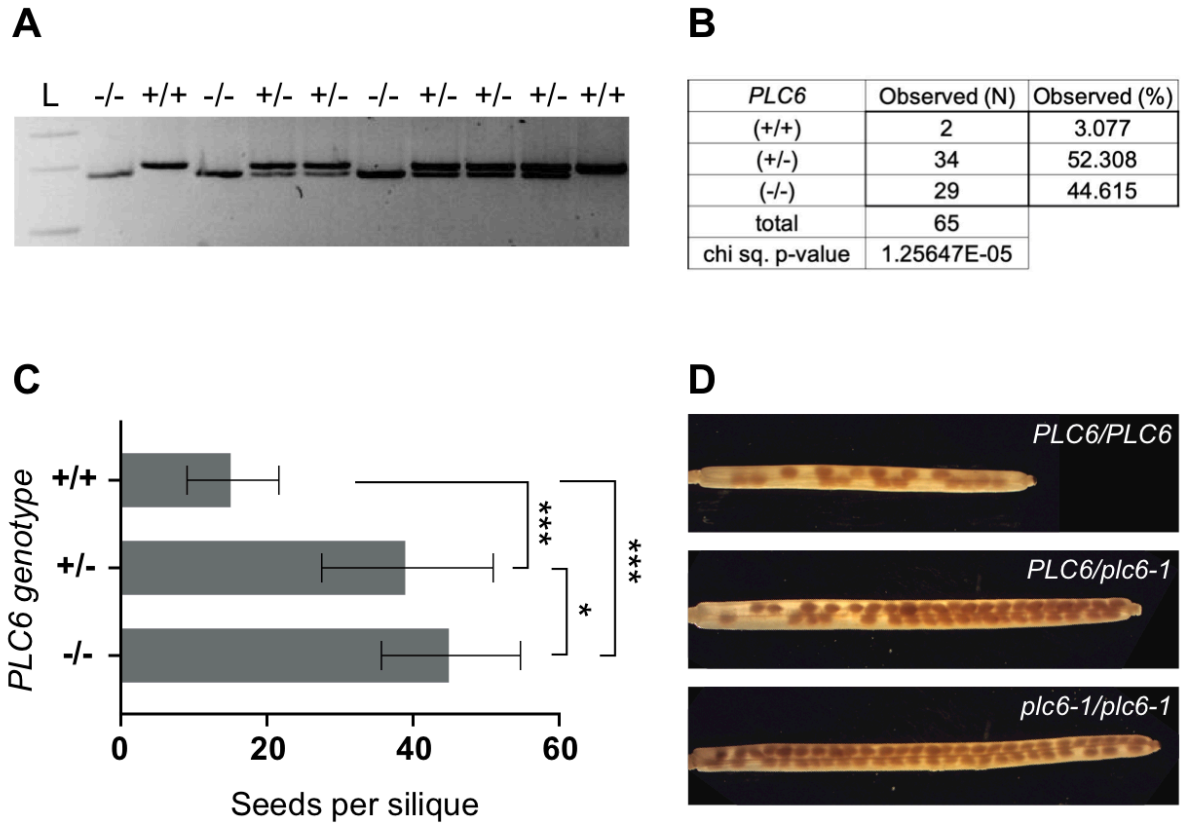

PLC6	Observed (N)	Observed (%)
(+/+)	2	3.077
(+/-)	34	52.308
(-/-)	29	44.615
total	65	
chi sq. p-value	1.25647E-05	

*Figure 4-2. hpat1/3 suppression phenotype co-segregates with plc6-1 mutation in BC5F2 generation frh3 plants. A) Genotyping of plc6-1 mutation. PCR products were amplified using dCAPS primers, treated with HYP188III restriction enzyme, and run on a 2% agarose gel. Full-length (WT) PCR product = 207 bp. PCR product containing the plc6-1 mutation is cleaved at the 3' end of primer resulting in 183 and 24 bp bands. B) Genotype segregation ratios of BC5F2 individuals. C) Seed counts for BC5F2s based on PLC6 genotype. (+) denotes the WT allele, and (-) denotes plc6-1 mutant allele. Statistics performed using Student's t-test; * indicates p-value < 0.05. D) Representative siliques of each genotype cleared with 70% ethanol.*

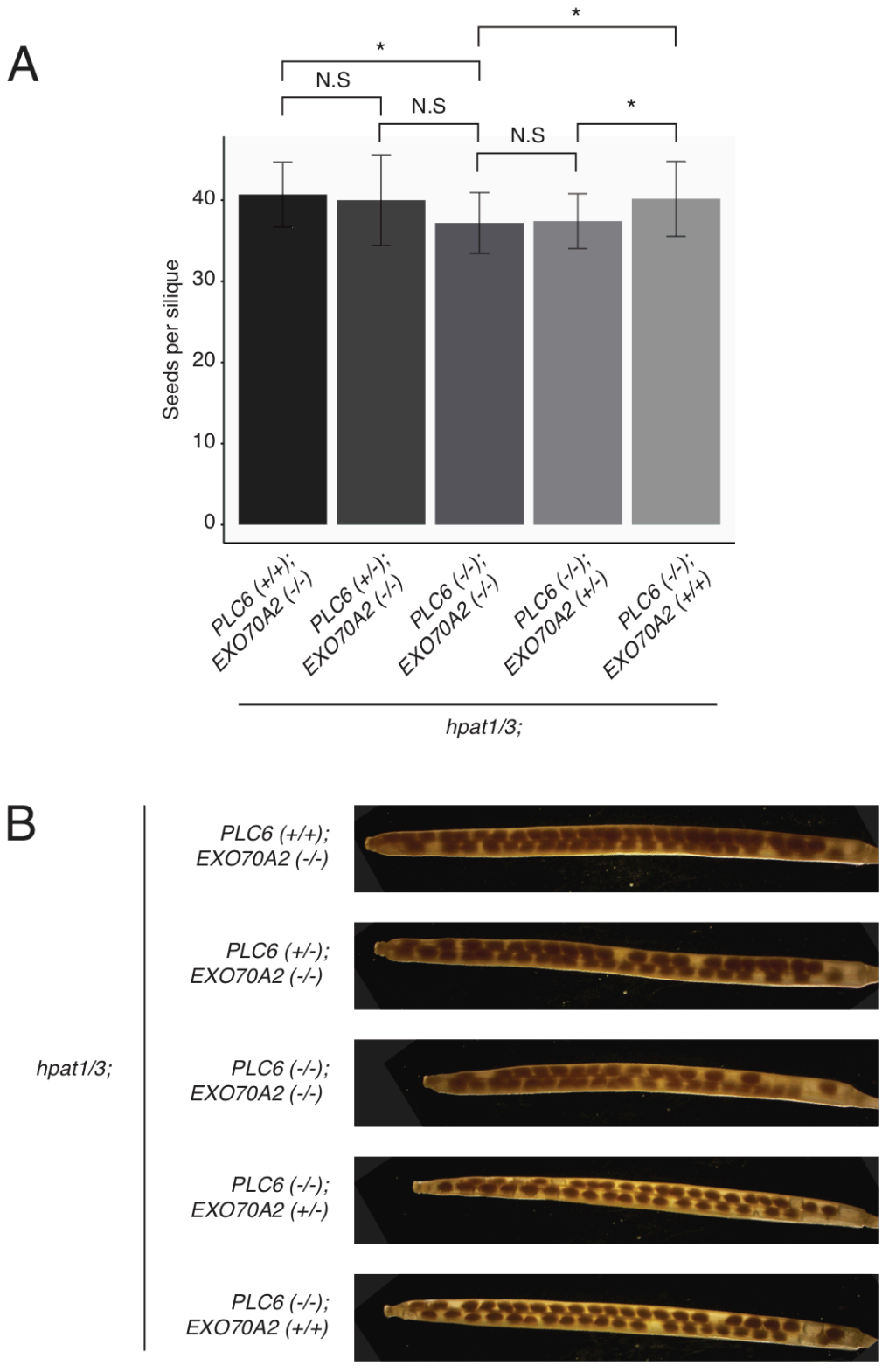

Figure 4-3. frh3/plc6-1 and frh1/exo70a2-2 seed production is not increased in frh3; frh1 "double suppressor". A) Seed counts of hpat1/3 plants carrying WT or mutant alleles of PLC6 [PLC6 (+) or plc6-1 (-)] or EXO70A2 [EXO70A2 (+) or exo70a2-2 (-)]. NWT =10 siliques, N ≥17 siliques for other genotypes.

Statistical analysis performed using Student's t-test. B) Representative siliques for each genotype cleared in 70% ethanol.

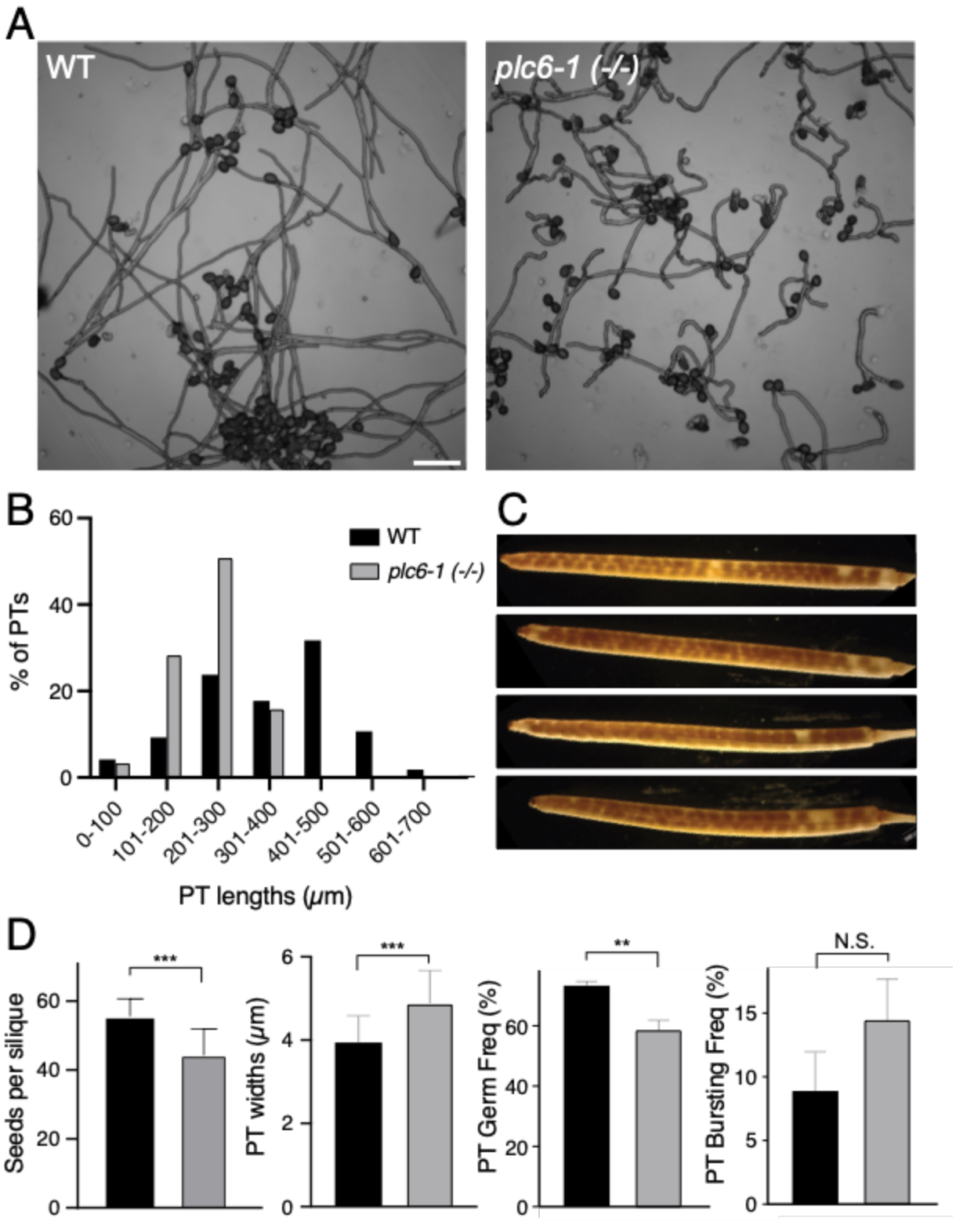

Figure 4-4. plc6-1 PTs are curlier, wider, and germinate less frequently than WT. A) PTs grown in vitro for four hours and imaged with DIC optics at 10X magnification; scale bar represents 100 microns. B) Quantification of PT lengths after 5 hours growth in vitro N ≤ 202 PTs per genotype. C) Pictures of plc6-1

*siliques. D) Reproductive phenotypes. Far left- seed counts for WT (N = 14) and plc6-1 (N= 13). Left middle- PT width measurements after 1 hours of growth; N ≥ 200 PTs per genotype. Right middle and far right- Germination and bursting frequencies after 2 hours of in vitro growth. Both bursting and germination experiments were repeated in triplicate for each genotype. Nbursting ≥ 159 PTs analyzed per experiment, per genotype. Ngermination ≥ 404 pollen grains analyzed per experiment per genotype. Statistical analyses performed using Student's t-test; ** represents p-value < 0.005.*

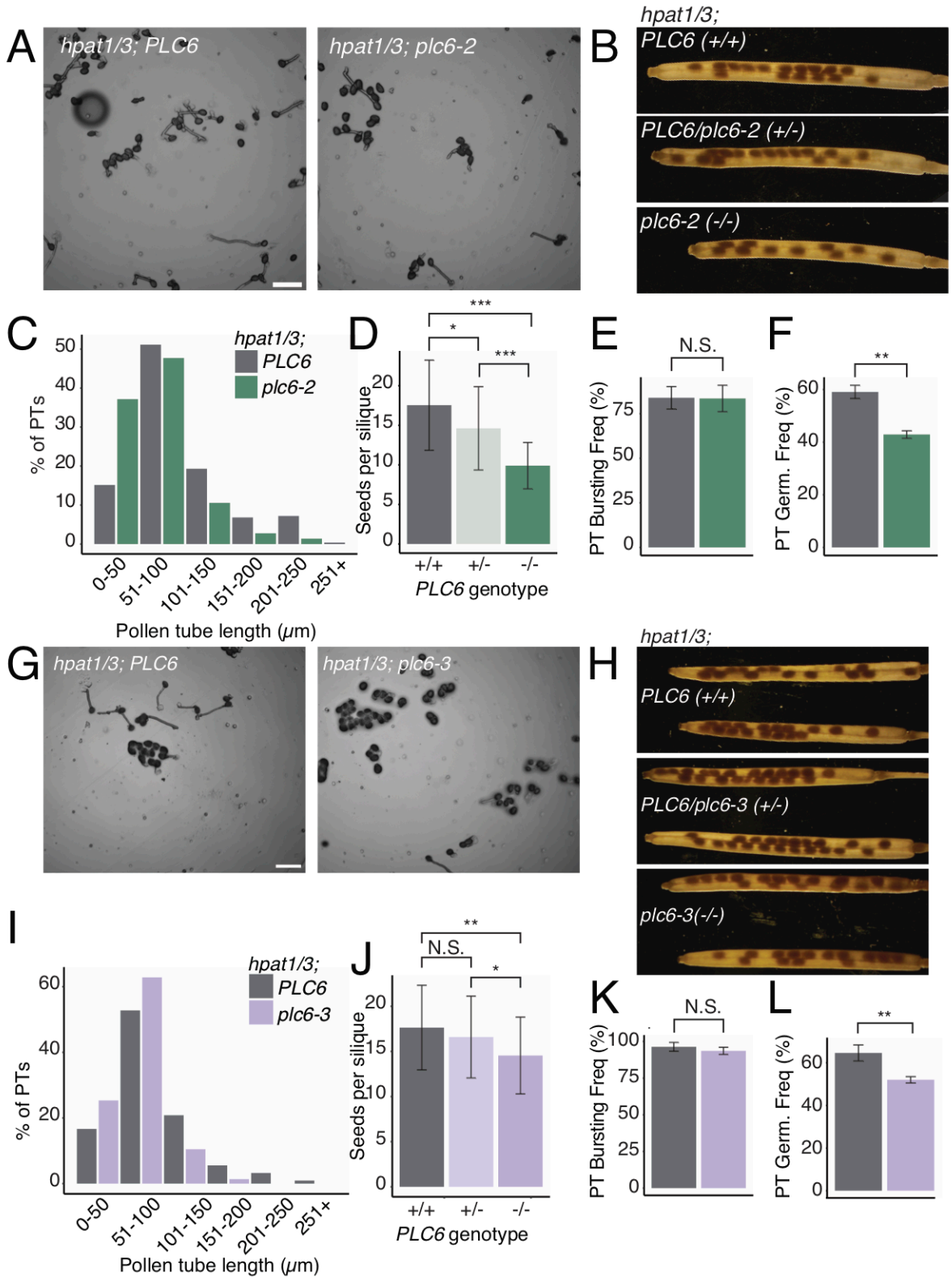

Figure 4-5. plc6 TDNA insertion mutations do not improve hpat1/3 pollen fertility. A) PTs grown in vitro for 2 hours and imaged with DIC optics at 10X magnification; scale bar represents 100 microns. B) Representative siliques for each genotype cleared with 70% ethanol. C) Quantification of PT lengths after

2 hours growth in vitro N ≥ 218 PTs per genotype. D) Seed counts based on plant genotype; (-) denotes plc6-2 mutant allele. N ≥ 19 siliques per genotype. Bars represent average seed counts and error bars represent standard deviation. E) PT bursting frequencies after 2 hours in vitro growth. Experiment repeated three times with N ≥ 112 PTs per genotype per experiment. F) PT germination frequencies after 2 hours in vitro growth. Experiment repeated three times with N ≥ 332 pollen grains measured per genotype per experiment. G) PTs grown in vitro for 2 hours and imaged with DIC optics at 10X magnification; scale bar represents 100 microns. H) Representative siliques for each genotype cleared with 70% ethanol. I) Quantification of PT lengths after 2 hours growth in vitro N ≥ 216 PTs per genotype. J) Seed counts based on plant genotype; (-) denotes plc6-3 mutant allele. N ≥ 22 siliques per genotype. K) PT bursting frequencies after 2 hours in vitro growth. Experiments repeated twice for each genotype with N ≥ 150 pollen grains examined, except in one experiment, the Nhpat1/3=66. L) PT germination frequencies after 2 hours in vitro growth. Experiment repeated three times for hpat1/3 (N ≥ 239 per experiment) and twice for hpat1/3; plc6-3 (N ≥ 501 per experiment). Statistical analyses performed using Student's t-test.

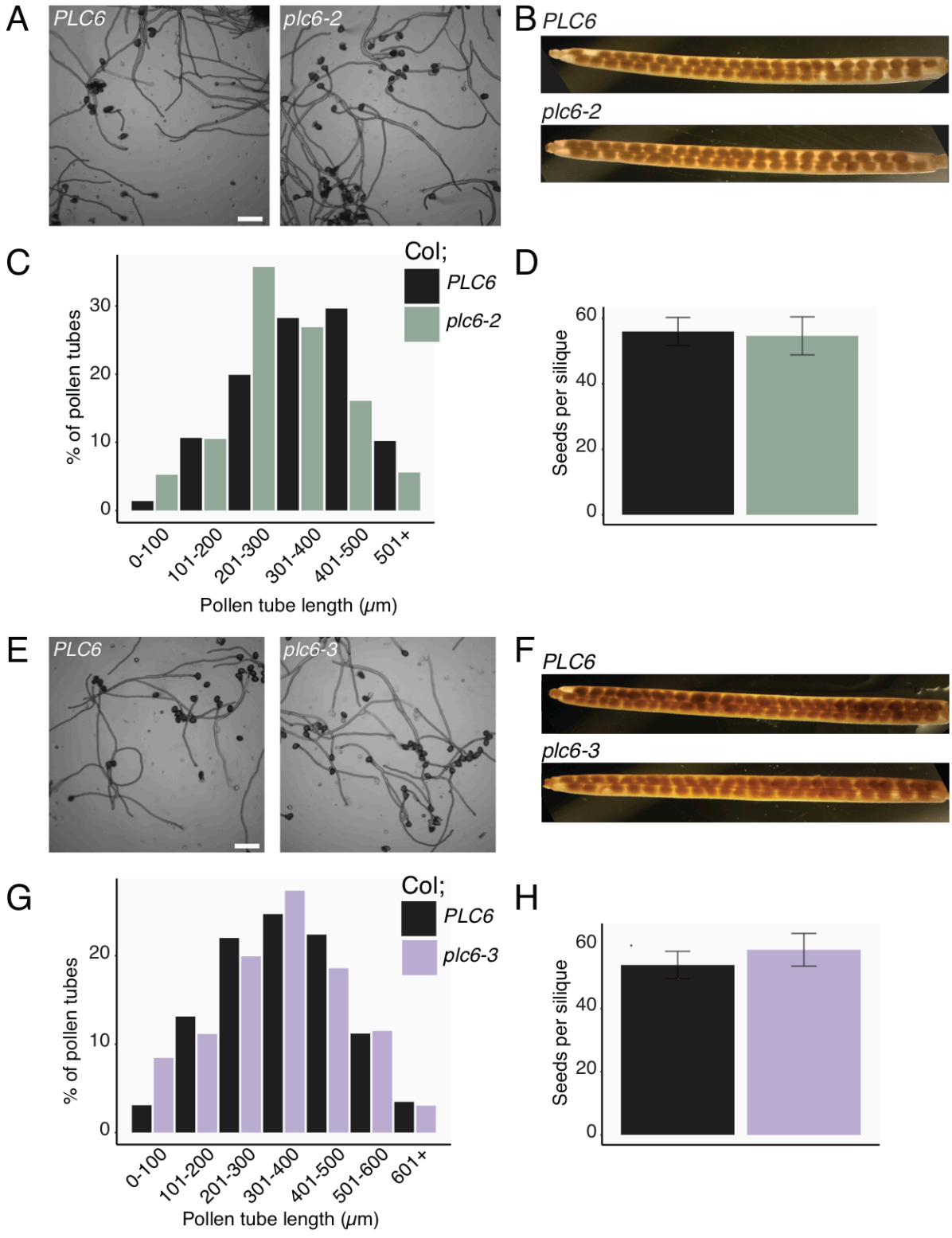

Figure 4-6. Seed production and in vitro PT growth are not disrupted in Col plc6 TDNA insertion mutants.A-D) Reproductive phenotypes in WT vs plc6-2 mutant. A) PTs grown in vitro for 4 hours and imaged with DIC optics at 10X magnification; scale bar represents 100 microns. B) Representative

siliques for each genotype cleared with 70% ethanol. C) Quantification of PT lengths after 4 hours growth in vitro. N ≥ 216 PTs per genotype. D) Seed counts for each genotype; (-) denotes plc6-2 mutant allele. N ≥ 19 siliques per genotype. E-H) Reproductive phenotypes in WT vs plc6-3 mutant. E) PTs grown in vitro for 4 hours and imaged with DIC optics at 10X magnification; scale bar represents 100 microns. F) Representative siliques for each genotype cleared with 70% ethanol. G) Quantification of PT lengths after 4 hours growth in vitro. N ≥ 259 PTs per genotype. H) Seed counts for each genotype; (-) denotes plc6-3 mutant allele. N ≥ 19 siliques per genotype. Statistical analyses performed using Student's t-test.

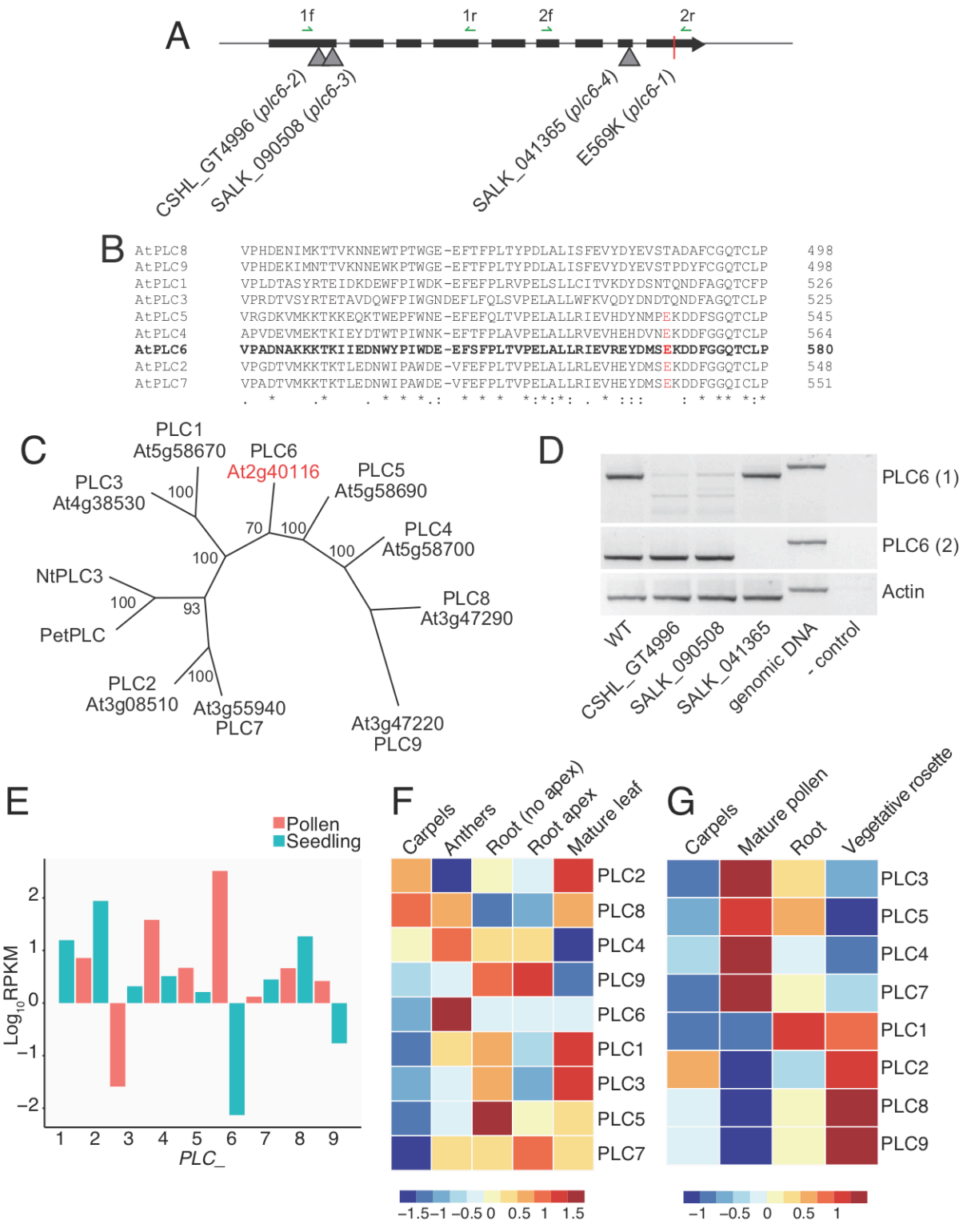

Figure 4-7. PLC6 gene map and RT-PCR for TDNA insertion mutants. A) Map of the PLC6 gene indicating exons (boxes), introns, and locations of transgene insertions for plc6-2, plc6-3 and plc6-4, as well as the location of the plc6-1 SNP mutation. Also shown are primer combinations to detect the PLC6

transcript in part D. B) Partial protein sequences for Arabidopsis PLCs with the E569 position indicated in red. Alignment performed with CLUSTAL omega. "" indicates perfect alignment, ":" indicates site among group with strong similarity, and "." Indicates site among group with weak similarity. C) Phylogenetic analysis of PLCs from Arabidopsis, Petunia, and tobacco. Unrooted maximum likelihood tree shown with bootstrap values for each node. D) Gel showing RT-PCR products amplified using primer combinations 1 (1F + 1R) and 2 (2F + 2R), and actin. cDNA libraries were prepared from flower mRNA, except for the genomic DNA and no template (-) controls. E) RNA sequencing analysis showing RPKM values transformed to log10 scale for each PLC gene in Arabidopsis pollen or seedling samples. Dataset obtained from Klepikova et al. 2016.*

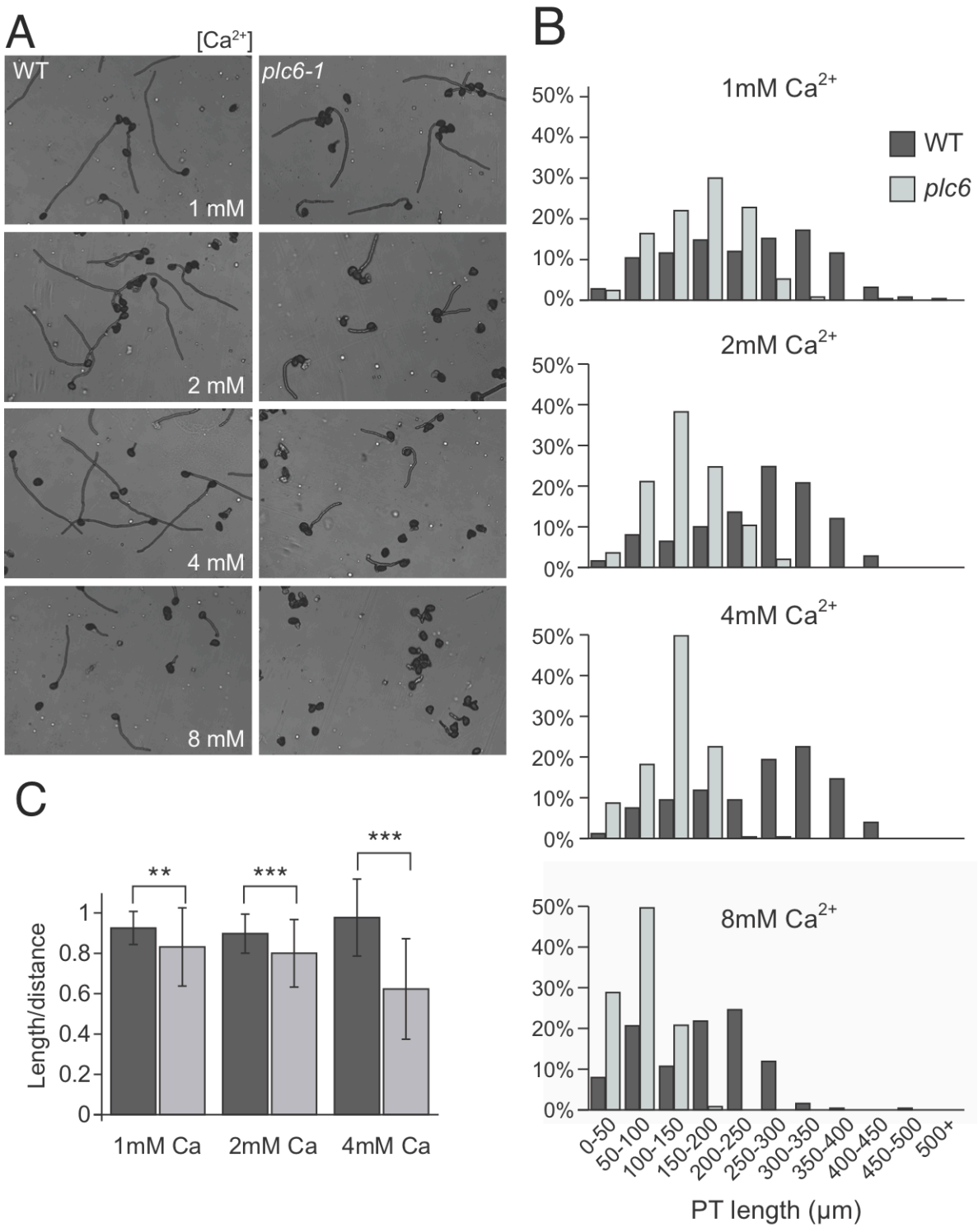

Figure 4-8. plc6-1 PT growth in vitro is inhibited by increased calcium levels. A) PTs grown for 2.5 hours and imaged with DIC optics at 10X magnification; B) PT lengths quantified after 2.5 hours, with N ≥ 250 PTs per experiment per genotype. C) Length/distance ratios to measure PT curliness. Measurements

taken after 2.5 hours of growth. N ≥ 64 PTs per genotype per experiment. Statistical analyses performed using Student's t-test.

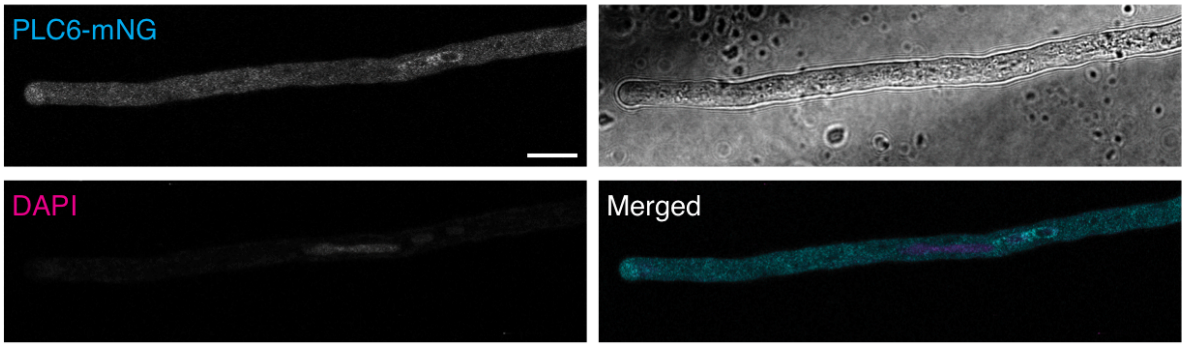

Figure 4-9. PLCp:PLC6-mNG is expressed in PTs and is enriched around sperm nuclei.
Medial z-slice of a representative PT expressing PLC6p:PLC6-mNG, imaged with confocal microscopy at 100X magnification. In merged image, mNG is false-colored cyan and DAPI is false-colored magenta. Scale bar represents 10 microns.

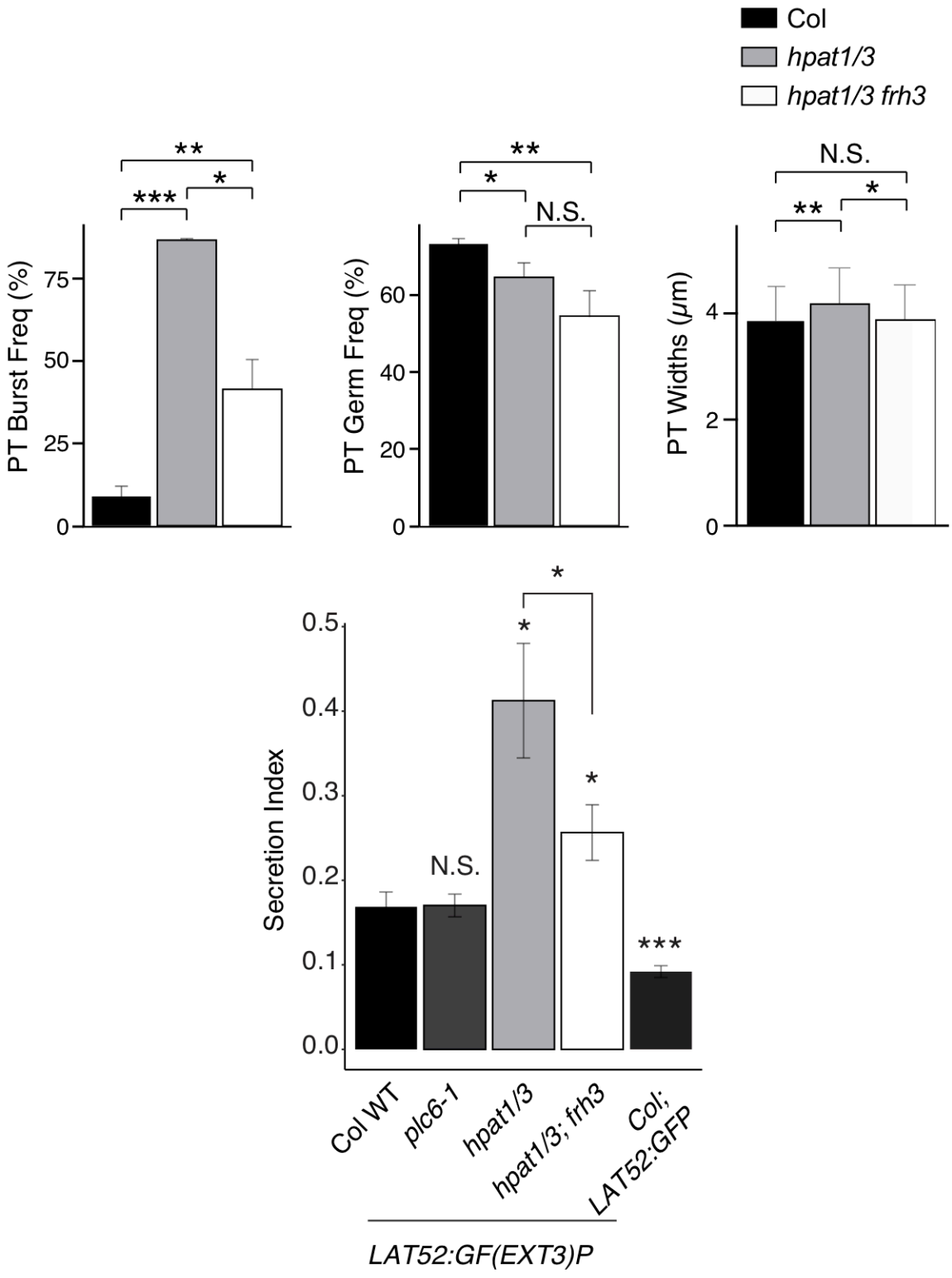

Figure 4-10 (Supplemental Figure 1). hpat1/3 cell wall-related defects are also suppressed in frh3 PTs. Left and middle: PT bursting and germination frequencies measured after 2 hours growth in vitro. Experiments were repeated in triplicate for each genotype. Nbursting ≥ 155 PTs analyzed per experiment

per genotype. Ngermation ≥ 239 per experiment per genotype. PT widths measured after 1 hours, with N ≥ 101 PTs per genotype. Statistical analyses performed using Student's t-test. A) Secretion indices for PTs expressing LAT52:GF(EXT3)P reporter, as well as the non-secreted control LAT52:GFP. Bars represent average ratios and error bars represent standard error.

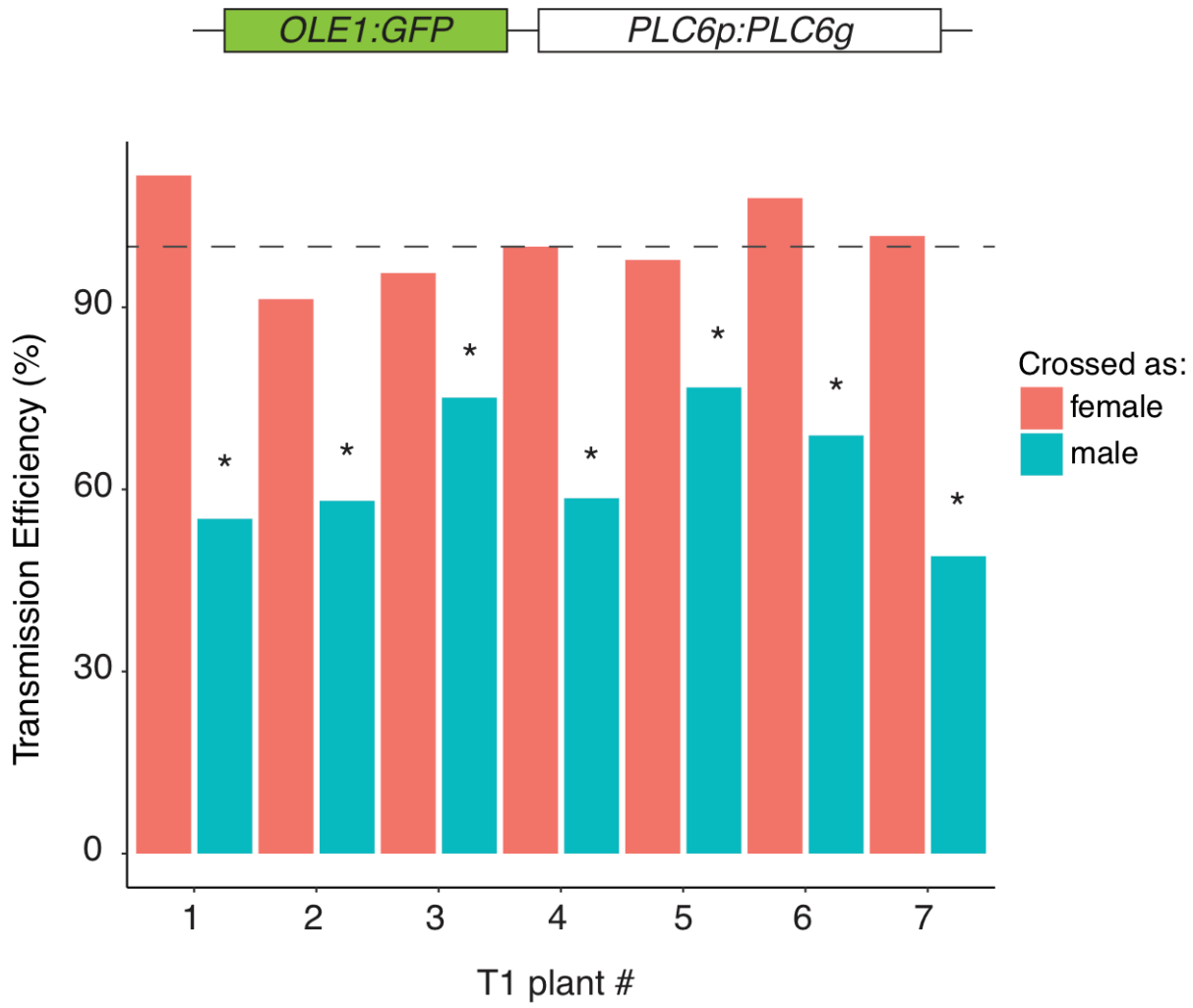

*Figure 4-11 (Supplemental Figure 2). Transmission efficiency is decreased in frh3 PTs carrying PLC6 genomic transgene. Top- schematic of the construct cloned into pFASTG01 (Shimada et al. 2010) and transformed into frh3 plants, which includes the OLE1:GFP selection marker and the genomic PLC6 sequence. Bottom- transmission efficiency calculated as percent of GFP+ seeds produced from a cross using transformed plants (T1-T7), and scaled to 100% by multiplying by 2 (50% GFP+ seeds means 100% transmission efficiency). Nfemale ≥ 69 seeds analyzed from each cross with a female T1 parent; Nmale crosses ≥ 86 seeds from each cross with a male T1 parent. Statistical analyses performed using chi-squared test, comparing the observed numbers of GFP+ and GFP- seeds to 50% GFP+ seeds (1:1 GFP+:GFP-), which is expected if transmission is not affected by the transgene insertion. * represents chi-squared p-value < 0.05.*

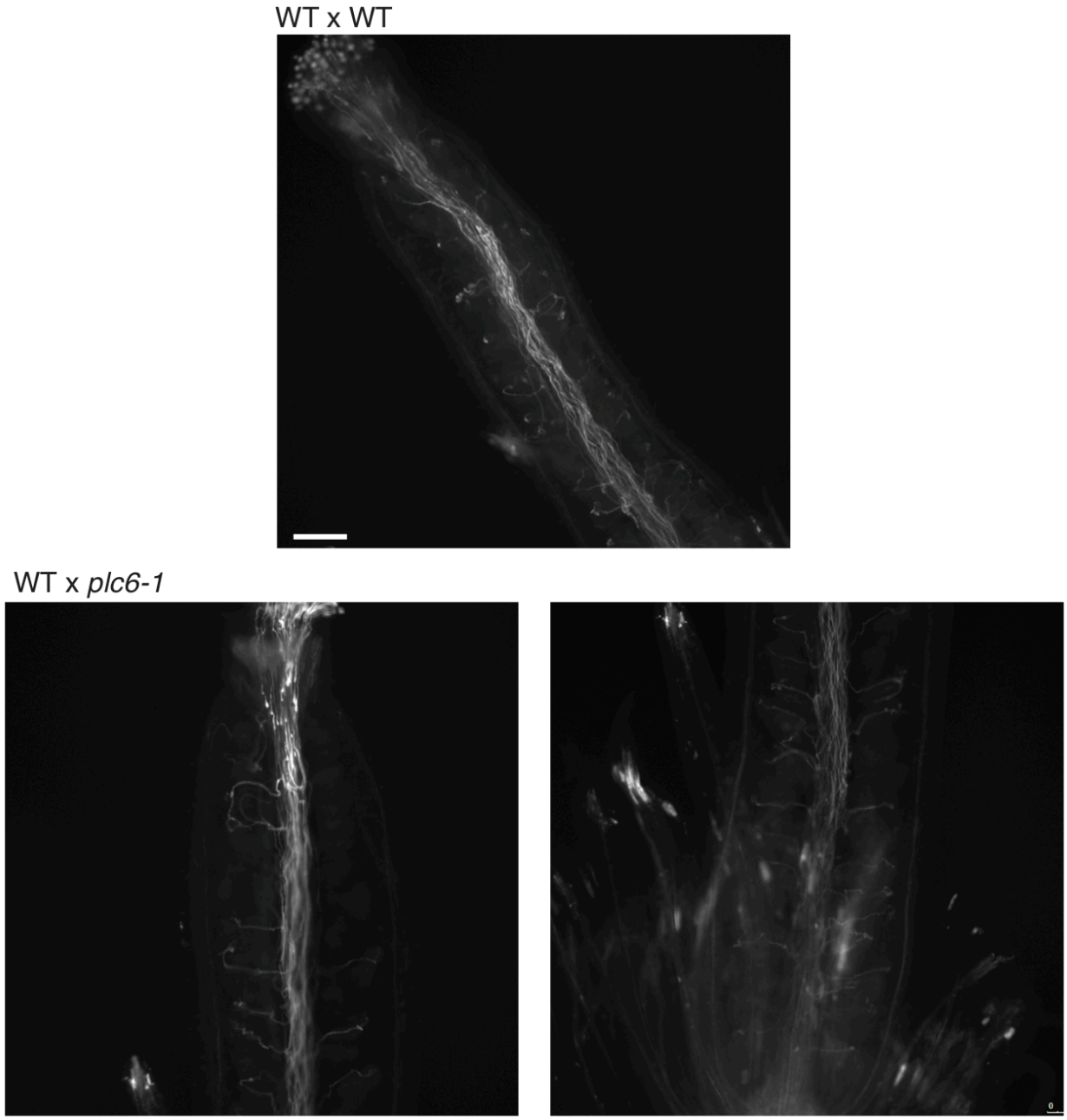

Figure 4-12 (Supplemental Figure 3). Aniline blue staining of WT and plc6-1 PTs in vivo. WT pistils imaged 24 hours after manual pollination with WT (top) or plc6-1 (bottom) pollen. Imaged at 10X magnification and scale bar represents 100 microns.

A

```
AtPLC6              LIGWTHGAQMIAFNMQGYGKSLWLMHGMFRANGGCGYVKKPNFLMKKGFHDEVFDPRKKL 480
RnPKC alpha 2UZP    ------------------------------------S-----MHTERRGRLQL-EIRA 16
HsPKC gamma 1DSY    ---------------------------------------HTEKRGRIYL-KAE- 13
RnPKC beta 1A25     -------------------------GSPGISGGGGGIL-----DSMERRGRIYI-QAH- 27
                                                            :..:   . .

AtPLC6              PVKETLKVKVYMGDGWRMDFSHTHFDAYSPPDFYTKMFIVGVPADNAKKKTKIIEDNWYP 540
2UZP_1|Chains       PTADEIHV--TVGEA----RNLIPMDPNGLSDPYVKLKLIPDPRNLTKQKTRTVKATLNP 70
1DSY_1|Chain        VTDEKLHV--TVRDA----KNLIPMDPNGLSDPYVKLKLIPDPKNESKQKTKTIRSTLNP 67
1A25_1|Chains       IDREVLIV--VVRDA----KNLVPMDPNGLSDPYVKLKLIPDPKSESKQKTKTIKCSLNP 81
                       : : *   : :.     .   :*  .  * *.*: ::  * . :*:**: :. .  *

AtPLC6              IWDEEFSFPLTVPEL-ALLRIEVREYDMSEKDDFGGQTCLPVAELRPGIR---------- 589
2UZP_1|Chains       VWNETFVFNLKPGDVERRLSVEVWDWDRTSRNDFMGAMSFGVSELLKAPVDGWYKLLNQE 130
1DSY_1|Chain        QWNESFTFKLKPSDKDRRLSVEIWDWDRTTRNDFMGSLSFGVSELMKMPASGWYKLLNQE 127
1A25_1|Chains       EWNETFRFQLKESDKDRRLSVEIWDWDLTSRNDFMGSLSFGISELQKAGVDGWFKLLSQE 141
                     *:* * * *.  :    * :*: ::* : ::** *  .: ::**

AtPLC6              -----SVPLYDKKGEKMKSVRLLMRFIFE      613
2UZP_1|Chains       EGEYYNVPVADADN---------------      144
1DSY_1|Chain        EGEYYNVPIPEG-----------------      139
1A25_1|Chains       EGEYFNVP---------------------      149
```

B

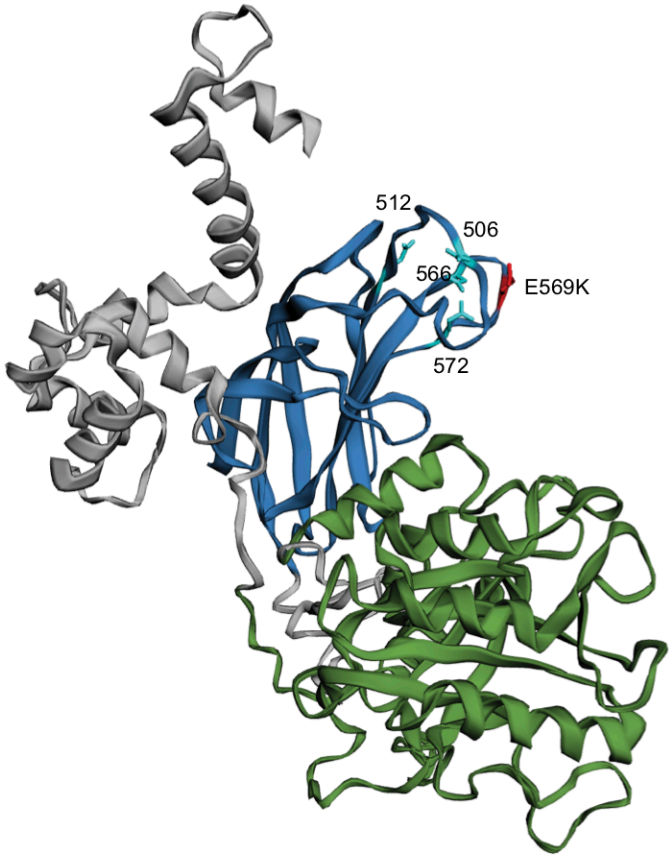

Figure 4-13 (Supplemental Figure 4). Protein structure of PLC6 C2 domain. A) Alignment of PLC6 C2 domain with the C2 domains of protein kinase Cs from human and rat. Yellow aspartic acid residues are involved in calcium coordination, and blue residues are important for interacting with phosphoinositides.

B) 3D protein structure model of PLC6 with calcium-coordinating aspartic acid residues indicated, along with E569.

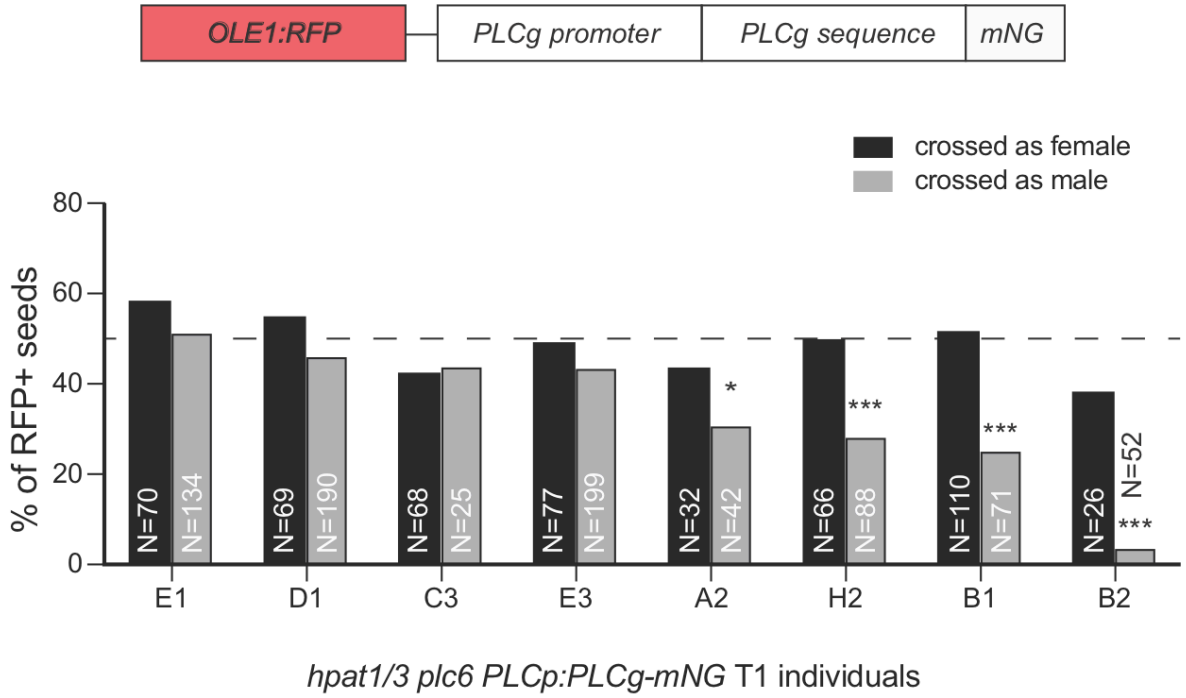

Figure 4-14 (Supplemental Figure 5).Transmission efficiency of PLC6p:PLC-mNG in hpat1/3; plc6-1/frh3 background. Top) Schematic of PLC6p:PLC6-mNG construct used for expression in WT PTs shown in Figure 9. Bottom) Reciprocal crosses showing %RFP seeds recovered when crossed with WT either as male or femle. Statistical analysis performed using chi-squared test.

Table 4-1. Col WT x Col; PLC6-1.

PLC6 geno	# progeny genotyped (obs)	# progeny expected	% obs
+/+	32	49	32.6530612
+/-	66	49	67.3469388
chi sq p-value	**0.00059361**		

Table 4-2. Col WT x Col; PLC6-2 (CSHL).

PLC6 geno	# progeny genotyped (obs)	# progeny expected	% obs
+/+	37	39.5	46.835443
+/-	42	39.5	53.164557
chi sq p-value	0.57374547		

Table 4-3. Col WT x hpat1/3; PLC6-2 (CSHL).

PLC6 geno	# progeny genotyped (obs)	# progeny expected	% obs
+/+	42	25.5	82.3529412
+/-	9	25.5	17.6470588
chi sq p-value	**3.8203E-06**		

Table 4-4. Col WT x Col PLC6-3 (SALK).

PLC6 geno	# progeny genotyped (obs)	# progeny expected	% obs
+/+	20	21	47.6190476
+/-	22	21	52.3809524
chi sq p-value	0.75762072		

Table 4-5. Col WT x hpat1/3; PLC6-3 (SALK).

PLC6 geno	# progeny genotyped (obs)	# progeny expected	% obs
+/+	40	27	74.11
+/-	14	27	25.9
chi sq p-value	**0.0004029**		

Table 4-6. Col WT x hpat1/3; exo70a2-2; PLC6/plc6-1.

PLC6 geno	# progeny genotyped (obs)	# progeny expected	% obs
+/+	55	34	80.8823529
+/-	13	34	19.1176471
chi sq p-value	3.51981E-07		

Table 4-7. Col WT x hpat1/3; plc6-1; EXO70A2/exo70a2-2.

EXO70A2 geno	# progeny genotyped (obs)	# progeny expected	% obs

+/+	56	35	80
+/-	14	35	20
chi sq p-value	5.16822E-07		

Table 4-8 (Supplementary Table 1). Primers used in this study.

Purpose	**Target amplicon**	**recomniation sites attached?**	**Primer Sequence**
plc6-1 genotyping	region of PLC6 gene surrounding plc6-1 SNP		GTAAGAGAGTATGATATCTCG
			Ggtgcaaattctttctcagagac
PLC6p:PLC6-mNG cloning	mNG	attb5	ggggacaactttgtatacaaaagttgATGGTGAGCAAGGGCGAG
		attb2	ggggaccactttgtacaagaaagctgggtTTACTTGTACAGCTCGTCCATGCC
	PLC6 promoter	attb1	ggggacaagtttgtacaaaaaagcaggctACACAAGTTTAAAGAAAAAC
	PLC6 gene without stop	attb2	ggggaccactttgtacaagaaagctgggtaTTCGAAGATGAAACGCATAA
PLC6p:PLC6 cloning	PLC6 gene with stop	attb2	ggggaccactttgtacaagaaagctgggtCAGTTTTTCTTCTTTCATAA
genotyping for SALK_090508 TDNA insertion	PLC6 genomic sequence		TCAGAAAAGACAAACGATCCC
			CACAGGGACTTCGCTACAATC
	SALK TDNA insertion		ATTTTGCCGATTTCGGAAC
genotyping for CSHL_GT4996/6221 TDNA insertion	PLC6 genomic sequence		CTTTGGCTTGAAGATCAGGTG
			AGATTCAAGTGATGGTGACGG
	CSHL TDNA insertion		ACCCGACCGGATCGTATCGGT

Appendix

A Loss of Function Mutation in Protein phosphatase 1 Regulatory Subunit (Inhibitor of Protein-Phosphatase 1) *INH3* Improves Poor *hpat1/3* Fertility and PT Growth.

Prior to whole-genome sequencing of BC4F2 generation suppressors from one mutagenized *hpat1/3* family (B10-6B), tests crosses revealed that all the suppressor plants from this family were heterozygous for the suppression-causing mutation, and no homozygous BC4F2 suppressors were recovered. Additionally, the suppressed individuals had a proportion of shriveled seeds, suggesting that the suppression-causing mutation was also inhibiting normal embryonic and/or seed development. Whole-genome sequencing identified a candidate mutation that was mapped to a G to A substitution in the coding sequence of *INH3,* which is predicted to cause an early truncation at the W43 position of the INH3 protein (*inh3-3*). After identifying this mutation, we discovered that another group could not recover plants that were homozygous for a loss of function transgene insertion mutation in *INH3* (*inh3-1*) from self-fertilized *INH3/inh3-1* heterozygotes, and approximately 25% of the seeds recovered were aborted (Takemiya et al., 2009). Approximately 25% embryos dissected from immature siliques of self-fertilized *inh3-1* heterozygotes grew slower and arrested prior to reaching the heart stage- consistent with the pattern of inheritance of a recessive mutation. Reduced fertility was also reported for *INH3* knockdown lines (by

RNA-interference), but the mechanism was not described. This generated two interesting questions: (1) how does *INH3* promote proper embryonic development, and (2), how does loss of *INH3* improve *hpat1/3* pollen fertility? Here, we report of our findings from addressing the latter question.

To demonstrate that *inh3-3* was indeed the *hpat1/3*- suppressor mutation, we backcrossed BC4F2 suppressors to *hpat1/3,* allowed them to self-fertilize, and then genotyped the resulting BC5F2 generation. We designed dCAPS primers to detect the *inh3-3* mutation through PCR and restriction enzyme digest, which selectively cuts the mutant sequence in the PCR product (Figure 1A). Because *inh3-3* homozygous mutants are inviable on soil, we expected to observe a 1:2 ratio of WT: heterozygotes in the BC5F2 generation if *inh3-3* did not affect transmission of *hpat1/3* gametes. We observed a significant bias towards the presence of the mutation, indicating that *inh3-3* improves fertility of *hpat1/3* gametes (Figure 1B). Plants that inherited the mutation had significantly higher seed counts and PT lengths (grown *in vitro*), indicating that improved PT growth is increasing seed counts in *inh3-3* heterozygote plants. To corroborate these results, we wanted to determine if the *inh3-1* knock out mutation could also suppress *hpat1/3* pollen fertility defects. We crossed the *inh3-1* mutation from Columbia WT into *hpat1/3* and observed a significant increase in seed counts and PT lengths in *hpat1/3; inh3-1/+* plants compared to *hpat1/3* (Figure 2A, B, D, E). We performed reciprocal crosses with WT and *hpat1/3; inh3-1/+* plants and observed a significant transmission bias in favor of the *inh3-1* mutation through the pollen only, and no effect of transmission through the female, indicating that *inh3-1* specifically improves poor

hpat1/3 PT fertility (Figure 2C). This also supports the notion that the *INH3-3* mutation is acting as a loss of function allele.

To learn more about *inh3-3* affects PT fertility, we performed reciprocal crosses of *inh3-3/*+ plants (in the Columbia WT background) with WT. Conversely to the *hpat1/3* background, the presence of *inh3-3* mutation specifically decreased transmission through the pollen (Figure 3C bottom). No effect on transmission was observed through the female tissue (Figure 3C top). Seed counts were unaffected in *inh3-3/*+ self-fertilized plants, likely due to the abundance of WT pollen still being produced (Figure 3A).

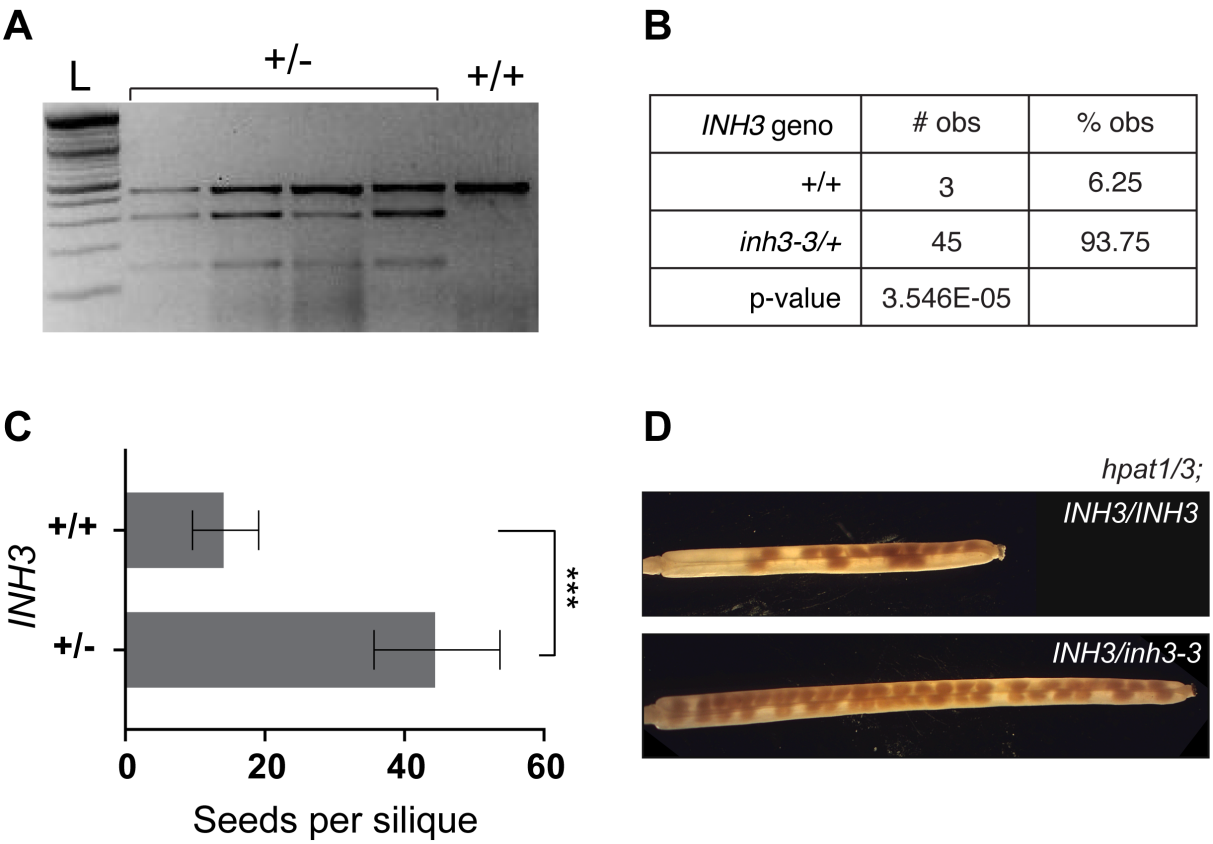

INH3 geno	# obs	% obs
+/+	3	6.25
inh3-3/+	45	93.75
p-value	3.546E-05	

*Appendix Figure 1. Suppression of hpat1/3 fertility defects co-segregates with inh3-3 mutation.enotyping of INH3. PCR products were treated with BspHI restriction enzyme and run on 2% agarose gel. Full length PCR product = 430 bp. PCR product with inh3-3 mutation is cleaved resulting in 297 and 133 bp bands. B) Segregation ratios of BC5F2 individuals. Statistics performed using chi-squared test. C) Average seed counts grouped by INH3 genotype. Error bars represent standard deviation. N ≥ 30 siliques per genotype. Statistics performed using Student's t-test; *** indicates p-value < 0.001. D) Representative siliques of each INH3 genotype in the hpat1/3 genetic background cleared with 70% ethanol.*

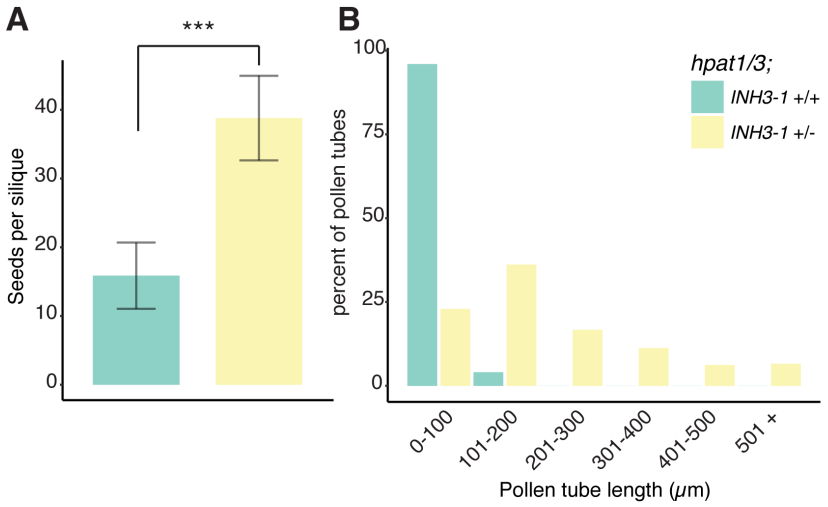

C

hpat1/3;	# obs	% obs
INH3-1 +/+	3	13.04
INH3-1 +/-	20	86.96
p-value	0.039	

	# obs	% obs
TG-	4	4.7
TG+	81	95.3
p-value	6.72E-17	

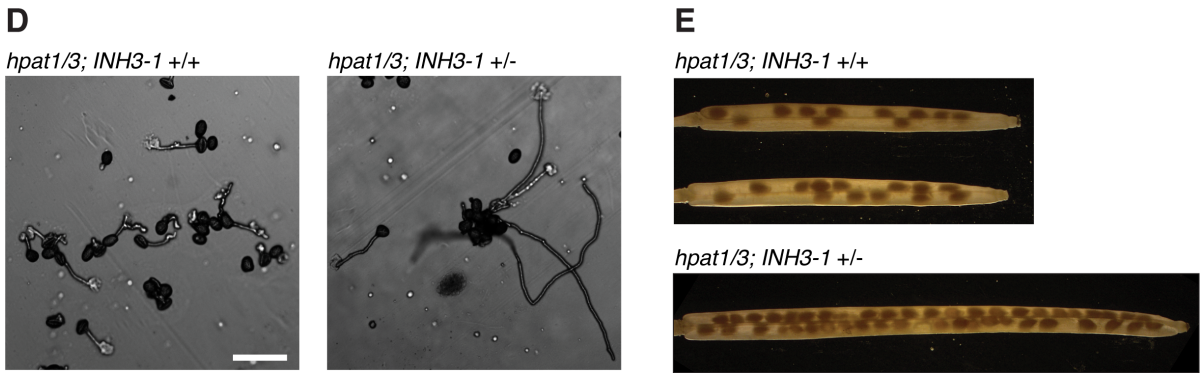

Appendix Figure 2. inh3-1 mutation improves transmission, pollen tube growth and seed set phenotypes in hpat1/3. A) Seed counts for each genotype. N ≥ 29 siliques per genotype B) Pollen tube lengths after 2.5 hours growth in vitro; N ≥ 201 pollen tubes per genotype. C) Top- Segregation of inh3-1 in self-fertilized progeny of hpat1/3; inh3-1 +/- parents. Bottom- Segregation of inh3-1 (TG+) in progeny of hpat1/3 inh3-1 +/- outcrossed as a male with WT female parent. D) Pollen tubes imaged in (A) with DIC at 10x magnification; scale bar represents 100 μm. E) Siliques cleared with ethanol.

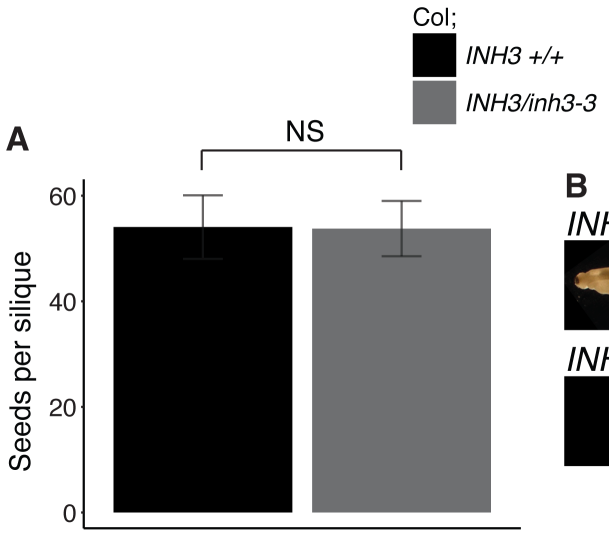

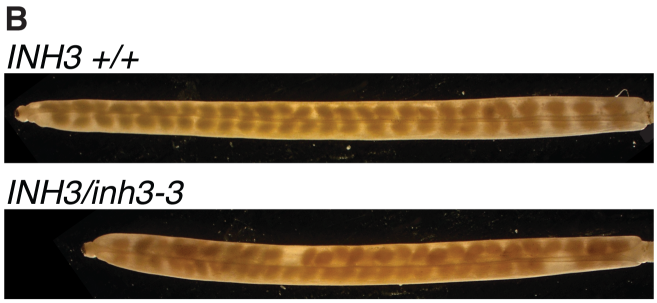

C

inh3-3/+ x WT	# obs	% obs
WT	24	51
het	23	49
p-value	0.884	

WT x *inh3-3/+*	# obs	% obs
WT	38	83
het	8	17
p-value	9.72E-06	

Appendix Figure 3. inh3-3 causes pollen-specific transmission defect in WT background. A) Seed counts based on each genotype. N≥ 37 per genotype. Statistics performed using Student's t-test. D) Representative siliques of each genotype. C) Reciprocal crosses of inh3-3 heterozygotes with WT. Statistics performed using chi-squared test.

Conclusion

HPATs modify extensins, and likely other cell wall-associated proteins, and loss of protein *O*-arabinosylation changes how the other components of the cell wall are organized, which affects the mechanical properties of the cell wall. This has a major impact on pollen tube growth and plant fertility, although the molecular mechanism through which HPATs promote proper pollen tube growth is not clear. The data generated in Chapter 2 created avenues to further explore this pathway, which we describe in Chapters 3 and 4. Furthermore, the contents/workflow of Chapter 2 functions as a template for other researchers to use to aid in the design of their own genetic screens, particularly if these screens involve mutations that affect fertility and transmission.

In Chapter 3, we show that *hpat1/3* pollen fertility was improved by mutations that decreased the overall flux of components secreted into the cell wall. These *hpat1/3*-suppressor mutations strongly rescued poor pollen tube tip-growth and the disrupted organization of cell wall materials. These findings demonstrate that the relationship between protein glycosylation and cell wall structure is also regulated by the rate at which materials are secreted into the cell wall by the exocyst complex- which likely includes HPAT-modified proteins and other cargo types such as pectins and/or pectin-remodeling enzymes. Another important result described in Chapter 3 is the validation of our suppressor screen and bioinformatic analysis pipeline (Chapter 2), where we

confirmed that the mapped mutations were actually present in the plants' genomes and performed genetic rescue experiments to confirm the identities of causal mutations for each *hpat1/3*- suppressor family.

In Chapter 4, we characterized another suppressor mutation that similarly rescued poor *hpat1/3* pollen tube growth and fertility. The mutation was mapped to a gene involved in regulating phosphoinositide (PI)- signaling and belongs to a family with no previously- reported function in *Arabidopsis* pollen tubes. We characterized the effect of this mutation in both *hpat1/3* and wild type backgrounds and described phenotypic similarities and differences compared to the *hpat1/3* suppressors described in Chapter 3. How this gene regulates PI signaling, and how this activity functions to influence pollen tube growth, are important questions that will be addressed in the future.

In conclusion, we have learned much more about HPATs regulate pollen tube growth and fertility in *Arabidopsis*; however, there is still much more to learn about how HPATs regulate the structure of the cell wall to promote proper pollen tube tip growth. For example, how the loss of *O*-arabinosylation affects extensin structure and function in the cell wall, and how this affects other cell wall components, are important questions moving forward. Additionally, what are the identities the exocyst- trafficked cargos, and is the exocyst- mediated secretion pathway described in Chapter 3 the only pathway active in pollen tubes? By addressing these questions, we will ultimately learn more about how the structural and mechanical properties of the cell wall are regulated and control plant cell growth.

Bibliography

Adams, E., & Frank, L. (1980). Metabolism of proline and the hydroxyprolines. In *Annual review of biochemistry* (Vol. 49, pp. 1005–1061). Annu Rev Biochem. https://doi.org/10.1146/annurev.bi.49.070180.005041

Akiyama, Y., Mori, M., & Kato, K. (1980). 13c-nmr analysis of hydroxy- proline arabinosides from nicotiana tabacum. *Agricultural and Biological Chemistry*, *44*(10), 2487–2489. https://doi.org/10.1080/00021369.1980.10864347

Baek, K., Knödler, A., Lee, S. H., Zhang, X., Orlando, K., Zhang, J., Foskett, T. J., Guo, W., & Dominguez, R. (2010). Structure-function study of the N-terminal domain of exocyst subunit Sec3. *Journal of Biological Chemistry*, *285*(14), 10424–10433. https://doi.org/10.1074/jbc.M109.096966

Balestrieri, C., Castaldo, D., Giovane, A., Quagliuolo, L., & Servillo, L. (1990). A glycoprotein inhibitor of pectin methylesterase in kiwi fruit (Actinidia chinensis). *European Journal of Biochemistry*, *193*(1), 183–187. https://doi.org/10.1111/j.1432-1033.1990.tb19321.x

Bate, N., & Twell, D. (1998). Functional architecture of a late pollen promoter: Pollen-specific transcription is developmentally regulated by multiple stage-specific and co-dependent activator elements. *Plant Molecular Biology*, *37*(5), 859–869. https://doi.org/10.1023/A:1006095023050

Baumberger, N., Ringli, C., & Keller, B. (2001). The chimeric leucine-rich repeat/extensin cell wall protein LRX1 is required for root hair morphogenesis in Arabidopsis thaliana. *Genes and Development*, *15*(9), 1128–1139. https://doi.org/10.1101/gad.200201

Beuder, S., Dorchak, A., Bhide, A., Moeller, S. R., Petersen, B. L., & MacAlister, C. A. (2020). Exocyst mutants suppress pollen tube growth and cell wall structural defects of hydroxyproline O-arabinosyltransferase mutants. *Plant Journal*, *103*(4), 1399–1419. https://doi.org/10.1111/tpj.14808

Beuder, S., & MacAlister, C. A. (2020). Isolation and cloning of suppressor mutants with improved pollen fertility. In *Methods in Molecular Biology* (Vol. 2160, pp. 93–108). Methods Mol Biol. https://doi.org/10.1007/978-1-0716-0672-8_7

Bill, C. A., & Vines, C. M. (2020). Phospholipase C. In *Advances in Experimental*

Medicine and Biology (Vol. 1131, pp. 215–242). Springer New York LLC. https://doi.org/10.1007/978-3-030-12457-1_9

Bloch, D., Pleskot, R., Pejchar, P., Potocký, M., Trpkošová, P., Cwiklik, L., Vukašinović, N., Sternberg, H., Yalovsky, S., & Žárský, V. (2016). Exocyst SEC3 and phosphoinositides define sites of exocytosis in pollen tube initiation and growth. *Plant Physiology*, *172*(2), 980–1002. https://doi.org/10.1104/pp.16.00690

Borassi, C., Sede, A. R., Mecchia, M. A., Salgado Salter, J. D., Marzol, E., Muschietti, J. P., & Estevez, J. M. (2016). An update on cell surface proteins containing extensin-motifs. In *Journal of Experimental Botany* (Vol. 67, Issue 2, pp. 477–487). Oxford University Press. https://doi.org/10.1093/jxb/erv455

Bordenave, M., & Goldberg, R. (1993). Purification and characterization of pectin methylesterases from mung bean hypocotyl cell walls. *Phytochemistry*, *33*(5), 999–1003. https://doi.org/10.1016/0031-9422(93)85011-F

Bosch, M., Cheung, A. Y., & Hepler, P. K. (2005). Pectin methylesterase, a regulator of pollen tube growth. *Plant Physiology*, *138*(3), 1334–1346. https://doi.org/10.1104/pp.105.059865

Bosch, M., & Hepler, P. K. (2005). Pectin methylesterases and pectin dynamics in pollen tubes. In *Plant Cell* (Vol. 17, Issue 12, pp. 3219–3226). American Society of Plant Biologists. https://doi.org/10.1105/tpc.105.037473

Bosch, M., & Hepler, P. K. (2006). Silencing of the tobacco pollen pectin methylesterase NtPPME1 results in retarded in vivo pollen tube growth. *Planta*, *223*(4), 736–745. https://doi.org/10.1007/s00425-005-0131-x

Bove, J., Vaillancourt, B., Kroeger, J., Hepler, P. K., Wiseman, P. W., & Geitmann, A. (2008). Magnitude and direction of vesicle dynamics in growing pollen tubes using spatiotemporal image correlation spectroscopy and fluorescence recovery after photobleaching. *Plant Physiology*, *147*(4), 1646–1658. https://doi.org/10.1104/pp.108.120212

Boyd, C., Hughes, T., Pypaert, M., & Novick, P. (2004). Vesicles carry most exocyst subunits to exocytic sites marked by the remaining two subunits, Sec3p and Exo70p. *Journal of Cell Biology*, *167*(5), 889–901. https://doi.org/10.1083/jcb.200408124

Braccini, I., & Pérez, S. (2001). Molecular basis of Ca2+-induced gelation in alginates and pectins: The egg-box model revisited. *Biomacromolecules*, *2*(4), 1089–1096. https://doi.org/10.1021/bm010008g

Brownleader, M. D., & Dey, P. M. (1993). Purification of extensin from cell walls of tomato (hybrid of Lycopersicon esculentum and L. peruvianum) cells in suspension

culture. *Planta*, *191*(4), 457–469. https://doi.org/10.1007/BF00195747

Cai, H., Reinisch, K., & Ferro-Novick, S. (2007). Coats, Tethers, Rabs, and SNAREs Work Together to Mediate the Intracellular Destination of a Transport Vesicle. In *Developmental Cell* (Vol. 12, Issue 5, pp. 671–682). Cell Press. https://doi.org/10.1016/j.devcel.2007.04.005

Camardella, L., Carratore, V., Ciardiello, M. A., Servillo, L., Balestrieri, C., & Giovane, A. (2000). Kiwi protein inhibitor of pectin methylesterase: Amino-acid sequence and structural importance of two disulfide bridges. *European Journal of Biochemistry*, *267*(14), 4561–4565. https://doi.org/10.1046/j.1432-1327.2000.01510.x

Campanoni, P., & Blatt, M. R. (2007). Membrane trafficking and polar growth in root hairs and pollen tubes. *Journal of Experimental Botany*, *58*(1), 65–74. https://doi.org/10.1093/jxb/erl059

Campàs, O., & Mahadevan, L. (2009). Shape and Dynamics of Tip-Growing Cells. *Current Biology*, *19*(24), 2102–2107. https://doi.org/10.1016/j.cub.2009.10.075

Cannon, M. C., Terneus, K., Hall, Q., Tan, L., Wang, Y., Wegenhart, B. L., Chen, L., Lamport, D. T. A., Chen, Y., & Kieliszewski, M. J. (2008). Self-assembly of the plant cell wall requires an extensin scaffold. *Proceedings of the National Academy of Sciences of the United States of America*, *105*(6), 2226–2231. https://doi.org/10.1073/pnas.0711980105

Carpita, N. C., & Gibeaut, D. M. (1993). Structural models of primary cell walls in flowering plants: Consistency of molecular structure with the physical properties of the walls during growth. *Plant Journal*, *3*(1), 1–30. https://doi.org/10.1111/j.1365-313X.1993.tb00007.x

Catoire, L., Pierron, M., Morvan, C., Du Penhoat, C. H., & Goldberg, R. (1998). Investigation of the action patterns of pectinmethylesterase isoforms through kinetic analyses and NMR spectroscopy: Implications in cell wall expansion. *Journal of Biological Chemistry*, *273*(50), 33150–33156. https://doi.org/10.1074/jbc.273.50.33150

Chang, M., & Huang, S. (2017). Rapid Isolation of Total Protein from Arabidopsis Pollen. *BIO-PROTOCOL*, *7*(8). https://doi.org/10.21769/bioprotoc.2227

Chebli, Y., Kaneda, M., Zerzour, R., & Geitmann, A. (2012). The cell wall of the Arabidopsis pollen tube--spatial distribution, recycling, and network formation of polysaccharides. *Plant Physiology*, *160*(4), 1940–1955. https://doi.org/10.1104/pp.112.199729

Chen, L.-Y., Shi, D.-Q., Zhang, W.-J., Tang, Z.-S., Liu, J., & Yang, W.-C. (2015). The Arabidopsis alkaline ceramidase TOD1 is a key turgor pressure regulator in plant

cells. *Nature Communications*, *6*, 6030. https://doi.org/10.1038/ncomms7030

Cheung, A. Y., Niroomand, S., Zou, Y., & Wu, H. M. (2010). A transmembrane formin nucleates subapical actin assembly and controls tip-focused growth in pollen tubes. *Proceedings of the National Academy of Sciences of the United States of America*, *107*(37), 16390–16395. https://doi.org/10.1073/pnas.1008527107

Cheung, A. Y., & Wu, H. M. (2004). Overexpression of an Arabidopsis Formin Stimulates Supernumerary Actin Cable Formation from Pollen Tube Cell Membrane. *Plant Cell*, *16*(1), 257–269. https://doi.org/10.1105/tpc.016550

Chong, Y. T., Gidda, S. K., Sanford, C., Parkinson, J., Mullen, R. T., & Goring, D. R. (2010). Characterization of the Arabidopsis thaliana exocyst complex gene families by phylogenetic, expression profiling, and subcellular localization studies. *New Phytologist*, *185*(2), 401–419. https://doi.org/10.1111/j.1469-8137.2009.03070.x

Chormova, D., Messenger, D. J., & Fry, S. C. (2014). Boron bridging of rhamnogalacturonan-II, monitored by gel electrophoresis, occurs during polysaccharide synthesis and secretion but not post-secretion. *Plant Journal*, *77*(4), 534–546. https://doi.org/10.1111/tpj.12403

Choudhary, P., Saha, P., Ray, T., Tang, Y., Yang, D., & Cannon, M. C. (2015). EXTENSIN18 is required for full male fertility as well as normal vegetative growth in Arabidopsis. *Frontiers in Plant Science*, *6*(JULY), 1–14. https://doi.org/10.3389/fpls.2015.00553

Christensen, C. A., Subramanian, S., & Drews, G. N. (1998). Identification of gametophytic mutations affecting female gametophyte development in arabidopsis. *Developmental Biology*, *202*(1), 136–151. https://doi.org/10.1006/dbio.1998.8980

Ciardiello, M. A., D'Avino, R., Amoresano, A., Tuppo, L., Carpentieri, A., Carratore, V., Tamburrini, M., Giovane, A., Pucci, P., & Camardella, L. (2008). The peculiar structural features of kiwi fruit pectin methylesterase: Amino acid sequence, oligosaccharides structure, and modeling of the interaction with its natural proteinaceous inhibitor. *Proteins: Structure, Function and Genetics*, *71*(1), 195–206. https://doi.org/10.1002/prot.21681

Clark, S. E., Running, M. P., & Meyerowitz, E. M. (1995). CLAVATA3 is a specific regulator of shoot and floral meristem development affecting the same processes as CLAVATA1. *Development*, *121*(7), 2057–2067. https://doi.org/10.1242/dev.121.7.2057

Cleland, R., & Karlsnes, A. M. (1967). A possible role of hydroxyproline-containing proteins in the cessation of cell elongation. *Plant Physiology*, *42*(5), 669–671. http://www.ncbi.nlm.nih.gov/pubmed/16656553

Cole, R. A., McInally, S. A., & Fowler, J. E. (2014). Developmentally distinct activities of the exocyst enable rapid cell elongation and determine meristem size during primary root growth in Arabidopsis. *BMC Plant Biology*, *14*(1), 1–20. https://doi.org/10.1186/s12870-014-0386-0

Cole, R. A., Synek, L., Zarsky, V., & Fowler, J. E. (2005). SEC8, a subunit of the putative arabidopsis exocyst complex, facilitates pollen germination and competitive pollen tube growth. *Plant Physiology*, *138*(4), 2005–2018. https://doi.org/10.1104/pp.105.062273

Corbalan-Garcia, S., & Gómez-Fernández, J. C. (2014). Signaling through C2 domains: More than one lipid target. In *Biochimica et Biophysica Acta - Biomembranes* (Vol. 1838, Issue 6, pp. 1536–1547). Elsevier. https://doi.org/10.1016/j.bbamem.2014.01.008

Cosgrove, D. J. (2005). Growth of the plant cell wall. In *Nature Reviews Molecular Cell Biology* (Vol. 6, Issue 11, pp. 850–861). Nature Publishing Group. https://doi.org/10.1038/nrm1746

Costa, A., Navazio, L., & Szabo, I. (2018). The contribution of organelles to plant intracellular calcium signalling. In *Journal of Experimental Botany* (Vol. 69, Issue 17, pp. 4175–4193). Oxford Academic. https://doi.org/10.1093/jxb/ery185

Costello, S., Michelangeli, F., Nash, K., Lefievre, L., Morris, J., Machado-Oliveira, G., Barratt, C., Kirkman-Brown, J., & Publicover, S. (2009). Ca2+-stores in sperm: Their identities and functions. In *Reproduction* (Vol. 138, Issue 3, pp. 425–437). Europe PMC Funders. https://doi.org/10.1530/REP-09-0134

Daher, F. B., & Braybrook, S. A. (2015). How to let go: Pectin and plant cell adhesion. In *Frontiers in Plant Science* (Vol. 6, Issue JULY, p. 523). Frontiers. https://doi.org/10.3389/fpls.2015.00523

Dardelle, F., Lehner, A., Ramdani, Y., Bardor, M., Lerouge, P., Driouich, A., & Mollet, J.-C. (2010). Biochemical and immunocytological characterizations of Arabidopsis pollen tube cell wall. *Plant Physiology*, *153*(4), 1563–1576. https://doi.org/10.1104/pp.110.158881

de Souza, A., Hull, P. A., Gille, S., & Pauly, M. (2014). Identification and functional characterization of the distinct plant pectin esterases PAE8 and PAE9 and their deletion mutants. *Planta*, *240*(5), 1123–1138. https://doi.org/10.1007/s00425-014-2139-6

Di Fino, L. M., D'Ambrosio, J. M., Tejos, R., van Wijk, R., Lamattina, L., Munnik, T., Pagnussat, G. C., & Laxalt, A. M. (2017). Arabidopsis phosphatidylinositol-phospholipase C2 (PLC2) is required for female gametogenesis and embryo development. *Planta*, *245*(4), 717–728. https://doi.org/10.1007/s00425-016-2634-z

Di Matteo, A., Giovane, A., Raiola, A., Camardella, L., Bonivento, D., De Lorenzo, G., Cervone, F., Bellincampi, D., & Tsemoglou, D. (2005). Structural basis for the interaction between pectin methylesterase and a specific inhibitor protein. *Plant Cell*, *17*(3), 849–858. https://doi.org/10.1105/tpc.104.028886

Dinh, T. T., Luscher, E., Li, S., Liu, X., Won, S. Y., & Chen, X. (2014). Genetic screens for floral mutants in Arabidopsis thaliana: Enhancers and suppressors. *Methods in Molecular Biology*, *1110*, 127–156. https://doi.org/10.1007/978-1-4614-9408-9_6

Dong, G., Hutagalung, A. H., Fu, C., Novick, P., & Reinisch, K. M. (2005). The structures of exocyst subunit Exo70p and the Exo84p C-terminal domains reveal a common motif. *Nature Structural and Molecular Biology*, *12*(12), 1094–1100. https://doi.org/10.1038/nsmb1017

Dowd, P. E., Coursol, S., Skirpan, A. L., Kao, T. H., & Gilroy, S. (2006). Petunia phospholipase C1 is involved in pollen tube growth. *Plant Cell*, *18*(6), 1438–1453. https://doi.org/10.1105/tpc.106.041582

Egelund, J., Obel, N., Ulvskov, P., Geshi, N., Pauly, M., Bacic, A., & Petersen, B. L. (2007). Molecular characterization of two Arabidopsis thaliana glycosyltransferase mutants, rra1 and rra2, which have a reduced residual arabinose content in a polymer tightly associated with the cellulosic wall residue. *Plant Molecular Biology*, *64*(4), 439–451. https://doi.org/10.1007/s11103-007-9162-y

Esquerré-Tugayé, M.-T., Lafitte, C., Mazau, D., Toppan, A., & Touzé, A. (1979). Cell Surfaces in Plant-Microorganism Interactions. *Plant Physiology*, *64*(2), 320–326. https://doi.org/10.1104/pp.64.2.320

Essen, L. O., Perisic, O., Katan, M., Yiqin, W., Roberts, M. F., & Williams, R. L. (1997). Structural mapping of the catalytic mechanism for a mammalian phosphoinositide-specific phospholipase C. *Biochemistry*, *36*(7), 1704–1718. https://doi.org/10.1021/bi962512p

Everdeen, D. S., Kiefer, S., Willard, J. J., Muldoon, E. P., Dey, P. M., Li, X., & Lamport, D. T. A. (1988). Enzymic Cross-Linkage of Monomeric Extensin Precursors in Vitro. *Plant Physiology*, *87*(3), 616. https://doi.org/10.1104/PP.87.3.616

Fabrice, T. N., Vogler, H., Draeger, C., Munglani, G., Gupta, S., Herger, A. G., Knox, P., Grossniklaus, U., & Ringli, C. (2018). LRX proteins play a crucial role in pollen grain and pollen tube cell wall development. *Plant Physiology*, *176*(3), 1981–1992. https://doi.org/10.1104/pp.17.01374

Feng, C., Wang, J.-G., Liu, H.-H., Li, S., & Zhang, Y. (2017). *Arabidopsis* adaptor protein 1G is critical for pollen development. *Journal of Integrative Plant Biology*, *59*(9), 594–599. https://doi.org/10.1111/jipb.12556

Finger, F. P., Hughes, T. E., & Novick, P. (1998). Sec3p is a spatial landmark for polarized secretion in budding yeast. *Cell*, *92*(4), 559–571. https://doi.org/10.1016/S0092-8674(00)80948-4

Finger, F. P., & Novick, P. (1997). Sec3p is involved in secretion and morphogenesis in Saccharomyces cerevisiae. *Molecular Biology of the Cell*, *8*(4), 647–662. https://doi.org/10.1091/mbc.8.4.647

Fry, S. C. (1988). The growing plant cell wall: chemical and metabolic analysis. *New York*, *203*, 333.

Gille, S., Hänsel, U., Ziemann, M., & Pauly, M. (2009). Identification of plant cell wall mutants by means of a forward chemical genetic approach using hydrolases. *Proceedings of the National Academy of Sciences of the United States of America*, *106*(34), 14699–14704. https://doi.org/10.1073/pnas.0905434106

Grant, G. T., Morris, E. R., Rees, D. A., Smith, P. J. C., & Thom, D. (1973). Biological interactions between polysaccharides and divalent cations: The egg-box model. *FEBS Letters*, *32*(1), 195–198. https://doi.org/10.1016/0014-5793(73)80770-7

Grobei, M. A., Qeli, E., Brunner, E., Rehrauer, H., Zhang, R., Roschitzki, B., Basler, K., Ahrens, C. H., & Grossniklaus, U. (2009). Deterministic protein inference for shotgun proteomics data provides new insights into Arabidopsis pollen development and function. *Genome Research*, *19*(10), 1786–1800. https://doi.org/10.1101/gr.089060.108

Guo, W., Tamanoi, F., & Novick, P. (2001). Spatial regulation of the exocyst complex by Rho1 GTPase. *Nature Cell Biology*, *3*(4), 353–360. https://doi.org/10.1038/35070029

Hála, M., Cole, R., Synek, L., Drdová, E., Pečenková, T., Nordheim, A., Lamkemeyer, T., Madlung, J., Hochholdinger, F., Fowler, J. E., & Žárskýa, V. (2008). An exocyst complex functions in plant cell growth in Arabidopsis and tobacco. *Plant Cell*, *20*(5), 1330–1345. https://doi.org/10.1105/tpc.108.059105

Hall, Q., & Cannon, M. C. (2002). The cell wall hydroxyproline-rich glycoprotein RSH is essential for normal embryo development in Arabidopsis. *The Plant Cell*, *14*(5), 1161–1172. http://www.ncbi.nlm.nih.gov/pubmed/12034904

Hamburger, Z. A., Hamburger, A. E., West, A. P., & Weis, W. I. (2006). Crystal structure of the S. cerevisiae exocyst component Exo70p. *Journal of Molecular Biology*, *356*(1), 9–21. https://doi.org/10.1016/j.jmb.2005.09.099

Hammerschmidt, R., Lamport, D. T. A., & Muldoon, E. P. (1984). Cell wall hydroxyproline enhancement and lignin deposition as an early event in the

resistance of cucumber to Cladosporium cucumerinum. *Physiological Plant Pathology*, *24*(1), 43–47. https://doi.org/10.1016/0048-4059(84)90072-9

Harsay, E., & Bretscher, A. (1995). Parallel secretory pathways to the cell surface in yeast. *Journal of Cell Biology*, *131*(2), 297–310. https://doi.org/10.1083/jcb.131.2.297

He, B., & Guo, W. (2009). The exocyst complex in polarized exocytosis. In *Current Opinion in Cell Biology* (Vol. 21, Issue 4, pp. 537–542). https://doi.org/10.1016/j.ceb.2009.04.007

He, B., Xi, F., Zhang, J., TerBush, D., Zhang, X., & Guo, W. (2007). Exo70p mediates the secretion of specific exocytic vesicles at early stages of the cell cycle for polarized cell growth. *Journal of Cell Biology*, *176*(6), 771–777. https://doi.org/10.1083/jcb.200606134

Held, M. A., Tan, L., Kamyabi, A., Hare, M., Shpak, E., & Kieliszewski, M. J. (2004). Di-isodityrosine is the intermolecular cross-link of isodityrosine-rich extensin analogs cross-linked in vitro. *Journal of Biological Chemistry*, *279*(53), 55474–55482. https://doi.org/10.1074/jbc.M408396200

Helling, D., Possart, A., Cottier, S., Klahre, U., & Kost, B. (2006). Pollen tube tip growth depends on plasma membrane polarization mediated by tobacco PLC3 activity and endocytic membrane recycling. *Plant Cell*, *18*(12), 3519–3534. https://doi.org/10.1105/tpc.106.047373

Herbell, S., Gutermuth, T., & Konrad, K. R. (2018). An interconnection between tip-focused Ca2+ and anion homeostasis controls pollen tube growth. *Plant Signaling & Behavior*, *13*(11), e1529521. https://doi.org/10.1080/15592324.2018.1529521

Higashiyama, T., & Takeuchi, H. (2015). The Mechanism and Key Molecules Involved in Pollen Tube Guidance. *Annual Review of Plant Biology*, *66*. https://doi.org/10.1146/annurev-arplant-043014-115635

Hill, A. E., Shachar-Hill, B., Skepper, J. N., Powell, J., & Shachar-Hill, Y. (2012). An osmotic model of the growing pollen tube. *PLoS ONE*, *7*(5), e36585. https://doi.org/10.1371/journal.pone.0036585

Hocq, L., Sénéchal, F., Lefebvre, V., Lehner, A., Domon, J. M., Mollet, J. C., Dehors, J., Pageau, K., Marcelo, P., Guérineau, F., Kolšek, K., Mercadante, D., & Pelloux, J. (2017). Combined experimental and computational approaches reveal distinct pH dependence of pectin Methylesterase Inhibitors. *Plant Physiology*, *173*(2), 1075–1093. https://doi.org/10.1104/pp.16.01790

Hruz, T., Laule, O., Szabo, G., Wessendorp, F., Bleuler, S., Oertle, L., Widmayer, P., Gruissem, W., & Zimmermann, P. (2008). Genevestigator V3: A Reference

Expression Database for the Meta-Analysis of Transcriptomes. *Advances in Bioinformatics*, *2008*, 1–5. https://doi.org/10.1155/2008/420747

Hunt, L., Otterhag, L., Lee, J. C., Lasheen, T., Hunt, J., Seki, M., Shinozaki, K., Sommarin, M., Gilmour, D. J., Pical, C., & Gray, J. E. (2004). Gene-specific expression and calcium activation of Arabidopsis thaliana phospholipase C isoforms. *New Phytologist*, *162*(3), 643–654. https://doi.org/10.1111/j.1469-8137.2004.01069.x

Imin, N., Patel, N., Corcilius, L., Payne, R. J., & Djordjevic, M. A. (2018). CLE peptide tri-arabinosylation and peptide domain sequence composition are essential for SUNN-dependent autoregulation of nodulation in Medicago truncatula. *New Phytologist*, *218*(1), 73–80. https://doi.org/10.1111/nph.15019

Ingouff, M., Fitz Gerald, J. N., Guérin, C., Robert, H., Sørensen, M. B., Van Damme, D., Geelen, D., Blanchoin, L., & Berger, F. (2005). Plant formin AtFH5 is an evolutionarily conserved actin nucleator involved in cytokinesis. *Nature Cell Biology*, *7*(4), 374–380. https://doi.org/10.1038/ncb1238

Ischebeck, T., Stenzel, I., & Heilmann, I. (2008). Type B phosphatidylinositol-4-phosphate 5-kinases mediate Arabidopsis and Nicotiana tabacum pollen tube growth by regulating apical pectin secretion. *Plant Cell*, *20*(12), 3312–3330. https://doi.org/10.1105/tpc.108.059568

Iwai, H., Hokura, A., Oishi, M., Chida, H., Ishii, T., Sakai, S., & Satoh, S. (2006). The gene responsible for borate cross-linking of pectin Rhamnogalacturonan-II is required for plant reproductive tissue development and fertilization. *Proceedings of the National Academy of Sciences of the United States of America*, *103*(44), 16592–16597. https://doi.org/10.1073/pnas.0605141103

Iwai, H., Masaoka, N., Ishii, T., & Satoh, S. (2002). A pectin glucuronyltransferase gene is essential for intercellular attachment in the plant meristem. *Proceedings of the National Academy of Sciences of the United States of America*, *99*(25), 16319–16324. https://doi.org/10.1073/pnas.252530499

James, G. V., Patel, V., Nordström, K. J., Klasen, J. R., Salomé, P. A., Weigel, D., & Schneeberger, K. (2013). User guide for mapping-by-sequencing in Arabidopsis. *Genome Biology*, *14*(6), 1–13. https://doi.org/10.1186/gb-2013-14-6-r61

Jiang, L., Yang, S. L., Xie, L. F., Puah, C. S., Zhang, X. Q., Yang, W. C., Sundaresan, V., & Ye, D. (2005). VANGUARD1 encodes a pectin methylesterase that enhances pollen tube growth in the Arabidopsis style and transmitting tract. *Plant Cell*, *17*(2), 584–596. https://doi.org/10.1105/tpc.104.027631

Johnson, M. A., von Besser, K., Zhou, Q., Smith, E., Aux, G., Patton, D., Levin, J. Z., & Preuss, D. (2004). Arabidopsis hapless mutations define essential gametophytic

functions. *Genetics*, *168*(2), 971–982. https://doi.org/10.1534/genetics.104.029447

Jolie, R. P., Duvetter, T., Van Loey, A. M., & Hendrickx, M. E. (2010). Pectin methylesterase and its proteinaceous inhibitor: A review. In *Carbohydrate Research* (Vol. 345, Issue 18, pp. 2583–2595). Elsevier Ltd. https://doi.org/10.1016/j.carres.2010.10.002

Kalmbach, L., Hématy, K., De Bellis, D., Barberon, M., Fujita, S., Ursache, R., Daraspe, J., & Geldner, N. (2017). Transient cell-specific EXO70A1 activity in the CASP domain and Casparian strip localization. *Nature Plants*, *3*(5). https://doi.org/10.1038/nplants.2017.58

Kanaoka, M. M., & Higashiyama, T. (2015). Peptide signaling in pollen tube guidance. In *Current Opinion in Plant Biology* (Vol. 28). https://doi.org/10.1016/j.pbi.2015.10.006

Kanehara, K., Yu, C. Y., Cho, Y., Cheong, W. F., Torta, F., Shui, G., Wenk, M. R., & Nakamura, Y. (2015). Arabidopsis AtPLC2 Is a Primary Phosphoinositide-Specific Phospholipase C in Phosphoinositide Metabolism and the Endoplasmic Reticulum Stress Response. *PLoS Genetics*, *11*(9), e1005511. https://doi.org/10.1371/journal.pgen.1005511

Kassaw, T., Schnabel, S. N. E., & Frugoli, J. (2017). Root determined nodulation1 Is required for M. Truncatula CLE12, but not CLE13, peptide signaling through the SUNN receptor kinase. *Plant Physiology*, *174*(4), 2445–2456. https://doi.org/10.1104/pp.17.00278

Kee, Y., Yoo, J. S., Hazuka, C. D., Peterson, K. E., Hsu, S. C., & Scheller, R. H. (1997). Subunit structure of the mammalian exocyst complex. *Proceedings of the National Academy of Sciences of the United States of America*, *94*(26), 14438–14443. https://doi.org/10.1073/pnas.94.26.14438

Kelley, L. A., Mezulis, S., Yates, C. M., Wass, M. N., & Sternberg, M. J. E. (2015). The Phyre2 web portal for protein modeling, prediction and analysis. *Nature Protocols*, *10*(6), 845–858. https://doi.org/10.1038/nprot.2015.053

Kent, L. M., Loo, T. S., Melton, L. D., Mercadante, D., Williams, M. A. K., & Jameson, G. B. (2016). Structure and properties of a non-processive, salt-requiring, and acidophilic pectin methylesterase from aspergillus Niger provide insights into the key determinants of processivity control. *Journal of Biological Chemistry*, *291*(3), 1289–1306. https://doi.org/10.1074/jbc.M115.673152

Kieliszewski, M. J., & Shpak, E. (2001). Synthetic genes for the elucidation of glycosylation codes for arabinogalactan-proteins and other hydroxyproline-rich glycoproteins. In *Cellular and Molecular Life Sciences* (Vol. 58, Issue 10, pp. 1386–1398). Cell Mol Life Sci. https://doi.org/10.1007/PL00000783

Kim, Y. J., Jeong, H. Y., Kang, S. Y., Silva, J., Kim, E. J., Park, S. K., Jung, K. H., & Lee, C. (2020). Physiological importance of pectin modifying genes during rice pollen development. *International Journal of Molecular Sciences*, *21*(14), 1–16. https://doi.org/10.3390/ijms21144840

Klepikova, A. V., Kasianov, A. S., Gerasimov, E. S., Logacheva, M. D., & Penin, A. A. (2016). A high resolution map of the Arabidopsis thaliana developmental transcriptome based on RNA-seq profiling. *Plant Journal*, *88*(6), 1058–1070. https://doi.org/10.1111/tpj.13312

Krupková, E., Immerzeel, P., Pauly, M., & Schmülling, T. (2007). The Tumorous Shoot Development2 gene of Arabidopsis encoding a putative methyltransferase is required for cell adhesion and co-ordinated plant development. *Plant Journal*, *50*(4), 735–750. https://doi.org/10.1111/j.1365-313X.2007.03123.x

Kulich, I., Vojtíková, Z., Glanc, M., Ortmannová, J., Rasmann, S., & Zárský, V. (2015). Cell wall maturation of arabidopsis trichomes is dependent on exocyst subunit EXO70H4 and involves callose deposition. *Plant Physiology*, *168*(1), 120–131. https://doi.org/10.1104/pp.15.00112

Lalanne, E., Michaelidis, C., Moore, J. M., Gagliano, W., Johnson, A., Patel, R., Howden, R., Vielle-Calzada, J. P., Grossniklaus, U., & Twell, D. (2004). Analysis of transposon insertion mutants highlights the diversity of mechanisms underlying male progamic development in Arabidopsis. *Genetics*, *167*(4), 1975–1986. https://doi.org/10.1534/genetics.104.030270

Lamport, D. T. A. (1967). Hydroxyproline-O-glycosidic linkage of the plant cell wall glycoprotein extensin [21]. In *Nature* (Vol. 216, Issue 5122, pp. 1322–1324). Nature Publishing Group. https://doi.org/10.1038/2161322a0

Lamport, D. T. A., & Lamport, D. T. A. (1966). *The Protein Component of Primary Cell Walls* (pp. 151–218). https://doi.org/10.1016/S0065-2296(08)60251-7

Lamport, D. T. A., & Miller, D. H. (1971). Hydroxyproline Arabinosides in the Plant Kingdom. *Plant Physiology*, *48*(4), 454–456. https://doi.org/10.1104/pp.48.4.454

Lan, Y., Liu, X., Fu, Y., & Huang, S. (2018). Arabidopsis class I formins control membrane-originated actin polymerization at pollen tube tips. *PLoS Genetics*, *14*(11). https://doi.org/10.1371/journal.pgen.1007789

Lang, D., Eisinger, J., Reski, R., & Rensing, S. A. (2005). Representation and high-quality annotation of the Physcomitrella patens transcriptome demonstrates a high proportion of proteins involved in metabolism in mosses. *Plant Biology*, *7*(3), 238–250. https://doi.org/10.1055/s-2005-837578

Lemmon, M. A. (2008). Membrane recognition by phospholipid-binding domains. In *Nature Reviews Molecular Cell Biology* (Vol. 9, Issue 2, pp. 99–111). Nature Publishing Group. https://doi.org/10.1038/nrm2328

Lemtiri-Chlieh, F., MacRobbie, E. A. C., Webb, A. A. R., Manison, N. F., Brownlee, C., Skepper, J. N., Chen, J., Prestwich, G. D., & Brearley, C. A. (2003). Inositol hexakisphosphate mobilizes an endomembrane store of calcium in guard cells. *Proceedings of the National Academy of Sciences of the United States of America*, *100*(17), 10091–10095. https://doi.org/10.1073/pnas.1133289100

Leroux, C., Bouton, S., Kiefer-Meyer, M. C., Fabrice, T. N., Mareck, A., Guénin, S., Fournet, F., Ringli, C., Pelloux, J., Driouich, A., Lerouge, P., Lehner, A., & Mollet, J. C. (2015). PECTIN METHYLESTERASE48 is involved in arabidopsis pollen grain germination. *Plant Physiology*, *167*(2), 367–380. https://doi.org/10.1104/pp.114.250928

Leucci, M. R., Di Sansebastiano, G. Pietro, Gigante, M., Dalessandro, G., & Piro, G. (2007). Secretion marker proteins and cell-wall polysaccharides move through different secretory pathways. *Planta*, *225*(4), 1001–1017. https://doi.org/10.1007/s00425-006-0407-9

Levesque-Tremblay, G., Pelloux, J., Braybrook, S. A., & Müller, K. (2015). Tuning of pectin methylesterification: consequences for cell wall biomechanics and development. In *Planta* (Vol. 242, Issue 4, pp. 791–811). Springer Verlag. https://doi.org/10.1007/s00425-015-2358-5

Li, L., He, Y., Wang, Y., Zhao, S., Chen, X., Ye, T., Wu, Y., & Wu, Y. (2015). Arabidopsis PLC2 is involved in auxin-modulated reproductive development. *Plant Journal*, *84*(3), 504–515. https://doi.org/10.1111/tpj.13016

Li, S., Chen, M., Yu, D., Ren, S., Sun, S., Liu, L., Ketelaar, T., Emons, A. M. C., & Liu, C. M. (2013). EXO70A1-mediated vesicle trafficking is critical for tracheary element development in Arabidopsis. *Plant Cell*, *25*(5), 1774–1786. https://doi.org/10.1105/tpc.113.112144

Li, S., van Os, G. M. A., Ren, S., Yu, D., Ketelaar, T., Emons, A. M. C., & Liu, C. M. (2010). Expression and functional analyses of EXO70 genes in arabidopsis implicate their roles in regulating cell type-specific exocytosis. *Plant Physiology*, *154*(4), 1819–1830. https://doi.org/10.1104/pp.110.164178

Li, Y., Tan, X., Wang, M., Li, B., Zhao, Y., Wu, C., Rui, Q., Wang, J., Liu, Z., & Bao, Y. (2017). Exocyst subunit SEC3A marks the germination site and is essential for pollen germination in Arabidopsis thaliana. *Scientific Reports*, *7*. https://doi.org/10.1038/srep40279

Limberg, G., Körner, R., Buchholt, H. C., Christensen, T. M. I. E., Roepstorff, P., &

Mikkelsen, J. D. (2000). Analysis of different de-esterification mechanisms for pectin by enzymatic fingerprinting using endopectin lyase and endopolygalacturonase II from A. Niger. *Carbohydrate Research*, *327*(3), 293–307. https://doi.org/10.1016/S0008-6215(00)00067-7

Liu, J., Zuo, X., Yue, P., & Guo, W. (2007). Phosphatidylinositol 4,5-bisphosphate mediates the targeting of the exocyst to the plasma membrane for exocytosis in mammalian cells. *Molecular Biology of the Cell*, *18*(11), 4483–4492. https://doi.org/10.1091/mbc.E07-05-0461

Loraine, A. E., McCormick, S., Estrada, A., Patel, K., & Qin, P. (2013). RNA-seq of Arabidopsis pollen uncovers novel transcription and alternative splicing. *Plant Physiology*, *162*(2), 1092–1109. https://doi.org/10.1104/pp.112.211441

MacAlister, C. A., Ortiz-Ramírez, C., Becker, J. D., Feijó, J. A., & Lippman, Z. B. (2016). Hydroxyproline *O* -arabinosyltransferase mutants oppositely alter tip growth in *Arabidopsis thaliana* and *Physcomitrella patens*. *The Plant Journal*, *85*(2), 193–208. https://doi.org/10.1111/tpj.13079

MacDougall, A. J., Brett, G. M., Morris, V. J., Rigby, N. M., Ridout, M. J., & Ring, S. G. (2001). The effect of peptide–pectin interactions on the gelation behaviour of a plant cell wall pectin. *Carbohydrate Research*, *335*(2), 115–126. https://doi.org/10.1016/S0008-6215(01)00221-X

MacDougall, A. J., Needs, P. W., Rigby, N. M., & Ring, S. G. (1996). Calcium gelation of pectic polysaccharides isolated from unripe tomato fruit. *Carbohydrate Research*, *293*(2), 235–249. https://doi.org/10.1016/0008-6215(96)00197-8

Markovič, O., & Janeček, Š. (2004). Pectin methylesterases: Sequence-structural features and phylogenetic relationships. *Carbohydrate Research*, *339*(13), 2281–2295. https://doi.org/10.1016/j.carres.2004.06.023

Marković, V., Cvrčková, F., Potocký, M., Kulich, I., Pejchar, P., Kollárová, E., Synek, L., & Žárský, V. (2020). EXO70A2 is critical for exocyst complex function in pollen development. *Plant Physiology*, *184*(4), 1823–1839. https://doi.org/10.1104/pp.19.01340

Marković, V., Cvrčková, F., Potocký, M., Pejchar, P., Kollárová, E., Kulich, I., Synek, L., & Žárský, V. (2019). EXO70A2 is critical for the exocyst complex function in Arabidopsis pollen. *BioRxiv*, 831875. https://doi.org/10.1101/831875

Martinière, A., Gayral, P., Hawes, C., & Runions, J. (2011). Building bridges: Formin1 of Arabidopsis forms a connection between the cell wall and the actin cytoskeleton. *Plant Journal*, *66*(2), 354–365. https://doi.org/10.1111/j.1365-313X.2011.04497.x

McKenna, S. T., Kunkel, J. G., Bosch, M., Rounds, C. M., Vidali, L., Winship, L. J., &

Hepler, P. K. (2009). Exocytosis Precedes and Predicts the Increase in Growth in Oscillating Pollen Tubes. *The Plant Cell*, *21*(10), 3026–3040. https://doi.org/10.1105/tpc.109.069260

Mecchia, M. A., Santos-Fernandez, G., Duss, N. N., Somoza, S. C., Boisson-Dernier, A., Gagliardini, V., Martínez-Bernardini, A., Fabrice, T. N., Ringli, C., Muschietti, J. P., & Grossniklaus, U. (2017). RALF4/19 peptides interact with LRX proteins to control pollen tube growth in Arabidopsis. *Science*, *358*(6370), 1600–1603. https://doi.org/10.1126/science.aao5467

Mei, K., & Guo, W. (2018). The exocyst complex. In *Current Biology* (Vol. 28, Issue 17, pp. R922–R925). Cell Press. https://doi.org/10.1016/j.cub.2018.06.042

Michard, E., Lima, P. T., Borges, F., Catarina Silva, A., Teresa Portes, M., Carvalho, J. E., Gilliham, M., Liu, L. H., Obermeyer, G., & Feijó, J. A. (2011). Glutamate receptor-like genes form Ca2+ channels in pollen ubes and are regulated by pistil D-serine. *Science*, *332*(6028), 434–437. https://doi.org/10.1126/science.1201101

Micheli, F. (2001). Pectin methylesterases: Cell wall enzymes with important roles in plant physiology. In *Trends in Plant Science* (Vol. 6, Issue 9, pp. 414–419). https://doi.org/10.1016/S1360-1385(01)02045-3

Mohnen, D. (2008). Pectin structure and biosynthesis. In *Current Opinion in Plant Biology* (Vol. 11, Issue 3, pp. 266–277). Elsevier Current Trends. https://doi.org/10.1016/j.pbi.2008.03.006

Møller, S. R., Yi, X., Velásquez, S. M., Gille, S., Hansen, P. L. M., Poulsen, C. P., Olsen, C. E., Rejzek, M., Parsons, H., Zhang, Y., Wandall, H. H., Clausen, H., Field, R. A., Pauly, M., Estevez, J. M., Harholt, J., Ulvskov, P., & Petersen, B. L. (2017). Identification and evolution of a plant cell wall specific glycoprotein glycosyl transferase, ExAD. *Scientific Reports*, *7*, 45341. https://doi.org/10.1038/srep45341

Moore, J. P., Farrant, J. M., & Driouich, A. (2008). A role for pectin-associated arabinans in maintaining the flexibility of the plant cell wall during water deficit stress. *Plant Signaling and Behavior*, *3*(2), 102–104. https://doi.org/10.4161/psb.3.2.4959

Mouille, G., Ralet, M.-C., Cavelier, C., Eland, C., Effroy, D., Hématy, K., McCartney, L., Truong, H. N., Gaudon, V., Thibault, J.-F., Marchant, A., & Höfte, H. (2007). Homogalacturonan synthesis in Arabidopsis thaliana requires a Golgi-localized protein with a putative methyltransferase domain. *The Plant Journal*, *50*(4), 605–614. https://doi.org/10.1111/j.1365-313X.2007.03086.x

Munnik, T., Irvine, R. F., & Musgrave, A. (1998). Phospholipid signalling in plants. In *Biochimica et Biophysica Acta - Lipids and Lipid Metabolism* (Vol. 1389, Issue 3, pp. 222–272). Biochim Biophys Acta. https://doi.org/10.1016/S0005-

2760(97)00158-6

Munnik, Teun. (2014). *PI-PLC: Phosphoinositide-Phospholipase C in Plant Signaling* (pp. 27–54). Springer, Berlin, Heidelberg. https://doi.org/10.1007/978-3-642-42011-5_2

Munnik, Teun, & Testerink, C. (2009). Plant phospholipid signaling: “In a nutshell.” In *Journal of Lipid Research* (Vol. 50, Issue SUPPL., p. S260). American Society for Biochemistry and Molecular Biology. https://doi.org/10.1194/jlr.R800098-JLR200

Nagata, T., Iizumi, S., Satoh, K., Ooka, H., Kawai, J., Carninci, P., Hayashizaki, Y., Otomo, Y., Murakami, K., Matsubara, K., & Kikuchi, S. (2004). Comparative analysis of plant and animal calcium signal transduction element using plant full-length cDNA data. *Molecular Biology and Evolution*, *21*(10), 1855–1870. https://doi.org/10.1093/molbev/msh197

Nakhamchik, A., Zhao, Z., Provart, N. J., Shiu, S. H., Keatley, S. K., Cameron, R. K., & Goring, D. R. (2004). A comprehensive expression analysis of the Arabidopsis proline-rich extensin-like receptor kinase gene family using bioinformatic and experimental approaches. *Plant and Cell Physiology*, *45*(12), 1875–1881. https://doi.org/10.1093/pcp/pch206

Novick, P., Field, C., & Schekman, R. (1980). Identification of 23 complementation groups required for post-translational events in the yeast secretory pathway. *Cell*, *21*(1), 205–215. https://doi.org/10.1016/0092-8674(80)90128-2

O’Neill, M. A., Ishii, T., Albersheim, P., & Darvill, A. G. (2004). Rhamnogalacturonan II: Structure and function of a borate cross-linked cell wall pectic polysaccharide. In *Annual Review of Plant Biology* (Vol. 55, pp. 109–139). Annu Rev Plant Biol. https://doi.org/10.1146/annurev.arplant.55.031903.141750

O’Neill, M., Albersheim, P., & Darvill, A. (1990). *The Pectic Polysaccharides of Primary Cell Walls* (Vol. 2, pp. 415–441). Academic Press. https://doi.org/10.1016/b978-0-12-461012-5.50018-5

Ogawa-Ohnishi, M., Matsushita, W., & Matsubayashi, Y. (2013). Identification of three hydroxyproline O-arabinosyltransferases in Arabidopsis thaliana. *Nature Chemical Biology*, *9*(11), 726–730. https://doi.org/10.1038/nchembio.1351

Ohyama, K., Shinohara, H., Ogawa-Ohnishi, M., & Matsubayashi, Y. (2009). A glycopeptide regulating stem cell fate in Arabidopsis thaliana. *Nature Chemical Biology*, *5*(8), 578–580. https://doi.org/10.1038/nchembio.182

Otterhag, L., Sommarin, M., & Pical, C. (2001). N-terminal EF-hand-like domain is required for phosphoinositide-specific phospholipase C activity in Arabidopsis thaliana. *FEBS Letters*, *497*(2–3), 165–170. https://doi.org/10.1016/S0014-5793(01)02453-X

Pagnussat, G. C., Yu, H. J., Ngo, Q. A., Rajani, S., Mayalagu, S., Johnson, C. S., Capron, A., Xie, L. F., Ye, D., & Sundaresan, V. (2005). Genetic and molecular identification of genes required for female gametophyte development and function in Arabidopsis. *Development*, *132*(3), 603–614. https://doi.org/10.1242/dev.01595

Pelloux, J., Rustérucci, C., & Mellerowicz, E. J. (2007). New insights into pectin methylesterase structure and function. In *Trends in Plant Science* (Vol. 12, Issue 6, pp. 267–277). Elsevier Current Trends. https://doi.org/10.1016/j.tplants.2007.04.001

Petersen, B. L., MacAlister, C. A., & Ulvskov, P. (2021). Plant Protein O-Arabinosylation. In *Frontiers in Plant Science* (Vol. 12, p. 400). Frontiers. https://doi.org/10.3389/fpls.2021.645219

Peterson, R., Slovin, J. P., & Chen, C. (2010). A simplified method for differential staining of aborted and non-aborted pollen grains. *International Journal of Plant Biology*, *1*(2), 66–69. https://doi.org/10.4081/pb.2010.e13

Pike, A.C.W., Amos, A., Johansson, C., Sobott, F., Savitsky, P., Berridge, G., Fedorov, O., Umeano, C., Gorrec, F., Bunkoczi, G., Debreczeni, J., von Delft, F., Arrowsmith, C.H., Edwards, A., Weigelt, J., Sundstrom, M., Knapp, S. (2007). *RCSB PDB-2UZP: Crystal structure of the C2 domain of human protein kinase C gamma.* RCSB PDB- 2UZP: Crystal Structure of the C2 Domain of Human Protein Kinase C Gamma. https://doi.org/10.2210/pdb2UZP/pdb

Pleskot, R., Cwiklik, L., Jungwirth, P., Žárský, V., & Potocký, M. (2015). Membrane targeting of the yeast exocyst complex. *Biochimica et Biophysica Acta - Biomembranes*, *1848*(7), 1481–1489. https://doi.org/10.1016/j.bbamem.2015.03.026

Pokotylo, I., Kolesnikov, Y., Kravets, V., Zachowski, A., & Ruelland, E. (2014). Plant phosphoinositide-dependent phospholipases C: Variations around a canonical theme. In *Biochimie* (Vol. 96, Issue 1, pp. 144–157). Biochimie. https://doi.org/10.1016/j.biochi.2013.07.004

Qi Xiaoyang, Behrens Bing-Xie, West, P. R., & Mort, A. J. (1995). Solubilization and partial characterization of extensin fragments from cell walls of cotton suspension cultures. Evidence for a covalent cross-link between extensin and pectin. *Plant Physiology*, *108*(4), 1691–1701. https://doi.org/10.1104/pp.108.4.1691

Qu, L. J., & Qin, G. (2014). Generation and identification of arabidopsis EMS mutants. *Methods in Molecular Biology*, *1062*, 225–239. https://doi.org/10.1007/978-1-62703-580-4_12

Rebecchi, M. J., & Pentyala, S. N. (2000). Structure, function, and control of

phosphoinositide-specific phospholipase C. In *Physiological Reviews* (Vol. 80, Issue 4, pp. 1291–1335). American Physiological SocietyBethesda, MD. https://doi.org/10.1152/physrev.2000.80.4.1291

Ridley, B. L., O'Neill, M. A., & Mohnen, D. (2001). Pectins: Structure, biosynthesis, and oligogalacturonide-related signaling. In *Phytochemistry* (Vol. 57, Issue 6, pp. 929–967). https://doi.org/10.1016/S0031-9422(01)00113-3

Röckel, N., Wolf, S., Kost, B., Rausch, T., & Greiner, S. (2008). Elaborate spatial patterning of cell-wall PME and PMEI at the pollen tube tip involves PMEI endocytosis, and reflects the distribution of esterified and de-esterified pectins. *Plant Journal*, *53*(1), 133–143. https://doi.org/10.1111/j.1365-313X.2007.03325.x

Rodriguez-Enriquez, M. J., Mehdi, S., Dickinson, H. G., & Grant-Downton, R. T. (2013). A novel method for efficient in vitro germination and tube growth of Arabidopsis thaliana pollen. *New Phytologist*, *197*(2), 668–679. https://doi.org/10.1111/nph.12037

Rounds, C. M., Lubeck, E., Hepler, P. K., & Winship, L. J. (2011). Propidium iodide competes with Ca 2+ to label pectin in pollen tubes and arabidopsis root hairs. *Plant Physiology*, *157*(1), 175–187. https://doi.org/10.1104/pp.111.182196

Rupwate, S. D., & Rajasekharan, R. (2012). C2 domain is responsible for targeting rice phosphoinositide specific phospholipase C. *Plant Molecular Biology*, *78*(3), 247–258. https://doi.org/10.1007/s11103-011-9862-1

Sadava, D., & Chrispeels, M. J. (1973). Hydroxyproline-rich cell wall protein (extensin): Role in the cessation of elongation in excised pea epicotyls. *Developmental Biology*, *30*(1), 49–55. https://doi.org/10.1016/0012-1606(73)90047-X

Safavian, D., Zayed, Y., Indriolo, E., Chapman, L., Ahmed, A., & Goring, D. R. (2015). RNA silencing of exocyst genes in the stigma impairs the acceptance of compatible pollen in arabidopsis. *Plant Physiology*, *169*(4), 2526–2538. https://doi.org/10.1104/pp.15.00635

Samuel, M. A., Chong, Y. T., Haasen, K. E., Aldea-Brydges, M. G., Stone, S. L., & Goring, D. R. (2009). Cellular pathways regulating responses to compatible and self-incompatible pollen in brassica and arabidopsis stigmas intersect at exo70a1, a putative component of the exocyst complex. *Plant Cell*, *21*(9), 2655–2671. https://doi.org/10.1105/tpc.109.069740

Schlupmann, H., Bacic, A., & Read, S. M. (1994). Uridine diphosphate glucose metabolism and callose synthesis in cultured pollen tubes of Nicotiana alata Link et Otto. *Plant Physiology*, *105*(2), 659–670. https://doi.org/10.1104/pp.105.2.659

Schmid, M., Davison, T. S., Henz, S. R., Pape, U. J., Demar, M., Vingron, M.,

Schölkopf, B., Weigel, D., & Lohmann, J. U. (2005). A gene expression map of Arabidopsis thaliana development. *Nature Genetics*, *37*(5), 501–506. https://doi.org/10.1038/ng1543

Schnabel, E. L., Kassaw, T. K., Smith, L. S., Marsh, J. F., Oldroyd, G. E., Long, S. R., & Frugoli, J. A. (2011). The root determined nodulation1 gene regulates nodule number in roots of medicago truncatula and defines a highly conserved, uncharacterized plant gene family. *Plant Physiology*, *157*(1), 328–340. https://doi.org/10.1104/pp.111.178756

Schoof, H., Lenhard, M., Haecker, A., Mayer, K. F. X., Jürgens, G., & Laux, T. (2000). The stem cell population of Arabidopsis shoot meristems is maintained by a regulatory loop between the CLAVATA and WUSCHEL genes. *Cell*, *100*(6), 635–644. https://doi.org/10.1016/S0092-8674(00)80700-X

Sede, A. R., Borassi, C., Wengier, D. L., Mecchia, M. A., Estevez, J. M., & Muschietti, J. P. (2018). Arabidopsis pollen extensins LRX are required for cell wall integrity during pollen tube growth. *FEBS Letters*, *592*(2), 233–243. https://doi.org/10.1002/1873-3468.12947

Sénéchal, F., Graff, L., Surcouf, O., Marcelo, P., Rayon, C., Bouton, S., Mareck, A., Mouille, G., Stintzi, A., Höfte, H., Lerouge, P., Schaller, A., & Pelloux, J. (2014). Arabidopsis PECTIN METHYLESTERASE17 is co-expressed with and processed by SBT3.5, a subtilisin-like serine protease. *Annals of Botany*, *114*(6), 1161–1175. https://doi.org/10.1093/aob/mcu035

Sénéchal, F., L'Enfant, M., Domon, J. M., Rosiau, E., Crépeau, M. J., Surcouf, O., Esquivel-Rodriguez, J., Marcelo, P., Mareck, A., Guérineau, F., Kim, H. R., Mravec, J., Bonnin, E., Jamet, E., Kihara, D., Lerouge, P., Ralet, M. C., Pelloux, J., & Rayon, C. (2015). Tuning of pectin methylesterification: Pectin methylesterase inhibitor 7 modulates the processive activity of co-expressed pectin methylesterase 3 in a pH-dependentmanner. *Journal of Biological Chemistry*, *290*(38), 23320–23335. https://doi.org/10.1074/jbc.M115.639534

Shaner, N. C., Lambert, G. G., Chammas, A., Ni, Y., Cranfill, P. J., Baird, M. A., Sell, B. R., Allen, J. R., Day, R. N., Israelsson, M., Davidson, M. W., & Wang, J. (2013). A bright monomeric green fluorescent protein derived from Branchiostoma lanceolatum. *Nature Methods*, *10*(5), 407–409. https://doi.org/10.1038/nmeth.2413

Shimada, T. L., Shimada, T., & Hara-Nishimura, I. (2010). A rapid and non-destructive screenable marker, FAST, for identifying transformed seeds of Arabidopsis thaliana: TECHNICAL ADVANCE. *Plant Journal*, *61*(3), 519–528. https://doi.org/10.1111/j.1365-313X.2009.04060.x

Shinde, U. P., Li, Y., & Inouye, M. (1995). Propeptide mediated protein folding: intramolecular chaperones. In *Intramolecular chaperones and protein folding*.

https://ci.nii.ac.jp/naid/10027519559/

Shinohara, H., & Matsubayashi, Y. (2013). Chemical synthesis of arabidopsis CLV3 glycopeptide reveals the impact of hydroxyproline arabinosylation on peptide conformation and activity. *Plant and Cell Physiology*, *54*(3), 369–374. https://doi.org/10.1093/pcp/pcs174

Showalter, A. M. (1993). Structure and function of plant cell wall proteins. In *Plant Cell* (Vol. 5, Issue 1, pp. 9–23). American Society of Plant Biologists. https://doi.org/10.1105/tpc.5.1.9

Showalter, A. M., & Basu, D. (2016). Extensin and Arabinogalactan-Protein Biosynthesis: Glycosyltransferases, Research Challenges, and Biosensors. *Frontiers in Plant Science*, *7*, 814. https://doi.org/10.3389/fpls.2016.00814

Showalter, A. M., Keppler, B., Lichtenberg, J., Gu, D., & Welch, L. R. (2010). A bioinformatics approach to the identification, classification, and analysis of hydroxyproline-rich glycoproteins. *Plant Physiology*, *153*(2), 485–513. https://doi.org/10.1104/pp.110.156554

Sinclair, R., Rosquete, M. R., & Drakakaki, G. (2018). Post-golgi trafficking and transport of cell wall components. In *Frontiers in Plant Science* (Vol. 871, p. 1784). Frontiers. https://doi.org/10.3389/fpls.2018.01784

Sivaram, M. V. S., Furgason, M. L. M., Brewer, D. N., & Munson, M. (2006). The structure of the exocyst subunit Sec6p defines a conserved architecture with diverse roles. *Nature Structural and Molecular Biology*, *13*(6), 555–556. https://doi.org/10.1038/nsmb1096

Smallwood, M., Beven, A., Donovan, N., Neill, S. J., Peart, J., Roberts, K., & Knox, J. P. (1994). Localization of cell wall proteins in relation to the developmental anatomy of the carrot root apex. *The Plant Journal*, *5*(2), 237–246. https://doi.org/10.1046/j.1365-313X.1994.05020237.x

Smallwood, Margaret, Martin, H., & Knox, J. P. (1995). An epitope of rice threonine- and hydroxyproline-rich glycoprotein is common to cell wall and hydrophobic plasma-membrane glycoproteins. *Planta: An International Journal of Plant Biology*, *196*(3), 510–522. https://doi.org/10.1007/BF00203651

Smith, J. J., Muldoon, E. P., & Lamport, D. T. A. (1984). Isolation of extensin precursors by direct elution of intact tomato cell suspension cultures. *Phytochemistry*, *23*(6), 1233–1239. https://doi.org/10.1016/S0031-9422(00)80432-X

Stafstrom, J. P., & Staehelin, L. A. (1986a). Cross-Linking Patterns in Salt-Extractable Extensin from Carrot Cell Walls. *Plant Physiology*, *81*(1), 234–241. https://doi.org/10.1104/pp.81.1.234

Stafstrom, J. P., & Staehelin, L. A. (1986b). The Role of Carbohydrate in Maintaining Extensin in an Extended Conformation. *Plant Physiology*, *81*(1), 242–246. https://doi.org/10.1104/pp.81.1.242

Sterling, J. D., Atmodjo, M. A., Inwood, S. E., Kolli, V. S. K., Quigley, H. F., Hahn, M. G., & Mohnen, D. (2006). Functional identification of an Arabidopsis pectin biosynthetic homogalacturonan galacturonosyltransferase. *Proceedings of the National Academy of Sciences of the United States of America*, *103*(13), 5236–5241. https://doi.org/10.1073/pnas.0600120103

Sterling, J. D., Quigley, H. F., Orellana, A., & Mohnen, D. (2001). The catalytic site of the pectin biosynthetic enzyme α-1,4-galacturonosyltransferase is located in the lumen of the Golgi. *Plant Physiology*, *127*(1), 360–371. https://doi.org/10.1104/pp.127.1.360

Sutton, R. B., & Sprang, S. R. (1998). Structure of the protein kinase Cβ phospholipid-binding C2 domain complexed with Ca2+. *Structure*, *6*(11), 1395–1405. https://doi.org/10.1016/S0969-2126(98)00139-7

Synek, L., Schlager, N., Eliáš, M., Quentin, M., Hauser, M. T., & Žárský, V. (2006). AtEXO70A1, a member of a family of putative exocyst subunits specifically expanded in land plants, is important for polar growth and plant development. *Plant Journal*, *48*(1), 54–72. https://doi.org/10.1111/j.1365-313X.2006.02854.x

Synek, L., Vukašinović, N., Kulich, I., Hála, M., Aldorfová, K., Fendrych, M., & Žárský, V. (2017). EXO70C2 Is a Key Regulatory Factor for Optimal Tip Growth of Pollen. *Plant Physiology*, *174*(1), 223–240. https://doi.org/10.1104/pp.16.01282

Taiz, L. (1984). Plant Cell Expansion: Regulation of Cell Wall Mechanical Properties. *Annual Review of Plant Physiology*, *35*(1), 585–657. https://doi.org/10.1146/annurev.pp.35.060184.003101

Takemiya, A., Ariyoshi, C., & Shimazaki, K. I. (2009). Identification and functional characterization of inhibitor-3, a regulatory subunit of protein phosphatase 1 in plants1[W][OA]. *Plant Physiology*, *150*(1), 144–156. https://doi.org/10.1104/pp.109.135335

Tan, L., Varnai, P., Lamport, D. T. A., Yuan, C., Xu, J., Qiu, F., & Kieliszewski, M. J. (2010). Plant O-hydroxyproline arabinogalactans are composed of repeating trigalactosyl subunits with short bifurcated side chains. *Journal of Biological Chemistry*, *285*(32), 24575–24583. https://doi.org/10.1074/jbc.M109.100149

Tang, H., Wang, S., Wang, J., Song, M., Xu, M., Zhang, M., Shen, Y., Hou, J., & Bao, X. (2016). N-hypermannose glycosylation disruption enhances recombinant protein production by regulating secretory pathway and cell wall integrity in

Saccharomyces cerevisiae. *Scientific Reports*, *6*. https://doi.org/10.1038/srep25654

TerBush, D. R., & Novick, P. (1995). Sec6, Sec8, and Sec15 are components of a multisubunit complex which localizes to small bud tips in Saccharomyces cerevisiae. *Journal of Cell Biology*, *130*(2), 299–312. https://doi.org/10.1083/jcb.130.2.299

Tiainen, P., Myllyharju, J., & Koivunen, P. (2005). Characterization of a second Arabidopsis thaliana prolyl 4-hydroxylase with distinct substrate specificity. *Journal of Biological Chemistry*, *280*(2), 1142–1148. https://doi.org/10.1074/jbc.M411109200

Tian, G.-W., Chen, M.-H., Zaltsman, A., & Citovsky, V. (2006). Pollen-specific pectin methylesterase involved in pollen tube growth. *Developmental Biology*, *294*(1), 83–91. https://doi.org/10.1016/j.ydbio.2006.02.026

van Holst, G.-J., & Varner, J. E. (1984). Reinforced Polyproline II Conformation in a Hydroxyproline-Rich Cell Wall Glycoprotein from Carrot Root. *Plant Physiology*, *74*(2), 247–251. https://doi.org/10.1104/pp.74.2.247

Van Leeuwen, W., Vermeer, J. E. M., Gadella, T. W. J., & Munnik, T. (2007). Visualization of phosphatidylinositol 4,5-bisphosphate in the plasma membrane of suspension-cultured tobacco BY-2 cells and whole Arabidopsis seedlings. *Plant Journal*, *52*(6), 1014–1026. https://doi.org/10.1111/j.1365-313X.2007.03292.x

van Wijk, R., Zhang, Q., Zarza, X., Lamers, M., Marquez, F. R., Guardia, A., Scuffi, D., García-Mata, C., Ligterink, W., Haring, M. A., Laxalt, A. M., & Munnik, T. (2018). Role for arabidopsis PLC7 in stomatal movement, seed mucilage attachment, and leaf serration. *Frontiers in Plant Science*, *871*, 1721. https://doi.org/10.3389/fpls.2018.01721

VanDerWoude, W. J., Morré, D. J., & Bracker, C. E. (1971). Isolation and characterization of secretory vesicles in germinated pollen of Lilium longiflorum. *Journal of Cell Science*, *8*(2), 331–351. https://doi.org/10.1242/jcs.8.2.331

Vaughan, D., & Cusens, E. (1973). Effects of hydroxyproline on the growth of excised root segments of Pisum sativum under aseptic conditions. *Planta*, *112*(3), 243–252. https://doi.org/10.1007/BF00385328

Velasquez, S. M., Ricardi, M. M., Dorosz, J. G., Fernandez, P. V., Nadra, A. D., Pol-Fachin, L., Egelund, J., Gille, S., Harholt, J., Ciancia, M., Verli, H., Pauly, M., Bacic, A., Olsen, C. E., Ulvskov, P., Petersen, B. L., Somerville, C., Iusem, N. D., & Estevez, J. M. (2011). O-glycosylated cell wall proteins are essential in root hair growth. *Science*, *332*(6036), 1401–1403. https://doi.org/10.1126/science.1206657

Velasquez, S. M., Ricardi, M. M., Poulsen, C. P., Oikawa, A., Dilokpimol, A., Halim, A.,

Mangano, S., Denita Juarez, S. P., Marzol, E., Salgado Salter, J. D., Dorosz, J. G., Borassi, C., Möller, S. R., Buono, R., Ohsawa, Y., Matsuoka, K., Otegui, M. S., Scheller, H. V., Geshi, N., … Estevez, J. M. (2015). Complex regulation of prolyl-4-hydroxylases impacts root hair expansion. *Molecular Plant*, *8*(5), 734–746. https://doi.org/10.1016/j.molp.2014.11.017

Verdaguer, N., Corbalan-Garcia, S., Ochoa, W. F., Fita, I., & Gómez-Fernández, J. C. (1999). Ca2+ bridges the C2 membrane-binding domain of protein kinase Cα directly to phosphatidylserine. *EMBO Journal*, *18*(22), 6329–6338. https://doi.org/10.1093/emboj/18.22.6329

Verhertbruggen, Y., Marcus, S. E., Haeger, A., Ordaz-Ortiz, J. J., & Knox, J. P. (2009). An extended set of monoclonal antibodies to pectic homogalacturonan. *Carbohydrate Research*, *344*(14), 1858–1862. https://doi.org/10.1016/j.carres.2008.11.010

Vermeer, J. E. M., Thole, J. M., Goedhart, J., Nielsen, E., Munnik, T., & Gadella, T. W. J. (2009). Imaging phosphatidylinositol 4-phosphate dynamics in living plant cells. *Plant Journal*, *57*(2), 356–372. https://doi.org/10.1111/j.1365-313X.2008.03679.x

Vermeer, J. E. M., Van Leeuwen, W., Tobeña-Santamaria, R., Laxalt, A. M., Jones, D. R., Divecha, N., Gadella, T. W. J., & Munnik, T. (2006). Visualization of PtdIns3P dynamics in living plant cells. *Plant Journal*, *47*(5), 687–700. https://doi.org/10.1111/j.1365-313X.2006.02830.x

Wang, M., Yuan, D., Gao, W., Li, Y., Tan, J., & Zhang, X. (2013). A Comparative Genome Analysis of PME and PMEI Families Reveals the Evolution of Pectin Metabolism in Plant Cell Walls. *PLoS ONE*, *8*(8). https://doi.org/10.1371/journal.pone.0072082

Wang, S., Crisman, L., Miller, J., Datta, I., Gulbranson, D. R., Tian, Y., Yin, Q., Yu, H., & Shen, J. (2019). Inducible Exoc7/Exo70 knockout reveals a critical role of the exocyst in insulin-regulated GLUT4 exocytosis. *Journal of Biological Chemistry*, *294*(52), 19988–19996. https://doi.org/10.1074/jbc.RA119.010821

Weigel, D., & Glazebrook, J. (2006). EMS Mutagenesis of Arabidopsis Seed. *Cold Spring Harbor Protocols*, *2006*(5), pdb.prot4621. https://doi.org/10.1101/PDB.PROT4621

Wheeler, G. L., & Brownlee, C. (2008). Ca2+ signalling in plants and green algae - changing channels. In *Trends in Plant Science* (Vol. 13, Issue 9, pp. 506–514). Trends Plant Sci. https://doi.org/10.1016/j.tplants.2008.06.004

Wolf, S., Mouille, G., & Pelloux, J. (2009). Homogalacturonan methyl-esterification and plant development. *Molecular Plant*, *2*(5), 851–860. https://doi.org/10.1093/mp/ssp066

Woody, S. T., Austin-Phillips, S., Amasino, R. M., & Krysan, P. J. (2007). The WiscDsLox T-DNA collection: An arabidopsis community resource generated by using an improved high-throughput T-DNA sequencing pipeline. *Journal of Plant Research*, *120*(1), 157–165. https://doi.org/10.1007/s10265-006-0048-x

Woriedh, M., Wolf, S., Márton, M. L., Hinze, A., Gahrtz, M., Becker, D., & Dresselhaus, T. (2013). External application of gametophyte-specific ZmPMEI1 induces pollen tube burst in maize. *Plant Reproduction*, *26*(3), 255–266. https://doi.org/10.1007/s00497-013-0221-z

Wormit, A., & Usadel, B. (2018). The multifaceted role of pectin methylesterase inhibitors (PMEIs). In *International Journal of Molecular Sciences* (Vol. 19, Issue 10). MDPI AG. https://doi.org/10.3390/ijms19102878

Wu, S., Mehta, S. Q., Pichaud, F., Bellen, H. J., & Quiocho, F. A. (2005). Sec15 interacts with Rab11 via a novel domain and affects Rab11 localization in vivo. *Nature Structural and Molecular Biology*, *12*(10), 879–885. https://doi.org/10.1038/nsmb987

Wudick, M. M., Portes, M. T., Michard, E., Rosas-Santiago, P., Lizzio, M. A., Nunes, C. O., Campos, C., Santa Cruz Damineli, D., Carvalho, J. C., Lima, P. T., Pantoja, O., & Feijó, J. A. (2018). CORNICHON sorting and regulation of GLR channels underlie pollen tube Ca2+ homeostasis. *Science*, *360*(6388), 533–536. https://doi.org/10.1126/science.aar6464

Xia, K., Wang, B., Zhang, J., Li, Y., Yang, H., & Ren, D. (2017). Arabidopsis phosphoinositide-specific phospholipase C 4 negatively regulates seedling salt tolerance. *Plant Cell and Environment*, *40*(8), 1317–1331. https://doi.org/10.1111/pce.12918

Xiang, Y., Zhang, X., Nix, D. B., Katoh, T., Aoki, K., Tiemeyer, M., & Wang, Y. (2013). Regulation of protein glycosylation and sorting by the Golgi matrix proteins GRASP55/65. *Nature Communications*, *4*. https://doi.org/10.1038/ncomms2669

Xu, C., Liberatore, K. L., Macalister, C. A., Huang, Z., Chu, Y. H., Jiang, K., Brooks, C., Ogawa-Ohnishi, M., Xiong, G., Pauly, M., Van Eck, J., Matsubayashi, Y., Van Der Knaap, E., & Lippman, Z. B. (2015). A cascade of arabinosyltransferases controls shoot meristem size in tomato. *Nature Genetics*, *47*(7), 784–792. https://doi.org/10.1038/ng.3309

Yamochi, W., Tanaka, K., Nonaka, H., Maeda, A., Musha, T., & Takai, Y. (1994). Growth site localization of Rho1 small GTP-binding protein and its involvement in bud formation in Saccharomyces cerevisiae. *Journal of Cell Biology*, *125*(5), 1077–1093. https://doi.org/10.1083/jcb.125.5.1077

Yang, Z., Bennett, E. P., Jørgensen, B., Drew, D. P., Arigi, E., Mandel, U., Ulvskov, P., Levery, S. B., Clausen, H., & Petersen, B. L. (2012). Toward stable Genetic engineering of human O-glycosylation in plants. *Plant Physiology*, *160*(1), 450–463. https://doi.org/10.1104/pp.112.198200

Ye, J., Zheng, Y., Yan, A., Chen, N., Wang, Z., Huang, S., & Yang, Z. (2009). Arabidopsis formin3 directs the formation of actin cables and polarized growth in pollen tubes. *Plant Cell*, *21*(12), 3868–3884. https://doi.org/10.1105/tpc.109.068700

Yoro, E., Nishida, H., Ogawa-Ohnishi, M., Yoshida, C., Suzaki, T., Matsubayashi, Y., & Kawaguchi, M. (2019). PLENTY, a hydroxyproline O-arabinosyltransferase, negatively regulates root nodule symbiosis in Lotus japonicus. *Journal of Experimental Botany*, *70*(2), 507–517. https://doi.org/10.1093/jxb/ery364

Zhang, Q., Van Wijk, R., Shahbaz, M., Roels, W., Van Schooten, B., Vermeer, J. E. M., Zarza, X., Guardia, A., Scuffi, D., García-Mata, C., Laha, D., Williams, P., Willems, L. A. J., Ligterink, W., Hoffmann-Benning, S., Gillaspy, G., Schaaf, G., Haring, M. A., Laxalt, A. M., & Munnik, T. (2018). Arabidopsis phospholipase C3 is involved in lateral root initiation and ABA responses in seed germination and stomatal closure. *Plant and Cell Physiology*, *59*(3), 469–486. https://doi.org/10.1093/pcp/pcx194

Zhang, X., Bi, E., Novick, P., Du, L., Kozminski, K. G., Lipschutz, J. H., & Guo, W. (2001). Cdc42 Interacts with the Exocyst and Regulates Polarized Secretion. *Journal of Biological Chemistry*, *276*(50), 46745–46750. https://doi.org/10.1074/jbc.M107464200

Zhang, X., Orlando, K., He, B., Xi, F., Zhang, J., Zajac, A., & Guo, W. (2008). Membrane association and functional regulation of Sec3 by phospholipids and Cdc42. *Journal of Cell Biology*, *180*(1), 145–158. https://doi.org/10.1083/jcb.200704128

Zhao, Y., Yan, A., Feijó, J. A., Furutani, M., Takenawa, T., Hwang, I., Fu, Y., & Yang, Z. (2010). Phosphoinositides regulate clathrin-dependent endocytosis at the tip of pollen tubes in Arabidopsis and tobacco. *Plant Cell*, *22*(12), 4031–4044. https://doi.org/10.1105/tpc.110.076760

Zheng, S. Z., Liu, Y. L., Li, B., Shang, Z. L., Zhou, R. G., & Sun, D. Y. (2012). Phosphoinositide-specific phospholipase C9 is involved in the thermotolerance of Arabidopsis. *Plant Journal*, *69*(4), 689–700. https://doi.org/10.1111/j.1365-313X.2011.04823.x

Zhu, X., Li, S., Pan, S., Xin, X., & Gu, Y. (2018). CSI1, PATROL1, and exocyst complex cooperate in delivery of cellulose synthase complexes to the plasma membrane. *Proceedings of the National Academy of Sciences of the United States of America*, *115*(15), E3578–E3587. https://doi.org/10.1073/pnas.1800182115